ELECTRON TRANSFER AND DELOCALIZATION IN MIXED-VALENCE MONOCATIONS OF BIS- AND TRIS-(DIARYLAMINO) DERIVATIVES

A Dissertation
Presented to
The Academic Faculty

By

Susan Odom

In Partial Fulfillment
Of the Requirements for the Degree
Doctor of Philosophy in Organic Chemistry

Georgia Institute of Technology

December 2008

ELECTRON TRANSFER AND DELOCALIZATION IN MIXED-VALENCE MONOCATIONS OF BIS- AND TRIS-(DIARYLAMINO) DERIVATIVES

Approved by:

Dr. Seth R. Marder
School of Chemistry and Biochemistry
Georgia Institute of Technology

Dr. David Collard
School of Chemistry and Biochemistry
Georgia Institute of Technology

Dr. Laren Tolbert
School of Chemistry and Biochemistry
Georgia Institute of Technology

Dr. Jean-Luc Brédas
School of Chemistry and Biochemistry
Georgia Institute of Technology

Dr. Bernard Kippelen
School of Electrical and Computer Engineering
Georgia Institute of Technology

Date Approved: *November 14, 2008*

For my family.

ACKNOWLEDGEMENTS

The two people I have most to thank (or to blame!) for me sitting here writing an acknowledgements section to a Ph.D. thesis in organic chemistry are Robert Toreki and John Anthony. While many people have helped educate me in math, science, and in life lessons, it was ultimately the actions of Rob and John whose mentoring led me into graduate school. As a freshman at the University of Kentucky, I did not know what I wanted to study. I enrolled in General Chemistry 102 with Rob in the Spring semester. Rob made quite an effort to interest the students of his class in chemistry, getting everyone enthusiastic by playing two to three songs before class (first introducing me to the Talking Heads with "Particle Man") and showed us many demonstrations for proof of concept. I spent many hours in Rob's office discussion both the course material and chemistry and life in general. Rob eventually introduced me to John Anthony, the purpose of which was to have John be a faculty advisor for starting a chapter of the Kiwanis Club at the university. Although the club failed to gain interest from the student body, I had the advantage of meeting John. I wanted to join his research group in my second year of undergraduate studies, but he didn't want me to make up my mind too early and required me to wait until I had completed both semesters of organic chemistry. That Summer, I participated in an REU student where I was a student in Geoffrey Coates' research group at Cornell University. There I was mentored by Anna Cherion, who guided me patiently despite my regular inability to arrive to the lab at her desired time of nine a.m.

When I first met John, the graduate students were in a debate over whether or not they should start calling him John instead of Dr. Anthony. They also called him The Man, and I quickly picked up on Herr Mann as my knick name for him. To this day I still have trouble calling him John! The informalities of our faculty-student relationship allowed me to overcome many of my fears about working on the unknown. John was always there to guide me to the next step, or, I should say, *push* me to the next step. When he thought I had learned enough about a project, he switched me to something more difficult. While I started in the group on a project that was several steps of organic synthesis, a year later I was fabricating OLEDs from scratch. John pushed me outside of my comfort zone. I loved working with John and his students. I would have stayed there for graduate school – at least a master's degree – if he had let me, but he pushed me out the door for my own good, which is why I am here.

Before I met John and Rob, the person who most helped develop my interest in science was Brenda Haven. She was my high school chemistry instructor when I was at McLean County High School. Mrs. Haven, despite my class's attempts to prevent her from teaching, managed to inspire many of us to go onto study chemistry with patience, enthusiasm, and skill in teaching. I regret that Mrs. Haven died a few weeks after my defense, and I never told her about it.

My utmost gratitude belongs to Seth Marder, Steve Barlow, and Simon Jones, who helped me in different ways to accomplish the research in this thesis. Knowing Seth has opened my mind to many new perspectives, both scientifically and personally, that I am not sure I could have found in another advisor. I am eternally grateful to Seth for his regular pursuit of cracking my stubborn personality, despite my protests. Seth has been a

wonderful mentor to me, and I will always value what I've learned, even if I manage to forget it again! During my second year when the going seemed tough, Simon became my mentor and pulled me out of several synthetic ruts and gave me guidance and encouragement in the lab. More importantly, Simon was the first person to suggest generating radical cation of the thiophene-based bis(diarylamine)s, which led to my ultimate involvement in projects on mixed-valence chemistry and the study of several other classes of radical cations and anions. I will forever be indebted to Steve more even more specific project guidance, both helping me make decisions to take my research in reasonable directions as well as helping me interpret data with which the rest of the group was not familiar. His efforts to work with me go beyond any expectations I ever had.

I am infinitely thankful to Harry Anderson for letting me join his group at the University of Oxford for five months in 2005. The opportunity to live and work in another country and interact with many people from different cultures was quite eye-opening. Harry's input and advice helped start projects that have led to two papers from the synthetic work I did in his group. Within Harry's group, I am especially thankful to Craig Wilson and Michael Frampton for advice on synthesis and purification, as well as to Emma Dahlset and Milan Balaz. Although the projects from my work there are not in this thesis, hopefully you will be able to read about them in publications soon.

Yulia Getmanenko has been a great help synthetically, both with advice and with help in making compounds. In addition to synthesizing a few of the compounds in this thesis, she also worked on purification of some compounds at the end when I ran out of time. I am grateful to my undergraduate students Daniel Sweat and Kelly Lefler who

contributed to some of the synthetic work in this thesis and provided me with some entertainment in the lab.

Kelly Lancaster has been great to work with, and all of my chapters have relied on her computational expertise and hard work. I thank her for being patient with my experimental difficulties and procrastinations and especially for being so supportive of me. She is a joy to work with. I also thank Slava Coropceanu for his help, even if his conversations with me were often beyond my understanding!

I thank Laura Clapp for helping me with the set-up of the variable temperature EPR apparatus in Boggs, and I am especially thankful to David Jensen for helping me run some of the variable temperature EPR experiments.

I am grateful to the time and effort provided by Peter Hotchkiss, Gäelle Deshayes, Kelly Lancaster, and Stephen Barlow in proofreading and editing this thesis, which was pretty miserably written until they tore it to pieces. I officially blame the commonwealth of Kentucky and its KERA program for my poor writing skills.

Lastly I must acknowledge the friends and family who have supported me significantly over the years I have been in Atlanta. Thank you to LaKeisha McClary, Sandeep Patel, Steve Arnstein, Peter Hotchkiss, Gäelle Deshayes, Jon Matichak, Michal Malicki, Simon Jones, Crissie Bauer, and Steve Barlow for being wonderful friends during my time here. I thank my family members for being supportive, even if they did not understand most of my problems. My mom has always been there when I have needed her, making regular trips to Atlanta to visit me. I will miss my father and sister who were there for me as much as they could be. My grandparents, aunts, and uncles have done a wonderful job of supporting me as well. Lastly, I thank my two favorite cats

Wotan and Mona Lisa for being wonderful yet challenging for past two and a half years.

Their love and affection is my reward.

TABLE OF CONTENTS

LIST OF TABLES

LIST OF FIGURES

LIST OF SCHEMES

LIST OF ABBREVIATIONS

Cp	Cyclopentadienyl, C_5H_5
DFT	Density Functional Theory
EPR	Electron Paramagnetic Resonance
HOMO	Highest Occupied Molecular Orbital
HRMS	High Resolution Mass Spectrometry
IP	Ionization Potential
IR	Infrared
LUMO	Lowest Unoccupied Molecular Orbital
MO	Molecular Orbital
MV	Mixed-valent
NIR	Near Infrared
NMR	Nuclear Magnetic Resonance
THF	Tetrahydrofuran
UV-vis	Ultra Violet – Visible

Other abbreviations and symbols are explained in the text.

SUMMARY

To better understand the optical and electronic properties of thiophene- and pyrrole-based organic compounds on a molecular level, several aromatic compounds and their corresponding monocations were analyzed by a variety of solution-based spectroscopic techniques. The derivatives were initially synthesized using palladium-catalyzed amination reactions, condensation reactions, Horner-Emmons reactions, and Stille coupling reactions. Once isolated, the neutral compounds were analyzed by UV-visible-NIR absorption spectroscopy, fluorescence spectroscopy, cyclic voltammetry, and / or differential pulse voltammetry. Monocations were generated by chemical oxidation and were analyzed by visible-NIR absorption spectroscopy and electron paramagnetic resonance spectroscopy. By quantifying the extent of the electron-donor abilities of some chromophores and the electron delocalization of positive charge in the monocations, a more thorough understanding of the optical and electronic properties of the compounds was obtained.

CHAPTER 1

INTRODUCTION

1.1 Mixed-Valent Species

Mixed valency is a term that is used to describe a chemical species with two or more redox centers that have different formal oxidation states. Mixed-valence (MV) species can be in the form of two atoms of the same element, in a molecule, or in a lattice. The concept of mixed valency, once called "oscillating valency," was described in 1915 by Hofmann and Hoeschele.[1]

Mixed valence compounds were recognized over one hundred years ago because of their unusual colors and stoichiometries. MV species are often highly colored because of unique electronic transitions associated with intervalence electron transfer (ET) (see later discussion in Section 1.3.2) that may occur in the visible region. For example, Prussian blue, a pigment discovered in 1710,[2] is a MV species containing Fe(II)-Fe(III) centers with a cyanide bridge. Several other inorganic MV compounds were used as dyes and pigments because of the unique colors, including Wells' Salt and Wolfram's Red Salt. It was in 1896 that Alfred Werner recognized[3] and in 1924 when Zintl and Rausch explicitly stated[4] that: "To produce colors…which are not given by the sum of the individual colors of the components…it is necessary that the distribution of oxidation states within the molecule can exchange under the influence of light so as to produce this light absorption and hence the color. This situation occurs most frequently in inorganic chemistry when the same element is present in different valence states in the same molecule."

The first designed MV species, prepared by Creutz and Taube in the 1970s, was a pyrazine-bridged ruthenium dimer (Figure 1.1).[5,6] Assignment of this compound as a delocalized or localized system has proven problematic despite an abundance of analytical data; the consensus now leans toward a delocalized species. In the same decade, Cowan and coworkers also synthesized biferrocenyl monocation (Figure 1.1).[7,8] Many inorganic and organometallic MV species have been synthesized since then, including several analogs of the Creutz-Taube ion and several derivatives incorporating biferrocenyl monocations. This thesis will focus more on the properties of organic-based MV species, which have attracted attention more recently.
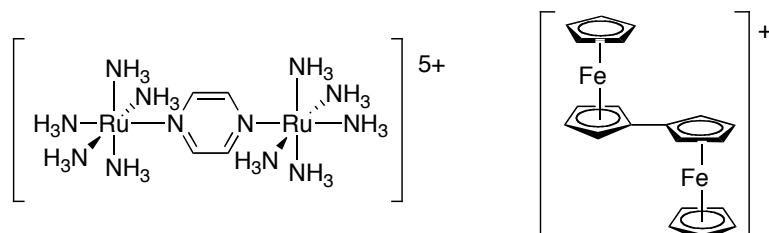
Figure 1.1. Creutze-Taube ion)[5,6] (left) and biferrocenyl monocation[7,8] (right).

Organic MV systems have been studied because they often exhibit stronger coupling and often also larger reorganizaton energies than analogs based on transition metals,[9] and because of their potential relevance to organic electronics. For anionic organic MV species, some of the redox groups that have been investigated include quinones and imides,[10,11] diketones,[12,13] dioxaborines,[14] nitro groups,[15,16] and perchlorotriphenylmethyl centers,[17] some of which are shown in Figure 1.2.
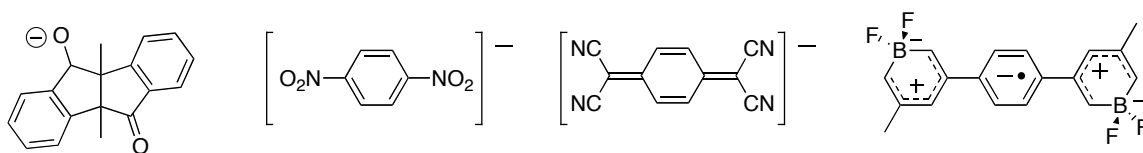
Figure 1.2. Some examples of anionic organic mixed-valent species.

Among cationic organic MV species, 1,4-dialkoxybenzenes,[18,19] hydrazines,[20,21] and alkylamines and arylamines[22-31] have been investigated, some of which are shown in Figure 1.3.
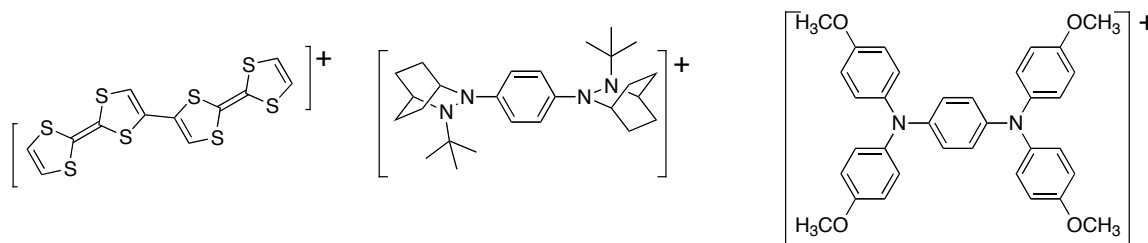
Figure 1.3. Some examples of cationic organic mixed-valent species.

The study of MV species aids in developing an understanding of ET and delocalization, which is relevant to systems in biochemistry, including the processes that control mechanisms ranging from photosynthesis and respiration to electrochemical energy systems and corrosion.[32-35] ET and delocalization is also relevant in organic electronics in which the active charge carriers in organic hole- and electron-transporting semiconductors are often MV cation and anionic species, respectively.[36] ET is also relevant to classic reactions in organic chemistry, including the SET (single electron transfer) reaction and in exciplexes. By studying MV species, it is sometimes possible to measure rate constants and activation barriers for intramolecular ET, which is usually difficult to study. Nelsen's studies on bis(hydrazine) monocations[37-39] and Elliot's study

3

of polypyridyl-linked Fe(II)-Fe(III) centers are among the few studies involving MV species.[40]

1.2 Electron Transfer and Delocalization in Mixed-Valent Species

In the 1940s, the principles of ET were described with transition state theory[41] and Kramers theory,[42] that described reaction rates on a microscopic basis. In the 1950s, Rudy Marcus developed an empirical concept for understanding the dependence of rate constants on thermodynamic and molecular dynamics parameters for outer-sphere ET, including subsequent justification by derivation from basic principles.[43-45] In the 1960s, two groups of scientists independently summarized MV species. Robin and Day proposed a classification of MV species based on electronic coupling.[46] Allen and Hush modified Marcus theory to include inner-sphere ET, thus developing a theory to explain the electronic transition unique to MV species, the intervalence charge transfer (IVCT) band.[47] The next section discusses Robin and Day's classification system of MV species.

1.2.1 Robin-Day Classification of Mixed-Valent Species

In 1967 Robin and Day presented a classification of MV species based on the electronic coupling between the redox centers.[46] Robin and Day divided MV species into three classes. In Class I, there is no electronic coupling between redox centers. In Class II, there are localized valences with measurable electronic coupling, which gives rise to an invervalence charge transfer (IVCT) band and a thermal barrier to electron exchange. In Class III, the redox centers – having non-integral valence – are indistinguishable, and the lone electron / hole is delocalized equally over both redox sites.

Representations of the potential energy surfaces for the ET reaction coordinates are shown in Figure 1.4. In Class I species (Figure 1.4a), two parabolae represent the potential energy wells of two redox centers. Because there is no electronic coupling, there is no mixing of the two parabolae; the redox centers remain isolated from one another. The distance between the centers of the redox sites and is equivalent to the diabatic ET distance, which is the distance between two redox centers when there is no electronic coupling. In Class II species (Figure 1.4b), when electronic coupling is present, the two parabolae representing the diabatic potential surfaces mix, creating two adiabatic potential energy surfaces. In this case, the distance between the two minima of the merged parabolae – now equivalent to the adiabatic ET distance, the real distance the electron moves – is smaller than that of the diabatic ET distance in Class I species. For Class II species, ET can occur both by photoexcitation with energy equivalent to the reorganization energy between the geometries of the two MV states (λ) or by overcoming the barrier to thermal ET ($\Delta G^{\ddagger}$). Lastly, in Class III MV species (Figure 1.4c), the electronic coupling is so large that there is one minimum to the potential energy surface, and the redox centers are equivalent and non-integral in oxidation state. The adiabatic ET distance is zero, and the energy absorbed upon photoexcitation is equivalent to that of twice the electronic coupling ($2V$).
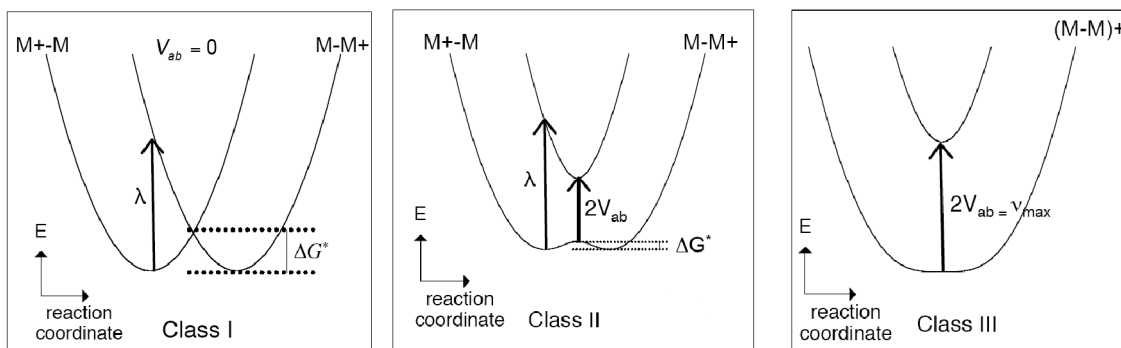
Figure 1.4. Potential energy surfaces of Class I (a), II (b), and III (c) MV species containing two equivalent redox centers with different formal oxidation states.

The next section focuses on the various experimental techniques that are used to determine the electronic coupling (*V*) in MV species, how Class II or III assignment is determined, and – for Class II MV species – how the rate of intramolecular ET is measured.

1.3 Experimental Techniques for Analyzing Mixed-Valent Species

MV species have been analyzed by numerous techniques to determine the electronic coupling (*V*), Class II or III assignment, and the rate of ET in Class II species. Electronic coupling has been estimated by electrochemical experiments such as cyclic voltammetry (CV) and differential pulse voltammetry (DPV),[17,26,27,48-54] analysis of the intervalence charge transfer (IVCT) band,[26-28,47,55-60] and indirectly from the activation barrier to ET ($\Delta G^{\ddagger}$).[61-63] Class II or III assignment is based on electronic spectroscopy; the broadness and line shape of the IVCT transition is analyzed in this case. IR and Raman spectroscopies can be used in some cases to distinguish Class II and III systems.[64-69] Mössbauer spectroscopy is useful in determining class assignment in MV species containing iron and a few other elements.[70-73] Electron paramagnetic resonance (EPR)

spectroscopy can be used to determine whether a MV species appears localized or delocalized on the EPR time scale.[28,73-77] X-ray crystallography can be used to examine bond symmetry within a redox center and from one redox center to another as well as bond order within a bridge. [7,28,67,78] Solvatochromism and Stark spectroscopy have been used to determine whether a MV species belongs to Class II or III.[27,79-82] Rates of ET can be determined from rate-dependent experiments such as IR/Raman,[64,65] Mössbauer,[70-73] and EPR[28,73-77] spectroscopy. By varying the temperatures at which spectra are recorded, rates can be extracted if the spectra change with temperature.

1.3.1 Electrochemical Techniques

CV and DPV are useful for obtaining a general idea of how stable one ionic species will be with respect to disproportionation, using the comproportionation constant (K_c). For example, when studying MV species, it is relevant to know how easy it will be to form a monocation rather than a mixture of neutral species, monocation, and dication. A large comproportionation constant – meaning a substantial difference between redox potentials – is necessary for the isolation of MV species separately of other oxidation states of the species.[54]

If a MV species is a monocation of a neutral species, then the difference between first and second oxidation potentials ($\Delta E_{1/2}$) can be used to calculate the comproportionation constant (K_c), which has been used to estimate the electronic interaction between electron-transfer sites. [52,60,83] K_c is defined as

$$K_c = \exp[(\Delta E_{1/2} n_1 n_2 F)/RT] \tag{1.1}$$

7

where n_1 and n_2 are the numbers of electrons transferred in each redox process, F is the Faraday constant, R is the gas constant, and T is temperature in Kelvin. When $n_1 = n_2 = 1$, the equation simplifies to

$$K_c = \exp(\Delta E_{1/2}/25.69) \qquad\qquad (1.2)$$

at 298 K when $\Delta E_{1/2}$ is given in mV.[84] As an example, the cyclic voltammogram of a bis(ruthenium) complex is shown below (Figure 1.5), which displays two reversible oxidations and one reversible reduction. The difference between the oxidation potentials (0.34 V) gave a K_c of ca. 6×10^5.[85]
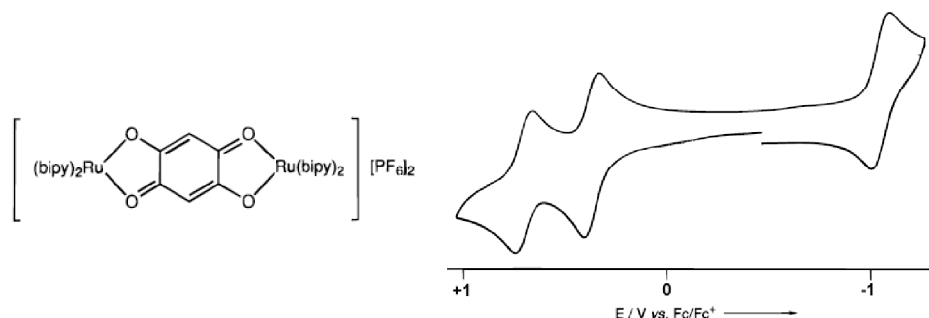
Figure 1.5. A dinuclear Ru(II) complex with the dianion of 2,5-dihydroxy-1,4-benzoquinone as bridging ligand (left) and its cyclic voltammogram (right).[85]

K_c has often been used to quantify "communication" between redox centers, although often not specifying exactly what is meant. While it is true that V should contribute to K_c, and in fact

$$\Delta G_V = V^2 / \lambda \text{ (for Class II)} = V / 2 \text{ (for Class III)}$$

the factors leading to the free energy associated with the comproportionation constant (ΔG_c) can outweigh those from ΔG_V, especially those from electrostatic forces in Class II systems, and also from ion-pairing, antiferromagnetic exchange, inductive effects, and entropy. Numerous examples have shown a discrepancy between correlating V and K_c.[54] Sutton and Taube found that for a series of Class II bis(ruthenium) derivatives, the

resonance (electronic coupling) contribution to ΔG_c is less than 10% of the total.[50] However, it should be noted that within some series of Class III systems, $\Delta E_{1/2}$ does seem to be a good measure of V.[56]

It should also be noted that values for K_c are determined in solvents with electrolyte when many other measurements are conducted in solvents without electrolyte, which can also affect K_c. Different electrolytes can also affect the value of K_c. Geiger demonstrated this with a tetra(ferrocenyl)-nickel dithiolene complex, showing how the separation between the four oxidations changed depending on electrolyte used (Figure 1.6).[86]
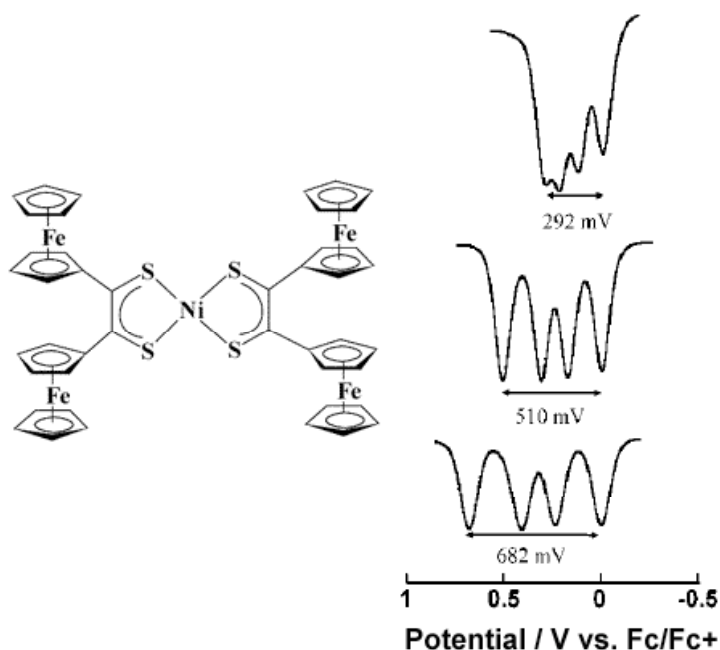
Figure 1.6.   Tetra(ferrocenyl)nickel dithiolane complex (left) and differential pulse voltammograms in tetra(*n*-butyl)ammonium hexafluorophosphate (left, top), tetra(*n*-butylammonium) tetra(pentaphenyl)borate (left, middle), and sodium tetra[3,5-di(trifluoromethyl)phenyl]borate in dichloromethane[86]

1.3.2 Marcus-Hush Theory for Inner-Sphere Electron Transfer

In 1967, Hush provided a theoretical model for linking the activation barriers for ET derived from Marcus theory with the parameters of the IVCT absorption bands in the equation

$$\nu_{max} = h\nu = \lambda_i + \lambda_o + \Delta E_0 + \Delta E^{'} \tag{1.3}$$

where $\lambda_i + \lambda_o$ are the Franck-Condon factors that correspond to inner- and outer-sphere reorganization energies, ΔE_0 is the difference in energy between the vibrationally relaxed initial and final states in the absence of electronic coupling, and ΔE reflects additional contributions due to electronic coupling.[47]

In Class I MV species, when the redox centers are not electronically coupled, IVCT transitions are not possible due to a zero transition dipole moment associated with the transition because the donor wave function is entirely based on one redox center, and the acceptor wave function is entirely based on the other redox center, with no overlap of the two orbitals. In Class II MV species, where electronic coupling is present, IVCT bands occur due to the vertical transition between the adiabatic states of the redox centers, corresponding to λ in Figure 1.5b. For Gaussian-shaped IVCT bands, the electronic coupling (V) is given by

$$V = \frac{\mu_{ge}\bar{\nu}_{max}}{eR_{ab}} \tag{1.4}$$

in which μ_{ge} is the transition dipole moment, ν_{max} is energy of maximum absorption, e is the charge of one electron, and R_{ab} is the diabatic ET distance, i.e, the distance between redox centers in the absence of electronic coupling. In metal-based systems, R_{ab} is often taken as the metal-metal distance. In many organic systems where the redox center is a group, R_{ab} is less clear-cut., e.g with nitro groups, dioxaborines, and quinones, the redox

center is a group rather than an atom. Moreover, in both organic and inorganic systems with strong electronic coupling, the redox sites may be somewhat displaced onto the bridges, making R_{ab} even more difficult to estimate. It has previously been noted that the Hush equation may underestimate values of V because values of R_{ab} are often overestimated.[87]

It should be noted that, while R_{ab} is difficult to determine in organic MV species and in strongly coupled MV species, it is possible to measure experimentally. The diabatic ET distance is defined by

$$R_{ab} = \frac{\sqrt{\Delta\mu_{12}^2 + \Delta\mu_{ge}^2}}{e} \tag{1.5}$$

where μ_{12} is the adiabatic dipole moment shift and can be determined from solvatochromism in Stark spectroscopy and quantum-mechanical calculations,[88] and μ_{ge} is the transition dipole moment, which can be calculated from analysis of the IVCT band.

For class III systems, V can also be calculated by equation 1.6 and is simply half the energy of the absorption energy of the so-called IVCT band

$$V = \bar{v}_{max}/2 \tag{1.6}$$

although a true Class III system no longer has a *mixture* of valency because each redox center is identical; the adiabatic ET distance is zero, so there is no redistribution of the symmetry of the electron from one redox center to another as happens in Class II species. Comparison of the values of V from equations 1.4 and 1.6 for Class III systems can be used to estimate the error in R_{ab}, thus providing a better indication of the true value of R_{ab}.

Hush theory also predicts the thermal barrier to ET based on analysis of the IVCT band in Class II species. In a conventional semi-classical model, the barrier ($\Delta G^{\ddagger}$) to thermal intramolecular ET is defined as

$$\Delta G^{\mp} = \frac{(\lambda - 2V)^2}{4\lambda} \tag{1.7}$$

for which V can be obtained from equation 1.4, and λ is the value the energy of maximum absorption of the IVCT band. If $\Delta G^{\ddagger}$ is known from another method, such as a variable temperature rate-dependent spectroscopy (specifics for which will be discussed in later sections) and if the reorganization energy (λ) is known from the energy of maximum absorption of the IVCT band (ν_{max}), then it is possible to indirectly calculate V using equation 1.7.

Analysis of the line broadness and line shape of the IVCT band is also used to determine whether a MV species belongs to Class II or III. Hush theory provides a simple relationship between the reorganization energy and the band width in class II MV species

$$\nu_{1/2} = \sqrt{16RT\ln 2(\lambda)} \tag{1.8}$$

where $\nu_{1/2}$ is the band width at half height, R is the gas constant, and T is the temperature in Kelvin. This equation simplifies to

$$\nu_{1/2} = \sqrt{2310\lambda} = \sqrt{2310\nu_{max}} \tag{1.9}$$

at 298 K when ν_{max} is given in cm^{-1}. If a Gaussian-shaped band has a $\nu_{1/2}$ larger than that predicted by equation 1.9, this result is suggestive that the IVCT band belongs to a Class II species. If the band is narrower than that predicted by equation 1.9, this result is suggestive of a Class III species.

It should be noted that in many metal-based systems, the IVCT bands are narrow and fairly symmetric. In organic systems, the IVCT bands of Class III systems often exhibit well-marked vibrational structure, as has been seen in bis(dialkylamino)benzene monocations, dinitrobenzene monoanions, and bis(dioxaborine) monocations.[14-16,25]

1.3.3 Solvatochromism and Stark Spectroscopy

Solvatochromism is a common technique used to determine if a MV species belongs to Class II or III. Usually the IVCT band is analyzed. While solvatochromism can be very useful in determining class assignment, a drawback of solvatochromism is that it requires the species of interest to be soluble in a range of solvents. In a Class II MV species, the change in dipole moment is non-zero, and, therefore, the IVCT bands of Class II MV species should be solvatochromic. In a Class II MV species, the dipoles of the solvent molecules in polar solvents will organize around each redox center because of the asymmetric charge distribution in the MV species. Upon photoexcitation, the excited state of the MV species will be destabilized because of having a different dipole moment to the ground state, resulting in blue shift of IVCT bands in more polar solvents (Figure 1.7). Class III MV species are expected to be much less solvatochromic than Class II species.
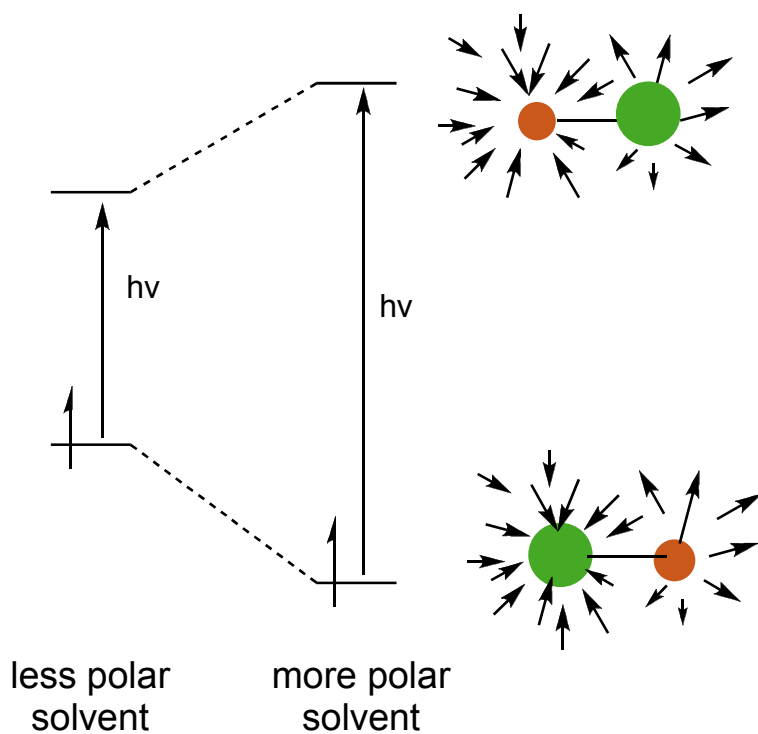
Figure 1.7. Solvatochromic effect in Class II MV species.

An example of the solvatochromism of a biferrocenyl MV species is shown in Figure 1.8.[89]
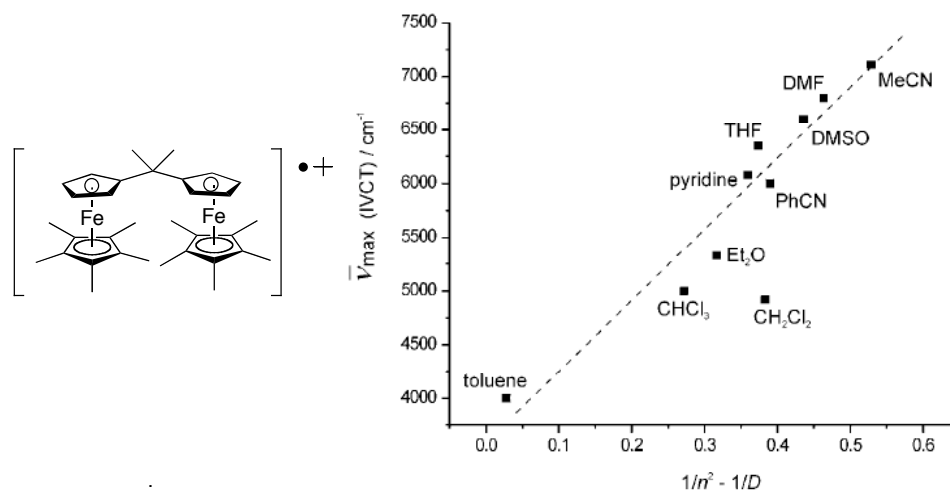
Figure 1.8. A biferrocenium monocation (left) and solvatochromism of the IVCT band (right).[89]

Solvatochromism can also be used in Stark spectroscopy to determine the adiabatic dipole moment shift.[79,82] Stark spectroscopy, which is an electroabsorption technique, measures the effect of an externally applied electric field on the molar extinction absorptivity and absorption energy of a sample. In many cases, Stark spectroscopy has yielded quantitative measurements about the changes in permanent electric dipole moment and polarizability between two states involved in an optical transition. Additionally, Stark spectroscopy provides the susceptibility of the transition dipole moment to an electric field. This experiment provides an experimental approach for the assignment of charge-transfer bands and for quantifying the degree of electronic delocalization.

1.3.4 X-ray Crystallography

X-ray crystallography is another technique employed to analyzed MV species. In this technique, the bond lengths and angles from one redox center to another are compared to examine the symmetry (or lack thereof) between and within the redox centers as well as patterns of bond lengths. X-ray crystallography can be a difficult technique to employ for such studies because it first requires the ability to grow a suitable crystal of the MV species, and it is also necessary to have a sample that is pure from other oxidation states of the compound, which is especially difficult for organic MV species. Once a crystal structure is obtained, conclusive data to support a Class III species is often difficult to obtain because sometimes a species that is symmetric in solution may be unsymmetric in the crystal due to position of a counterion or other packing forces. Additionally, if a structure is poorly resolved due to static or dynamic

crystallographic disorder, asymmetric bonds may appear symmetric due to the error in atom placement. The crystal structure of 4,4'-bis(dianisylamino)stilbene monocation–hexachloroantimate salt, which was assigned as a Class III monocation, is shown in Figure 1.9.[28] Bond lengths between redox centers were compared, some of which are listed in the figure below. The authors found little difference in bond lengths from one redox center to another but observed a difference in the C-N bond lengths to the anisyl rings (red) compared to the central stilbene bridge (blue), which suggested that the monocation is not localized on one triarylamine center, for which one would expect all of the C-N bond lengths within a triarylamine moiety to be of similar length.
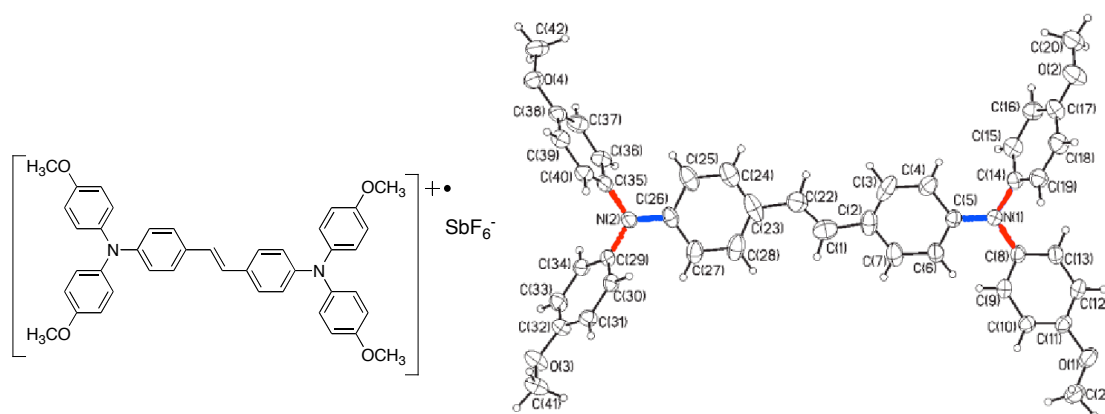
Figure 1.9. 4,4'-bis(dianisylamino)stilbene monocation $SbCl_6^-$ salt (left) and a view of the crystal structure (right). Selected bond lengths (Å) for N1 center: N1-C5: 1.377(4); N1-C8: 1.424(4); N1-C14: 1.427(4) and N2 center: N2-C26: 1.361 (4); N2-C29: 1.434(4); N2-C35: 1.437(4).[28]

1.3.5 Infrared and Raman Spectroscopies

Infrared (IR) and Raman spectroscopies, which provide information on molecular vibrations, can also be used to determine delocalization in MV species. When a species appears delocalized on the time scale of IR and Raman spectroscopy, the intramolecular ET rate is faster than 10^{11}–10^{12} s^{-1}. IR and Raman spectroscopies can be used to

determine differences in symmetry within the bonds of multiple redox centers and within

bridges. In the example shown below (Figure 1.10), the substitutents in bridging and

ancillary ligands in dimers of ruthenium trinuclear clusters with pyrazine-based bridges

were systematically varied. The carbonyl stretching frequencies were examined by IR

spectroscopy. Weaker electronic coupling between the redox centers resulted in greater

separations of the energies at which the carbonyl stretching vibration occurred.[90]
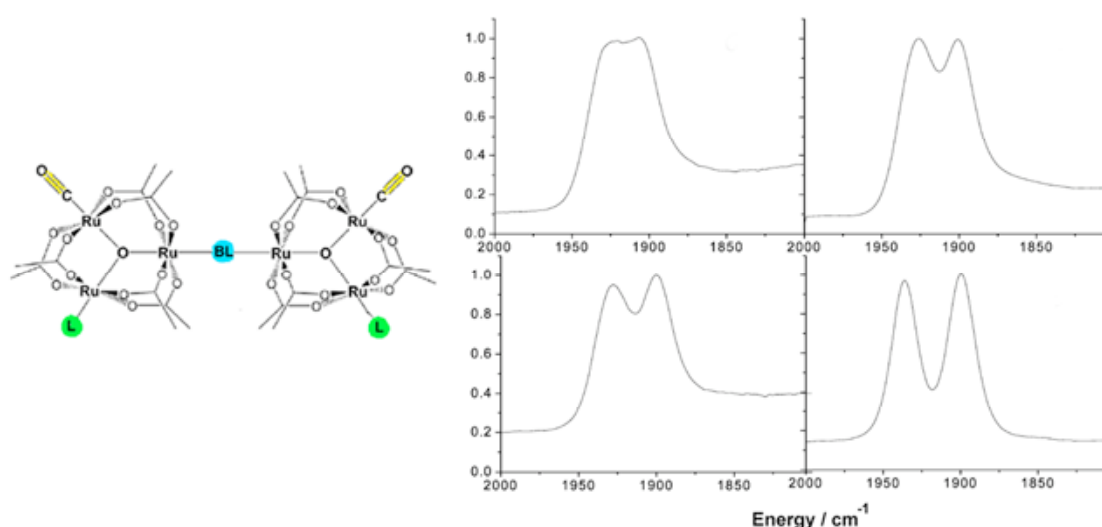
Figure 1.10. A Bis(triruthenium) complex with variations in the pyrazine-based bridging ligand (blue) and ancillary ligands (green) (left) and IR spectra of the carbonyl (yellow) stretches of some of the derivatives (right).[90]

IR spectroscopy can also be used to determine rates of intramolecular ET.

Coalescence and line broadening have been used in NMR spectroscopy to determine the

rates of dynamic chemical-exchange processes.[91] Using vibrational spectroscopies for the

same purposes have been much less wide spread, and the time scale is much shorter than

in NMR spectroscopy, ranging from femtoseconds to picoseconds. In addition to probing

intramolecular ET, other processes can occur on this time scale, including environmental

relaxation, fast intramolecular structural changes, dephasing of high-frequency

vibrational modes, and rapid self-exchange proton transfer. The combination of these possibilities leads to difficulty in interpreting variable temperature IR (VT-IR) spectroscopy. VT-IR spectroscopy was first reported for a MV system by Wu and coworkers,[92] although not quantitatively. More recently, Kubiak and coworkers have examined the rates of intramolecular ET by examination of the carbonyl stretching frequencies for bis(triruthenium) complexes using different solvents.[65] An example of the carbonyl stretching frequencies measured in multiple solvents is shown below (Figure 1.11) for a derivative with structure the same as that shown in Figure 1.10 where BL = pyrazine and the ancillary ligand = 4-N,N'-dimethylaminopyridine.   The carbonyl stretching frequencies occur at with different separations depending on the solvent used.
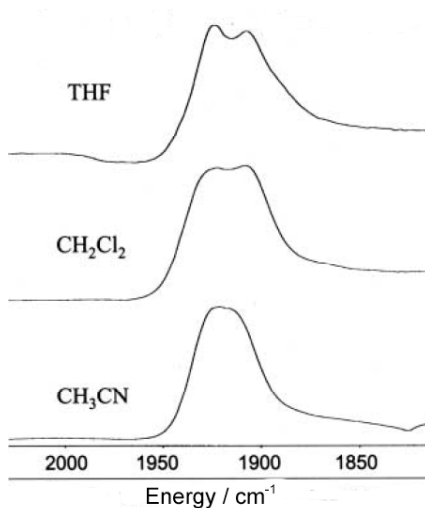
Figure 1.11. Carbonyl stretching frequencies shown for bis(triruthenium) complex (BL = pyrazine, ancillary ligand = 4-N,N'-dimethylaminopyridine) in different solvents.[65]

The authors showed that the coalescence observed for the two peaks could be simulated with different rates of intramolecular ET between the two ruthenium redox centers.   Simulations at different rates are shown in Figure 1.12, along with an experimental spectrum that matches the rate of one simulation.
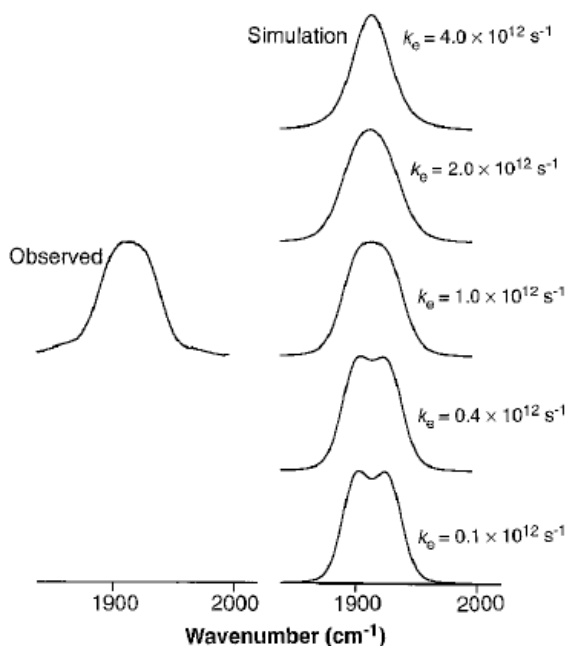
Figure 1.12. An observed IR spectrum for the carbonyl stretching frequencies of a bis(triruthenium) complex (right) and spectra simulated at different rates of intramolecular ET (right).[65]

1.3.6 EPR Spectroscopy

EPR spectroscopy is a time-dependent technique that is useful for analyzing MV species with spin-active nuclei. Analysis of EPR spectra can indicate whether a MV species is either a localized or is in a delocalized or fast-exchange regime, i.e. with intramolecular ET rates greater than ca. 10^7 s^{-1}. When hyperfine coupling is present in an EPR spectrum, the spectrum can be simulated to determine to what types of nuclei and how many nuclei a lone electron is coupled. In a two-site MV species, if the electron is coupled to the spin-active nuclei of one redox center only, for example, this result implies that the MV species is localized, so is a Class II species. If the electron is coupled to the nuclei of two redox centers, then the electron is either delocalized over multiple redox

centers and is therefore a Class III MV species, or the electron may be in a fast-exchange regime between the redox centers, overcoming the barrier to ET on the time scale of the EPR experiment, which result from a Class II species. In the example shown below (Figure 1.13), the EPR spectrum of the monoanion of a complex is shown.[93] The 11-line spectrum of anion of a bismanganese complex, which was assigned to Class III based on analysis of the IVCT band, is consistent with coupling to two ^{55}Mn centers ($I = 5/2$).
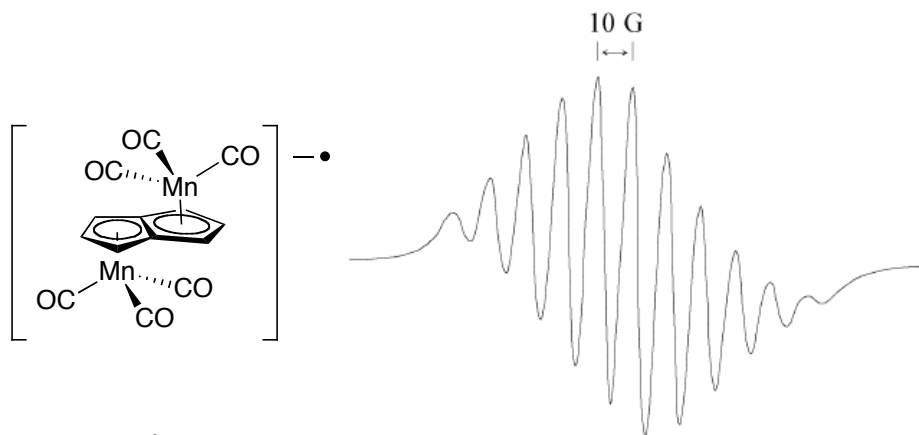
Figure 1.13. An anionic bimanganese complex (left) and its EPR spectrum (right).[93]

Variable temperature EPR (VT-EPR) spectroscopy can be used to determine rates of ET and barriers to intramolecular ET because, in some cases, the rate of ET is in the fast regime at higher temperatures and in the slow regime at lower temperatures on the EPR time scale. In the example shown in Figure 1.14, VT-EPR spectra were recorded for an anionic bis(CpMn(CO)$_2$) moietyl with pyrazolate bridge.[94] The 11-line room temperature spectrum was assigned to a delocalized species, with coupling to two ^{55}Mn nuclei. The spectrum at 123 K was described as typical of other [CpMn(II)(CO)$_2$L] compounds, indicating coupling to a single ^{55}Mn nucleus.

20
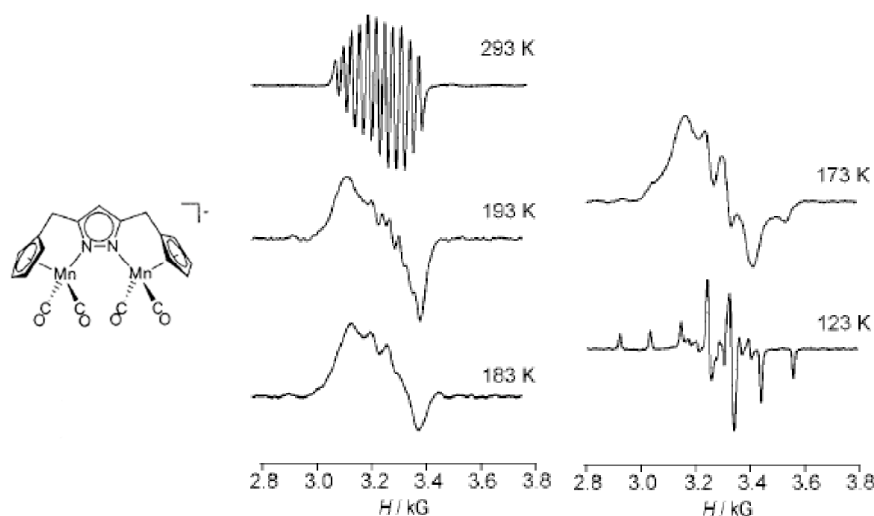
Figure 1.14. An anionic bis(CpMn(CO)$_2$) moiety with pyrazolate bridge (right) and its VT-EPR spectra (right).[94]

From this data, the authors provided a rough estimate for the activation energy ($\Delta G^{\ddagger}$) based on a coalescence temperature of 185 K, estimating the barrier to electron transfer to be 13.6 kJ mol^{-1} with a rate of ET of 2.6×10^{10} s^{-1} at 298 K using Gagne's approximation

$$k_{TH} = (kT/h)\exp(-\Delta G^{\ddagger}/RT) \tag{1.6}$$

in which k_{TH} is taken to be equal to the EPR lifetime (5.5×10^8 s^{-1}), h is Plank's constant, R is the gas constant, T is the temperature in Kelvin, and k is the Boltzmann constant.[95]

In some cases it is possible for VT-EPR spectra to be obtained from simulations with different exchange rates, and from this data, the slope of the plot of the natural log of the rate of ET versus the inverse of temperature can be used to determine the barrier to ET. In one example, VT-EPR spectra of a bis(donor)biphenylene monocation were recorded and were simulated with different rates of ET.[19] The spectra and simulations at select temperatures are shown in Figure 1.15.

21
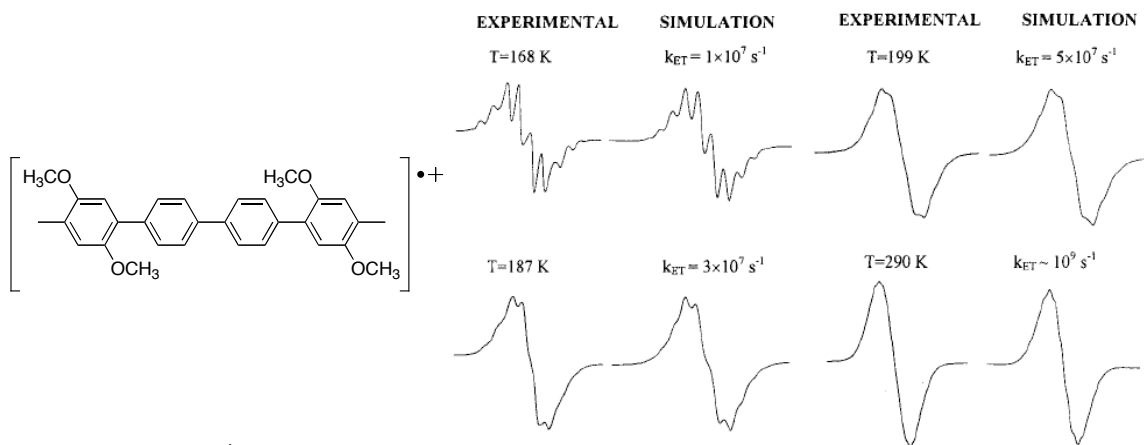
Figure 1.15. A bis(donor)-substituted biphenylene monocation (left) and VT-EPR spectra with simulations at different rates (right).[19]

1.3.7 Mössbauer Spectroscopy

Mössbauer spectroscopy is a time-dependent technique used for the analysis the nuclear transitions of atoms, often of ^{57}Fe-containing systems. In Mössbauer spectroscopy, a solid sample is exposed to a beam of gamma radiation; atoms absorb gamma rays and re-emit them, and the transmittance of gamma rays is measured. Other atoms such as ^{119}Sn, ^{129}I, and ^{121}Sb can also be analyzed given the appropriate source of gamma rays. Mössbauer spectra show two peaks for each ^{57}Fe environment, the separation between which is called the quadrupolar splitting, the magnitude of which depends on changes in the quadrupolar moment of the nucleus between the ground and excited state and in changes in the electric field gradient at the nucleus. If the ET rate in multiple ^{57}Fe environments is slower than 10^7 s^{-1}, it is possible to spectroscopically observe the different ^{57}Fe environments. For example, the Mössbauer spectra of two biferrocenium salts at 4.2 K are shown below (Figure 1.16).[73] In dibromobiferrocenium

triiodide, there is one doublet, which suggests that both iron atoms are equivalent on the time scale of the Mössbauer experiment. For dichlorobiferrocenium octaiodide, there are two sets of doublets, indicating two different iron environments, suggesting two different iron environments.
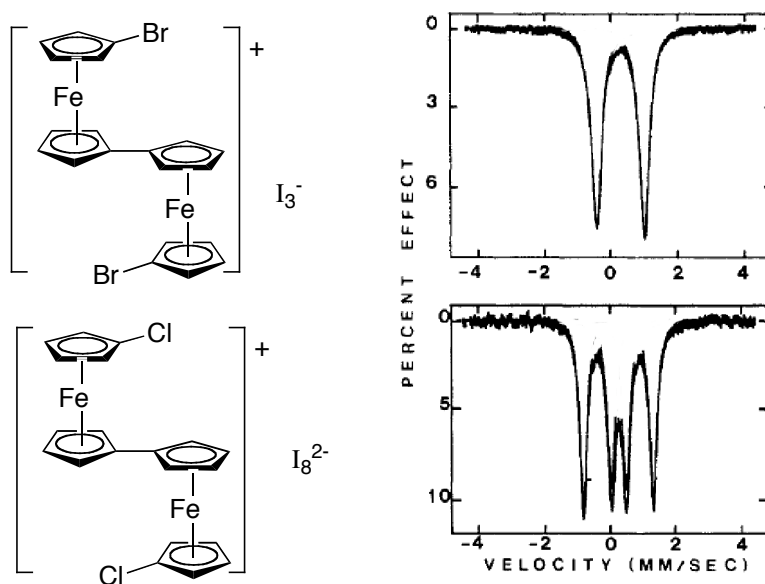
Figure 1.16. Biferrocenium salts (left) and their Mössbauer spectra at 4.2 K (right).[73]

Variable temperature Mössbauer spectroscopy can also be used to analyze the change in delocalization with temperature in MV species. The "break" temperature (the localized-to-delocalized transition) is obtained from a plot of the natural log of the area of each Mössbauer spectrum versus the temperature at which the spectrum was recorded. In the example shown below for microcrystalline samples of diethylbiferrocenium triiodide (Figure 1.17), there is an assigned "break" at approximately 220 K.[72]
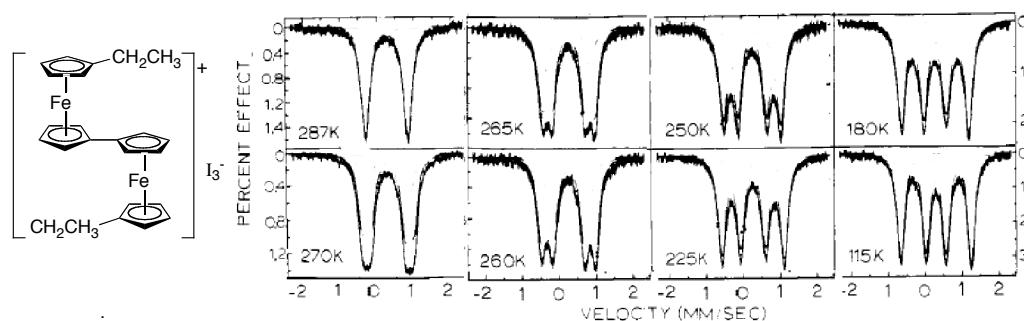
Figure 1.17. Diethylbiferrocenium triiodide (left) and its VT Mössbauer spectra (right).[72]

1.3.8 Photoelectron Spectroscopy

Gas phase ultraviolet photoelectron spectroscopy (UPS) has been shown to be a reasonable probe for understanding electronic coupling in MV species. In a recent study by Coropceanu and coworkers, UPS results on bis(dialkyl)- and bis(diaryl)-amines, the monocations of which had previously been assigned as Class III and Class II/Class III borderline MV species.[96] The difference between the second and third ionization potentials should be roughly equivalent to twice the value of the electronic coupling of in the equivalent monocationic MV species, as shown in Figure 1.18 for a Class II MV species (note: the same data for a Class III MV species should also give twice the electronic coupling).
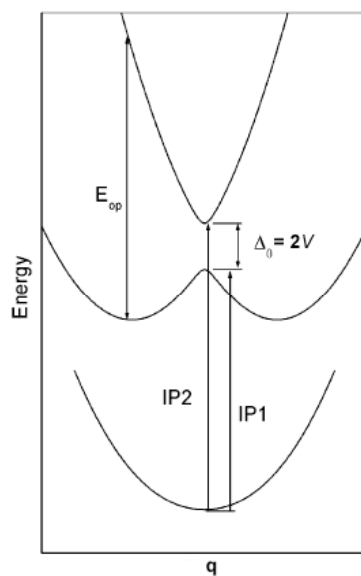
Figure 1.18. Typical adiabatic potential energy surfaces for a Class II MV system with ionization potentials (IP) noted.[96]

In the study by Coropceanu, the results of comparing the various diamino derivatives showed a correlation with the difference in the first and second ionizations with the electronic coupling calculated from the Hush analysis of the IVCT band.[96] As an example, the low energy portion of the UPS spectrum of 1,4-bis(dianisylamino)benzene, for which the monocation is a Class III MV species, is shown below for one of the derivatives (Figure 1.19).
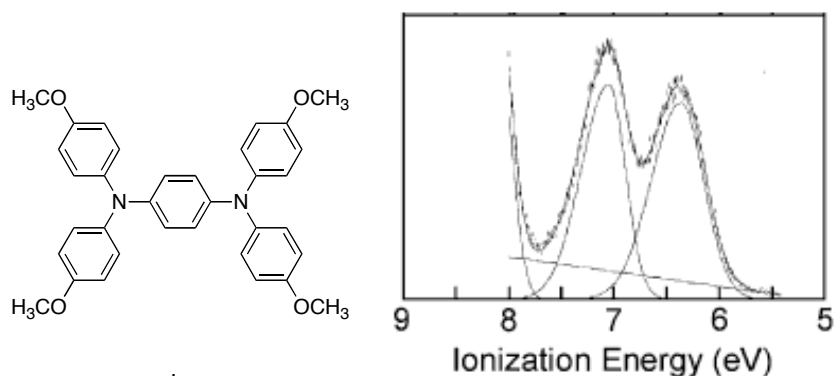
Figure 1.19. 1,4-Bis(dianisylamino)benzene (left) and the low energy region of its UV-PES spectrum (right).[96]

X-ray photoelectron spectroscopy (XPS) also provides a method for measuring the electronic coupling in MV species, operating on the same principles as UPS but at different energies. XPS has been used to distinguish between Classes II, II/III and III in several MV species with metal-based redox centers,[97-100] although it has been noted that interpretation of the data can sometimes be difficult.[101,102]

1.4 Triarylamine-based Mixed-Valent Species

Organic MV species are receiving increasing attention as MV species because of their relevance in understanding ET phenomena and because of their relevance to organic electronic materials. Triarylamine-based monocations have been among the MV species studied. For example, bis(diarylamino)biphenyl derivatives are commonly incorporated as hole-transporting organic semiconductors in organic light-emitting diodes[36] in which the active charge transport material is the monocation of the bis(diarylamino) derivative, which is a MV species. Additionally, MV species based on organic compounds have been proposed as switching devices.[103-105]

Triarylamine derivatives are particularly attractive to study as MV species because they are generally straightforward to synthesize and often have stable monocations, making them relatively easy MV species to study. Triarylamine monocations have absorption spectra that usually span the visible region, leaving most the near-infrared (NIR) window open to the observation of transitions due to potential IVCT bands. This section will focus on electronic properties of some monocations of bis- and tris-(diarylamino) derivatives.

1.4.1 Monocations of Bis(diarylamino)-substituted Derivatives

Several studies have investigated the electronic coupling of the monocations of bis(diarylamino) derivatives. Many of these studies have included analysis of the IVCT band. In addition to analysis of the IVCT bands based on Hush theory, some monocations of bis(diarylamino) derivatives have also been studied by IR and Raman spectroscopy, x-ray crystallography, and EPR spectroscopy. This section will describe MV species in which the two (or three) redox centers are identical in the neutral versions of the triarylamine derivatives.

1.4.1.1 Bis(diarylamino) Derivatives Studied by Low

Several examples of the monocations of bis(triarylamine)s have been reported as MV species. Low and coworkers studied a series of bis(diarylamino)biphenyl derivatives (**I–III**, Figure 1.20) and their monocations.[106] In addition to CV experiments, the IVCT bands of the monocations were measured, and for some of monocations, their solid state structures were investigated by x-ray crystallography. The first oxidation potentials of

the derivatives ranged from 0.09 – 0.29 V versus ferrocenium / ferrocene. The IVCT bands, which had a minimal solvatochromic response, had absorption maxima ranging from 6360–7380 cm^{-1}, and the monocations were assigned as Class II/III with electronic coupling values ranging from 2800 – 3300 cm^{-1}.
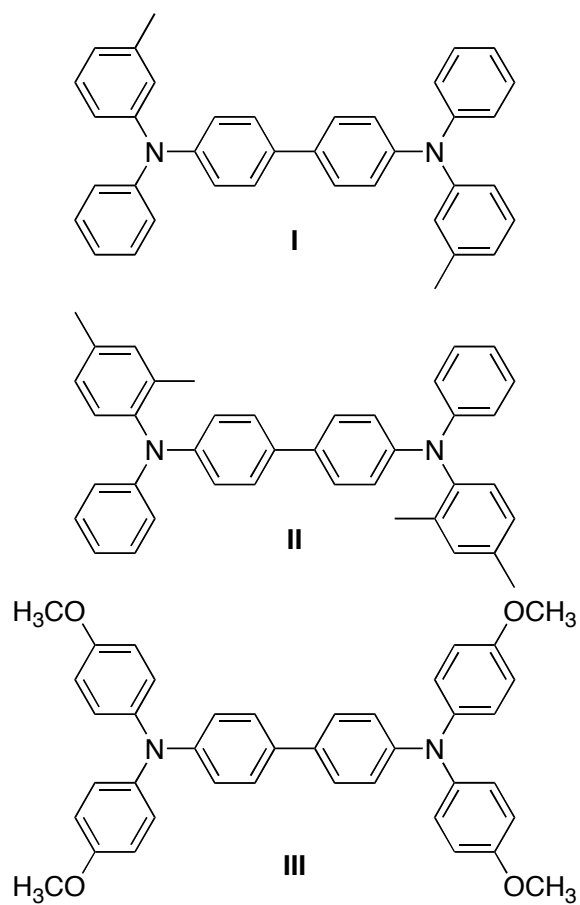
Figure 1.20. Bis(diarylamino)biphenyl derivatives studied by Low and coworkers.[106]

The data obtained from analysis of the IVCT bands of the monocations of compounds **I–III** is summarized in Table 1.1. The barrier to intramolecular ET was also calculated for these monocations. The electronic coupling is presumably lower in **III⁺** than in the other monocations because there of the decrease in ionization potential of the alkoxyphenyl end groups in comparison to the alkylphenyl end groups, which should result in more electron density on the end groups in **III⁺**, which should increase the distance between the redox centers.

Table 1.1. Electronic coupling (*V*), barrier to electron transfer ($\Delta G^{\ddagger}$), and class assignment for monocations studied by Low and coworkers.[106]

Compound	$V_{\text{eqn 1.6}}$ / cm^{-1}	$\Delta G^{\ddagger}$ / cm^{-1}	Class Assignment
I	3200	50	II/III
II	3300	50	II/III
III	2800	60	II/III

1.4.1.2 Bis(diarylamino) Derivatives Studied by Lambert and Nöll

Lambert and Nöll have studied the properties of bis(triarylamine) monocations with methoxy substitutents at the *para* positions of the terminal aryl groups. The bridges incorporated into these derivatives include phenylene, biphenyl, and phenylene-ethynylene groups (Figure 1.21).[24,26,107] The monocations of these bis(diarylamino)-substituted monocations had electronic coupling values ranging from 500 – 3250 cm^{-1} and thermal barriers to ET ranging from 1900 – 240 cm^{-1}. Lambert and Nöll assigned these monocations as class II or Class II/III borderline MV species, based on the values of *V* obtained from equation 1.4 and from line shape analyses, in which some of the IVCT

bands were asymmetric.[26] The asymmetric line shapes were interpreted as a narrowing of the bandwidths on the low-energy side due to cut-off of the of the Gaussian-shaped absorption upon increase of V.[26] This was later interpreted by Coropceanu to be due to coupling of Class III transitions to symmetric vibrations,[108] and some the monocations were reassigned to new classes.
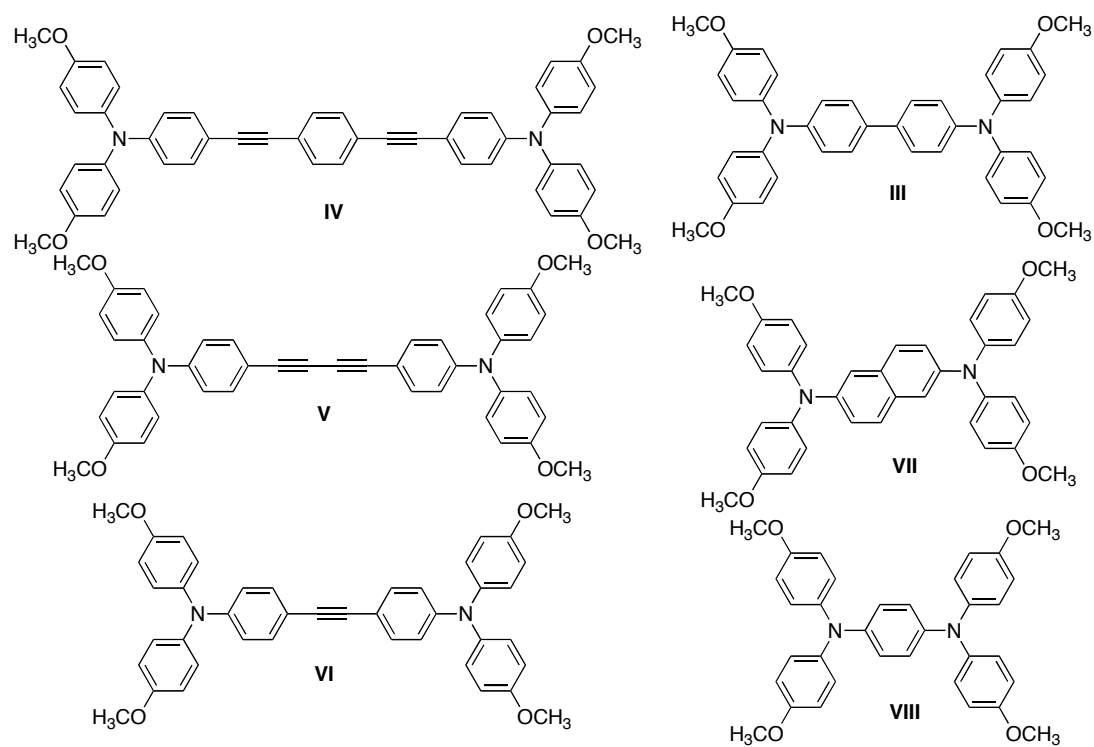
Figure 1.21. Bis(diarylamino) derivatives studied by Lambert and Nöll.[26]

Table 1.2 summarizes the values for electronic coupling, the barriers to thermal ET, and the class assignment (and re-assignment by Coropceanu and coworkers in some cases) of the MV monocations studied by Lambert and Nöll. It was observed that the monocations with shorter bridge lengths generally exhibited stronger electronic coupling, the change bridge length resulting in a change in classification from Class II to Class III in some cases.

Table 1.2. Electronic coupling, barrier to thermal ET, and class assignment of monocations of MV bis(diarylamino) derivatives **III–VIII** studied by Lambert and Nöll.

Compound	$V_{eqn\ 1.4}$ / cm^{-1}	$V_{eqn\ 1.6}$ / cm^{-1}	$\Delta G^{\ddagger}$ / cm^{-1}	Class Assignment
III	1550	3180	420	II/III → III
IV	500	–	1900	II
V	710	–	1280	II
VI	1200	–	580	II
VII	2250	3810	320	II/III*
VIII	3250	4765	240	II/III → III

*not examined by Coropceanu and coworkers

1.4.1.3 Bis(diarylamino) Derivatives Studied by Barlow and Coropceanu

Barlow and coworkers have reported bis(di(4-alkoxyphenyl)amino)-substituted analogs with stilbene and extended phenylene-ethylene bridges to determine the effect on the electronic coupling in comparison to the alkyne-based equivalents.[27,28] Barlow and coworkers synthesized derivatives with multiple bridge lengths, which are shown below (Figure 1.22).
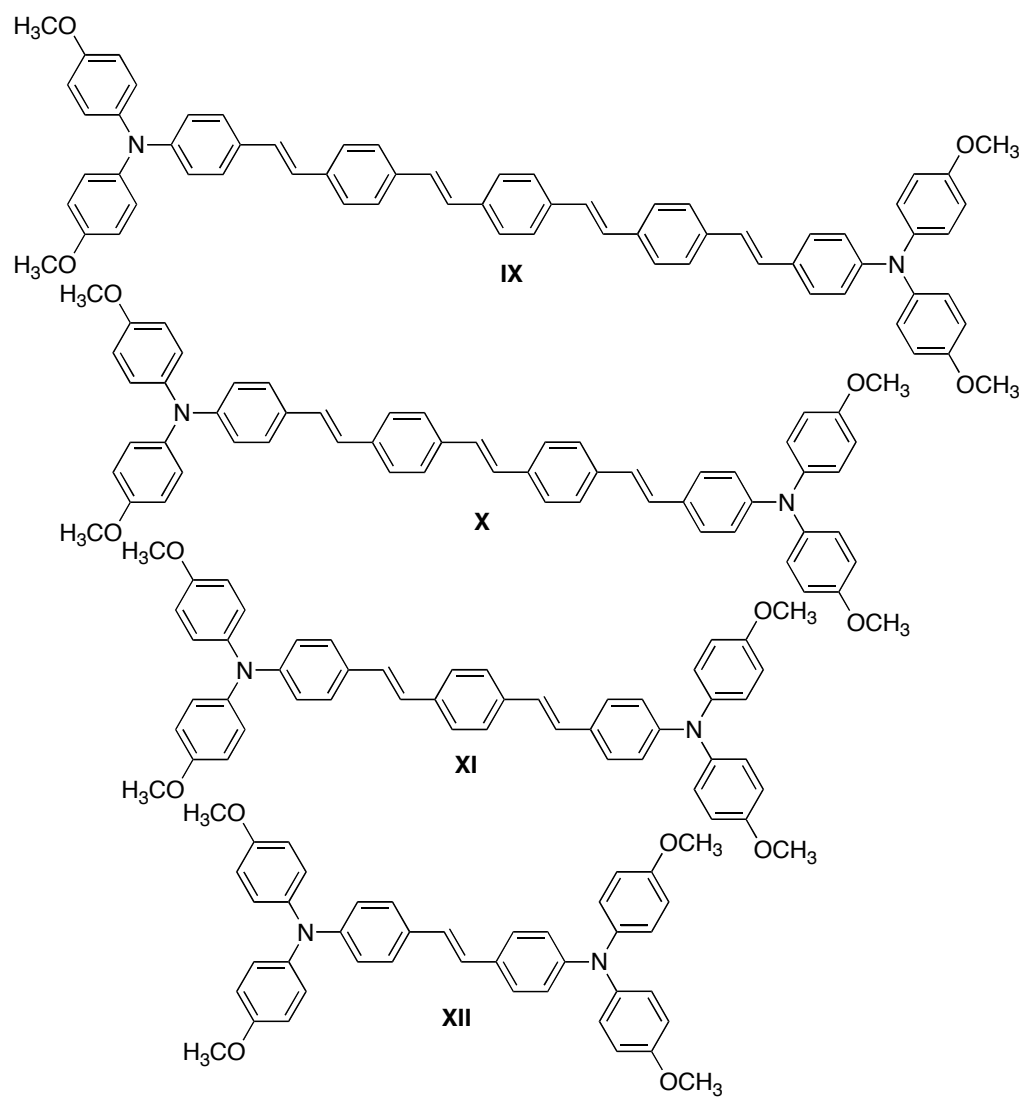
Figure 1.22. Bis(diarylamino) derivatives studied by Barlow and coworkers.[27,28]

Barlow found that, in comparison to the equivalent alkene-based monocation (**VI⁺**), the alkene-based monocation (**XII⁺**) exhibited stronger electronic coupling, resulting in Class III assignment for **XII⁺** (**VI⁺** was assigned to Class II) (Table 1.2). In comparison of the longer alkyne-based monocation (**IV⁺**) in which $V = 500$ cm^{-1}, the electronic coupling in the alkene-based derivative (**XI⁺**) increased to 700 cm^{-1}, though it remained a Class II MV species (Table 1.3). From the comparison of these derivatives with each other and with those studied by Lambert and Nöll, one can see that generally when the bridge length is increased, the electronic coupling decreases. Also, when alkene- and alkyne-based derivatives are compared, the derivative with the alkene has stronger electronic coupling.

Table 1.3. Electronic coupling and class assignment of monocations of MV bis(diarylamino) derivatives **IX–XII** studied by Barlow.[27,28]

Compound	$V_{\text{eqn 1.4}}$ / cm^{-1}	$V_{\text{eqn 1.6}}$ / cm^{-1}	Class Assignment
IX	*	–	II
X	*	–	II
XI	700	–	II
XII	1400	3020	III

*not provided using Hush analysis of the experimental parameters

EPR studies of monocations **III⁺** and **XII⁺** gave spectra that were both consistent with coupling to two nitrogen atoms.[28] Recall that coupling to two redox centers does not guarantee delocalization; although it *can* be consistent with delocalization, this result implies that the monocation is either delocalized or that the rate of intramolecular ET is faster than the time scale of the EPR experiment. Analysis of the crystal structure of the monocation salt of **XII** (crystal structure previously shown in Figure 1.7) is also consistent with assignment to Class III. The C–N bond lengths were compared among

the carbon atoms of the stilbene and anisyl moieties. If the monocation were localized, it was assumed that the C–N bond lengths would be similar within each redox center, so the difference in C–N bond lengths (0.050 Å) supports delocalization. Additionally the C–C bond lengths in the stilbene bridge show a quinoidal pattern of bond-length alternation, which also supports delocalization.[28]

More recently, Barlow and coworkers analyzed the properties of bis[di(4-alkoxyphenyl)aminostyryl]arene derivatives and their monocations in which the central arene ring was modified to vary the ionization potentials of the bridges relative to that of the di(alkoxyphenyl)amino end groups.[109] Specifically, the central phenylene group was either substituted with cyano groups (**XIII**), was unsubstituted (**XIV**), or was replaced with a 3,4-di(*n*-butoxy)thiophene group (**XV**) (Figure 1.23).
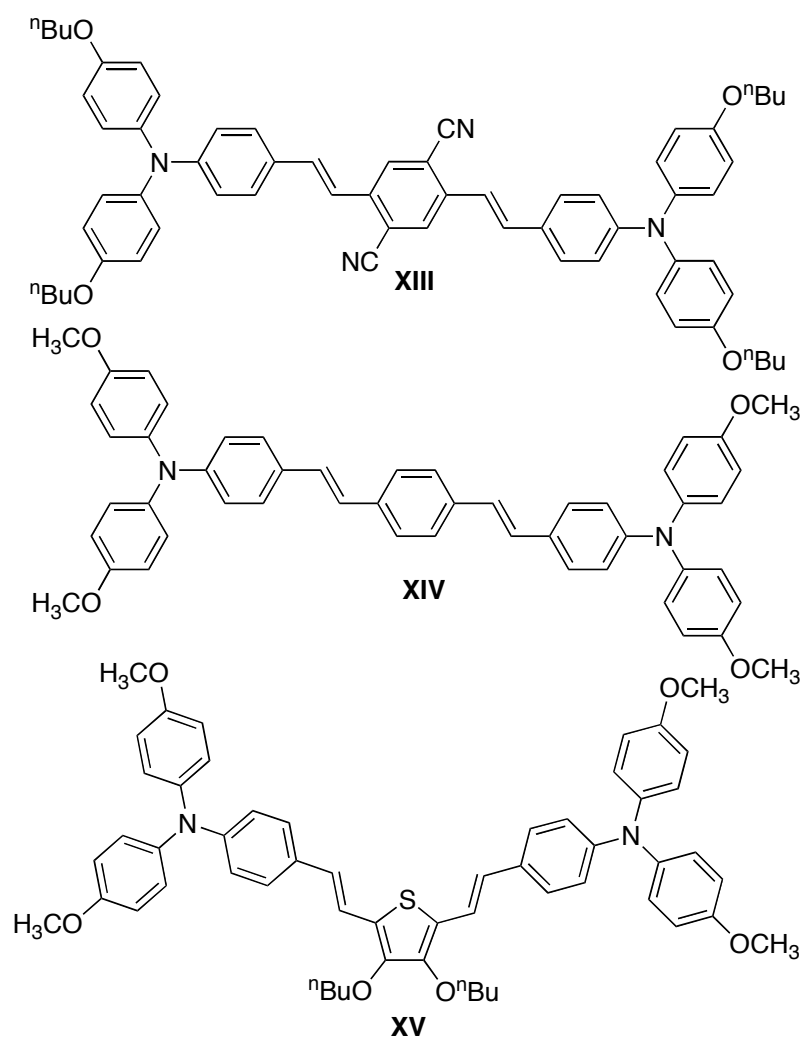
Figure 1.23. Bis[di(4-alkoxyphenyl)aminostyryl]arene derivatives studied by Barlow.[109]

The oxidation potentials of the bis(diarylaminostyryl)arene derivatives were investigated by CV; the first oxidation potentials of the derivatives decreased as the cores became more easily ionizable (Table 1.4).[109] Additionally, as the central arene group became more easily ionizable, resulting in the frontier molecular orbital energy approaching that of the di(alkoxyphenyl)amino end groups, the electronic coupling in the monocations increased – as determined by Hush analysis of the IVCT bands (Table 1.3).[109] The monocations varied from Class II to Class III by changing the core substitution alone.

Table 1.4. Electronic coupling, barrier to thermal ET, and class assignment of monocations of MV bis(diarylamino) monocations **XIII–XV** studied by Barlow.[109]

Compound	$E_{1/2}^{+/0}$ / V	$V_{eqn\ 1.4}$ / cm^{-1}	$V_{eqn\ 1.6}$ / cm^{-1}	Class Assignment
XIII	+0.26	480	–	II
XIV	+0.20	700	–	II
XV	+0.05	960	2830	III

Barlow and coworkers also studied a similar series of bis(diarylaminostyryl)arene derivatives in which the end groups were either diphenylamino or had an occasional alkyl group at the *meta* position of the terminal phenyl groups.[109] The ionization potentials of the central arene ring was again varied, including dicyanophenylene (**XVI**), dibromophenylene (**XVII**), phenylene (**XVIII**), di(*n*-dodecyloxy)phenylene (**XIX**), and 3,4-di(*n*-butoxy)thiophene (**XX**) derivatives (Figure 1.19).
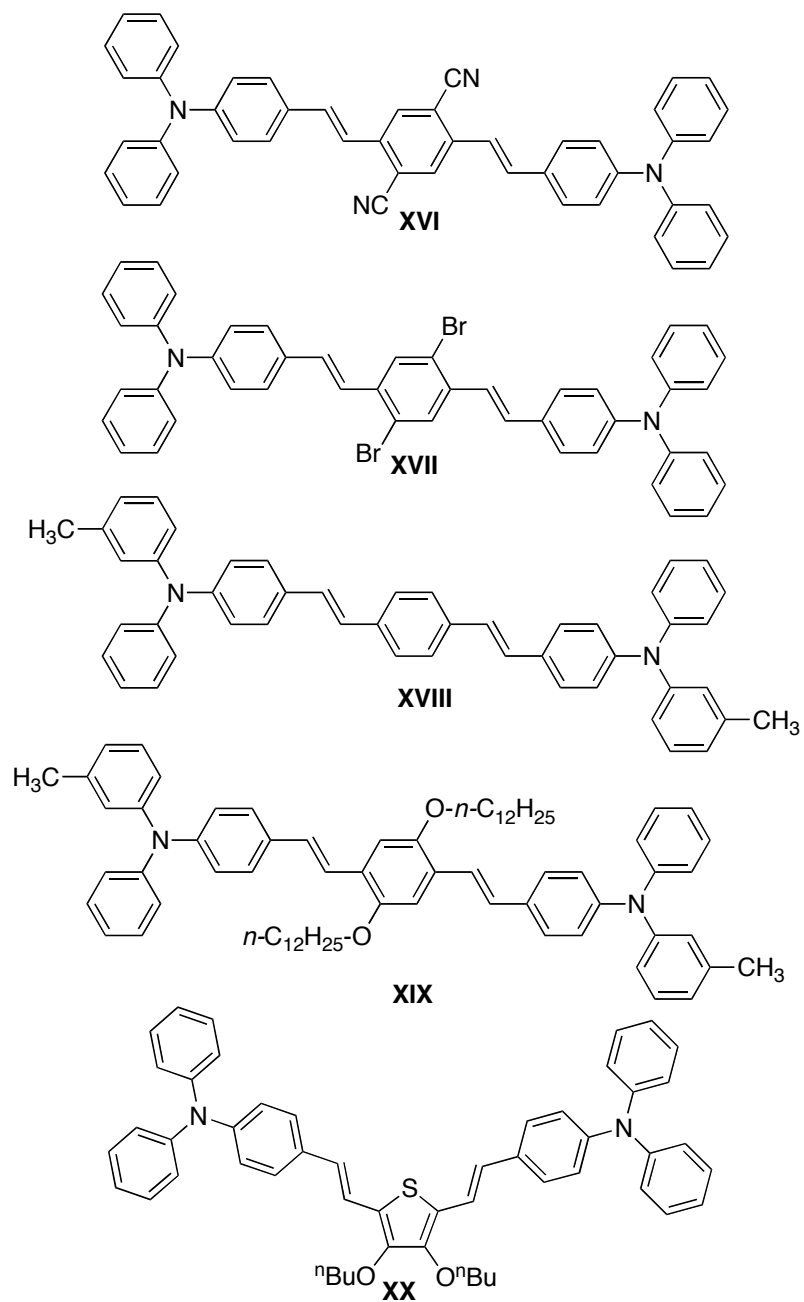
Figure 1.24. Bis(diarylaminostyryl)arene derivatives recently studied by Barlow and coworkers.[109]

Again the first oxidation potential of these derivatives occurred at lower potentials when the cores were more easily ionizable (Table 1.4).[109] Hush analysis of the IVCT bands of the monocations indicated that the electronic coupling increased as the ionization potentials of the cores increased (Table 1.4).[109] By comparing the values for V for Class III systems calculated from equations 1.4 and 1.5, one can see that the difference in values of V is quite large, which suggests that the use of the nitrogen-nitrogen distance as R_{ab} in equation 1.4 becomes increasingly erroneous as the electronic coupling increases.

Table 1.5.   Electronic coupling, barrier to thermal ET, and class assignment of monocations of MV bis(diarylamino) monocations **XVI–XX** studied by Barlow.[109]

Compound	$E_{1/2}^{+/0}$ / V	$V_{\text{eqn 1.4}}$ / cm^{-1}	$V_{\text{eqn 1.6}}$ / cm^{-1}	Class Assignment
XVI	+0.51	480	–	II
XVII	+0.44	670	–	II
XVIII	+0.31	640	–	II
XIX	+0.24	810	2700	III
XX	+0.15	1000	3200	III

From the studies by Barlow and coworkers, one can see that when a more electron-rich aryl group is incorporated into the conjugated bridge – thus raising the energies of the frontier molecular orbitals of the bridge closer to the energies of the diarylamine end groups – the electronic coupling is increased with increasing ease in oxidation of the bridges, i.e. when the energies of the frontier molecular orbitals of the bridges become closer to the energies of the end groups.

1.4.1.4 Bis(diarylamino) Derivative with Thiophene-based Bridges Studied by Hartmann and Navarrete

The monocations of some bis(diarylamino) derivatives with thiophene-based cores have been studied experimentally and computationally. The visible-NIR absorption spectrum was reported for monocation **XXI-2** (n = 2, Figure 1.25), for which the energy of maximum absorption of the IVCT band was ca. 900 cm^{-1}, but this band was not analyzed in the context of Hush theory.[110] Additionally, the EPR spectra were reported for monocations in this series where n = 1 – 7. Of the monocations, the spectra for n = 1 – 4 showed hyperfine coupling (when n = 5 – 7, the spectra were featureless), consistent with coupling to nitrogen and hydrogen nuclei; the hyperfine coupling constant to nitrogen decreased as the bridge length was increased.

XXI-*n*
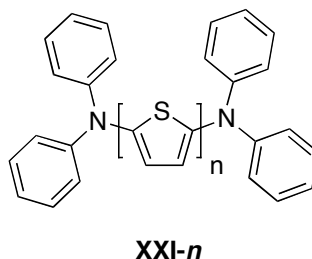
Figure 1.25. Bis(diphenylamino)oligothiophene derivatives studied by Hartmann and coworkers.[110]

The visible-NIR absorption spectra for monocations **XXII** and **XXIII** (Figure 1.26) have been reported. The absorption maxima of the IVCT bands were 1323 and 1420 cm^{-1}, respectively, but again the IVCT bands were not analyzed by Hush theory.[111]
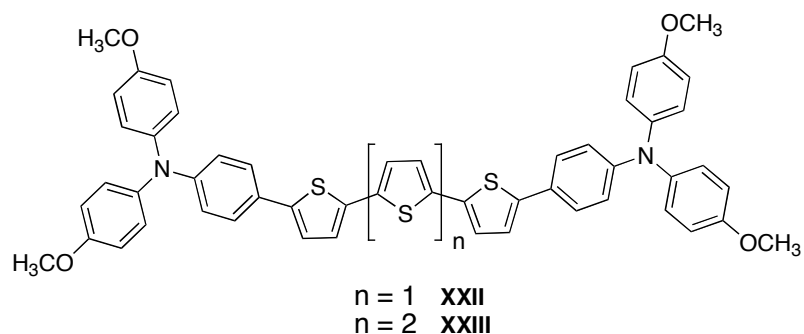
Figure 1.26. Bis(dianisylaminophenyl)oligothiphene derivatives studied by Navarrete and coworkers.[111]

1.4.1.5 Bis(diarylamino) Derivative Studied by Hirao and Tanaka

Hirao and Tanaka studied the monocation of a spiro-fused bis(triarylamine) (**XXIV**). EPR spectra of a spiro-fused bis(triarylamine). EPR spectra of the monocation were recorded at multiple temperatures (Figure 1.27).[62] The spectra showed changes upon cooling; the intensity of the peaks in the central portion of the spectrum – originally approximately a 5-line spectrum – decreased upon cooling. The spectra were simulated with an EPR-EXN program using optimization of rate constants for ET between two nitrogen nuclei (Figure 1.20).[62]
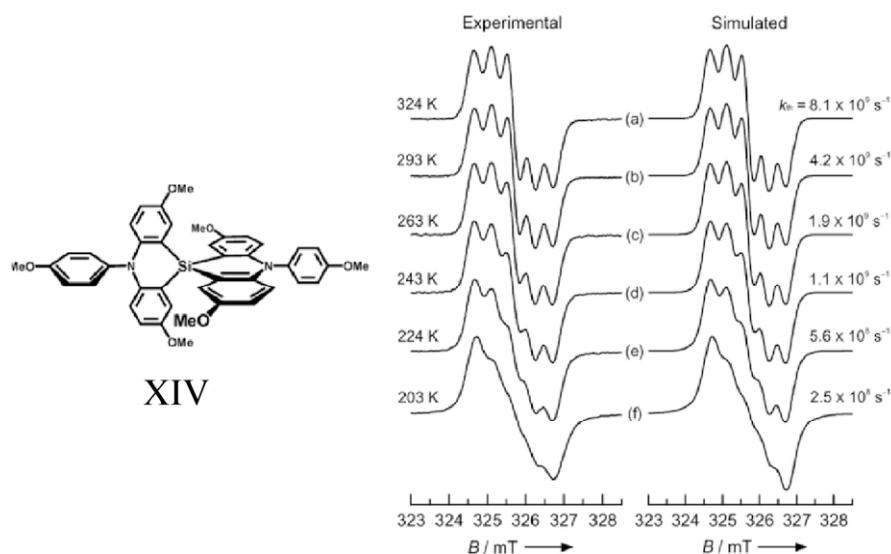
Figure 1.27. A spiro-fused bis(triarylamine) derivative (left) and experimental and simulated VT-EPR spectra of its monocation (right).[62]

By plotting the natural log of the rate constants versus the inverse of the temperature at which each spectrum was recorded, the authors obtained a linear fit of the data and were able to extract information relevant to the barriers to ET in this species.[62] Unfortunately, the monocation showed no IVCT band in the region probed by the authors (450 – 2000 nm), so the kinetic data obtained from the thermally varied EPR experiment could not be compared to the same terms that could potentially have been extracted from IVCT band analysis.

1.4.2 Monocations of Tris(diarylamino)-substituted Derivatives

Relatively few examples of monocations of three-site triarylamine-based monocations have been studied in the literature. Bonviosin and coworkers reported two studies of the monocation (and di- and tri-cations) of 1,3,5-tris(bis(4-ethylphenyl)amino)phenyl)benzene (XV, Figure 1.28).[23,112] Additionally, related three-site and two-site molecules have been studied for comparison (Figure 1.27).[23]
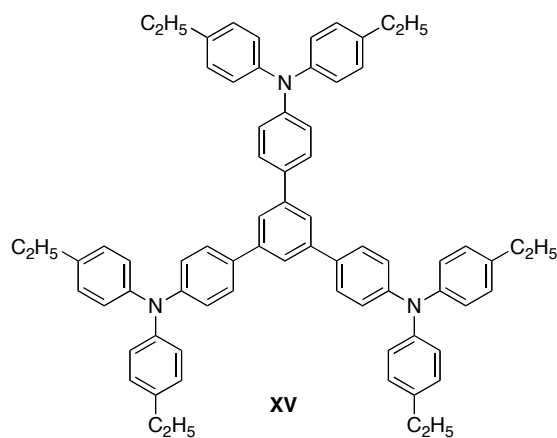
Figure 1.28. 1,3,5-Tris(bis(4-ethylphenyl)amino)phenyl)benzene.[112]

In the case of the 3-fold symmetric monocation, CV experiments were consistent with three non-separable one-electron oxidations, and the analysis of the monocation indicated a class II MV species with weak electronic coupling (V = ca. 200 cm^{-1}).[112] The IVCT band overlapped somewhat with the absorption bands of triarylamine monocation moiety, preventing observation of the band on its own, requiring Gaussian fits to analyze the band shape. The weak coupling presumably results from the *meta* substitution around the central benzene ring.

The monocation of 1,3,5-tris(di(4-methoxyphenyl)amino)benzene (**XVI**, Figure 1.28) was reported.[113] One might expect this monocation to be more strongly coupled than the analog with phenylene bridges in Figure 1.29 because of the decrease in nitrogen-nitrogen distance.
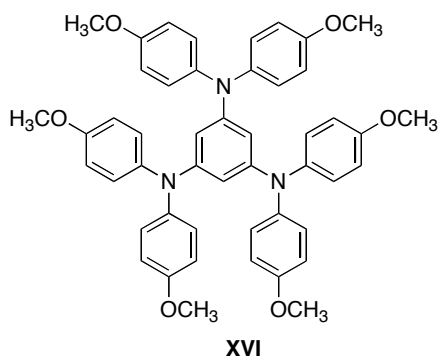
Figure 1.29. 1,3,5-tris[di(4-methoxyphenyl)amino]benzene.

Unfortunately, the monocation could not be studied at room temperature because of its instability. The EPR spectrum was reported at -65 ºC, which was consistent with coupling to three nitrogen (3.4 G) and three hydrogen (2.6 G) nuclei. This result means that the monocation is either delocalized or has a rate of intramolecular ET faster than that of the EPR time scale. No visible-NIR spectra were reported for this monocation, so the electronic coupling could not be determined from IVCT band analysis.

1.5 Thesis Overview

The goals of this thesis were to study ET and electron delocalization in bis- and tris-(diarylamino) substituted MV monocations in order to determine the degree of electronic coupling in the various series of derivatives (Figure 1.30). One study investigates the extent to which strongly coupled monocations of bis(diarylamino) derivatives can still be considered MV species. Another study focuses on the incorporation of electron-rich bridges into a series of bis(diarylamino) monocations in which the energies of the frontier molecular orbitals of the bridges versus end groups have been systematically varied, to determine if continuing to increase the bridge group

energy changes the trends observed in IVCT absorption bands. Another study sought to correlate the energy barrier to ET in Class II MV monocations, based both on thermal ET data and optical data of the IVCT bands. The last study focuses on analysis of three-site MV monocations with more electron-rich bridges than previously reported examples of weakly coupled tris(diarylamino) derivatives, in hopes of obtaining clearly defined IVCT bands, in order to better understand the nature of in three-site MV species.
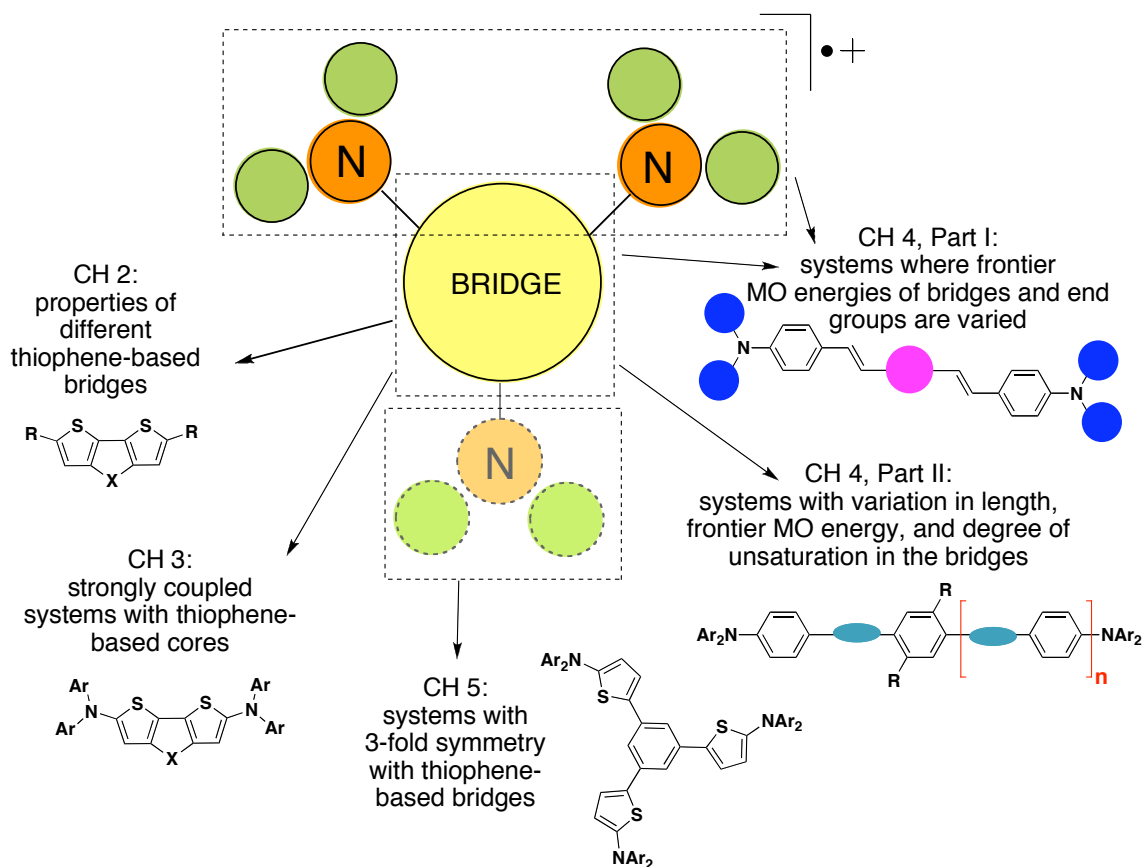
Figure 1.30. Overview of thesis projects.

Specifically, Chapter 2 describes the analysis of some thiophene-based small molecules that will later be studied as bridges in the monocations of bis(diarylamino) derivatives. The electron donating properties of various thiophene-based bridges and their derivatives were explored in order to determine, among other properties, the ease of oxidation of the bridges upon modifications such as ring fusion and incorporation of different atoms into the fused rings. These bridges are incorporated into bis(diarylamino) derivatives, which are discussed in Chapter 3. In this chapter, the monocations of the bis(diarylamino) derivatives are all strongly coupled class III MV species based on Hush analysis of the IVCT bands. Of interest in this chapter is to what extent the monocations can still be considered MV species, or if the bridges have become so electron rich that the monocations become bridge-based.

In Chapter 4, a series of bis(diarylaminostyryl)arene derivatives are presented with variation in the relative energies of the frontier molecular orbitals of the bis(styryl)arene bridges versus the diarylamino end groups. The objectives of this chapter include determining how the relative energies of the bridges versus end groups effects the electronic coupling in the monocations of these derivatives, and if a bridge that is easily ionizable continues to follow the trends of the main series or becomes a bridge-based monocation.

The second part of Chapter 4 focuses on using an alternate method to analysis of the IVCT band – in this case VT-EPR spectroscopy – to determine the rate constants and, thus, the activation barrier to ET in class II bis(diarylamino) monocations. The resultant barriers to ET obtained from the VT-EPR experiments were compared with those

obtained from Hush analysis of the IVCT band, thus shedding more light into the true diabatic ET distance in these monocations.

Finally, in Chapter 5, the properties of new symmetrical three-site diarylamino derivatives were studied in comparison to the monocation presented in Figure 1.21. In attempt to increase the electronic coupling in comparison to the weakly coupled Class II tris(triarylamino) derivative with phenylene-based bridges, derivatives with thiophene-based bridges were synthesized, which was based in part on the results from Chapter 3. The goal of this chapter was to increase the electronic coupling and, therefore, the intensity of the IVCT band, making it easier to analyze a symmetric three-site MV species.

Enjoy!

1.6 References

(1)   Hofmann, K. A.; Hoeschele, K. *Ber. Deut. Chem. Ges.* 1915, *48*, 20-28.
(2)   Woodward, J. *Philos. Trans. R. Soc. London* 1724, *33*, 15.
(3)   Werner, A. *Z. anorg. Chem* 1896, *12*, 46.
(4)   Zintl, E.; Rauch, A. *Ber. Deut. Chem. Ges.* 1924, *57*, 1739.
(5)   Creutz, C.; Taube, H. *J. Am. Chem. Soc.* 1969, *91*, 3988.
(6)   Creutz, C.; Taube, H. *J. Am. Chem. Soc.* 1973, *95*, 1086.
(7)   Cowan, D. O.; Levanada, C.; Park, J.; Kaufman, F. *Acc. Chem. Res.* 1973, *6*, 1.
(8)   Vanda, C. L.; Bechgaard, K.; Cowan, D. O.; Rausch, M. D. *J. Am. Chem. Soc.* 1977, *99*, 2964.
(9)   Nelsen, S. F.; Tran, H. Q.; Nagy, M. A. *J. Am. Chem. Soc.* 1998, *120*, 298-304.
(10)   Jozefiak, T. H.; Miller, L. L. *J. Am. Chem. Soc.* 1987, *109*, 6560.
(11)   Rak, S. F.; Miller, L. L. *J. Am. Chem. Soc.* 1992, *114*, 1388.
(12)   Mazur, S.; Sreekumar, C.; Schroeder, A. H. *J. Am. Chem. Soc.* 1976, *98*.
(13)   Schroeder, A. H.; Mazur, S. *J. Am. Chem. Soc.* 1978, *100*, 7339.
(14)   Risko, C.; Barlow, S.; Coropceanu, V.; Halik, M.; Brédas, J.-L.; Marder, S. R. *Chem. Commun.* 2003, *2*, 194-195.
(15)   Nelsen, S. F.; Konradsson, A. E.; Weaver, M. N.; Telo, J. P. *J. Am. Chem. Soc.* 2003, *125*, 12493.
(16)   Nelsen, S. F.; Weaver, M. N.; Zink, J. I. *J. Am. Chem. Soc.* 2005, *127*, 10611.
(17)   Bonvoisin, J.; Launay, J.-P.; Rovira, C.; Veciana, J. *Angew. Chem. Int. Ed.* 1994, *33*, 2106.
(18)   Rosokha, S. V.; Sun, D.-L.; Kochi, J. K. *J. Phys. Chem. A* 2002, *106*, 2283.
(19)   Lindeman, S. V.; Rosokha, S. V.; Sun, D.; Kochi, J. K. *J. Am. Chem. Soc.* 2002, *124*, 843.
(20)   Nelsen, S. F.; Chang, H.; Wolff, J. J.; Adamus, J. J. *J. Am. Chem. Soc.* 1993, *115*, 12276.
(21)   Nelsen, S. F.; Ismagilov, R. F.; Powell, D. R. *J. Am. Chem. Soc.* 1996, *118*, 6313.
(22)   Bonvoisin, J.; Launay, J.-P.; Auweraer, M. V. d.; Schryver, F. C. D. *J. Phys. Chem.* 1994, *98*, 5052.
(23)   Bonvoisin, J.; Launay, J.-P.; Verbouwe, W.; Auweraer, M. V. d.; Schryver, F. C. D. *J. Phys. Chem.* 1996, *100*, 17097.
(24)   Lambert, C.; Nöll, G.; Schelter, J. *Nature Mater.* 2002, *1*, 69-73.
(25)   Lambert, C.; Noll, G. *Angew. Chem. Int. Ed.* 1998, *37*, 2107-2110.
(26)   Lambert, C.; Nöll, G. *J. Am. Chem. Soc.* 1999, *1999*, 8434-8442.
(27)   Barlow, S.; Risko, C.; Chung, S.-J.; Tucker, N. M.; Coropceanu, V.; Jones, S. C.; Levi, Z.; Brédas, J. L.; Marder, S. R. *J. Am. Chem. Soc.* 2005, *127*, 16900-16911.
(28)   Barlow, S.; Risko, C.; Coropceanu, V.; Tucker, N. M.; Jones, S. C.; Levi, Z.; Khrustalev, V. N.; Antipin, M. Y.; Kinnibrugh, T. L.; Timofeeva, T.; Marder, S. R.; Brédas, J. L. *Chem. Commun.* 2005, 764-766.
(29)   Nöll, G.; Avola, M. *J. Phys. Org. Chem.* 2006, *19*, 238-241.
(30)   Lambert, C.; Risko, C.; Coropceanu, V.; Schelter, J.; Amthor, S.; Gruhn, N. E.; Durivage, J. C.; Brédas, J. L. *J. Am. Chem. Soc.* 2005, *127*, 8508-8516.
(31)   Jones, S. C.; Coropceanu, V.; Barlow, S.; Kinnibrugh, T.; Timofeeva, T.; Brédas, J.-L.; Marder, S. R. *J. Am. Chem. Soc.* 2004, *126*, 11782-11783.

(32)   Mabad, B.; Tuchagues, J.-P.; Hwang, Y.-T.; Hendrickson, D. N. *J. Am. Chem. Soc.* 1985, *107*, 2801-2.

(33)   Wedlock, D. J.; Bradshaw, F.; Phillips, G. O. *Int. J. Biol. Macromol.* 1981, *3*, 275-277.

(34)   Root, D. E.; Henson, M. J.; Machonkin, T.; Mukherjee, P.; Stack, T. D. P.; Solomon, D. I. *J. Am. Chem. Soc.* 1998, *120*, 4982-4990.

(35)   Bominaar, E. L.; Borshch, S. A.; Girerd, J.-J. *J. Am. Chem. Soc.* 1994, *116*, 5362-5372.

(36)   Kido, J.; Kimura, M.; Hagai, K. *Science* 1995, *267*, 1332.

(37)   Nelsen, S. F.; Ismagilov, R. F.; II, D. A. T. *Science* 1997, *289*, 846.

(38)   Nelsen, S. F.; Ismagilov, R. F.; Powell, D. R. *J. Am. Chem. Soc.* 1998, *119*, 10213.

(39)   Nelsen, S. F.; Ismagilov, R. F.; Powell, D. R. *J. Am. Chem. Soc.* 1998, *120*, 1924.

(40)   Elliott, C. M.; Derr, D. L.; Matyushov, D. V.; Newton, M. D. *J. Am. Chem. Soc* 1998, *120*, 11714.

(41)   Gladstone, S.; Laider, K.; Eyring, H. *The Theory of Rate Processes* 1941, *McGraw-Hill, New York.*

(42)   Kramers, H. A. *Physicia* 1940, *7*, 284.

(43)   Marcus, R. A. *J. Chem. Phys.* 1956, *24*, 966.

(44)   Marcus, R. A. *J. Chem. Phys.* 1956, *24*, 979.

(45)   Marcus, R. A. *Can. J. Chem.* 1959, *37*, 155.

(46)   Robin, M. B.; Day, P. *Adv. Inorg. Chem. Radiochem.* 1967, *10*, 247-422.

(47)   Hush, N. S. *Prog. Inorg. Chem.* 1967, *8*, 391-444.

(48)   Evans, D. H.; O'Connell, K. M.; Peterson, R. A.; Kelly, M. J. *J. Chem. Educ.* 1983, *60*, 290-293.

(49)   Kissinger, P. T.; Heineman, W. R. *J. Chem. Educ.* 1983, *60*, 702-706.

(50)   Sutton, J. E.; Taube, H. *Inorg. Chem.* 1981, *20*, 3125.

(51)   Barriere, F.; Camire, N.; Geiger, W. E.; Mueller-Westerhoff, U. T.; Sanders, R. *J. Am. Chem. Soc.* 2002, *124*, 7262 -7263.

(52)   Astruc, D. *Acc. Chem. Res.* 1997, *30*, 383.

(53)   Mabbot, G. A. *J. Chem. Educ.* 1983, *60*, 702-706.

(54)   D'Alessandro, D. M.; Keene, F. R. *Dalton Trans.* 2004, 3950-3954.

(55)   Hush, N. S. *Electrochim. Acta.* 1968, *13*, 1005.

(56)   Creutz, C. *Prog. Inorg. Chem.* 1983, *30*, 1.

(57)   Kaim, W.; Bruns, W.; Poppe, J.; Kasack, V. *J. Mol. Struct.* 1993, *292*, 221.

(58)   Richardson, D. E.; Taube, H. *Coord. Chem. Rev.* 1984, *60*, 107.

(59)   Crutchley, R. J. *Inorg. Chem.* 1994, *41*, 273.

(60)   Ward, M. D. *Chem. Soc. Rev.* 1995, *24*, 121.

(61)   Sun, D.-L.; Rosokha, S. V.; Lindeman, S. V.; Kochi, J. K. *J. Am. Chem. Soc.* 2003, *125*, 15950-15963.

(62)   Hirao, Y.; Urabe, M.; Ito, A.; Tanaka, K. *Angew. Chem. Int. Ed.* 2007, *36*, 3300-3303.

(63)   Ranganathan, S.; Murray, R. W. *J. Phys. Chem. B* 2004, *108*, 19982-19989.

(64)   Grevels, F.-W.; Kerpen, K.; Klotzbucher, W. E.; McClurg, R. E.; Russel, G.; Viotte, M.; Schaffner, K. *J. Am. Chem. Soc.* 1998, *120*, 10423.

(65)   Ito, T.; Hamaguchi, T.; Nagino, H.; Yamaguchi, T.; Washington, J.; Kubiak, C. P. *Science* 1997, *277*, 660-663.

(66)   Furholz, U.; Burgi, H. A.; Wagner, F. E.; Stebler, A.; Ammeter, J. H.; Krausz, E.; Clark, R. J. H.; Stead, M. J.; Ludi, A. *J. Am. Chem. Soc.* 1984, *106*, 121.

(67)   Furholz, U.; Joss, S.; Burgi, H. A.; Ludi, A. *Inorg. Chem.* 1985, *24*, 9143.

(68)   Myers, A. B. *Chem. Phys.* 1994, *180*, 215.

(69)   Heller, E. J. *Acc. Chem. Res.* 1981, *14*, 368.

(70)   Oh, S. M.; Wilson, S. R.; Hendrickson, D. N.; Woehler, S. E.; Wittebort, R. J.; Inniss, D.; Strouse, C. E. *J. Am. Chem. Soc.* 1987, *109*, 1073.

(71)   Sorai, M.; Hendrickson, D. N. *Pure Appl. Chem.* 1991, *63*, 1503.

(72)   Dong, T.-Y.; Hendrickson, D. N.; Iwai, K.; Cohn, M. J.; Geib, S. J.; Rheingold, A. L.; Sano, H.; Motoyama, I.; Nakashima, S. *J. Am. Chem. Soc* 1985, *107*, 7996-8008.

(73)   Dong, T.-Y.; Hendrickson, D. N.; Pierpont, C. G.; Moore, M. F. *J. Am. Chem. Soc.* 1986, *108*, 963-971.

(74)   Smart, J. C.; Pinksy, B. L. *J. Am. Chem. Soc.* 1980, *103*, 1009-1015.

(75)   Kramer, J. A.; Hendrickson, D. N. *Inorg. Chem.* 1980, *19*, 3330-3337.

(76)   Stebler, A.; Ammeter, J. H.; Furholz, U.; Ludi, A. *Inorg. Chem.* 1984, *23*, 2764.

(77)   Beattie, J. K.; Hush, N. S.; Taylor, P. R. *Inorg. Chem.* 1976, *15*, 992.

(78)   Che, C.-M.; Lam, H.-W.; Tong, W.-F.; Lai, T.-F.; Lau, T.-C. *Chem. Commun.* 1989, 1883.

(79)   Oh, D. H.; Sano, M.; Boxer, S. G. *J. Am. Chem. Soc.* 1991, *113*, 6880-6890.

(80)   Bublitz, G. U.; Laidlaw, W. M.; Denning, R. G.; Boxer, S. G. *J. Am. Chem. Soc.* 1998, *120*, 6068.

(81)   Karki, L.; Lu, H. P.; Hupp, J. T. *J. Phys. Chem.* 1996, *100*, 15637.

(82)   Treynor, T. P.; Boxer, S. G. *J. Phys. Chem. A* 2004, *108*, 1764-1778.

(83)   Demadis, K. D.; Hartshorn, C. M.; Meyer, T. J. *Chem. Rev.* 2001, *101*, 2655-2685.

(84)   Richardson, D. E.; Taube, H. *Inorg. Chem.* 1981, *20*, 1278.

(85)   Ward, M. D. *Inorg. Chem.* 1996, *35*, 1712-1714.

(86)   Barriere, F.; Camire, N.; Geiger, W. E.; Mueller-Westerhoff, U. T.; Sanders, R. *J. Am. Chem. Soc.* 2002, *124*, 7262-7263.

(87)   Rovira, C.; Ruiz-Molina, D.; Elsner, O.; Vidal-Gancedo, J.; Bonvoisin, J.; Launay, J. P.; Veciana, J. *Chem. Eur. J.* 2001, *7*, 240.

(88)   Cave, R. J. *Chem. Phys. Lett* 1996, *249*, 15.

(89)   Jones, S. C.; Barlow, S.; O'Hare, D. *Chem. Eur. J.* 2005, *11*, 4473-4481.

(90)   Salsman, J. C.; Ronco, S.; Londergan, C. H.; Kubiak, C. P. *Inorg. Chem.* 2006, *45*, 547-554.

(91)   Sandstrom, J. *Dynamic NMR Spectroscopy* 1982, Academic Press, New York.

(92)   Wu, R.; Koske, S. K. A.; White, R. P.; Anson, C. E.; Jayasooriya, U. A.; Cannon, R. D. *J. Chem. Soc. Chem. Commun.* 1994, 1657.

(93)   Jones, S. C.; Hascall, T.; Barlow, S.; O'Hare, D. *J. Am. Chem. Soc.* 2002, *124*, 11610-11611.

(94)   Roder, J. C.; Meyer, F.; Hyla-Kryspin, I.; Winter, R. F.; Kaifer, E. *Chem. Eur. J.* 2003, *9*, 2636-2648.

(95)   Gagne, R. R.; Koval, C. A.; Smith, T. J.; Cimlino, M. C. *J. Am. Chem. Soc.* 1979, *101*, 4571-4580.

(96)   Coropceanu, V.; Gruhn, N. E.; Barlow, S.; Lambert, C.; Durivage, J. C.; Bill, T. G.; Nöll, G.; Marder, S. R.; Brédas, J.-L. *J. Am. Chem. Soc*. 2004, *126*, 2727-2731.

(97)   Spreer, L. O.; Allan, C. B.; MacQueen, D. B.; Otvos, J. W.; Calvin, M. *J. Am. Chem. Soc*. 1994, *116*, 2187.

(98)   Kaim, W.; Kasack, V.; Binder, H.; Roth, E.; Jordanov, J. *Angew. Chem. Int. Ed*. 1988, *27*, 1174.

(99)   Kasack, V.; Kaim, W.; Binder, H.; Jordonav, J.; Roth, E. *Inorg. Chem*. 1995, *34*, 1924.

(100)   Lay, P. A.; Magnuson, R. H.; Sen, J.; Taube, H. *J. Am. Chem. Soc*. 1982, *104*, 7658.

(101)   Hush, N. S. *Chem. Phys*. 1975, *10*, 361.

(102)   Citrin, P. H.; Ginsberg, A. P. *J. Am. Chem. Soc* 1981, *103*, 3673.

(103)   Launay, J. P. *Chem. Soc. Rev*. 2001, *30*, 386.

(104)   Demadis, K. D.; Hartshorn, C. M.; Meyer, T. M. *Chem. Rev*. 2001, *101*, 2655.

(105)   Brunschwig, B. S.; Creutz, C.; Sutin, N. *Chem. Soc. Rev*. 2002, *31*, 168.

(106)   Low, P. J.; Paterson, M. A. J.; Puschmann, H.; Goeta, A. E.; Howard, J. A. K.; Lambert, C.; Cherryman, J. C.; Tackley, D. R.; Leeming, S.; Brown, B. *Chem. Eur. J*. 2004, *10*, 83-91.

(107)   Lambert, C.; Amthor, S.; Schelter, J. *J. Phys. Chem. A* 2004, *108*, 6474-6486.

(108)   Coropceanu, V.; Malagoli, M.; Andre, J. M.; Brédas, J. L. *J. Chem. Phys*. 2001, *115*, 10409.

(109)   Barlow, S.; Zheng, S.; Beverina, L.; Marder, S. R. *Unpublished Work*.

(110)   Rohde, D.; Dunsch, L.; Tabet, A.; Hartmann, H.; Fabian, J. *J. Phys. Chem. B*. 2006, *110*, 8223-8231.

(111)   Casado, J.; Ruiz Delgado, M. C.; Shirota, Y.; López, V. H.; Navarrete, J. T. *J. Phys. Chem. B* 2003, *107*, 2637-2644.

(112)   Bonvoisin, J.; Launay, J.-P.; Auweraer, M. V. d.; Schryver, F. C. D. *J. Phys. Chem*. 1994, *98*, 5052-5057.

(113)   Stickley, K. R.; Blackstock, S. C. *J. Am. Chem. Soc*. 1994, *116*, 11576-11577.

CHAPTER 2

A COMPARISON OF 2,2'-BITHIOPHENE, DITHIENO[3,2-b:2,3-d]THIOPHENE

AND DITHIENO[3,2-b:2,3-d]PYRROLE AS ELECTRON DONORS

2.1. Introduction

This chapter focuses on the properties of 2,2'-bithiophene, dithieno[3,2-*b*;2,3-*d*]thiophene, and dithieno[3,2-*b*;2,3-*d*]pyrrole derivatives, including dialkyl- and bis(5-alkylthien-2-yl)-substituted derivatives. Properties of the neutral compounds were investigated including UV-visible absorption spectroscopy, fluorescence spectroscopy, and cyclic voltammetry (CV). Additionally, monocations of the derivatives were generated and were analyzed by visible-NIR absorption and electron paramagnetic resonance (EPR) spectroscopies.

2.1.1 Applications of Oligothiophene Derivatives

Thiophene has been incorporated into many small molecule and polymer derivatives as materials for use as organic semiconductors.[1-6] The simplest oligothiophene is 2,2'-bithiophene (BIT). Many examples of longer oligothiophenes of defined length have been explored, including up to a 48-mer[7] and 96-mer.[8] Because of their properties, oligothiphenes and their derivatives have been incorporated into several optical and electronic devices. For example, oligothiophenes and poly(3-alkylthiophene)s have been used as hole-transporting semiconductors in organic field effect transistors.[1,2] Polythiophenes have been employed as chemical sensors.[9] Perylene-oligothiophene-perylene triads have been reported for photovoltaic applications. [3]

Oligomeric thiophene-ethynylenes terminated with terminal *p*-phenylisocyanide groups have been reported for use as molecular wires.[4]

2.1.2 Properties of Oligothiophenes

The ideal optical and electronic properties for oligothiophene derivatives vary depending on the application for which an oligothiophene derivative is being used. There are several ways in which oligothiophenes can be modified to change their optical and electronic properties. Increasing the number of repeat units in an oligothiophene lowers the energy of maximum absorption and lowers the oxidation potential, which is relevant to having the appropriate ionization potential (IP) and electron affinity (EA) for incorporation into devices such as organic field-effect transistors, photovoltaics, and light-emitting diodes among others.[7,8] Optical and electronic properties can also be modified by changing the IP and EA of the parent oligothiophene; several derivatives of oligothiophenes have been reported with substitutents at the 3- and 4-positions of the thiophene ring, which have been shown to modify the properties – i.e. the absorption maxima, oxidation potentials, solid-state order – of the parent chromophores.[10-12] Forcing the thiophene rings into planarity by fusing them into an acene-like systems is yet another way of modification of optoelectronic properties: examples include dithieno[3,2-*b*;2,3-*d*]thiophene (DTT)[13] and dithieno[3,2-*b*;2,3-*d*]pyrrole (DTP),[14] which have been reported as fused-ring derivatives of 2,2'-bithiophene (BIT).

It is important to understand how the modification of an oligothiophene – whether by chain length, introduction of substitutents, and flexibility of the thiophene rings with respect to one another – affects the optical and electronic properties of the oligothiophene

derivative so that an oligothiophene with certain desired properties can be designed for a specific application. With a thorough understanding of the basic properties of various oligothiophene derivatives, an appropriate derivative can be designed and/or selected to meet the needs of a given application. BIT (**I**), DTT (**II**), DTP (**III**) (Figure 2.1) have been synthesized and characterized by standard techniques.[15,16] [13,17,18] However, additional insight into the electronic structure and properties of these aromatic moieties will be useful for the rational design of organic compounds for organic electronic applications.
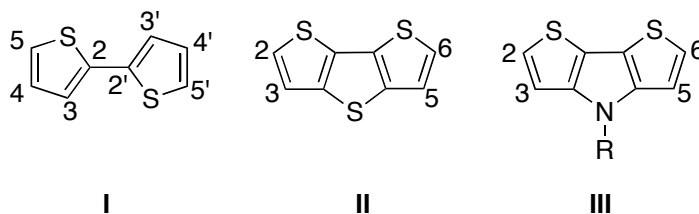
Figure 2.1. BIT (**I**), DTT (**II**) and DTP (**III**), shown with numbering of carbon atoms.

In order to design chromophores for optoelectronic devices that incorporate BIT, DTT, and/or DTP derivatives, it is beneficial to know both the electron-donor strength of each chromophore, which is defined both by their IP, as well as their π-donating abilities, which is also influenced by the strength of coupling to an external π-accepting system, which will depend on position of substitution, i.e, for a disubstitued system, the donor strength of the cores with 2,6-disubstitution could be different from 3,5-disubstitution (or 5,5'- versus 4,4'-disubsstitution in the case of BIT). This chapter focuses on the basic electronic properties of new DTT and DTP derivatives, also in comparison to similar BIT derivatives, in order to determine the influence of the ring fusion and of the specific atoms used to link the ring

systems – where BIT is linked by sulfur or nitrogen – in the oligothiophene dimers and tetramers on their properties.

2.1.3 Reported Properties of BIT, DTT, and DTP

Various optical and electronic properties of **I**, **II**, and **III** have been reported in the literature.[13,15,17,18]   For example, the UV-visible absorption spectra of BIT,[15] DTT,[13] and *N*-functionalized-DTP derivatives[17,18] have been reported. The absorption spectra of **I**, **II**, and **IIIa** (*N*-phenyl-DTP) in dichloromethane are shown below (Figure 2.2). Compared to non-fused BIT, both DTT and *N*-phenyl-DTP exhibit more vibronic structure, which is expected for rigid fused systems compared to their flexible counterparts, as has been shown in previous studies of fused and non-fused oligothiophenes.[19] The blue shift of **II** and **IIIa** compared to **I** is presumably do to a destabilizing of the LUMOS of **II** and **IIIa** due to the central heteroatoms.
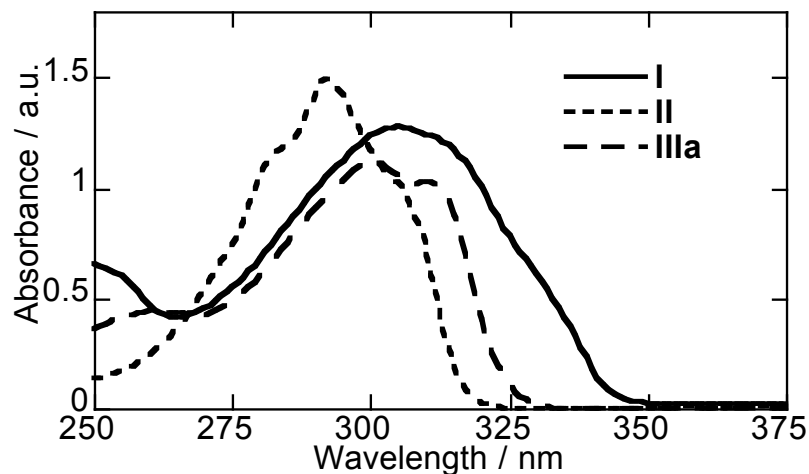
Figure 2.2. UV-visible absorption spectra of **I**, **II**, and **IIIa** in dichloromethane.

CV experiments have been reported for **II** and some *N*-functionalized derivatives of **III**.[16,20-22] However, these simple aromatic molecules were not substituted at their most reactive 2- and 6-positions. These unsubstituted positions lead to the possibility of subsequent reactions upon oxidation in the CV experiments. Specifically, polymerization reaction have been shown to occur at the 2- and 5-positions of 3-alkylthiophenes upon oxidation, either using chemical or electrochemical oxidative conditions.[20-22] In fact, electrochemical polymerizations have been used to obtain polymers of *N*-functionalized derivatives of **III**.[23] Shown below (Figure 2.3) is an example of the irreversible oxidation observed in a CV experiment for *N*-phenyl-DTP (**IIIa**).
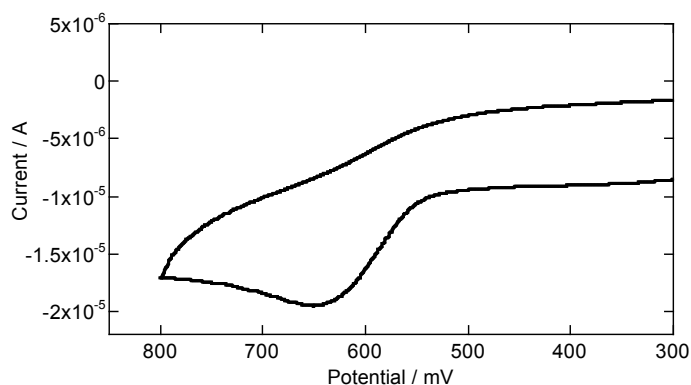
Figure 2.3. Cyclic voltammogram of **IIIa** in 0.1 M Bu$_4$NPF$_6$ in dichloromethane at 50 mV/s.

A reliable oxidation potential cannot be determined from the CV experiment when oxidations are irreversible, such as the one shown above (Figure 2.3). In order to obtain a reliable oxidation (or reduction) potential, it is necessary to observe both the forward and reverse waves of the electron transfer event, then to take the average potential of the forward and reverse peaks. Blocking the presumably most reactive 5,5'-

positions of BIT and the 2- and 6-positions of DTT and *N*-substituted DTP could give rise to reversible oxidations in the CV experiments, because this would block the positions at which the polymerization reactions are presumably occurring.

To determine the oxidation potentials of the DTT and *N*-functionalized-DTP cores, and to compare the values to less complex aromatic moieties such as BIT, it is necessary to have simple derivatives that are functionalized in such a way as to not significantly affect the electronic properties of the aromatic moiety, and which are placed at the reactive positions of the aromatic core so that irreversible chemical reactions do not follow the removal of an electron. To determine the oxidation potentials, and, therefore, a measure of the electron-donating abilities of BIT, DTT, and *N*-functionalized DTP derivatives, the most reasonable targets are 2,6-di(alkyl)-functionalized derivatives (**1–4**, Figure 2.4). In addition to the derivatives functionalized with *n*-butyl (^{n}Bu) groups including DTT (**2**, R = ^{n}Bu) and DTP (**3** and **4**, R = ^{n}Bu) targets, a commercially available 2,2'-bithiophene derivative (**1**, R = *n*-C_6H_{13}) was studied for comparison.
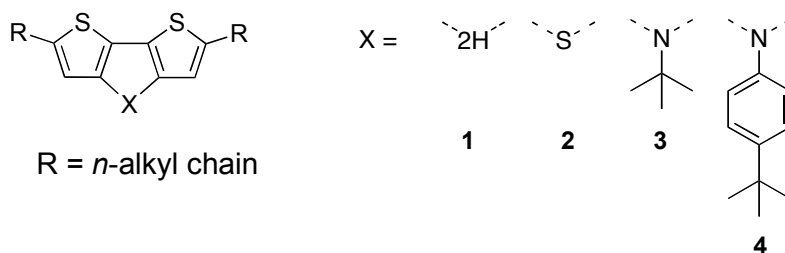
Figure 2.4. 2,6-Di(alkyl)-functionalized BIT, DTT, and DTP derivatives.

In addition to determining the oxidation potentials of simple dialkyl-substituted-BIT, -DTT and -DTP derivatives, it is also of interest to analyze the properties of

derivatives in which conjugation is extended with two additional thiophene rings, leading to oligothiophene tetramers and derivatives thereof. Previous reports of oligothiophene tetramers include quarterthiophene (**IV**), 2,6-bis(3-*n*-hexyl-thien-2-yl)-DTT (**V**)[24] and *N*-(*n*-octyl)-2,6-bis(thien-2-yl)-DTP (**VI**)[25] (Figure 2.5).
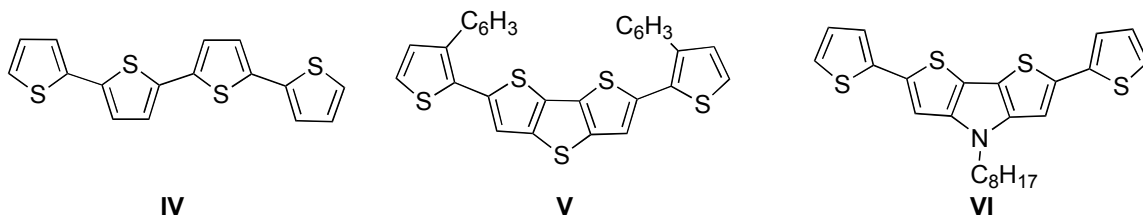
Figure 2.5. Prevoiusly published compounds: quarterthiophene (**IV**), 2,6-bis(3-*n*-hexyl-thien-2-yl)-DTT (**V**),[24] and *N*-(*n*-octyl)-2,6-bis(thien-2-yl)-DTP (**VI**).

Although the authors of the papers describing compounds **V** and **VI** suggested the incorporation of these derivatives into organic electronic devices, no characterization by CV experiments was provided. Additionally, the published derivatives lacked functional groups at the 5-positions of the external thiophene rings, potentially leaving these compounds open to chemical reactions upon oxidation. As a result, new targets were designed in which the 5-positions of the thiophene rings were functionalized with alkyl chains, in this case *n*-heptyl groups (**5–7**, Figure 2.6). *n*-Heptyl groups were chosen because of the convenience of having starting materials with that specific chain length.
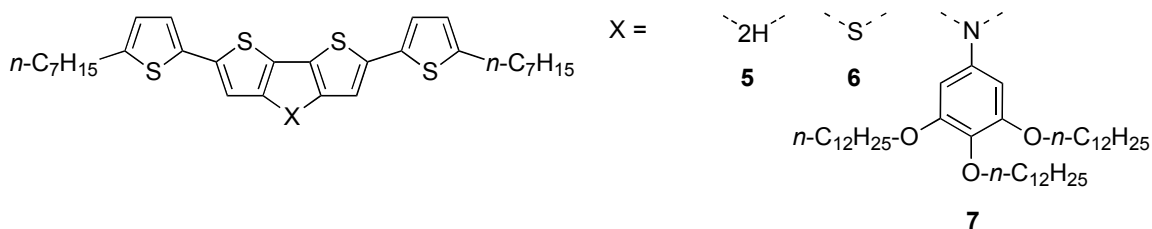
Figure 2.6. 2,6-Bis(5-*n*-heptylthien-2-yl)-BIT (**5**), 2,6-Bis(5-*n*-heptylthien-2-yl)-DTT (**6**), and 2,6-Bis(5-*n*-heptylthien-2-yl)-*N*-(1,3,5-tri(*n*-dodecyloxy)phenyl)DTP (**7**).

The next sections will focus on the synthesis of compounds **2**–**7** and their relevant precursors.

2.2. Synthesis of BIT, DTT, and DTP Derivatives

2.2.1 Previous Reports for the Synthesis of DTT and DTP Derivatives

The synthesis of DTT has been reported by a variety of methods.[13,24,26,27] For this study, the route reported by Holmes *et al*. (Scheme 2.1)[24] was used for the synthesis of DTT. Initially 2,3,4,5-tetrabromothiophene underwent a double halogen-metal exchange reaction at the 2- and 5-positions, and the lithiated species was quenched with 1-formylpiperidine, the aqueous work-up of which gave a 2,5-dialdehyde. Reaction of ethyl-2-mercaptoacetate in basic solution gave a 2,6-diester-functionalized DTT core. Reaction with lithium hydroxide gave the 2,6-dicarboxylic acid, which was decarboxylated in the presence of copper to give DTT (**II**).
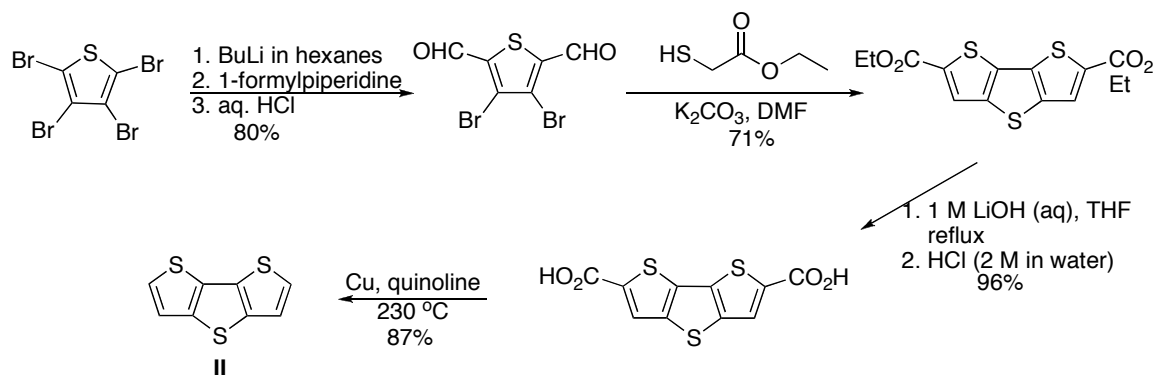
Scheme 2.1. Synthesis of DTT using Holmes' route.[24]

DTP derivatives have been reported by two basic routes. [14,17] The first published route is the palladium-catalyzed amination of 3,3'-bromo-2,2'-bithiophene with a primary amine (Scheme 2.2). This route has the advantage of incorporating the specific amine in the last step of the synthesis, allowing for the synthesis of a variety of *N*-functionalized DTP derivatives using one common intermediate. The initial report using this route described the reaction of 3,3'-dibromo-2,2'-bithiophene with aniline, giving *N*-phenyl-DTP (**IIIa**) in 38% yield over 50 hours.[14] In more recent reports, *n*-alkylamines have been reacted 3,3'-dibromo-2,2'-bithiophene in reasonable yields (65–80%) in palladium-catalyzed reactions.[28]
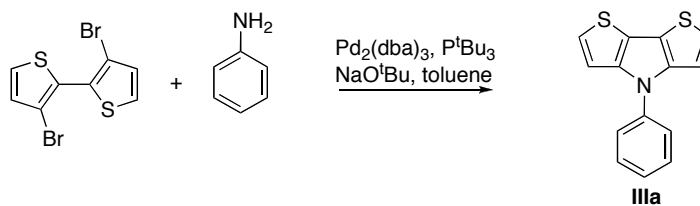
Scheme 2.2. Nozaki's synthesis of *N*-phenyl-DTP.[14]

The second reported route involved the palladium-catalyzed amination of two equivalents of 3-bromothiophene with one equivalent of a primary amine, which was followed

by an *in situ* bromination with *N*-bromosuccinimide (NBS) and a copper-catalyzed carbon-carbon bond-formation (Scheme 2.3).[17] This route requires fewer steps to obtain the *N*-substituted DTP derivative from commercially available materials and gives both *N*-alkyl- and *N*-aryl-substituted DTP derivatives in reasonable yields (65-82%). However, this route has the disadvantage of requiring that each unique DTP derivative be synthesized using the entire synthetic route, because it requires that the specific amine substitutent be incorporated in the first step of the synthesis.
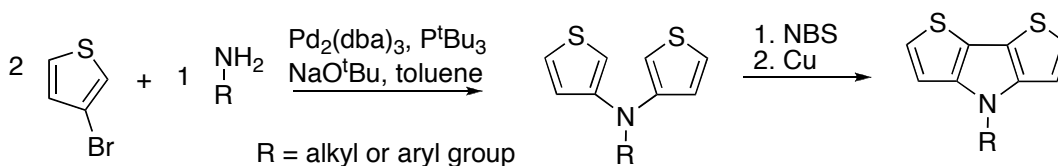
Scheme 2.3. Rasmussen's synthesis of *N*-alkyl- and *N*-aryl-DTP derivatives.[17]

Although the literature yields using Nozaki's route were low, it seemed worthwhile to optimize this reaction (Scheme 2.1) in order to be able to incorporate the amine in the last step, rather than using the second route, which required repetitive synthetic steps to obtain multiple DTP derivatives. For the optimization of the synthesis of *N*-substituted DTP derivatives, 3,3'-dibromo-2,2'-bithiophene[29] and aniline were chosen as the starting materials.

2.2.2 Optimization of the Synthesis of N-Substituted DTP Derivatives

For the synthesis of *N*-substituted-DTP derivatives, the same catalyst, base, and solvent as were reported for first route (Scheme 2.2) were used in the optimization trials

(Scheme 2.4). Conventional heating and microwave irradiation were compared as heating sources to determine if either was advantageous. The only report available at that time gave a 38% yield for *N*-phenyl-DTP when reacted for 50 hours at 80 ºC.[14] Initially the reaction mixture was simply heated to reflux in toluene (boiling point 110 ºC), otherwise under the same conditions, and the reaction was complete within one hour. Additionally, the yields of *N*-functionalized-DTP derivatives were usually good (28-94%). By simply refluxing the reaction mixture, the reaction yield was improved and the reaction time significantly decreased.

Using microwave irradiation sometimes resulted in high yields in short reaction times, but it was difficult to control the progress of the reaction, and often the reaction yield was low due to the formation of dark red or purple byproducts, the analysis of which (by ^{1}H NMR and mass spectrometry) could not be correlated with specific DTP-based chemical structures, such as a homopolymer of the DTP derivative. As a result of the difficulty in controlling the reaction yields conducted under microwave irradiation, further reactions to synthesize *N*-functionalized-DTP derivatives used conventional heating.
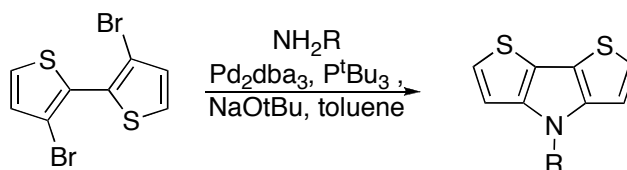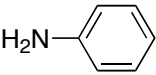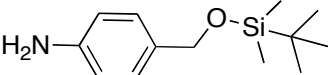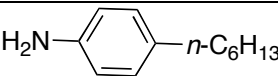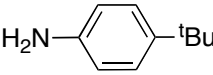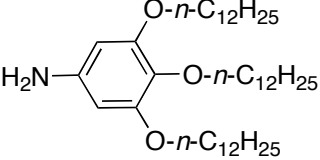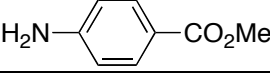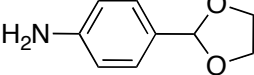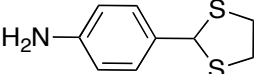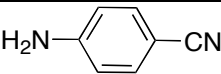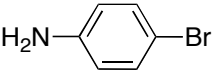
Scheme 2.4. Various substituted aniline derivatives and reactions with 3,3'-dibromo-2,2'-bithiophene.

The outcomes of the attempted syntheses of various *N*-functionalized-DTP derivatives are summarized in Table 2.1. While the reaction with amines bearing some functional groups occurred without difficulty (giving products **IIIb** and **IIIe**), the presence of some other

functional groups resulted in the reaction not leading to the desired product. In one cases decomposition of the starting amine occurred (attempt to synthesize **IIIg**). In another case the presumed homo-polymerization of the primary amine with its functional group (attempt to synthesize **IIIf**, **IIIi**, and **IIIj**) hindered DTP formation. In one case, presumed catalyst poisoning by the functional group (attempt to synthesize **IIIh**) occurred. In the cases of reaction failure due to presumed reaction of the starting aniline derivative with itself, control reactions were conducted in the absence of 3,3'-dibromo-2,2'-bithiophene, and in these reactions, the starting aniline derivative was consumed, supporting the hypothesis of self-polymerization under the amination conditions.

Table 2.1. Result of reaction of various primary amines with 3,3'-dibromo-2,2'-bithiophene.

Product	R-group	Yield of desired product or description of outcome
IIIa[a]	H_2N—⟨benzene⟩	94%
IIIb	H_2N—⟨benzene⟩—O-Si-^tBu	28%
IIIc[a]	H_2N—⟨benzene⟩—n-C_6H_{13}	75%
IIId	H_2N—⟨benzene⟩—^tBu	84%
IIIe	H_2N—⟨benzene⟩ with O-n-$C_{12}H_{25}$, O-n-$C_{12}H_{25}$, O-n-$C_{12}H_{25}$	59%
IIIf	H_2N—⟨benzene⟩—CO_2Me	Amine homo-polymerized with ester[b]
IIIg	H_2N—⟨benzene⟩—⟨dioxolane O,O⟩	Starting amine itself was unstable in ambient conditions, decomposed during reaction
IIIh	H_2N—⟨benzene⟩—⟨dithiolane S,S⟩	Amine failed to react
IIIi	H_2N—⟨benzene⟩—CN	Amine homo-polymerized with cyano group[b]
IIIj	H_2N—⟨benzene⟩—Br	62% was best yield, competition with homo-polymerization limited the yields in most cases[b]
IIIk	H_2N-^tBu	75%

[a] DTP derivative has been previously reported[14,17]
[b] As a control, the reaction was also run without 3,3'-dibromo-2,2'-bithiophene.

2.2.3 Synthesis of 2,6-Dialkylated-DTT and –DTP Derivatives

Alkylation of DTT and DTP may provide derivatives that have reversible oxidations in CV experiments, due to blocking the presumably most reactive position in these aromatic moieties. Many examples have been reported for the alkylation of thiophene derivatives at the 2-position by lithiation with n-butyllithium, followed by quenching with an alkylhalide.[30,31] Similarly, to obtain the 2,6-dialkylated derivatives of DTT (**2**) and DTP (**3** and **4**), the parent compound was doubly lithiated, then reacted with 1-iodobutane (Scheme 2.5). The crude product, which was often a mixture of the dialkylated and monoalkylated species as well as the starting material, were purified using column chromatography, recrystallization, and/or bulb-to-bulb distillation under vacuum.
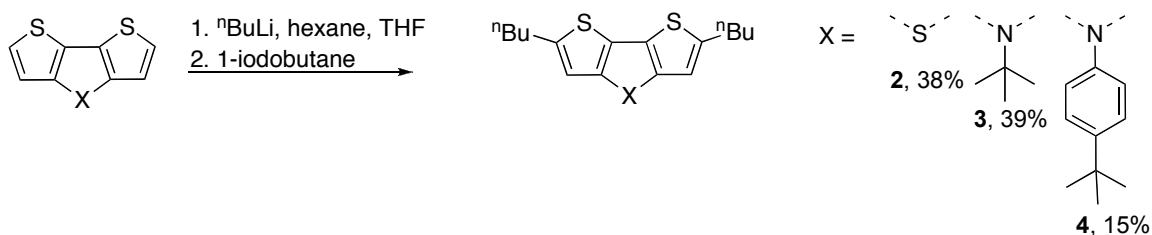
Scheme 2.5. Synthesis of the 2,6-di(n-butyl)-DTT (**2**), N-($tert$-butyl)-2,6-di(n-butyl)-DTP (**3**), and N-(4-$tert$-butylphenyl)-2,6-di(n-butyl)-DTP (**4**).

2.2.4 Synthesis of Bis(alkylthien-2-yl)-BIT, -DTT, and –DTP

The bis(5-alkylthien-2-yl)-substituted derivatives were synthesized using palladium-catalyzed Stille reactions[32] from the dibromo- or diiodo-substituted derivative of the core with 2-n-heptyl-5-[tri(n-butyl)stannyl]thiophene. The halogenated cores were obtained by reaction with NBS or N-iodosuccinimde (NIS) (Scheme 2.8). The

bromination of DTT has been reported with NBS in DMF,[33] although in this case, a combination of acetic acid and chloroform was used as the solvent instead of DMF. Similarly, whether the *N*-position of the DTP housed an aryl or tertiary alkyl group, the DTP derivative was brominated with NBS selectively at the 2- and 6-positions without brominating the *N*-substituent. However, when the *N*-substituent is an *n*-alkyl chain, bromination with NBS results in decomposition of the DTP moiety, as determined by monitoring with TLC, GCMS, and ^{1}H NMR spectroscopy.
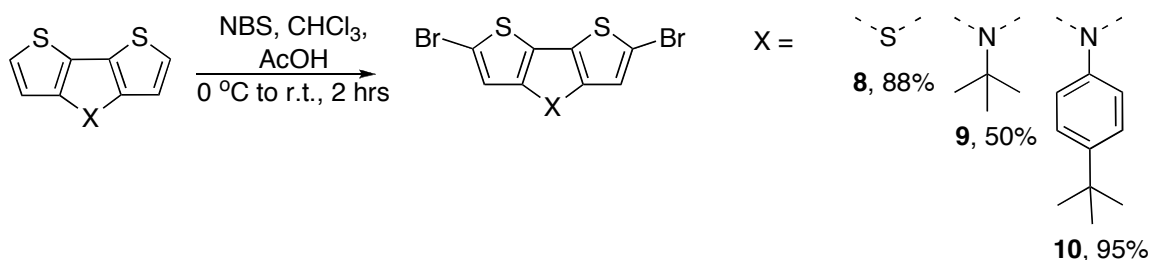
Scheme 2.6. Bromination of DTT and *N*-functionalized DTP derivatives with NBS.

Iodination of DTT and *N*-functionalized DTP was accomplished by reaction with NIS in chloroform/acetic acid (Scheme 2.9). For DTT and *N*-aryl-DTP derivatives, the iodination proceeded in high yields. For *N*-(*n*-alkyl)-substituted-DTP derivatives, however – as was the case in bromination reactions with NBS – the reactions resulted in decomposition of the DTP starting material and desired products, as monitored by TLC and GCMS. In this case, the reaction has not been tested with a tertiary alkyl group at the *N*-position of DTP.
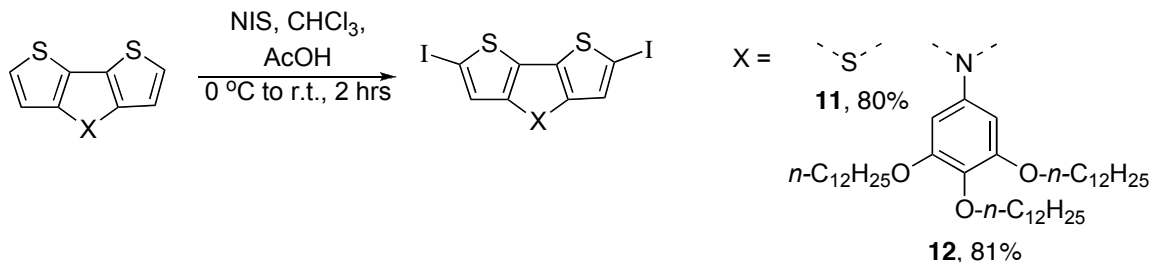
Scheme 2.7. Iodination of DTT and an *N*-[1,3,5-tri(*n*-dodecyloxy)]DTP with NIS.

In order to characterize the properties of BIT, DTT, and DTP derivatives with extended conjugation, 2,6-bis(*n*-heptylthien-2-yl)substituted derivatives were designed as simple derivatives with substitutents at the most reactive positions of the external thiophene rings. These derivatives of quarterthiophene were synthesized by palladium-catalyzed Stille coupling reactions, reacting the 5,5'-dibromo-BIT, 2,6-dibromo-DTT, or the 2,6-diiodide of the DTP derivative with 2-*n*-heptyl-5-(tri(*n*-butyl)stannyl)thiophene. All compounds were isolated as bright yellow solids. The DTT- and DTP-based derivatives were heated under microwave irradiation for 5 minutes at 80 W, while the BIT-based derivative was allowed to react at room temperature for two hours, giving yields from 29–66%.
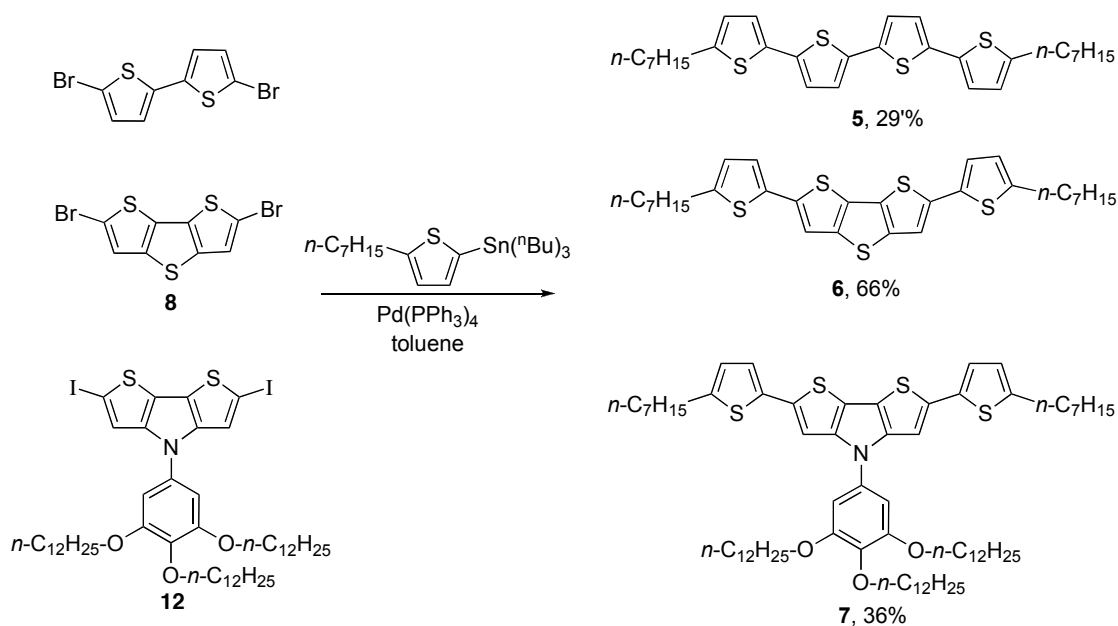
Scheme 2.8. Synthesis of bis(5-*n*-heptylthien-2-yl)-BIT (**5**), -DTT (**6**) and -*N*-(3,4,5-tri(*n*-dodecyloxy)phenyl)DTP (**7**).

The next sections describe the characterization of compounds **1**-**7**. Characterization of the neutral compounds includes CV and UV-visible absorption spectra. Characterization of the monocations includes visible-NIR absorption and EPR spectra.
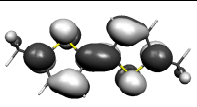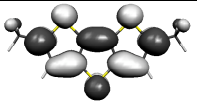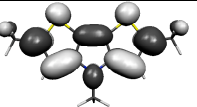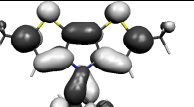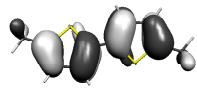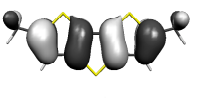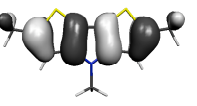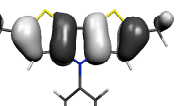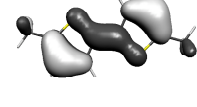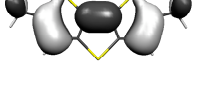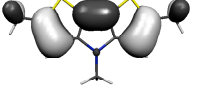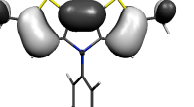
2.3 Characterization of the Properties of BIT, DTT, and DTP Derivatives

2.3.1. Molecular Orbital Pictures for BIT, DTT, and DTP Derivatives

To better understand the properties reported in later sections, the molecular orbitals were calculated for versions of compounds **1**–**7** in which the alkyl chains were replaced with methyl groups. In all cases, the geometries were minimized before calculating orbital structure and energies. In the case of the BIT derivatives, this lack of restriction on the dihedral angle yielded a geometry minima with the central thiophene

rings facing opposite directions. The orbitals shown below include the highest occupied molecular orbital (HOMO), lowest unoccupied molecular orbital (LUMO), and HOMO-1. In addition to the molecular orbital pictures, energies for these orbitals were also calculated, which are relevant to CV experiments and to the optical gap determined by the energy of the intersection of UV-visible absorption and emission spectra. Also, the calculation of the transition energies with relevant orbitals and of the transition dipole moments, which were calculated using TD-DFT, is relevant in predicting which orbitals give rise to transitions in the UV-visible absorption spectra in the neutral molecules and in the monocations. The HOMO-1, HOMO, and LUMO pictures for versions of compounds **1**, **2**, **3**, and **4** with methyl groups replacing the alkyl chains are shown in Table 2.2. The HOMOs can be regarded as out-of-phase combinations of two thiophene HOMOs and are consistent with the pattern of single and double bonds implied by valence-bond representations of the structures. The LUMOs are similar to an in-phase pair of thiophene LUMOs with an out-of-phase contribution from the bridging heteroatoms. The origin of the HOMO-1 orbitals is less clear but have some relation to in-phase combinations of two thiophene HOMOs. The molecular orbital pictures for the SOMOs of the monocations (not shown) are similar to those computed for the HOMO of the neutral compounds.
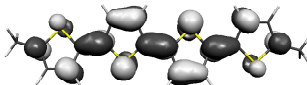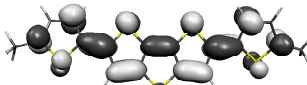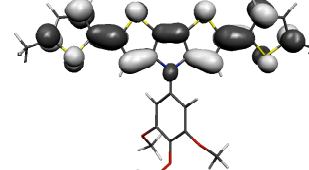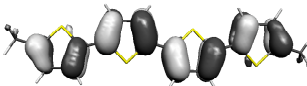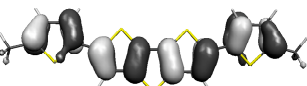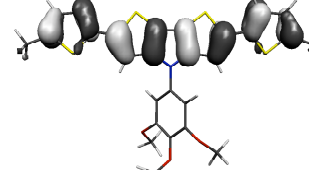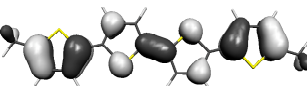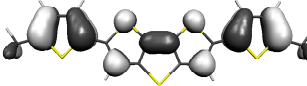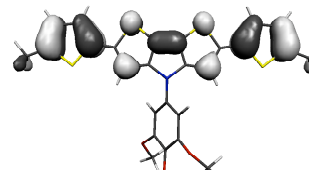
Table 2.2. HOMO-1s, HOMOs and LUMOs **1**, **2**, **3**, and **4** from gas-phase DFT calculations.

	1	**2**	**3**	**4**
LUMO				
HOMO				
HOMO-1				

The HOMO-1, HOMO, and LUMO for methyl versions of bis(5-alkylthien-2-yl) derivatives **5**, **6**, and **7** are shown in Table 2.3. As was the case for the dialkylated derivatives, the HOMOs are again consistent with the pattern of single and double bonds implied by valence-bond representations of the structures, and essentially appear to be the in-phase combination of four thiophene HOMOs. The BIT, DTT, and DTP cores of the LUMOs are very similar to those observed for the LUMOs of **1**–**4**, with outer thiophene rings in an out-of-phase combination with the cores. The cores of the HOMO-1 orbitals have essentially the same character as is observed in the HOMO-1 orbitals of **1**–**4**, with in-phase orbitals of the HOMOs of two thiophene rings. As was the case in compounds **3**

and **4**, in compound **7**, there is also little orbital density at nitrogen and the aryl group in the HOMO and HOMO-1.

Table 2.3.   HOMO-1s, HOMOs and LUMOs for **5**, **6**, and **7** from gas-phase DFT calculations.

	5	6	7
LUMO			
HOMO			
HOMO-1			

The calculated energies for the HOMO-1s, HOMOs, and LUMOs for the methyl versions of compounds **1**–**7** are shown in Figure 2.7. When each dialkylated derivative is compared to its relevant bis(5-alkylthien-2-yl) derivative, (**1** to **5**, **2** to **6**, and **3** & **4** to **7**), one can see that the bis(5alkylthien-2-yl)-substituted derivative has a higher HOMO energy and a lower LUMO energy than its dialkylated equivalent. This drop in HOMO-LUMO gap is consistent with the increase in conjugation length in the bis(5-alkylthien-2-yl) derivatives in comparison to the dialkylated derivatives. From the HOMO energies determined from the calculations, it is expected that the DTP derivatives (**3**, **4**, and **7**) should be the easiest to oxidize for each set of compounds.
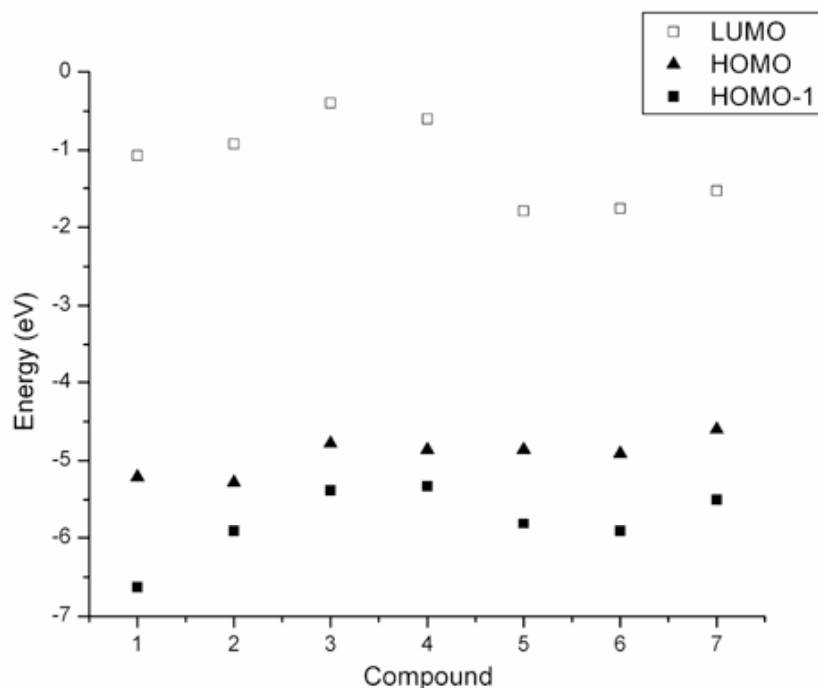
Figure 2.7. HOMO-1, HOMO, and LUMO energies calculated in the gas phase DFT calculations for versions of compounds **1–7** in which the alkyl chains were replaced with methyl groups.

When comparing BIT derivatives to DTT derivatives, the energy gap is larger in the case of DTT derivatives, with the HOMO being lower energy and the LUMO being higher energy for DTT than for BIT. One would expect that the incorporation of the additional sulfur atom in DTT would result in a stabilization of the orbitals due to the σ-electron withdrawing effects of the electronegative atom, which should lower the energies of the HOMO and LUMO of DTT relative to BIT. In the LUMO of DTT, however, there is significant molecular orbital density on sulfur, so in this case, the π-donation can raise the energy of the orbital more than the σ-electron withdrawing stabilizes it. An additional factor to take into account would be the dihedral angle of the two outer thiophene rings, which freely rotate in BIT and are fused in DTT. The

74

calculation used the minimum energy geometry for BIT, so the this question is currently unanswered. If the same calculations were performed on a BIT geometry where the rings were locked in the same plane with a C2V-type symmetery, calculations based on this geometry could better answer the question of how ring geometry affects the orbital energies.

2.3.2 Cyclic Voltammetry of the BIT, DTT, and DTP Derivatives

CV experiments were performed on compounds **1–4** in order to determine their half-wave potentials for oxidation and, therefore, which correlates with the electron-donor strengths. All CV experiments were run in 0.1 M $^{n}Bu_4NPF_6$ in dichloromethane using ferrocenium / ferrocene ($Cp_2Fe^{+/0}$ at 0 V) or decamethylferrocenium / decamethylferrocene ($Cp_2Fe^{+/0}$, at -0.55 V versus $Cp_2Fe^{+/0}$) as an internal reference, referencing the potentials to $Cp_2Fe^{+/0}$. All CV experiments were run at scan rates of 50 mV/s.

The cyclic voltammograms of compounds **1–4** are shown in Figure 2.8. For the oxidations of **1** and **2**, the ratios of the current of the reverse and forward waves (I_{red}/I_{ox}), were ca. 0.2 and 0.3, respectively, indicative of an electrochemical-type process, which gives the irreversible character to the oxidation. The cyclic voltammograms of **3** and **4** have I_{red}/I_{ox} values of ca. 1, indicating reversible oxidations. Of the dialkylated derivatives, compounds **1** and **2** were oxidized at similar energies. As expected from the DFT calculations of the HOMO energies, both **3** and **4** were easier to oxidize than **1** and **2**, with **3** being slightly easier to oxidize than **4**.
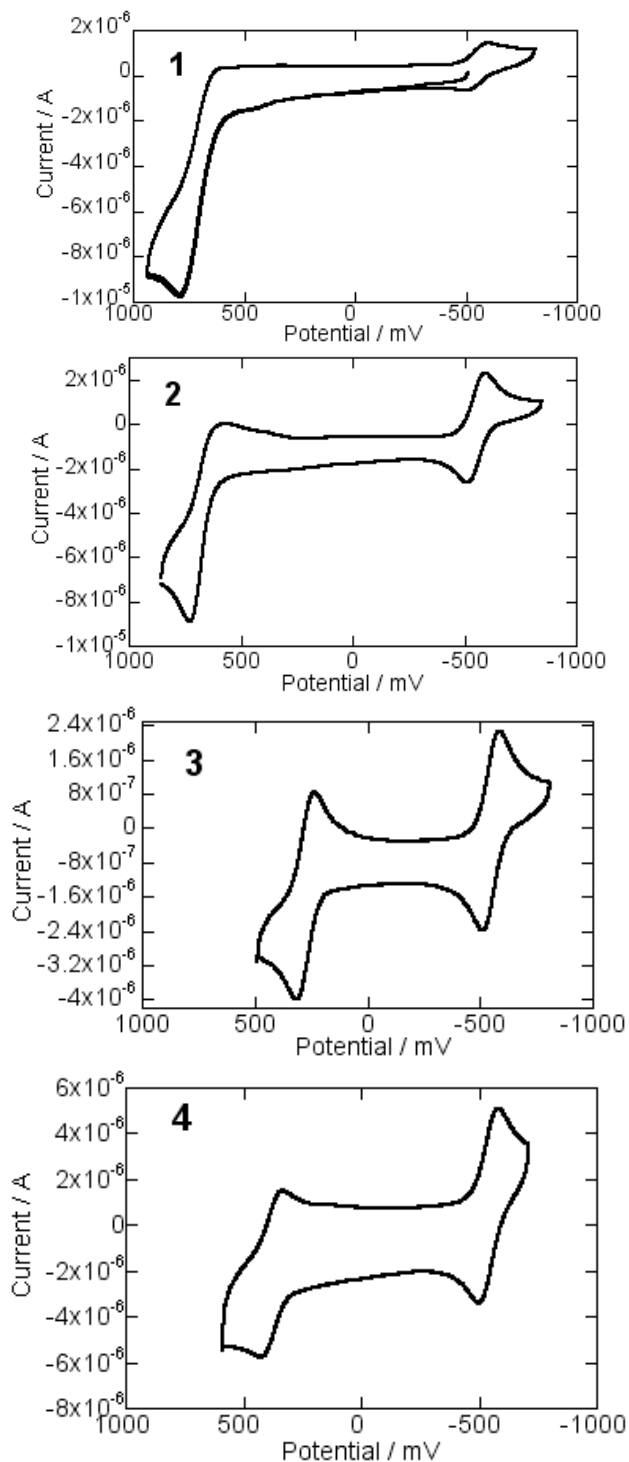
Figure 2.8. Cyclic voltammograms for compounds **1–4** in 0.1 M ^{n}Bu$_4$NPF$_6$ in dichloromethane, all shown with Cp*$_2$Fe$^{+/0}$ at –0.55 V as an internal reference, potentials referenced to Cp$_2$Fe$^{+/0}$ at 0 V.

The half-wave [oxidation] potentials of **1**–**4** and related derivatives are summarized in Table 2.4. The half-wave potentials for compounds **1** and **2** are not as reliable as the potentials for compounds **3** and **4** because of the irreversibility of the oxidations for **1** and **2**.

Table 2.4. Half-wave potentials ($E_{1/2}^{+/0}$, V) of compounds **1**–**4** in 0.1 M $^nBu_4NPF_6$ in dichloromethane, referenced to $Cp_2Fe^{+/0}$ at 0 V.

Compound	$E_{1/2}^{+/0}$ / V
1	0.69
2	0.66
3	0.23
4	0.38

CV experiments were also performed for compounds **5**–**7**. The cyclic voltammograms for compounds **5**–**7** are shown in Figure 2.9. The CV experiments indicate that compound **7** is the easiest to oxidize of the series, which was expected since the oxidation potentials of the fused aromatic cores have the same trend (**3** and **4** being easier to oxidize than **1** and **2**). As was the case for the dialkylated BIT and DTT derivatives (**1** and **2**), **5** had a similar oxidation potential to that of **6**.
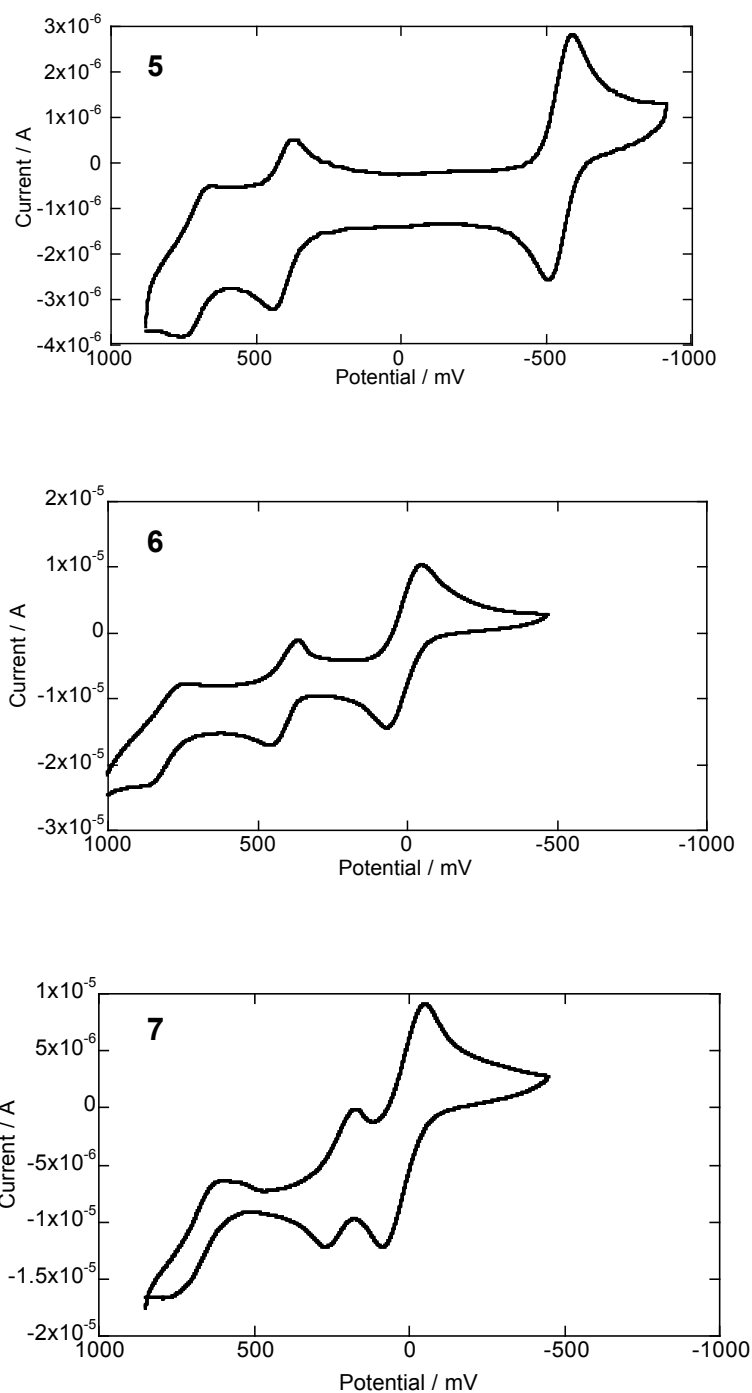
Figure 2.9. Cyclic voltammograms of **5** (top) shown with $Cp^*_2Fe^{+/0}$ as the internal reference at -0.55 V; **6** (middle) and **7** (bottom) both shown with $Cp_2Fe^{+/0}$ as the internal reference, all potentials referenced to $Cp_2Fe^{+/0}$ at 0 V.

A summary of the oxidation potentials of compounds **5–7** is shown in Table 2.5. The separation between the oxidation potentials (ΔE) is the largest in the case of the DTP derivative and smallest for the BIT derivative.

Table 2.5. Half-wave oxidation potentials (V) and separation of first and second oxidation potentials (ΔE) of **5**, **6**, and **7** in 0.1 M Bu_4NPF_6 in dichloromethane, referenced to $Cp_2Fe^{+/0}$ at 0 V.

Compound	$E_{1/2}^{2+/}$ / V	$E_{1/2}^{+/0}$ / V	ΔE / V
5	0.71	0.47	0.24
6	0.79	0.40	0.39
7	0.68	0.20	0.48

The values computed for the energies of the HOMOs of the compounds **5–7** correlate with energies of the first oxidation potentials (Figure 2.10). In each series of compounds (**1–4** and **5–7**), there is a correlation with the calculated HOMO energies and the first oxidation potential.
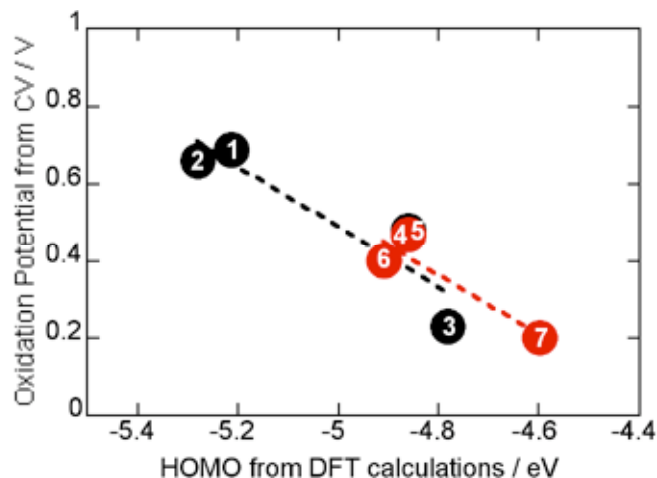
Figure 2.10. Half-wave oxidation potentials from CV experiment versus HOMO energies from DFT calculations for compounds **1**–**7**.

2.3.3 UV-Visible Absorption Spectra of BIT, DTT, and DTP Derivatives

UV-visible absorption spectra of compounds **1**–**4** were recorded in dichloromethane (Figure 2.11). All of the cores have similar energies of absorption maxima, although the fused-ring systems have more vibronic structure than does the BIT system (**1**). This is consistent with the increased vibrational freedom in **1**, which doesn't have the central atom (sulfur or nitrogen) locking the rings in a more planar conformation as is the case for **2**, **3**, and **4**. These results are also consistent with previous studies of the absorption spectra of fused and non-fused oligothiophenes.[19]
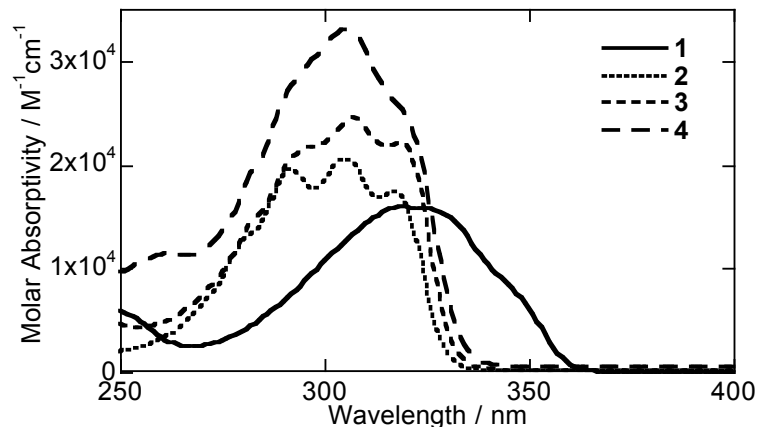
Figure 2.11. UV-visible absorption spectra of compounds **1–4** in dichloromethane.

UV-visible absorption spectra of compounds **5–7** were recorded in dichloromethane (Figure 2.12).   The absorption spectrum of **5** is less intense and has less vibronic structure than that of **6** and **7**; this is not surprising because the central ring system in **5** is not fused. The absorption spectra of **6** and **7** are nearly identically shaped spectra and extinction coefficients are on the same order of magnitude; the wavelengths of maximum absorption of **6** and **7** are few nanometers apart. The absorption maxima of compounds **5** and **7** are red-shifted compared to related quarterthiophene (**IV**) and 2,6-*N*-(*n*-octyl)bis(thien-2-yl)DTP (**VI**),[25] consistent with the dialkyl-substitution in **5** and **7**. The absorption spectrum of 2,6-bis(3-*n*-hexylthien-2-yl)DTT (**V**) has not been reported.
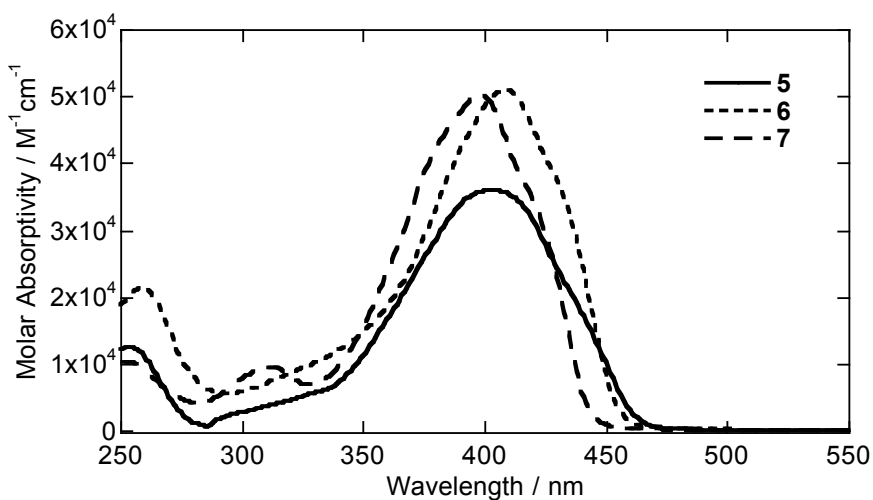
Figure 2.12. UV-visible absorption spectra of compounds **5**, **6**, and **7** in dichloromethane.

The absorption maxima for each compound are shown in the Table 2.6, as well as the value for the transition dipole moments. TD-DFT calculations predict that – for all of the compounds – the lowest energy absorption in the visible region corresponds to a HOMO-to-LUMO transition. TD-DFT values for the transition energies and transition dipole moments are also shown in the same table, and although the values are similar to what was measured experimentally, the trends do not match those of the experimental values for all cases.

Table 2.6. Absorption maxima (ν_{max}), molar absorptivity (ε), and transition dipole moments (μ_{ge}) for compounds **1–7** in dichloromethane with TD-DFT values in parentheses.

Compound	ν_{max} / nm	ν_{max} / cm^{-1}	ε / M^{-1}cm^{-1}	μ_{ge} / D
1	319 (317)	31300 (31500)	15900	5.1 (6.1)
2	305 (301)	32800 (33200)	20600	5.4 (5.7)
3	307 (296)	32600 (33800)	24500	6.0 (6.0)
4	305 (321)	32800 (31200)	33100	6.9 (3.3)
5	403 (436)	24800 (22900)	36000	6.7 (11.1)
6	409 (422)	24500 (23700)	51000	9.3 (11.1)
7	398 (430)	25100 (23300)	50100	8.9 (11.3)

2.3.4 Emission Spectra of Bis(5-alkylthien-2-yl)-BIT, -DTT, and –DTP Derivatives

The energy of the relaxed excited state relative to the ground state in solution – sometimes called the solution HOMO-LUMO gap – was measured from the intersection of the normalized absorption and emission spectra of compounds **5**–**7**. The emission spectra, recorded in dichloromethane, were very similar, showing vibronic structure in all cases. Interestingly there is more vibronic structure in the emission than in the absorption spectra, which may be due to planarization in the relaxed excited state, which is similar to spectra obtained for other fused and non-fused oligothiophene derivatives.[19] The emission maxima for compounds **5** and **7** are red-shifted by ca. 15 – 20 nm compared that published for related compounds **IV** and **VI**,[25] which is consistent with the effects of alkylation in compounds **5** and **7**. Emission data for **V** has not been published. Normalized emission spectra for **5**–**7** are shown in Figure 2.13, with normalized absorption spectra to show the intersection of the absorption and emission spectra.
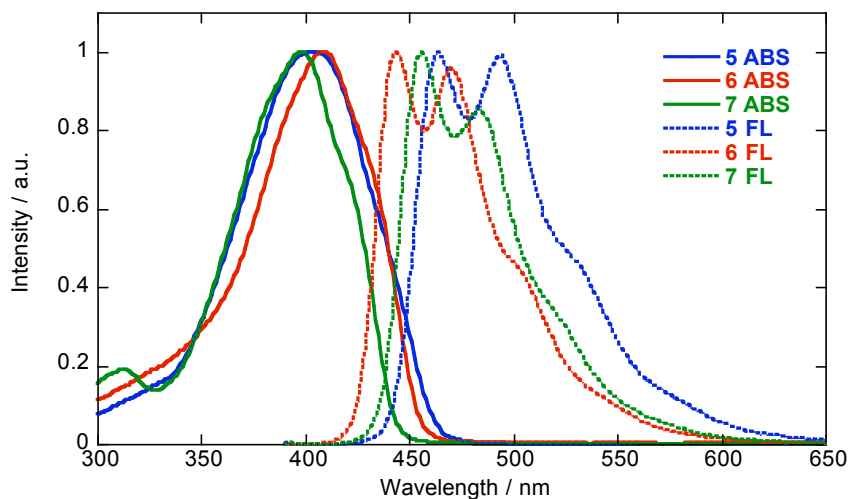
Figure 2.13. Normalized absorption and emission spectra for **5**–**7** in dichloromethane.

Table 2.7 summarizes the absorption and emission spectral features for the emission spectra of compounds **5**–**7**, as well as those of related published compounds **IV** and **VI** for comparison.[25]

Table 2.7. Summary of features from emission spectra of compounds **5**-**7** in dichloromethane, with related data for published compounds **IV** and **VI**.[25]

Compound	Emission Maxima / nm	Related Compound	Emission Maxima / nm
5	464 494 532	**IV**	437 478 510
6	443 470 505	–	–
7	456 484 525	**VI**	444 470 506

From the intersection of the absorption and emission spectra, the solution HOMO-LUMO gap was calculated for compounds **5**–**7**. The results are similar for each compound and are shown in Table 2.8.

Table 2.8. Intersection of normalized absorption and fluorescence spectra for compounds **5**–**7**, estimated solution HOMO-LUMO gap from intersection of absorption and emission spectra.

Compound	Intersection of absorption and emission spectra / nm	Estimate of HOMO-LUMO gap / eV
5	448	2.77
6	435	2.85
7	438	2.83

2.3.5 Visible-NIR Absorption Spectra of Monocations

If the BIT, DTT, and DTP derivatives were to be used as hole-transporting organic semiconductors, the active charge carrier were these compounds would be the monocations. In order to better understand the properties of the monocations of compounds **3**–**7**, the visible-NIR absorption spectra of monocations **3$^+$**–**7$^+$** were recorded in dichloromethane (Figures 2.12 and 2.13). The monocations were generated in solution by adding a 10-fold excess of neutral compound to a solution of tris(4-bromophenyl)aminium hexachloroantimonate in dry dichloromethane. Multiple scans of the solutions in the visible-NIR region showed that the monocations were relatively stable in solution over time. Attempts at acquiring absorption spectra for monocations **1$^+$** and **2$^+$** resulted in spectra that changed dramatically over time, consistent with expectations – from the irreversibility of the oxidations in CV experiments – that these

monocations were unstable; the data for the absorption spectra of **1⁺** and **2⁺** are therefore not included.

The absorption spectra of **3⁺** and **4⁺** are shown in Figure 2.14. Although the spectra are plotted from 400–800 nm, the data was collected from 400–2500 nm, and no absorption bands were observed lower than 800 nm. The monocation absorption spectra were relatively stable over a period of ca. 20 minutes, although a band at ca. 725 nm grew within a few minutes, so is expected not to be from the monocations themselves but instead were due to a decomposition product. TD-DFT calculations predicted a HOMO-1 to HOMO transition at similar energies to where the lowest energy transition (before decomposition) was observed. The shapes and energies of the lowest energy absorption features in **3⁺** and **4⁺** are similar, which was expected based on the similarities of the HOMO-1 and HOMO orbitals for these monocations (the MOs for the monocations are not shown but are similar to those for the neutral molecules). When plotted in energy (cm⁻¹), the spacing between peaks of each spectrum is ca 1300 cm⁻¹ and 1380 cm⁻¹ for **3⁺** and **4⁺**, respectively.
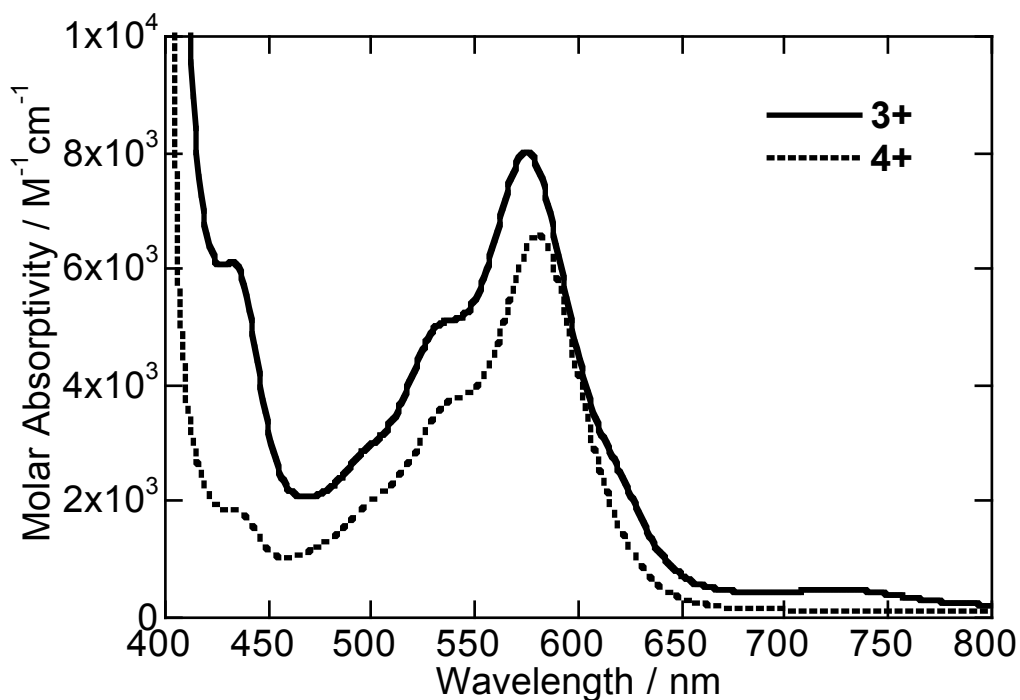
Figure 2.14. Visible-NIR absorption spectra for monocations 3^+ and 4^+ in dichloromethane.

The absorption spectra of monocations 5^+–7^+ are shown in Figure 2.15. The monocations show absorption bands at similar energies and with similar features, although the transitions for the 7^+ are slightly less intense and occur at higher energy than those for 5^+ and 6^+. The energy of the lowest energy transition of bis(5-alkylthien-2-yl)-substituted DTP-based monocation 7^+ is red-shifted by ca. 350 nm compared to the lowest energy transitions in dialkyl-substitued DTP-based monocations 3^+ and 4^+. As was the case for 3^+ and 4^+, the lowest energy absorption features for the monocations show evidence of vibronic structure; when the absorption spectra of 5^+–7^+ are plotted in energy (cm^{-1}), the spacing between the lowest energy absorption and next highest energy

feature are ca. 1400–1500 cm^{-1}. The transition dipole moments are similar for **5⁺**, **6⁺** and

7⁺, despite the difference in transition energies in **7⁺** compared to **5⁺** and **6⁺**.
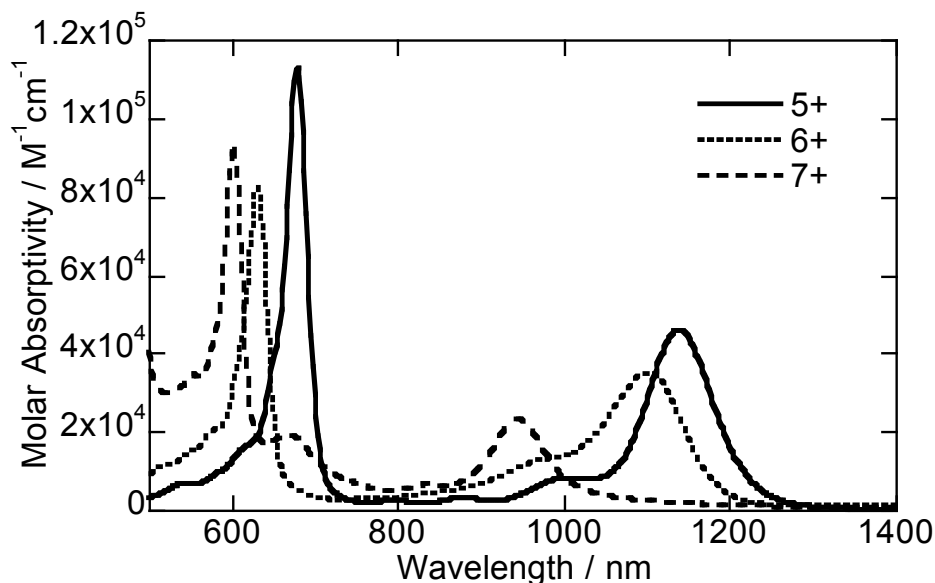
Figure 2.15.   Visible-NIR absorption spectra of monocations **5⁺**, **6⁺**, and **7⁺** in dichloromethane.

TD-DFT calculations predict that the intense low energy transition occurs from the SOMO-1 to SOMO in all three monocations. Table 2.9 summarizes the experimental and theoretical data for the lowest energy feature in the monocation absorption spectra, including absorption maxima (ν_{max}), extinction coefficients(ε), and transition dipole moments (μ_{ge}). Also included are values from TD-DFT calculations, for which the trends in the predictions for the energies of lowest absorbtion transition follow those of the experimental data.

Table 2.9. Absorption maxima (ν_{max}), extinction coefficients (ε), and transition dipole moments (μ_{ge}) for compounds **4–7** in dichloromethane, both from experimental data and predicted from TD-DFT calculations (in parentheses).

Compound	ν_{max} / nm	ν_{max} / cm^{-1}	ε/ M^{-1}cm^{-1}	μ_{ge} / D
1	–* (566)	–* (17700)	–*	–* (2.5)
2	–* (542)	–* (18500)	–*	–* (3.0)
3	577 (506)	17300 (19800)	7960	3.7 (2.7)
4	581 (506)	17200 (19800)	6560	3.1 (2.7)
5	1140 (995)	8770 (10100)	46000	6.3 (6.3)
6	1095 (954)	9130 (10500)	35000	7.7 (6.6)
7	943 (877)	10600 (11400)	23300	6.6 (5.7)

* reliable experimental data could not be obtained for this value

2.3.6 EPR Spectra of Mono of BIT, DTT, and DTP Derivatives

In order to study the spin distribution in the monocations, and ultimately to determine which of the monocations of BIT, DTT, and DTP is a better electron acceptor, EPR spectra were acquired for monocations **5⁺–7⁺**. Initially, it was planned that the EPR spectra of **5⁺–7⁺** would be compared to those of monocations **1⁺–4⁺**, but since monocations **1⁺** and **2⁺** are presumably unstable – as indicated by the irreversible oxidations in the CV experiments – it is possible that the EPR spectra may not represent the monocations themselves (at least for **1⁺** and **2⁺**) but rather could be a mixture of the desired monocation and other byproduct(s) or completely of byproduct(s). For this reason, multiple scans of all monocations were recorded to determine if the spectra changed significantly over time, and, if they did change, the spectra would be deemed less reliable. As was the case for the visible-NIR absorption spectra, the monocations were generated by chemical oxidation with tris(4-bromophenyl)aminium hexachloroantimonate in dichloromethane and were recorded at concentrations of ca. 5 × 10⁻⁴ M in monocation.

The EPR spectra at room temperature for 3^+ and 4^+ are shown in Figure 2.16. As expected, the EPR spectra of 1^+ and 2^+ changed over time; the spectra could not be simulated with WinSim, and thus the seemingly unreliable spectra are not shown here. However, monocations 3^+ and 4^+ were stable over time, so their EPR spectra were considered reliable. It is interesting that although the SOMOs for 3^+ and 4^+ look nearly the same, the EPR spectra are very different. From the simulations of the EPR spectra of 3^+ and 4^+ using WinSim, which are overlaid with the experimental spectra, it was determined that the values of the hyperfine coupling constants (HFCCs, Table 2.10) for 3^+ and 4^+ are very similar despite the spectral differences.
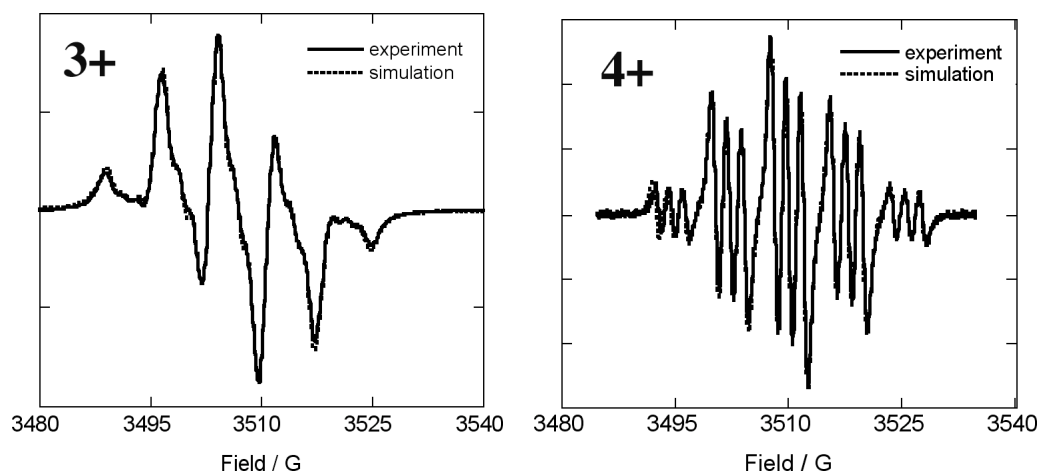
Figure 2.16. EPR of the monocations 3^+ (left) and 4^+ (right) in dichloromethane, shown with simulations overlaid with experimental spectra.

The HFCCs were predicted from DFT calculations of the spin densities of the monocations. A labeling scheme for the nuclei used in Table 2.10 is shown in Figure 2.17.
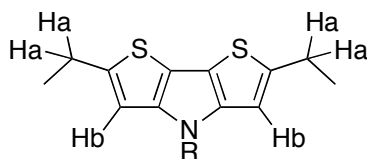
Figure 2.17. Labeling scheme for nuclei for which HFCCs were obtained from DFT calculations.

The HFCCs from the simulations of the experimental spectra are summarized in Table 2.10 for 3^+ and 4^+. The HFCCs to nitrogen (A_N) and to hydrogen (A_H) nuclei were similar for both monocations. The large HFCCs to hydrogen nuclei were predicted by DFT calculations to be the four hydrogen nuclei on the benzylic position of the alkyl chain.

Table 2.10. Absolute values for the HFCCs (A_x) for 3^+ and 4^+ obtained from simulations of the experimental data and from DFT calculations (in parentheses).

compound	A_N / G	A_{Ha}/ G	A_{Hb}/ G
3^+	1.83 (1.80)	7.50 (9.93)	–* (0.84)
4^+	1.93 (1.79)	7.08 (9.89)	–* (0.92)

*coupling to these atoms was not necessary to give a good fit with WinSim

The EPR spectra of monocations of 5^+–7^+ were recorded in dichloromethane and were simulated with WinSim. The EPR spectral shapes stayed constant over time, so the EPR spectra were considered reliable for simulation. The spectra are shown in Figure 2.18, overlaid with simulations, which are nearly identical to the experimental spectra.
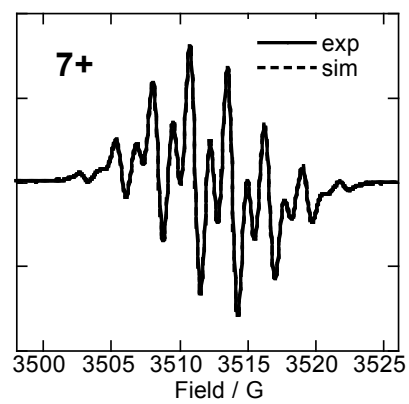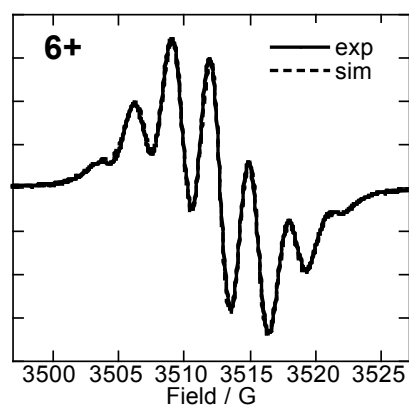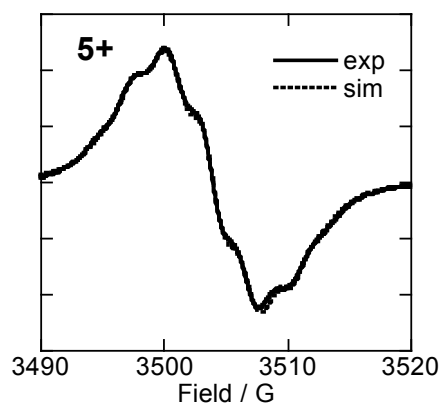
Figure 2.18. EPR spectra monocations **5⁺**, **6⁺**, and **7⁺** in dichloromethane, shown with simulations overlaid.

The HFCCs to various nuclei were extracted from the simulations of the EPR spectra of $\mathbf{5^+}$–$\mathbf{7^+}$. All three sets are shown in Table 2.11. For $\mathbf{5^+}$, the simulation is fitted with one set of four and another set of two hydrogen nuclei. Another set of two hydrogen nuclei could be added without changing the simulation shape significantly. The simulation of $\mathbf{6^+}$ was fitted using three sets of two equivalent hydrogen nuclei. The simulation for the $\mathbf{7^+}$ was fitted using three sets of two equivalent hydrogen nuclei and one nitrogen atom. In the case of $\mathbf{7^+}$, the HFCC to nitrogen was smaller ($A_N = 1.46$ G) than in the case of $\mathbf{3^+}$ ($A_N = 1.83$ G and $\mathbf{4^+}$ ($A_N = 1.93$ G), which suggests that some electron spin density has moved away from the core. Additionally, because there is coupling to the multiple sets of hydrogen nuclei, this fit is more supportive that the spin density has moved onto the to alkylthienyl rings. A diagram showing the labeling of the relevant nuclei for HFCCs in Table 2.11 is shown in Figure 2.19.

$X = 2\ H_c$, S, or NR
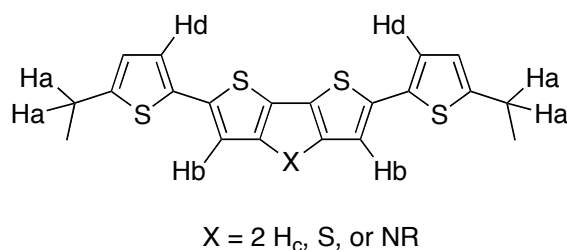
Figure 2.19. Labeling scheme for HFCCs for monocations $\mathbf{5^+}$, $\mathbf{6^+}$, and $\mathbf{7^+}$.

Table 2.11 shows the HFCCs obtained from simulations of the experimental spectra of monocations $\mathbf{5^+}$, $\mathbf{6^+}$, and $\mathbf{7^+}$. Note that in the case of $\mathbf{5^+}$, where there are two sets of two hydrogen nuclei, it cannot be certain that the experimental HFCCs were assigned to the correct hydrogen nuclei from Figure 2.19.

Table 2.11. HFCCs (in units of Gauss) for monocations 5^+, 6^+, and 7^+ obtained from simulations of the experimental EPR spectra.

compound	N	H_a	H_b	H_c	H_d
5^*	–	2.36 (4.38)	–* (1.06)	3.43, 2.43	0.78, (2.86)
6	–	2.63 (4.60)	–* (0.47)	–*, (–)	3.30 (2.99)
7	1.46 (1.20)	2.79 (4.31)	–* (0.29)	–*, (–)	2.56 (3.19)

*too small to be detected beyond the error of the fit

DFT calculations were used to estimate the percent of electron spin density for the monocations and were divided into various portions throughout the monocation: 1) the core (i.e. BIT, DTT, or DTP only), 2) both thiophene rings, and 3) the alkyl groups attached to each thiophene as shown in Figure 2.20.

n = 0 or 1
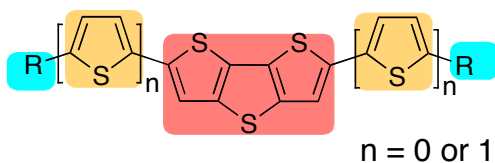
Figure 2.20. Division of monocation into core (red), thiophene rings (orange), and alkyl chains (blue).

Table 2.12 shows the percent of radical distribution over these three portions of the radical cations. The monocations of the bis(alkylthienyl)-substituted derivatives have lower percentages of spin density on their cores than do the dialkylated derivatives, which was expected because the positive charge can be more delocalized over the two additional thiophene rings in monocations 5^+–7^+, giving less spin density to the cores of those monocations. The spin densities on the alkyl chains have little variation, which was expected since the alkyl chains are not aromatic. The DTP-based monocation (7^+) shows a slightly higher percentage of radical cation density on the core compared to the DTT-

based monocation (**6⁺**), which suggests that DTP can better accept the positive charge than can DTT. The BIT monocation (**5⁺**) has a percent spin density between the equivalent DTT and DTP cores, which is not obvious.

Table 2.12. Percent spin density calculated for the different portions of monocations **1⁺–7⁺** predicted from DFT calculations.

Compound	core	thiophene rings	alkyl chains
1	98	–	2
2	97	–	3
3	99	–	1
4	98	–	2
5	57	43	1
6	55	44	1
7	59	40	1

2.4. Conclusions about BIT, DTT, and DTP Derivatives

The oxidation potentials of various BIT, DTT, and DTP derivatives have been determined by the synthesis of simple derivatives with modification of the presumably most reactive 2- and 6-positions of the aromatic cores. While BIT and DTT derivatives display similar electronic properties, the equivalent DTP derivatives are easier to oxidize. UV-visible absorption spectra of both sets of derivatives show that the transitions in the DTT and DTP derivatives have more similar characteristics, while the freely rotating BIT core tends to limit the detail of vibronic structure in the absorption spectra. Visible-NIR absorption spectra of the bis(5-alkylthien-2-yl)-substituted derivatives indicate that the presumably SOMO-to-SOMO-1 transition occurs at similar energy for the BIT and DTT derivatives, while the DTP derivative has similar characteristics at different energies; all

three compounds were stable as monocations, as evidenced by this experiment and by EPR experiments. EPR spectra of the monocations of some of the derivatives led to reasonable assignment of HFCCs, while others that showed partially reversible oxidations in CV experiments proved to be unstable in the EPR experiments.

Ultimately the bis(5-alkylthien-2-yl)-substituted derivatives are reasonably stable as monocations, at least on the time scale for recording spectroscopic measurements, such that it is possible that these derivatives could be – with the appropriate substitution – potential hole-transporting semiconductors. In this set of compounds, the specific derivative chosen would ultimately depend on the desired oxidation potential such that it was at the appropriate energy to match those in other semiconductors within an organic electronic device. To continue to explore the electronic properties of BIT, DTT, and DTP derivatives, and to compare the π-donor strengths of the cores, another system to study may be one in which simple π-acceptors are attached to the cores. Currently the purification of 2,6-bis(4-nitrostyryl)-substituted derivatives is underway. If the compounds are isolated and purified, CV measurements may better determine which core is a stronger π-donor by comparing the difference in oxidation potentials of the new derivatives to that of their parent cores.

2.5 Experimental Section for Chapter 2

2.5.1 DFT and TD-DFT Calculations

DFT and TD-DFT calculations were completed by Kelly Lancaster and Dr. Veaceslav Coropceanu of the research group of Prof. Jean-Luc Brédas at Georgia Institute of Technology.

The geometries of the BIT, DTT, and DTP derivatives for the neutral and radical cation ground and first excited states were optimized at the DFT level. The excitation energies and transition dipole moments of the low-lying excited states were calculated at the TD-DFT level. All DFT and TD-DFT calculations are performed using with the 6-31G(d,p) split valence plus double polarization basis set[34-37] and with the B3LYP functional.[38,39] All calculations were carried out using the Gaussian 03 suite of programs.[40]

Simulations of EPR experiments were accomplished using WinSim, a simulation program for Windows, which is currently provided for free download at the National Institutes for Environmental Health Sciences of the National Institutes of Health website at http://www.niehs.nih.gov/research/resources/software/tools/index.cfm.

2.5.2 Cyclic Voltammetry Experiments

Electrochemical measurements were carried out under nitrogen in dry deoxygenated dichloromethane solutions ca. 10^{-4} M in analyte and 0.1 M in tetra-*n*-butylammonium hexafluorophosphate using a BAS 100 B/W Potentiostat, a glassy carbon working electrode, a platinum auxiliary electrode, and, as a pseudo-reference electrode, a silver wire anodized in 1 M aqueous potassium chloride. Potentials were

referenced to ferrocenium / ferrocene by using cobaltocenium hexafluorophosphate (–1.32 V in dichloromethane) as an internal reference (since many of the redox events of interest were at similar potentials to that of ferrocene). Cyclic voltammograms were recorded at a scan rate of 50 mVs^{-1}.

2.5.3 UV-visible-NIR Absorption and Emission Spectra

UV-visible-NIR spectra were recorded in 1 cm cells using a Varian Cary 5E spectrometer. Monocation solutions (ca. 5×10^{-4} M) were generated by addition of < 0.1 eq. tris(4-bromophenyl)aminium hexafluoroantimonate (Aldrich) in dry CH_2Cl_2. Monocation absorptivities were calculated assuming all of the oxidizing agent added resulted in formation of monocation and that disproportionation is negligible at these concentration ratios. Emission spectra in dichloromethane were recorded on solutions for which the maximum absorbance had an absorbance less than 0.1 in 1 cm cells on a Horiba Jobin Yvon Fluorolog 3 fluorimeter.

2.5.4 EPR Experimental Details

Room-temperature EPR spectra were acquired using a Bruker EMX spectrometer. Monocation solutions (ca. 5×10^{-4} M) were generated by addition of less than 0.1 equivalents of tris(4-bromophenyl)aminium hexafluoroantimonate (Aldrich) in dry dichloromethane.

2.5.6 Synthetic Details

*Dr. Yulia Getmanenko, of the research group of Prof. Seth R. Marder at Georgia Institute of Technology, synthesized compounds **5** and **6**. Daniel Sweat, also of the same research group, assisted with the synthesis of **IIIe** and **12**.*

Starting materials were reagent grade and were used without further purification unless otherwise indicated. Starting materials were purchased from Acros Chemical Co. except for tris(dibenzylideneacetone)dipalladium(0) (Pd_2dba_3) and tri(t*ert*-butyl)phosphine solution in hexane, both of which were purchased from Strem. Solvents were dried by passing through columns of activated alumina in a manner similar to that described in the literature (tetrahydrofuran, toluene, dichloromethane)[41] or by distillation from CaH_2 (acetonitrile), or were obtained as anhydrous grade from Acros Organics. Chromatographic separations were performed using standard flash column chromatography methods using silica gel purchased from Sorbent Technologies (60 Å, 32-63 μm) or basic alumina purchased from Aldrich Chemical Company. Elemental analyses were performed by Atlantic Microlabs. The microwave used was a CEM Discover Labmate. Mass spec FAB was performed on a VG Instruments 70SE. GCMS data were acquired on an Agilent 5790 GC/ 6850 MS.

Dithieno[3,2-*b*:2',3'-*d*]dithiophene (II) was prepared as described by Holmes *et al.*[24] ^{1}H NMR (300 MHz, CDCl$_3$) δ 7.37 (d, *J* = 5.4 Hz, 2 H), 7.29 (d, *J* = 5.4 Hz, 2 H).

2,6-Dibromodithieno[3,2-*b*;2',3'-*d*]thiophene (8). Characterization data for the title compound has been reported, as synthesized from bromination with *N*-bromosuccinimide

in *N,N*-dimethylformamide.[33] Dithieno[3,2-*b*;2',3'-*d*]thiophene (0.81 g, 4.1 mmol), chloroform (45 mL), and acetic acid (45 mL) were combined in a 250 mL round-bottomed flask wrapped with aluminum foil, which was cooled to 0 °C. *N*-Bromosuccinimide (1.63 g, 9.1 mmol) was added, and the reaction mixture was stirred at 0 °C for one hour after which it was stirred at room temperature for 1 h. Dichloromethane (200 mL) was added, and the organic layer was washed with water and aqueous sodium bicarbonate, then was dried with anhydrous magnesium sulfate. The solution of crude product was run through a pad of silica gel, eluting with dichloromethane. The solvent was removed by rotary evaporation, yielding an off-white solid (1.29 g, 88%). ^{1}H NMR (300 MHz, CDCl$_3$) δ 7.28 (s, 2H). ^{13}C{^{1}H} NMR (75 MHz, CDCl$_3$) δ 138.9, 130.7, 123.1, 112.3. MS-EI (*m/z*): 353.8. Anal. calcd. for C$_8$H$_2$Br$_2$S$_3$: C, 27.13; H, 0.57. Found: C, 27.10; H, 0.57.

2,6-Diiododithieno[3,2-*b*:2',3'-*d*]thiophene (11). In a 100 mL round-bottomed flask, acetic acid (10 mL) and chloroform (10 mL) were added, and the reaction vessel was wrapped with aluminum foil and immersed in an ice water bath. Dithieno[3,2-*b*:2',3'-*d*]thiophene (0.20 g, 1.0 mmol) was added followed by *N*-iodosuccinimide (0.45 g, 2.0 mmol). After an hour of stirring, the reaction flask was removed from the cold bath. An hour later, dichloromethane (200 mL) was added, and the organic layer was washed with aqueous sodium carbonate (1 × 200 mL), then water (1 × 200 mL), and was then dried with anhydrous magnesium sulfate and was concentrated by rotary evaporation to obtain a white solid, which was recrystallized from toluene to obtain olive-colored crystals, 0.36 g (80%). ^{1}H NMR (300 MHz, C$_6$D$_6$) δ 6.64 (s, 2H). ^{1}H NMR (300 MHz, CD$_2$Cl$_2$) δ 7.46

(s, 2H). ^{13}C{1H} NMR (125 MHz, C$_6$D$_6$) δ 141.0, 135.2, 129.4, 73.2. MS-EI (*m/z*): 447.7. Anal. calcd. for C$_8$H$_2$I$_2$S$_2$: C, 21.44; H, 0.45. Found: C, 21.54; H, 0.41.

2,6-Di(*n*-butyl)dithieno[3,2-*b*:2',3'-*d*]thiophene (2). To an oven-dried Schlenk flask cooled under nitrogen was added dithieno[3,2-*b*;2',3'-*d*]thiophene (0.050 g, 2.56 mmol) and tetrahydrofuran (25 mL, freshly distilled from sodium/benzophenone). The reaction flask was immersed in a dry ice/acetone bath after which *n*-butyllithium (2.3 mL, 2.5 M solution in hexane) was added. The reaction flask was removed from the cold bath and was allowed to warm to room temperature. After 30 minutes, the reaction flask was returned to the dry ice / acetone bath, and 1-iodobutane (0.71 g, 3.8 mmol) was added. The reaction was removed from the cold bath again, and after two hours, water (3 mL) was added. The reaction mixture was concentrated by rotary evaporation, and the crude product was purified by column chromatography (silica gel, 3% ethyl acetate in hexanes) and Kugelrohr distillation, producing 0.30 g (38%) of the title compound as a colorless oil. ^{1}H NMR (300 MHz, CDCl$_3$) δ 6.94 (s, 2 H), 2.89 (t, *J* = 7.2 Hz, 4 H), 1.72 (quintet, *J* = 7.4 Hz, 4H), 1.43 (sextet, *J* = 7.5 Hz, 4H), 0.97 (t, *J* = 7.4 H, 6H). ^{13}C{^{1}H} NMR (75 MHz, CDCl$_3$) δ 146.2, 139.1, 129.0, 117.4, 33.7, 30.8, 22.1, 13.8. GC-MS *m/z* (% relative intensity): 308 (95), 265 (100), 222 (90), 190 (88), 145 (60). Anal. calcd. for C$_{16}$H$_{20}$S$_3$: C, 62.29; H, 6.53. Found: C, 62.52; H, 6.56. UV-visible absorption (dichloromethane) λ$_{max}$, nm (ε): 305 nm (2.06 × 10^4) M^{-1}cm^{-1}. Cyclic voltammetry in 0.1 M Bu$_4$NPF$_6$ in dichloromethane: E$_{1/2}$$^{+/0}$: 0.69 V versus Cp$_2Fe^{+/0}$ at 0 V.

5,5-Dibromo-2,2-bithiophene. This compound was prepared as previously described in the literature.[29] ^{1}H NMR (CDCl$_3$, 300 MHz) δ 7.79 (d, J = 8.1 Hz, 2H), 7.37 (d, J = 8.4 Hz, 2H). ^{13}C{^{1}H} NMR (CDCl$_3$, 75 MHz) δ 146.0, 135.1, 130.0, 127.1. GC-MS m/z (% relative intensity): 326 (45), 324 (100), 322 (45), 245 (20), 201 (20), 164 (70), 119 (18), 93 (10).

N-**Phenyl-dithieno[3,2-*b*:2',3'-*d*]pyrrole (IIIa)**. The characterization for this compound has been previously published using a different method (although the reagents are similar) for synthesis.[14] Anhydrous deoxygenated toluene (35 mL) was added to a tube-shaped Schlenk flask after which 3,3'-dibromo-2,2'-bithiophene (1.95 g, 6.05 mmol) and Tris(dibenzylideneacetone)dipalladium(0) (0.23 g, 0.25 mmol) were added. In a separate flask, anhydrous deoxygenated toluene (15 mL) was combined with tri(*tert*-butyl)phosphine (2 mL, 10% wt. solution in hexane) and aniline (0.60 g, 6.5 mmol), and the solution was cannulated into the Schlenk flask. Sodium *tert*-butoxide (1.15 g, 12.0 mmol) was added, and the reaction mixture was heated to reflux. After heating for 2 hours, the reaction flask was removed from the oil bath, and the reaction mixture was concentrated by rotary evaporation. The crude product was run through a pad of silica gel, eluting with hexanes / dichloromethane (9:1, then 4:1), yielding 1.44 g of product (94%). ^{1}H NMR (300 MHz, acetone-d_6) δ 7.72 (d, J = 7.5 Hz, 2H), 7.63 (dd, J = 7.5 Hz, 2H), 7.41 (t, J = 8.5 Hz, 1H), 7.40 (d, J = 5.5 Hz, 2H), 7.31 (d, J = 5.5 Hz, 2H). ^{13}C{^{1}H} NMR (75 MHz, CDCl$_3$) δ 143.8, 139.7, 129.7, 125.9, 123.3, 122.5, 116.8, 112.2. GC-MS m/z (% relative intensity): 266 (95), 238 (85), 223 (100), 195 (88), 151 (90), 125 (15), 93 (30).

N-(4-n-Hexylphenyl)-dithieno[3,2-b:2',3'-d]pyrrole (IIIc). The synthesis and characterization of this molecule has been published, using a different method for synthesis.[17]

To an oven-dried Schlenk flask cooled under nitrogen was added anhydrous deoxygenated toluene (20 mL), tris(dibenzylideneacetone)dipalladium(0) (0.078 g, 0.085 mmol) and tri(*tert*-butyl)phosphine (Strem, 1.0 mL, 10% wt. solution in hexanes). After the reaction mixture stirred for 20 minutes, 4-*n*-hexylaniline (0.90 g, 5.1 mmol), 3,3'-dibromo-2,2'-bithiophene (1.5 g, 4.8 mmol), and sodium *tert*-butoxide (2.07 g, 21.6 mmol) were added. A reflux condenser was attached, and the reaction mixture was heated to reflux under a slight flow of nitrogen. After heating for 50 minutes, the reaction flask was removed from the oil bath. The crude product was run first through a short pad of silica gel, eluting with 3% ethyl acetate in hexanes, then through a column of silica gel, eluting with 1% ethyl acetate in hexanes. After concentration by rotary evaporation, 1.23 g (75%) of an off-white semicrystalline solid was isolated. ^{1}H NMR (CD$_2$Cl$_2$, 300 MHz) δ 7.50 (d, *J* = 8.4 Hz, 2H), 7.35 (d, *J* = 8.4 Hz, 2H), 7.20 (d, *J* = 5.1 Hz, 2H), 7.18 (d, *J* = 5.1 Hz, 2H), 2.69 (t, 7.8 Hz, 2H), 1.67 (quintet, *J* = 7.5 Hz, 2H), 1.27 (m, 6H), 0.92 (t, *J* = 5.4 Hz, 3H). GC-MS *m/z* (% relative intensity): 339 (100), 268 (90), 253 (10), 223 (10), 178 (8), 152 (7), 134 (10). Anal. calcd. for C$_{20}$H$_{21}$NS$_2$: C, 70.75; H, 6.23; N, 4.12. Found: C, 70.83; H, 6.36; N, 4.15.

N-(*tert*-Butylphenyl)dithieno[3,2-b:2',3'-d]pyrrole (IIId). To a 100 mL round-bottomed flask was added anhydrous deoxygenated toluene (Acroseal, 20 mL),

tris(dibenzylideneacetone)dipalladium(0)   (0.075 g, 0.082 mmol), and tri(*tert*-butyl)phosphine (10% wt. solution in hexanes, 0.4 mmol) under nitrogen atmosphere. After the reaction mixture stirred for 20 minutes, 4-(*tert*-butyl)aniline (0.75 g, 5.1 mmol), 3,3'-dibromo-2,2'-bithiophene (1.5 g, 4.8 mmol), and sodium *tert*-butoxide (2.1 g, 22 mmol) were added. A reflux condenser was attached, and the reaction mixture was heated to reflux under slight flow of nitrogen. After 40 minutes, the reaction mixture was removed from the oil bath and was run through a pad of silica gel, eluting with 1% ethyl acetate in hexanes. After concentration by rotary evaporation, the crude product was run through a column of silica gel, eluting with hexanes/dichloromethane (9:1), yielding1.25 g (84%) of the desired product was isolated as a pale yellow solid. ^{1}H NMR (500 MHz, CDCl$_3$) δ 7.59 (d, J = 8.5 Hz, 2H), 7.54 (d, J = 8.5 Hz, 2H), 7.21 (d, J = 5.5 Hz, 2H), 7.19 (d, J = 5.0 Hz, 2H), 1.48 (s, 9H). ^{1}H NMR (300 MHz, C$_6$D$_6$) 7.24 (d, J = 9 Hz, 2 H), 7.20 (d, J = 9 Hz, 2 H), 6.88 (d, J = 5.4 Hz, 2 H), 6.72 (d, J = 5.4 Hz, 2 H), 1.20 (s, 9 H). ^{13}C{^{1}H} NMR (75 MHz, CDCl$_3$) δ 148.8, 143.9, 137.2, 126.5, 123.1, 122.1, 116.5, 122.3, 34.7, 31.5. GC-MS *m/z* (percent relative intensity) 311 (100), 296 (98), 281 (35), 268 (20), 254 (16), 223 (10), 178 (36), 134 (37). Anal. calcd. for C$_{18}$H$_{17}$NS$_2$: C, 69.41; H, 5.50; N, 4.50. Found: C, 69.65; H, 5.69; N, 4.45.

4-(*tert*-Butyldimethylsilyloxymethyl)aniline.   This compound was prepared as previously described.[42] ^{1}H NMR (300 MH, C$_6$D$_6$) d 7.09 (d, J = 8.4 Hz, 2H), 6.31 (J = 7.8 Hz, 2H), 4.54 (s, 2H), 2.83 (broad s, 2H), 0.93 (s, 9H), 0.03 (s, 6H).

***N*-(4-*tert*-Butyldimethylsilyloxymethylphenyl)-dithieno[3,2-*b*:2',3'-*d*]pyrrole   (IIIb)**. In an oven-dried 20 mL vial with stir bar cooled under nitrogen, anhydrous deoxygenated

toluene (4 mL), tri(*tert*-butyl)phosphine (1 mL, 10% weight solution in hexane), and tris(dibenzylideneacetone)dipalladium(0) (0.18 g, 0.17 mmol) were combined and stirred at room temperature under nitrogen. In a 100 mL oven-dried round-bottomed flask cooled under nitrogen, anhydrous deoxygenated toluene (35 mL), *N*-(4-*tert*-butyldimethylsilyloxymethyl)aniline (1.0 g, 4.2 mmol), 3,3'-dibromo-2,2'-bithiophene (1.42 g, 4.4 mmol), and sodium *tert*-butoxide (1.0 g, 10 mmol) were combined. Then the slurry from the 20 mL vial was added to the 100 mL flask, which was then assembled in a microwave reactor. The reaction was irradiated for 20 minutes at 75 W, 20 minutes at 85 W, and 20 minutes at 95 W. The reaction mixture was concentrated by rotary evaporation, and the crude product was redissolved in hexanes and ethyl acetate. The solution was run through a pad of silica gel, eluting with hexanes, 10% ethyl acetate in hexanes, then 20% ethyl acetate in hexanes. The crude product was concentrated and was then run through a second column, eluting with 2% ethyl acetate in hexanes. The resulting solid was recrystallized from hexanes and methanol, yielding a semicrystalline white solid, mass 0.47 g, 28%. ^{1}H NMR (300 MHz, C_6D_6) δ 7.23 (s, 4H), 6.83 (d, J = 5.1 Hz, 2H), 6.72 (d, J = 5.1 Hz, 2H), 4.58 (s, 2H), 1.01 (s, 9H), 0.85 (s, 6H). $^{13}C\{^1H\}$ NMR (75 MHz, C_6D_6) δ 144.4, 139.4, 139.0, 127.6, 123.6, 122.7, 117.5, 112.4, 64.8, 26.3, 18.7, -5.0. GC-MS *m/z* (% relative intensity): 399 (50, M+), 283 (15), 268 (100).

N-(4-Bromophenyl)-dithieno[3,2-b:2',3'-d]pyrrole (17). *Note: this reaction was difficult to reproduce, and this procedure represents the best yield.* To a 100 mL round-bottomed flask dried in the oven and cooled under nitrogen was added toluene (approx. 4 mL, solvent purification system). 3,3'-dibromo-2,2'-bithiophene (0.21 g, 0.65 mmol), 4-

bromoaniline (0.12 g, 0.7 mmol), and sodium *tert*-butoxide (0.15 g, 1.56 mmol) were added followed by a slurry of tri(*tert*-butyl)phosphine (0.27 mL, 10% wt. in hexane) and tris(dibenzylideneacetone)dipalladium(0) (0.030 g, 0.026 mmol) in anhydrous deoxygenated toluene (2 mL). The reaction was heated using microwave heating at 95 W for 10 minutes, 100 W for 10 minutes, then 110 W for an additional 20 minutes, monitoring the reaction progress by GCMS and TLC. Chloroform was added, and the crude reaction mixture was run through a pad of silica gel, eluting with dichloromethane. The crude product was concentrated by rotary evaporation and was run through a column of silica gel, eluting with hexanes/dichloromethane (9:1). The desired product was obtained as a white solid in 62% yield (0.13 g). ^{1}H NMR (CDCl$_3$) δ 7.67 (d, *J* = 8.7 Hz, 2H), 4.89 (d, *J* = 9 Hz, 2H), 7.22 (d, *J* = 5.1 Hz, 2H), 7.16 (d, *J* = 5.1 Hz, 2H). ^{13}C{1H} NMR (CDCl$_3$) δ 143.92, 139.11, 133.08, 124.31, 124.06, 119.15, 117.41. MS-EI (*m/z*): 334.9. Elemental analysis was not obtained for this derivative because it could not be synthesized again, and the material synthesized in this batch was consumed in attempts to make another compound.

N-(4-*tert*-Butylphenyl)-2,6-dibromodithieno[3,2-*b*;2',3'-*d*]pyrrole (10). To a 250 mL round-bottomed flask were added *N*-(4-*tert*-butylphenyl)dithieno[3,2-*b*;2',3'-*d*]pyrrole (1.25 g, 4.0 mmol), chloroform (50 mL) and acetic acid (50 mL). The flask was wrapped with aluminum foil and immersed in an ice-water bath. *N*-Bromosuccinimide (1.44 g, 8.1 mmol) was added, and the reaction mixture was stirred for 1 hour, after which it was removed from the bath and was stirred for another hour. Dichloromethane (100 mL) was then added to the reaction mixture, and the resulting mixture was washed with water (2 ×

150 mL) and saturated aqueous sodium bicarbonate (2 × 150 mL), and the organic layer was dried over MgSO₄. The solution was diluted by 50% with hexanes and was run through a short pad of silica gel, eluting with hexanes / dichloromethane (1:1). After recrystallization from boiling hexanes, the product was obtained as tan-yellow needle-like crystals (1.14 g, 95%). ^{1}H NMR (300 MHz, C₆D₆) δ 7.16 (d, *J* = 8 Hz, 2 H), 6.90 (d, *J* = 8 Hz, 2H), 6.78 (s, 2H), 1.23 (s, 9H). ^{13}C{^{1}H} NMR (75 MHz, C₆D₆) δ 149.6, 141.1, 136.6, 126.8, 122.7, 117.0, 115.8, 110.6, 34.5, 31.3. GC-MS *m/z* (%): 469 (100, M$^+$), 454 (46), 336 (26), 278 (11), 212 (12), 125 (14), 102 (10), 77 (8), 57 (6). Anal. calcd. for for C₁₈H₁₅NS₂Br₂ (468.9): C, 46.07; H, 3.22; N, 2.98. Found: C, 45.79; H, 3.19; N, 2.95.

N-4-*tert*-Butylphenyl-2,6-di(*n*-butyl)dithieno[3,2-*b*:2',3'-*d*]pyrrole (4). To an oven-dried Schlenk flask cooled under nitrogen was added anhydrous deoxygenated tetrahydrofuran (20 mL), *N*-(4-(*tert*-butyl)phenyl)-2,6-dibromo-dithieno[3,2-*b*:2',3'-*d*]pyrrole (0.40 g, 0.86 mmol). The reaction mixture was immersed in a dry ice / acetone bath after which *tert*-butyllithium (2.1 mL, 1.7 M in pentane) was added. The bright yellow reaction mixture was stirred for 15 minutes after which 1-bromobutane (1.50 g, 10.8 mmol) was added. The reaction was removed from the cold bath, and after warming to room temperature, water (100 mL) was added followed by dichloromethane (100 mL). The organic layer was separated and dried with anhydrous magnesium sulfate. After filtration and concentration, the product was redissolved in hexanes and was run through a column of silica gel, eluting with hexanes followed by hexanes / ethyl acetate (99:1). The product was isolated as a mixture with the monoalkylated product, as determined by

GCMS. The product was further purified by recrystallization from hexanes, collecting 0.055 g (15%) of the desired product as an off-white crystalline solid. ^{1}H NMR (400 MHz, C$_6$D$_6$) δ 7.48 (dd, J = 6.4, 1.6 Hz, 2 H), 7.36 (dd, J = 6.4, 1.6 Hz, 2 H), 6.92 (s, 2 H), 2.76 (t, J = 8 Hz, 4 H), 1.65 (quintet, J = 8 Hz, 4 H), 1.35 (sextet, J = 8 Hz, 4 H), 1.33 (s, 9 H), 0.93 (t, J = 7.2 Hz, 6 H). ^{13}C{^{1}H} NMR (125 MHz, CD$_2$Cl$_2$) δ 149.2, 144.1, 142.1, 137.8, 126.9, 122.3, 114.8, 110.0, 34.9, 34.3, 31.5, 31.4, 22.5, 14.0. GCMS m/z (percent relative intensity): 423 (95), 331 (100), 364 (90), 350 (40), 337 (90), 321 (80), 307 (30), 294 (40), 380 (35), 204 (25), 182 (45), 168 (75). Anal. calcd. for C$_{26}$H$_{33}$NS$_2$: C, 73.71; H, 7.85; N, 3.31. Found: C, 73.71; H, 7.87; N, 3.29. UV-visible absorption (dichloromethane) λ$_{max}$, nm (ε): 305 nm (3.3 × 10^4) M^{-1}cm^{-1}. Cyclic voltammetry in 0.1 M Bu$_4$NPF$_6$ in dichloromethane: E$_{1/2}$$^{+/0}$: 0.38 V versus Cp$_2Fe^{+/0}$ at 0 V.

N-tert-Butyl-dithieno[3,2-_b_;2',3'-_d_]pyrrole (IIIk). The synthesis and characterization of this compound was previously reported, using a different method for synthesis. [17]

To a 100 mL round-bottomed flask was added anhydrous deoxygenated toluene (20 mL), tris(dibenzylideneacetone)dipalladium(0) (0.050 g, 0.043 mmol), tri(_tert_-butyl)phosphine (10% wt. solution in hexanes, 2.0 mL) under nitrogen. After stirring for 20 min, 4-_tert_-butylamine (0.59 g, 7.0 mmol), 3,3'-dibromo-2,2'-bithiophene (2.0 g, 6.2 mmol), and sodium _tert_-butoxide (1.8 g, 19 mmol) were added. A reflux condenser was attached, and the reaction mixture was heated to reflux under nitrogen. After 4 hours, the reaction appeared complete by TLC, and the reaction mixture was run through a pad of silica gel, eluting with 2%, then 5%, ethyl acetate in hexanes to give the desired product as a pale yellow solid (1.05 g, 75%). ^{1}H NMR (500 MHz, C$_6$D$_6$) δ 6.86 (d, J = 5.5 Hz, 2H), 6.74

(d, $J = 5.5$ Hz, 2H), 1.36 (s, 9H). $^{13}C\{^1H\}$ NMR (125 MHz, C_6D_6) δ 143.8, 122.1, 116.6, 115.0, 57.5, 30.3. MS (GC-MS) *m/z* (%): 311 (100), 296 (100), 26 (35), 178 (55), 134 (65). Anal. calcd. for $C_{12}H_{13}NS_2$: C, 61.24; H, 5.57; N, 5.95. Found: C, 61.14; H, 5.47; N, 5.83.

N-*tert*-Butyl-2,6-dibromodithieno[3,2-*b*;2',3'-*d*]pyrrole **(9)**. *N*-(*tert*-Butyl)-dithieno[3,2-*b*;2',3'-*d*]pyrrole (0.25 g, 1.1 mmol), chloroform (25 mL) and acetic acid (25 mL) were added to a 250 mL round-bottomed flask, which was wrapped with aluminum foil and immersed in an ice-water bath. *N*-Bromosuccinimide (0.45 g, 2.5 mmol) was added and the reaction mixture was stirred for 1 hour. Ethyl acetate (100 mL) was added to the reaction mixture, and the resulting organic phase was washed with water (2 × 150 mL) and saturated aqueous sodium bicarbonate (2 × 150 mL). The organic layer was then dried over anhydrous magnesium sulfate, was concentrated under reduced pressure, and was run through a pad of basic alumina, eluting with hexanes / ethyl acetate (9:1). The product was recrystallized from boiling hexanes to give the desired product as tan crystals (0.27 g, 50%). ^1H NMR (500 MHz, C_6D_6) δ 6.97 (s, 2H), 1.07 (s, 9H). $^{13}C\{^1H\}$ NMR (125 MHz, C_6D_6) δ 140.3, 118.3, 116.5, 109.4, 58.0, 30.0. GC-MS *m/z* (% relative intensity): 393 (60, M$^+$), 337 (100), 258 (35), 207 (5), 176 (5), 125 (30). Anal. calcd. for $C_{12}H_{11}NS_2Br_2$: C, 36.66; H, 2.82; N, 3.56. Found: C, 36.93; H, 2.84; N, 3.58.

N-*tert*-Butyl-2,6-di(*n*-butyl)-dithieno[3,2-*b*;2',3'-*d*]pyrrole **(3)**. To an oven-dried Schlenk flask cooled under nitrogen was added *N-tert*-butyldithieno[3,2-*b*;2',3'-*d*]pyrrole and tetrahydrofuran (freshly distilled from sodium/benzophenone). The reaction flask

was immersed in a dry ice/acetone bath after which *n*-butyllithium (2.5 M solution in hexane) was added. The reaction flask was removed from the cold bath, and the reaction mixture was allowed to warm to room temperature. After 35 minutes, the reaction flask was returned to the dry ice / acetone bath, and 1-iodobutane was added. The reaction flask was removed from the cold bath again, and after 2 hours, water (3 mL) was added. The reaction mixture was concentrated by rotary evaporation, and the crude product was purified by column chromatography (silica gel, 3% ethyl acetate in hexanes), producing the title compound (0.17 g, 39%) as a colorless oil. ^{1}H NMR (300 MHz, C_6D_6) δ 6.85 (s, 2H), 2.72 (t, J = 7.5 Hz, 4H), 1.59 (quintet, J = 7.8 Hz, 4H), 1.44 (s, 9H), 1.30 (sextet, J = 7.5 Hz, 4H), 0.85 (t, J = 7.5 Hz, 6H). ^{13}C{^{1}H} NMR (75 MHz, C_6D_6) δ 142.0, 141.6, 115.0, 112.7, 57.3, 34.4, 31.6, 30.4, 22.5, 14.0. GCMS *m/z* (% relative intensity): 347 (90, M$^+$), 304 (85), 248 (90), 205 (95), 57 (100). Anal. calcd. for $C_{20}H_{27}S_2N$: C, 69.11; H, 8.41; N, 4.03. Found: C, 69.33; H, 8.41, N, 4.09. Cyclic voltammetry in 0.1 M $^nBu_4NPF_6$ in dichloromethane: $E_{1/2}^{+/0}$: 0.23 V versus $Cp_2Fe^{+/0}$ at 0 V. UV-visible absorption (dichloromethane) λ_{max}, nm (ε): 307 nm (2.45×10^4) M^{-1}cm^{-1}.

N-(3,4,5-Tri(*n*-dodecyloxy)phenyl)[3,2-*b*:2',3'-*d*]pyrrole (IIIe). To an oven-dried 100 mL round-bottomed flask cooled under nitrogen was added dry deoxygenated toluene (4 mL), 3,3'-dibromo-2,2'-bithiophene (0.21 g, 0.65 mmol), and 3,4,5-tri(*n*-dodecyloxyphenyl)aniline (0.45 g, 0.70 mmol). A solution of tris(dibenzylideneacetone)dipalladium(0) (0.030 g, 0.26 mmol) and tri(*tert*-butyl)phosphine (0.3 mL, 10% solution in hexane) in dry deoxygenated toluene (2 mL) was added to the reaction mixture, followed by sodium *tert*-butoxide (0.175 g, 1.82

mmol). The reaction flask was assembled in a microwave reactor with a reflux condenser and was heated at 90 W for 6 minutes (T_{max} = 57 °C), then for 19 minutes at 95 W (T_{max} = 82 °C), which was followed by an additional round of heating at 100 W for 20 minutes (T_{max} = 110 °C). The reaction mixture was run through a short pad of silica gel, eluting with hexanes / dichloromethane (9:1, then 4:1), and after concentration by rotary evaporation, the product was further purified by column chromatography on silica gel using hexanes / dichloromethane (9:1 gradually increasing the ration to 1:1) as the eluent. After concentration by rotary evaporation, a pale yellow oil was obtained, which was precipitated from acetone to give the title compound as an off-white powder (0.38 g, 59%). ^{1}H NMR (500 MHz, CD$_2$Cl$_2$) δ 7.20 (d, J = 5.0 Hz, 2H), 7.18 (d, J = 5.0 Hz, 2H), 6.76 (s, 2H), 3.98 (m, 6H), 1.84 (quintet, J = 7.0 Hz, 4H), 1.75 (quintet, J = 7.0 Hz, 2H), 1.49 (m, 6H), 1.28 (m, 24H), 0.89 (m, 9H). ^{13}C{^{1}H} NMR (75 MHz, CD$_2$Cl$_2$) δ 154.1, 144.4, 136.5, 135.4, 123.7, 116.7, 112.6, 101.7, 73.9, 69.6, 32.5, 32.1, 30.9, 30.3, 30.2 (2 peaks, 0.6 ppm apart), 29.9 (2 peaks, 0.04 ppm apart), 26.7, 26.6, 23.2 (2 peaks, 0.05 ppm apart), 14.4, 9 peaks missing in alkyl region, presumably due to overlap. EI-MS (*m/z*): 807.6. Anal. calcd. for C$_{50}$H$_{81}$NS$_2$O$_3$: C, 74.29; H, 10.10; N, 1.73. Found: C, 74.51; H, 10.19; N, 1.80.

N-(3,4,5-Tri(*n*-dodecyloxy)phenyl)-2,6-diiododithieno[3,2-*b*:2',3'-*d*]pyrrole (**12**). To a 250 mL round-bottomed flask was added chloroform and acetic acid, then *N*-(tri(dodecyloxy)phenyl)-dithienopyrrole (0.50 g, 0.62 mmol). The reaction flask was immersed in an ice water bath, and *N*-iodosuccinimde was added. After stirring for 2 hours from 0 °C to room temperature, sodium bicarbonate (saturated solution in water)

was added. Dichloromethane was added, and the organic layer was washed with aqueous sodium bicarbonate, then with water. The organic layer was dried with anhydrous magnesium sulfate. The crude product was concentrated by rotary evaporation and was recrystallized from dichloromethane/methanol, giving 0.52 g (81%) of the desired product as an off-white solid. ^{1}H NMR (500 MHz, CD$_2$Cl$_2$) δ 7.31 (s, 2 H), 6.65 (s, 2 H), 3.98 (m, 6 H), 1.82 (quintet, J = 7.5 Hz, 4 H), 1.75 (quintet, J = 7.5 Hz, 2 H), 1.49 (quintet, J = 6.5 Hz, 6 H), 1.22 – 1.42 (m, 48 H), 0.88 (m, 9 H). ^{1}H NMR (500 MHz, CD$_6$C$_6$) δ 7.13 (s, 2 H), 6.50 (s, 2 H), 4.28 (t, J = 6.5 Hz, 2 H), 3.62 (t, J = 6.5 Hz, 4 H), 1.98 (quintet, J = 7.5 Hz, 2 H), 1.67 (m, 6 H), 1.20 – 1.45 (m, 52 H), 0.92 (m, 9 H). ^{1}H NMR (500 MHz, C$_6$D$_6$) δ 6.99 (s, 2 H), 6.50 (s, 2 H), 4.28 (t, J = 6.5 Hz, 2 H), 3.62 (t, J = 6.5 Hz, 4 H), 1.98 (quintet, J = 6.4 Hz, 2 H), 1.67 (quintet, J = 6.5 Hz, 4 H), 1.20 – 1.50 (m, 54 H), 0.93 (m, 9 H). ^{13}C{^{1}H} NMR (125 MHz, C$_6$D$_6$) δ 154.6, 143.9, 138.1, 134.6, 128.5, 121.6, 121.1, 102.8, 73.7, 72.0, 69.3, 32.3, 31.1, 30.3, 30.2, 30.1, 29.87, 29.85, 29.82, 29.7, 26.8, 26.5, 23.1, 14.4. MS-EI (m/z): 1059.3 Anal. calcd. for C$_{50}$H$_{79}$I$_2$NO$_3$S$_2$: C, 56.65; H, 7.51; N, 1.32. Found: C, 57.09; H, 7.56; N, 1.40.

5,5'-Bis(5-*n*-heptylthien-2-yl)-2,2'-bithiophene **(5)**.   5,5'-Dibromo-2,2'-bithiophene (0.324 g, 1.0 mmol) and tri-*n*-butyl-(5-heptyl-thiophen-2-yl)-stannane (1.04 g, 2.2 mmol) were mixed in an oven-dried flask. Tetrakis(triphenylphosphino)palladium(0) (0.012 g, 0.01 mmol) and anhydrous DMF (10 mL) were added under nitrogen atmosphere, and the reaction mixture was stirred for 1.5 hours at room temperature. An orange precipitate formed, and the reaction mixture was stirred for another 3 hours, was treated with 30 mL of ice water, and the orange solid was isolated by vacuum filtration, rinsed with ethanol,

hexanes and dried under vacuum. The crude material was isolated in 63.9% yield (0.337 g). Additional amount of solid that formed in the mother liquor after evaporation of hexanes was vacuum filtered, combined with the crude material and chromatographed (250 ml of silica gel, hexanes / dichloromethane (5:2) as eluant). The solvents were removed from the combined fractions and the residue was recrystallized from hexanes. Purified material was obtained as orange-yellow solid (0.153 g, 29% purified yield). This material was combined with the 2nd crop of crystals and further purified by column chromatography (100 mL of basic alumina, hexanes, then hexanes / dichloromethane (1:1) as the eluants). The solvent was removed from combined fractions and the residue was recrystallized from hexanes (~50 mL) to give dark yellow polycrystalline material, which was further purified by column chromatography on silica gel and recrystallization from hexanes, and analytically pure compound was obtained as bright yellow solid (0.15 g, 29%). ^{1}H NMR (CDCl$_3$, 400 MHz) δ 7.03 (d, J = 3.8 Hz, 2H), 6.97 (m, 4H), 6.68 (d, J = 3.5 Hz, 2H), 2.79 (t, J = 7.6 Hz, 4H), 1.68 (m, 4H), 1.40-1.20 (m, 16H), 0.89 (t, J = 6.8 Hz, 6H). ^{13}C{^{1}H} NMR (CDCl$_3$, 100 MHz) δ 145.5, 136.6, 135.2, 134.3, 124.7, 123.8, 123.4, 123.2, 31.6, 31.5, 30.0, 28.9, 22.5, 14.0. HRMS (EI) calculated for C$_{30}$H$_{38}$S$_4$: 526.1856; found: 526.1848. Anal. calcd. for C$_{30}$H$_{38}$S$_4$: C, 68.39; H, 7.27. Found: C, 68.41; H, 7.16. UV-visible absorption (dichloromethane) λ_{max}, nm (ε): 403 nm (3.6 × 10^4) M^{-1}cm^{-1}. Cyclic voltammetry in 0.1 M ^{n}Bu$_4$NPF$_6$ in dichloromethane: E$_{1/2}$$^{+/0}$: 0.47; E$_{1/2}$$^{2+/+}$: 0.71 V versus Cp$_2Fe^{+/0}$ at 0 V.

2,6-Bis(5-*n*-heptylthien-2-yl)dithieno[3,2-b:2',3'-d]thiophene (**6**). 2,6-Dibromodithieno[3,2-b:2',3'-d]thiophene (0.10 g, 0.28 mmol), 2-*n*-heptyl-5-tri-*n*-

butylstannylthiophene (0.29 g, 0.62 mmol), tetrakis(triphenylphosphino)palladium(0) (0.006 g, 0.007 mmol), and *N,N'*-dimethylformamide (Acroseal, 1 mL) were mixed in a oven-dried 10 mL microwave reaction vessel cooled under nitrogen. The reaction vessel was sealed, and the reaction mixture was heated for 5 minutes at 80 W, reaching a maximum temperature of 130 °C. Yellow-orange needles formed on cooling of the reaction vessel. The reaction mixture was transferred to a 50 mL Erlenmeyer flask, and dichloromethane (20 mL) was added. The resulting mixture was heated and the orange slightly cloudy solution was purified by column chromatography on basic alumina, eluting with dichloromethane. The solvent was removed, and the crude material was recrystallized from 1,4-dioxane. A bright yellow solid (0.12 g, 76%) was isolated from filtration. ^{1}H NMR (CDCl$_3$, 500 MHz) δ 7.25 (s, 2H), 7.02 (d, *J* = 3.5 Hz, 2H), 6.70 (d, *J* = 3.5 Hz, 2H), 2.81 (t, *J* = 7.5 Hz, 4H), 1.70 (quintet, *J* = 7.5 Hz, 4H), 1.20-1.40 (m, 16H), 0.95 (t, *J* = 7.5 Hz, 6H). ^{13}C{^{1}H} NMR (125 MHz, CDCl$_3$) δ 146.0, 141.2, 138.5, 134.8, 129.1, 124.9, 123.6, 116.1, 31.8, 31.6, 30.2, 29.1, 29.0, 22.6, 14.1. MS-EI (*m/z*): 556.14622. Anal. calcd. for C$_{30}$H$_{36}$S$_5$: C, 64.70; H, 6.52; S, 28.79. Found: C, 64.53; H, 6.80; N, 28.46. UV-visible absorption (dichloromethane) λ$_{max}$, nm (ε): 409 nm (5.1 × 10^4) M^{-1}cm^{-1}. Cyclic Voltammetry in 0.1 M Bu$_4$NPF$_6$ in dichloromethane: E$_{1/2}^{+/0}$: 0.40; E$_{1/2}^{2+/+}$: 0.79 V versus Cp$_2$Fe$^{+/0}$ at 0 V.

N-(3,4,5-Tri(*n*-dodecyloxy)phenyl)-2,6-bis(5-*n*-heptylthien-2-yl)dithieno[3,2-*b*:2',3'-d]pyrrole (7). *N*-(3,4,5-tri(*n*-dodecyloxy)phenyl)-2,6-diiododithieno[3,2-*b*:2',3'-d]pyrrole (0.55 g, 0.53 mmol), 2-*n*-heptyl-5-(tri-*n*-butylstannyl)thiophene (0.67 g, 1.1 mmol), tetrakis(triphenylphosphine)palladium(0) (0.005 g, 0.004 mmol), and *N,N'*-

dimethylformamide (Acroseal, 1 mL) were added to a microwave reaction vessel under nitrogen, which was sealed. The reaction vessel was assembled in a microwave reactor and was heated for 5 minutes at 80 W, reaching a maximum temperature of 148 ℃. The reaction mixture was poured into aqueous potassium fluoride, and the product was extracted with hexanes, washing the organic layer with hydrochloric acid (2 M in water, 1 × 200 mL), then with water (1 × 200 mL). The organic layer was dried with anhydrous magnesium sulfate, was filtered, and concentrated by rotary evaporation to give the crude product as a dark red solid. The product was run through a column of silica gel, eluting with hexanes/toluene (4:1), giving the desired product as a yellow oil. The crude product was run through a size exclusion column (1% cross-linked polystyrene beads in tetrahydrofuran, Biorad S-X1 biobeads), and then was precipitated from dichloromethane/methanol, giving 0.21 g (33%) of the pure product as a bright yellow solid. ^{1}H NMR (300 MHz, C_6D_6) δ 7.35 (s, 2 H), 7.01 (d, J = 4.8 Hz, 2 H), 6.75 (s, 2 H), 6.51 (d, J = 3.6 Hz, 2 H), 4.27 (t, J = 6.6 Hz, 2 H), 3.73 (t, J = 6.0 Hz, 4 H), 2.57 (t, J = 7.2 Hz, 4 H), 1.97 (quintet, J = 7.8 Hz, 2 H), 1.71 (m, 4 H), 1.2-1.6 (m, 79 H), 0.92 (m, 15 H). ^{13}C{^{1}H} NMR (125 MHz, C_6D_6) δ 154.6, 145.2, 144.7, 138.0, 136.7, 136.6, 135.2, 125.3, 123.4, 115.8, 108.3, 102.9, 73.7, 69.3, 32.3, 32.1, 31.9, 31.1, 30.4, 30.3, 30.24, 30.19, 30.1, 30.0, 29.84, 29.76, 29.39, 29.3, 26.8, 26.5, 23.1, 23.0, 14.4, 14.3. MS (EI): 1166.9. Anal. calcd. for $C_{72}H_{113}NO_3S_4$: C, 73.98; H, 9.74; N, 1.20; found: C, 73.92; H, 9.90; N, 1.24. UV-visible absorption (dichloromethane) λ_{max}, nm (ε): 398 nm (5.0 × 10^4) $M^{-1}cm^{-1}$. Cyclic voltammetry in 0.1 M Bu_4NPF_6 in dichloromethane: $E_{1/2}^{+/0}$: 0.20; $E_{1/2}^{2+/+}$: 0.68 V versus $Cp_2Fe^{+/0}$ at 0 V.

2.6 References

(1)   Murphy, A. R.; Frechet, J. M.; Chang, P.; Lee, J.; Subramanian, V. *J. Am. Chem. Soc* **2004**, *126*, 1596-1597.

(2)   Garnier, F. *Electronic Materials: The Oligomer Approach* **1998**, *Wiley-VCH, Weinheim, Eds: K. Mullen and G. Wegner*.

(3)   Cremer, J.; Baeuerle, P. *Eur. J. Org. Chem.* **2005**, *17*, 3715-3723.

(4)   Tam, I. W.; Yan, J.; Breslow, R. *Org. Lett.* **2006**, *8*, 183-185.

(5)   Deman, A.-L.; Tardy, J.; Nicolas, Y.; Blanchard, P.; Roncali, J. *Syn. Met.* **2004**, *146*, 365-371.

(6)   Ashizawa, M.; Kato, R.; Takanishi, Y.; Takezoe, H. *Chem. Lett.* **2007**, *36*, 708-709.

(7)   Nakanishi, H.; Sumi, N.; Aso, Y.; Otsubo, T. *J. Org. Chem* **1998**, *63*, 8632-8633.

(8)   Izumi, T.; Kobashi, S.; Takimiya, K.; Aso, Y.; Otsubo, T. *J. Am. Chem. Soc* **2003**, *125*, 5286-5287.

(9)   Marsella, M. J.; Swager, T. M. *J. Am. Chem. Soc* **1993**, *115*, 12214-12215.

(10)   Garcia, P.; Pernaut, J. M.; Hapiot, P.; Wintgens, V.; Valat, P.; Garnier, F.; Delaboughlise, D. *J. Phys. Chem.* **1993**, *97*, 513-516.

(11)   Casado, J.; Delgado, M.; Ruiz, M. C.; Merchan, M.; Rey, C.; Hernandez, V.; Navarrete, J. T.; Lope, J. T.; Pappenfus, T. M.; Williams, N.; Stegner, W. J.; Johnson, J. C.; Edlund, B. A.; Janzen, D. E.; Mann, K. R.; Orduna, J.; Villacampa, B. *Chem. Eur. J.* **2006**, *12*, 5458-5470.

(12)   Wada, H.; Taguchi, T.; Goto, M.; Kambayashi, T.; Mori, T.; Ishikawa; Takezoe, H. *Chem. Lett.* **2006**, *35*, 280-281.

(13)   Jong, F. d.; Janssen, M. J. *J. Org. Chem* **1971**, *36*, 1645-1648.

(14)   Nozaki, K.; Takahashi, K.; Nakano, K.; Hiyama, T.; Tang, H.-Z.; Fujiki, M.; Yamaguchi, S.; Tamao, K. *Angew. Chem. Int. Ed.* **2003**, *42*, 2051-2053.

(15)   Belletete, M.; Leclerc, M.; Durocher, G. *J. Phys. Chem.* **1994**, *98*, 9450-9456.

(16)   Jow, T. R.; Jen, K. Y.; Elsenbaumer, R. L.; Scacklette, L. W. *Syn. Met.* **1986**, *14*, 53-60.

(17)   Ogawa, K.; Rasmussen, S. *J. Org. Chem* **2003**, *68*, 2921-2928.

(18)   Ogawa, K.; Stafford, J. A.; Roghstein, S. D.; Tallman, D. E.; Rasmussen, S. C. *Syn. Met.* **2005**, *152*, 137-140.

(19)   Zhang, X.; Matzger, A. *J. Org. Chem* **2003**, *68*, 9813-9815.

(20)   Wei, Y.; Tian, J.; Glahn, D.; Wang, B.; Chu, D. *J. Phys. Chem.* **1993**, *97*, 12842-12847.

(21)   Inaoka, S.; Collard, D. M. *Langmuir* **1999**, *15*, 3752-3758.

(22)   Hotta, S. *Syn. Met.* **1987**, *22*, 103-113.

(23)   Ogawa, K.; Rasmussed, S. *Macromolecules* **2006**, *39*, 1771-1778.

(24)   Frey, J.; Bond, A. D.; Holmes, A. B. *Chem. Commun* **2002**, 2424-2425.

(25)   Radke, K. R.; Ogaa, K.; Rasmussen, S. C. *Org. Lett.* **2005**, *7*, 5253.

(26)   Allared, F.; Hellberg, J.; Remonen, R. *Tet. Lett.* **2002**, *43*, 1553-1554.

(27)   Li, X.-C.; Sirringhaus, H.; Garnier, F.; Holmes, A. B.; Moratti, S. C.; Feeder, N.; Clegg, W.; Teat, S. J.; Friend, R. H. *J. Am. Chem. Soc* **1998**, *120*, 2206-2207.

(28)   Koeckelberghs, G.; Cremer, L. D.; Vanormelingen, W.; Dehaen, W.; Verbiest, T.; Persoons, A.; Samyn, C. *Tetrahedron* **2005**, *61*, 687-691.

(29)   Khor, E.; Ng, S. C.; Hwee, H. C.; Chai, S. *Heterocycles* **1991**, *32*, 1805-1812.

(30)   Getmanenko, Y.; Twieg, R. *J. Org. Chem* **2008**, *73*, 830-839.

(31)   Brusso, J. L.; Hirst, O. D.; Afshin, D.; Ganesan, S.; Cicoira, F.; Robertson, C. M.; Oakley, R. T.; Rosei, F.; Perepichka, D. F. *Chem. Mater.* **2008**, *20*, 2484-2494.

(32)   Milstein, D.; Stille, J. K. *J. Am. Chem. Soc* **1978**, *100*, 3636-3638.

(33)   Li, P.; Ahrens, B.; Feeder, N.; Raithby, P. R.; Teat, S. J.; Khan, M. S. *Dalton Trans.* **2005**, *5*, 874-883.

(34)   Ditchfield, R.; Hehre, W. J.; Pople, J. A. *J. Chem. Phys.* **1971**, *54*, 724.

(35)   Hehre, W. J.; Ditchfield, R.; Pople, J. A. *J. Chem. Phys.* **1972**, *56*, 2257.

(36)   Gordon, M. S. *Chem. Phys. Lett* **1980**, *76*, 163.

(37)   Hariharan, P. C.; Pople, J. A. *Theor. Chim. Acta* **1973**, *28*, 213.

(38)   Becke, A. D. *Phys. Rev. A* **1988**, *38*, 3098.

(39)   Becke, A. D. *J. Chem. Phys.* **1993**, *98*, 5648.

(40)   Frisch, M. J.; Trucks, G. W.; Schlegel, H. B.; Scuseria, G. E.; Robb, M. A.; Cheeseman, J. R.; J. A. Montgomery, J.; Vreven, T.; Kudin, K. N.; Burant, J. C.; Millam, J. M.; Iyengar, S. S.; Tomasi, J.; Barone, V.; Mennucci, B.; Cossi, M.; Scalmani, G.; Rega, N.; Petersson, G. A.; Nakatsuji, H.; Hada, M.; Ehara, M.; Toyota, K.; Fukuda, R.; Hasegawa, J.; Ishida, M.; Nakajima, T.; Honda, Y.; Kitao, O.; Nakai, H.; Klene, M.; Li, X.; Knox, J. E.; Hratchian, H. P.; Cross, J. B.; Adamo, C.; Jaramillo, J.; Gomperts, R.; Stratmann, R. E.; Yazyev, O.; Austin, A. J.; Cammi, R.; Pomelli, C.; Ochterski, J. W.; Ayala, P. Y.; Morokuma, K.; Voth, G. A.; Salvador, P.; Dannenberg, J. J.; Zakrzewski, V. G.; Dapprich, S.; Daniels, A. D.; Strain, M. C.; Farkas, O.; Malick, D. K.; Rabuck, A. D.; Raghavachari, K.; Foresman, J. B.; Ortiz, J. V.; Cui, Q.; Baboul, A. G.; Clifford, S.; Cioslowski, J.; Stefanov, B. B.; Liu, G.; Liashenko, A.; Piskorz, P.; Komaromi, I.; Martin, R. L.; Fox, D. J.; Keith, T.; Al-Laham, M. A.; Peng, C. Y.; Nanayakkara, A.; Challacombe, M.; Gill, P. M. W.; Johnson, B.; Chen, W.; Wong, M. W.; Gonzalez, C.; Pople, J. A. *Gaussian 03, Revision B.02* **2004**, Gaussian, Inc., Pittsburgh PA, 2003.

(41)   Pangborn, A. B.; Giardello, M. A.; Grubbs, R. H.; Rosen, R. K.; Timmers, J. F. *Organometallics* **1996**, *15*, 1518-1520.

(42)   Alaoui, A. E.; Schmidt, F.; Monneret, G.; Florent, J.-C. *J. Org. Chem* **2006**, *71*, 9628-9636.

CHAPTER 3

BIS(DIARYLAMINO) DERIVATIVES WITH THIOPHENE-BASED BRIDGES

AND MIXED-VALENCE CHARACTER OF THEIR RADICAL CATIONS

3.1 Introduction

This chapter focuses on the properties of bis(di(4-alkoxyphenyl)amino) derivatives with thiophene-based bridges. In addition to synthesis and characterization of the compounds by UV-visible absorption spectroscopy and cyclic voltammetry, the properties of the radical cations of the bis(diarylamine)s were studied by visible-NIR absorption and ESR spectroscopy.

3.1.1 Relevance of Diarylamines to Optoelectronic Applications

Diarylamino donor groups are important building blocks in a wide range of molecules with interesting nonlinear optical (NLO) and electronic properties. Quadrupolar[1,2] and octupolar[3] chromophores in which two or three triarylamines are linked by a conjugated bridge have been shown to exhibit high two-photon absorption cross-sections. Such octupolar species have also been studied as second-order NLO chromophores.[4] Dipolar chromophores with 4-(diarylamino)phenyl or 5-(diarylamino)-2-thienyl donors are promising for second-order NLO applications. In this context, 4-(diarylamino)phenyl-based chromophores have been shown to be more stable than their dialkylamino analogues.[5-8] Dipolar compounds of this type have also been used for third-order NLO applications[9,10] and as two-photon absorbing chromophores.[11] Triarylamines, in particular 4,4'-bis(diarylamino)biphenyl derivatives, have been widely studied as hole-

transport materials for xerography, organic light-emitting diodes, and in photorfefractive polymers.[12] The strong visible and NIR absorptions of radical cations and dications of bis(triarylamine)s can be potentially exploited in optical pulse suppression applications.[13]

Additionally, compounds containing two or more diarylamino redox groups have been employed in studies of electronic coupling and delocalization. NIR intervalence charge-transfer (IVCT) absorptions have been analyzed in the framework of Marcus-Hush theory for mixed-valence (MV) radical cations of species in which diarylamino groups are linked by bridging groups based on benzene and other arenes,[14-17] biphenyl,[14,18] phenylene-ethynylene,[14,19-21] phenylene-ethenylene,[22,23] cyclophane-based,[24] organoplatinum,[25] and phosphonium[26] moieties. Some examples of bis(diarylamine)s with various end groups and conjugated bridges are shown in Figure 3.1 and are used for comparisons later in this chapter.

Figure 3.1. Some examples of previously synthesized bis(diarylamine) compounds.

3.1.2 Motivation for Studying Bis(diarylamine) Derivatives with Thiophene-based Bridges

Replacement of phenylene with thienylene has been found to lead to stronger donor-acceptor coupling in dipolar chromophores, as shown, for example, in first hyperpolarizability data,[27] due to the reduced aromaticity of thiophene relative to that of

benzene. Since thiophene also has a lower ionization potential than benzene, replacement of phenylene with less aromatic and more easily ionized thienylene groups might lead to more effective mediation of coupling between two diarylamino groups (as has been shown for the case where phenylene groups are replaced by donor-substituted phenylene groups[19,20]). Although the NIR absorption spectra of the radical cations of 5,5'-bis(diphenylamino)[2,2']bithiophene[28] (**IVb⁺**, Figure 3.1) and of 5,5"-bis[4-(di-4-tolylamino)phenyl]-[2,2';5',2"]terthiophene[29] have been reported, and the radical cations of bis{(di-(4-methoxyphenyl)amino}oligothiophenes have been studied computationally,[30] no detailed experimental investigation from the standpoint of mixed valency of a bis(diarylamino) system with a thiophene-based bridge has been published before this work.

This chapter focuses on the synthesis of new bis(diarylamine) systems with thiophene-containing bridges (Figure 3.2): *E*-1,2-bis(5-{di[4-(*n*-butoxy)phenyl]amino}-2-thienyl)ethylene (**1**), 2,6-bis{di[4-(*n*-methoxy)phenyl]amino}-2,2'-bithiophene (**2**), 2,6-bis{di[4-(*n*-butoxy)phenyl]amino}dithieno[3,2-*b*:2',3'-*d*]thiophene (**3**), *N*-(4-*tert*-butylphenyl)-2,6-bis{di[4-methoxyphenyl]amino}dithieno[3,2-*b*:2',3'-*d*]pyrrole (**4a**), and *N*-*tert*-butyl-2,6-bis{di[4-methoxyphenyl]amino}dithieno[3,2-*b*:2',3'-*d*]pyrrole (**4b**). Also included is analysis of the neutral compounds by UV-visible absorption spectroscopy and cyclic voltammetry (CV) experiments; characterization of the corresponding radical cations by visible-NIR and ESR spectroscopies; analysis of the radical cation visible-NIR spectra in the framework of Hush theory;[31] and comparison to other bis(diarylamine) radical cations.
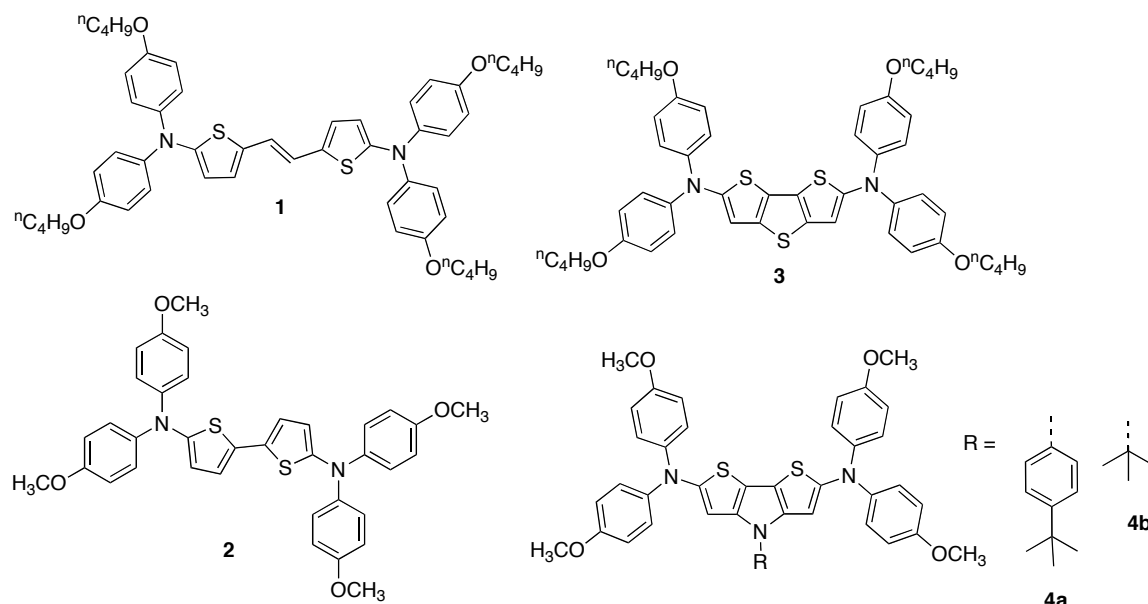
Figure 3.2. Bis(di(alkoxyphenyl)amine) derivatives with thiophene-based bridges.

3.1.2 Synthesis of Bis(di(4-alkoxyphenyl)amine) Derivatives

The syntheses of compounds **1-4** (Schemes 3.1 – 3.6) makes extensive use of palladium-catalyzed amination reactions.[32,33] Di[4-(*n*-butoxy)phenyl]amine (**7a**), an intermediate common to the synthesis of both compounds **1** and **3**, was obtained from the reaction of 1-bromo-4-(*n*-butoxy)benzene (**5**) and 4-(*n*-butoxy)aniline (**6**) using coupling conditions similar to those reported for the synthesis of bis(4-methoxyphenyl)amine (**7b**).[34] The reaction was complete after 1 hour of conventional heating. The product was obtained in good yield after recrystallization: 73% versus the yield of 89% yield reported for bis(4-methoxyphenyl)amine (**7b**) after 3 hours of heating.[34] The synthesis of compound **7a** was also carried out using single-mode microwave irradiation. However, this offered no particular advantage over conventional heating, giving a slightly lower yield and only a slightly reduced reaction time.

121

$O^nC_4H_9$ $O^nC_4H_9$ $^nC_4H_9O$ $O^nC_4H_9$

Br   +   NH$_2$ → (Pd(dppf)Cl$_2$, NaO^{t}Bu, PhMe, 73%) →   N / H

5   **6**   **7a**
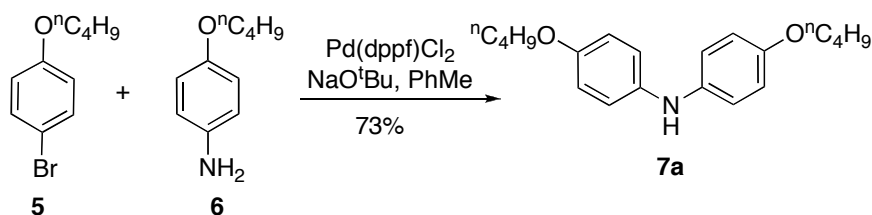
Scheme 3.1. Synthesis of di(*n*-butoxyphenyl)amine.

Although 2-(diarylamino)-3,4-diarylthiophenes have also been obtained from the reaction of *N,N*-2-triarylthioacetamides and 1-aryl-2-bromoethanones,[35] most published syntheses of 2-(diarylamino)thiophene derivatives have involved coupling of a diarylamine with a 2-halothiophene. Diphenylamine has been coupled with 2-halothiophenes, using a palladium source (Pd(OAc)$_2$[36,37] or Pd$_2$dba$_3$ {dba = dibenzylideneacetone}}[36]) in conjunction with P^{t}Bu$_3$ (36-78% from 2-bromothiophene[36-38]), or by using copper(I) iodide-mediated modified Ulmann conditions (40% yield from 2-iodothiophene).[39] Various other diarylamines including (4-alkoxyphenyl)amines have been coupled with α,α'-dibromo oligothiophenes and with 1,3-bis(5-bromothien-2-yl)benzo[*c*]thiophene in moderate yields using Pd(OAc)$_2$ / P^{t}Bu$_3$[40] or Pd(dppf)Cl$_2$ / dppf[41] (dppf = 1,1'-bis(diphenylphosphino)ferrocene) catalyst systems.

Initially the coupling of di(4-*n*-butoxyphenyl)amine (**7a**) with 2-bromothiophene (**8**) was attempted using Pd$_2$dba$_3$ / dppf as the catalyst system. Analysis of the reaction showed no evidence for the formation of desired 2-bis(4-*n*-butoxyphenyl)aminothiophene (**9**). However, compound **9** was successfully obtained after changing the catalyst system to Pd$_2$dba$_3$ / P^{t}Bu$_3$. The reaction was carried out both under conventional heating and in a

microwave reactor. After a few attempts in optimization of the conditions, analysis of the reaction mixtures showed that microwave heating could produce the desired product (**9**) in higher yields (95%) than conventional heating (73%). Moreover, under microwave conditions, fewer byproducts were obtained, which facilitated chromatographic isolation of the desired product (an oil). Consequently, microwave irradiation was used as the heating source for most of the subsequent reactions with 2-bromothiophene derivatives.
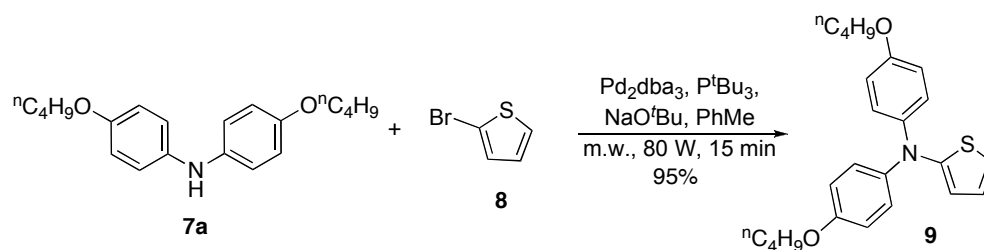
Scheme 3.2. Synthesis of 2-bis(4-*n*-butoxyphenyl)aminothiphene.

From compound **9**, the corresponding aldehyde (**10**) was readily obtained in good yield under Vilsmeier conditions, affording the pure product in 71% yield. Compound **10** can also be synthesized directly from the coupling of compound **7a** with 2-bromo-5-formylthiophene using Pd_2dba_3 / P^tBu_3 as a catalyst system. However, the formation of the desired aldehyde (**10**) was accompanied by a significant amount of the decarbonyated product (**9**). Compound **10** was reductively coupled under McMurry conditions to give the desired product (**1**) in moderate yield.
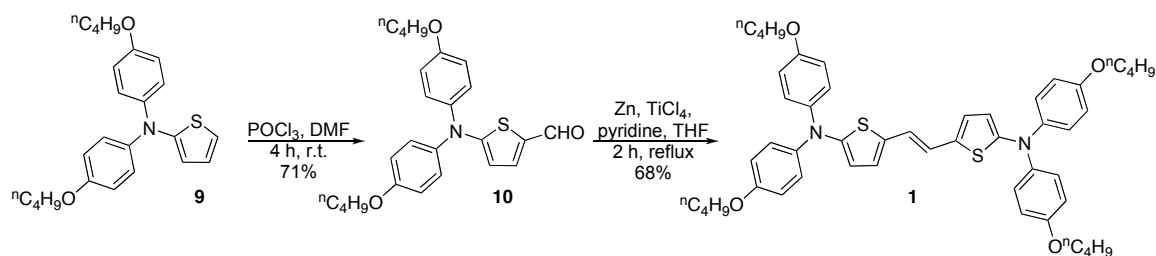
Scheme 3.3. Synthesis of bis(di(4-*n*-butoxyphenyl)amino-5-thien-2-yl)ethane.

In addition to its role as an intermediate in the synthesis of compound **1**, compound **10** is also of interest as a potential π-donor for dipolar chromophores, such as those used for electrooptic applications. Diarylamino-based donors would be expected to show superior thermal and photochemical stability to their dialkylamino analogues, [5-8] calculations suggest that di(4-alkoxyphenyl)amino-based donors show comparable π-donor strength to dialkylamino-based analogues,[42] and experimental[27] and theoretical[42] work suggests that the presence of the thienylene ring should lead to stronger donor-acceptor coupling than in phenylene analogues.

The same reagents were used to synthesize the previously reported[40] compound **2**, a yellow-orange solid, from 5,5'-dibromo-2,2'-bithiophene (**11**) and di(4-methoxyphenyl)amine (**7b**) in better yield (76% vs. 27%) than previously reported using Pd(OAc)$_2$ / P^{t}Bu$_3$.
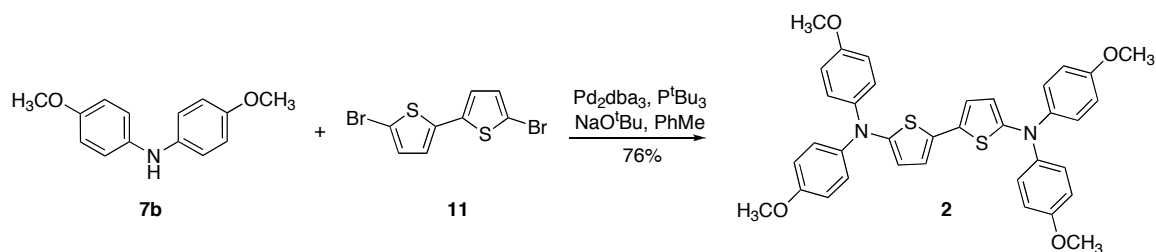
Scheme 3.4. Synthesis of bis(di(4-methoxyphenyl)amino)bithiophene.

Compound **3** was obtained in good yield as a glassy solid from the microwave-assisted palladium-catalyzed coupling of compound **7a** with 2,6-dibromodithieno[3,2-*b*:2',3'-*d*]thiophene (**12**), [43] which was prepared from bromination of the parent dithieno[3,2-*b*:2',3'-*d*]thiophene[44] with *N*-bromosuccinimide in chloroform / acetic acid. Additionally, the synthesis of bis(di(4-methoxyphenyl)amino[3,2-*b*:2',3'-*d*]thiophene (**3b**, not shown) was carried out using the same reagents with conventional heating, which is described in the experimental section.
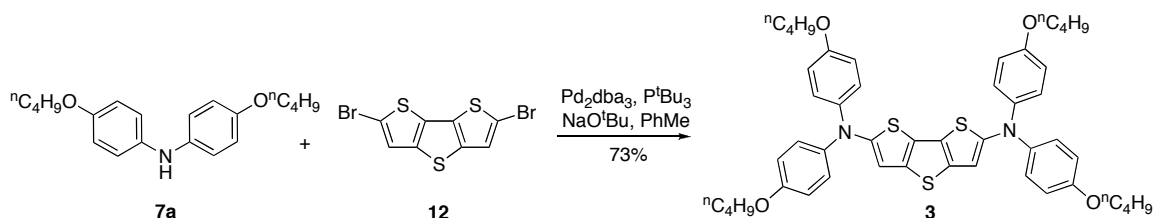
Scheme 3.5. Synthesis of 2,6-bis(di(4-*n*-butoxyphenyl)amino)dithienothiophene.

N-Substituted-dithieno[3,2-*b*:2',3'-*d*]pyrroles (**13a** and **13b**) were synthesized as described in Chapter 2. Treatment of compounds **13a** and **13b** with *N*-bromosuccinimide gave dibromides **14a** and **14b**, respectively, which were the first reported examples of 2,6-dibromo-dithieno[3,2-*b*:2',3'-*d*]pyrrole derivatives. As noted in Chapter 2, while the reaction was successful for *N*-aryl and *N*-*tert*-butyl species, analogues of **13b** with *n*-alkyl *N*-substitution decomposed under these conditions with no dibromo derivative isolable. Compounds **14a** and **14b** were converted to compounds **4a** and **4b**, respectively, using the same reagents used to form compounds **2** and **3**. However, in the synthesis of compounds **4a** and **4b**, microwave irradiation was not used due to the instability of the products.
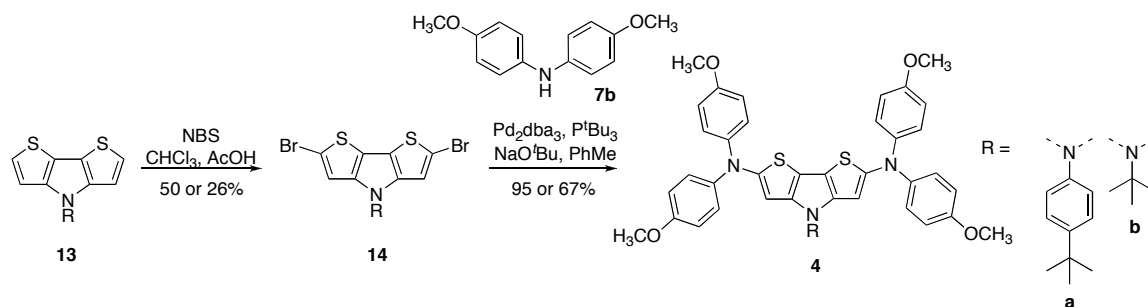
Scheme 3.6. Synthesis of 2,6-bis(di(4-methoxyphenyl)amino)dithienopyrrole derivatives.

3.1.2. Electronic Spectra of the Neutral Species

The UV-visible absorption spectra for the neutral species **1**, **2**, **3**, and **4a** are compared in Figure 3.3 (**4b** shows a very similar spectrum to **4a**, so it is shown separately).
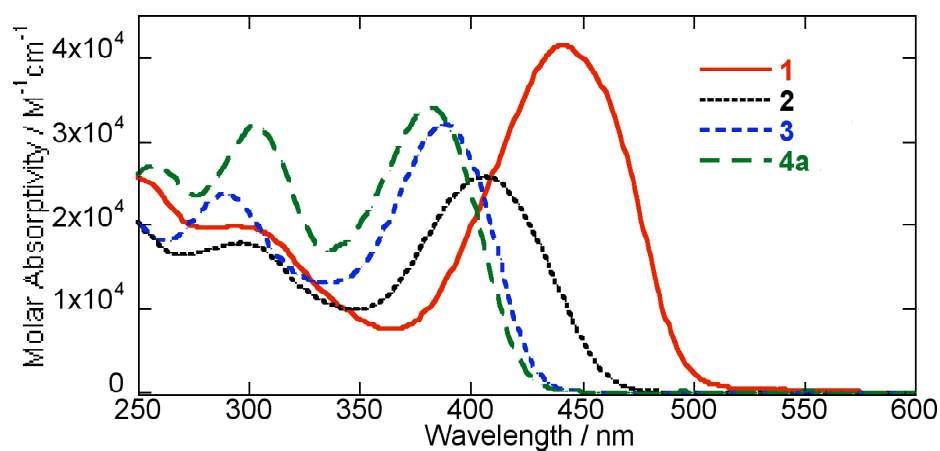
Figure 3.3. Molar absorptivities of bis(di(alkoxyphenyl)amine) derivatives **1**-**4a** in dichloromethane.

The UV-visible absorption spectra of compounds **4a** and **4b** in dichloromethane are very similar, which indicates that there is little effect of the *N*-substituent on the energy difference between the relevant orbitals associated with the visible absorption when the *N*-substituent is changed. The normalized spectra of both dithienopyrrole derivatives are shown below in Figure 3.4.
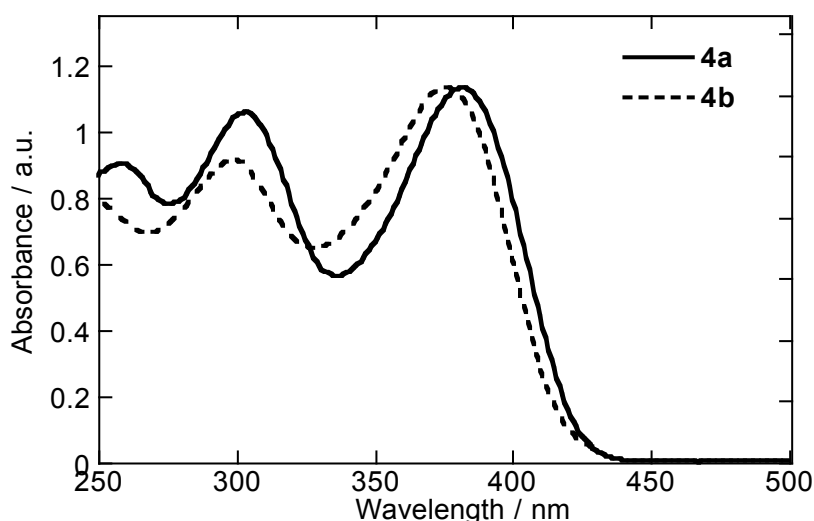
Figure 3.4. Normalized UV-visible absorption spectra of compounds **4a** and **4b** in dichloromethane.

The data for the lowest energy transitions are summarized in Table 3.1 along with transition dipole moments, μ_{ge}, estimated from the spectra. Data for the previously reported *E*-4,4'-bis{di-[4-(methoxy)phenyl]amino}stilbene (**I**)[23] are also included for comparison. Table 3.1 also includes absorption maxima and transition dipole moments obtained using time-dependent density functional theory (TD-DFT) for gas-phase **1**, **2**, **3**, **4a** and **I** (*n*-butyl groups were replaced by methyl for compounds **1** and **3**).

Table 3.1. Absorption maxima, absorptivities and transition dipole moments for the lowest-energy absorptions of the neutral compounds **1**, **2**, **3**, **4a**, and **I** in dichloromethane with TD-DFT gas-phase values[a] in italics.

Compound	λ_{max} ($\bar{v}_{max}$) / nm (cm^{-1})		ε_{max} / M^{-1}cm^{-1}	μ_{ge} / D	
1	442 (22600)	*488 (20500)*	41400	8.58	*11.9*
2	407 (24600)	*446 (22400)*	25800	6.57	*9.03*
3	388 (25800)	*420 (23800)*	32100	7.31	*8.79*
4a	382 (26200)	*412 (24300)*	34100	7.62	*8.31*
I	398 (25100[b])	*433 (23100)*	54900[b]	10.0[b]	*12.2*

[a] Computed with TD-DFT at the B3LYP/6-31G(d,p) level. [b] Data from reference.[23]

The calculated energies compare well with the experimental data, although are systematically underestimated by about 2000 cm^{-1} (this corresponds to less than 10% of the actual transition energy). The lowest energy transitions are seen for compound **1**, consistent with the expected effect of extending conjugation. Compounds **3** and **4a** show very similar transition energies, which are blue-shifted to that of compound **2**. This shift is presumably partly attributable to the destabilization of LUMOs of compounds **3** and **4a** from the central heteroatoms of the bridges. Both theory and experiment show larger transition dipole moments in the species with more extended conjugation, the vinylene-bridged compounds **1** and **I**, than in compounds **2**, **3** and **4a**, consistent with polarization of the transition along the long axis between the two amine groups.

The TD-DFT calculations show that that the lowest energy transition for each system is predominately a direct HOMO to LUMO excitation. The molecular orbitals involved in the transition are shown for each molecule in Figure 3.5, along with the HOMO–1, which is important in the spectra of the radical cations. In each case the HOMO and HOMO–1 are of opposite parity and can be regarded as an in- or out-of-phase linear combination of two diarylamine-based orbitals (dominated by nitrogen p-

orbitals). The HOMO orbital has significant bridge-based contributions from the local HOMO of the bridge, out of phase with those from the diarylamine-based orbitals. The LUMO in each case is principally bridge-based, resembling the LUMO of the isolated bridging moiety.
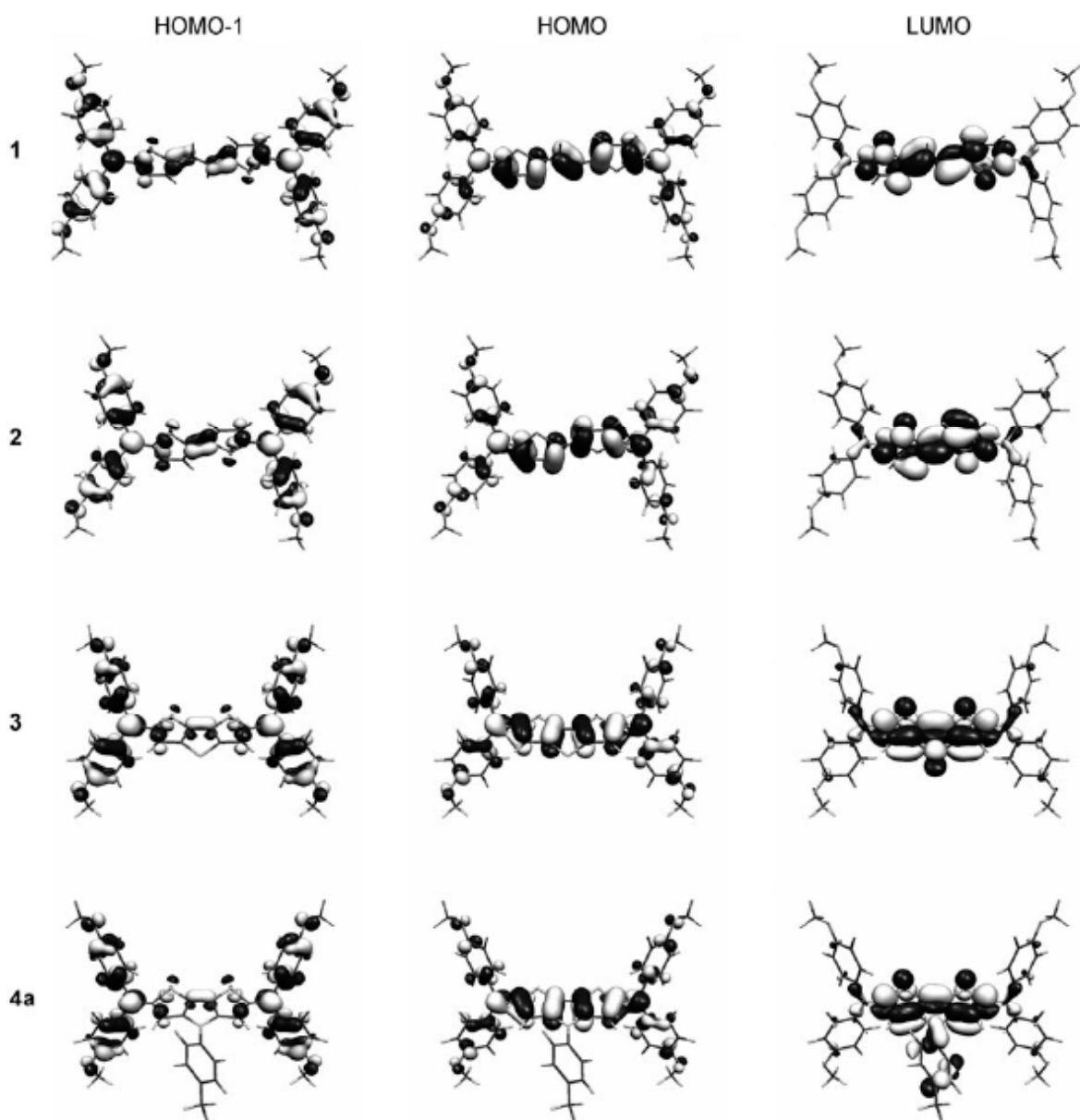
Figure 3.5. HOMO-1, HOMO, and LUMO for compounds **1**, **2**, **3**, and **4a** according to DFT calculations.

3.1.3. Electrochemistry of the Bis(diarylamino) Derivatives

In order to determine the ease of oxidation, cyclic voltammetry (CV) experiments were run for the bis(diarylamino) derivatives. Cyclic voltammograms of compounds **1**-**4** (Figure 3.6) indicate that all five compounds show two facile reversible oxidations at different potentials. In the voltammograms below, the compounds are shown along with cobaltocenium / cobaltocene as an internal reference (each time appearing at -1.32 V).
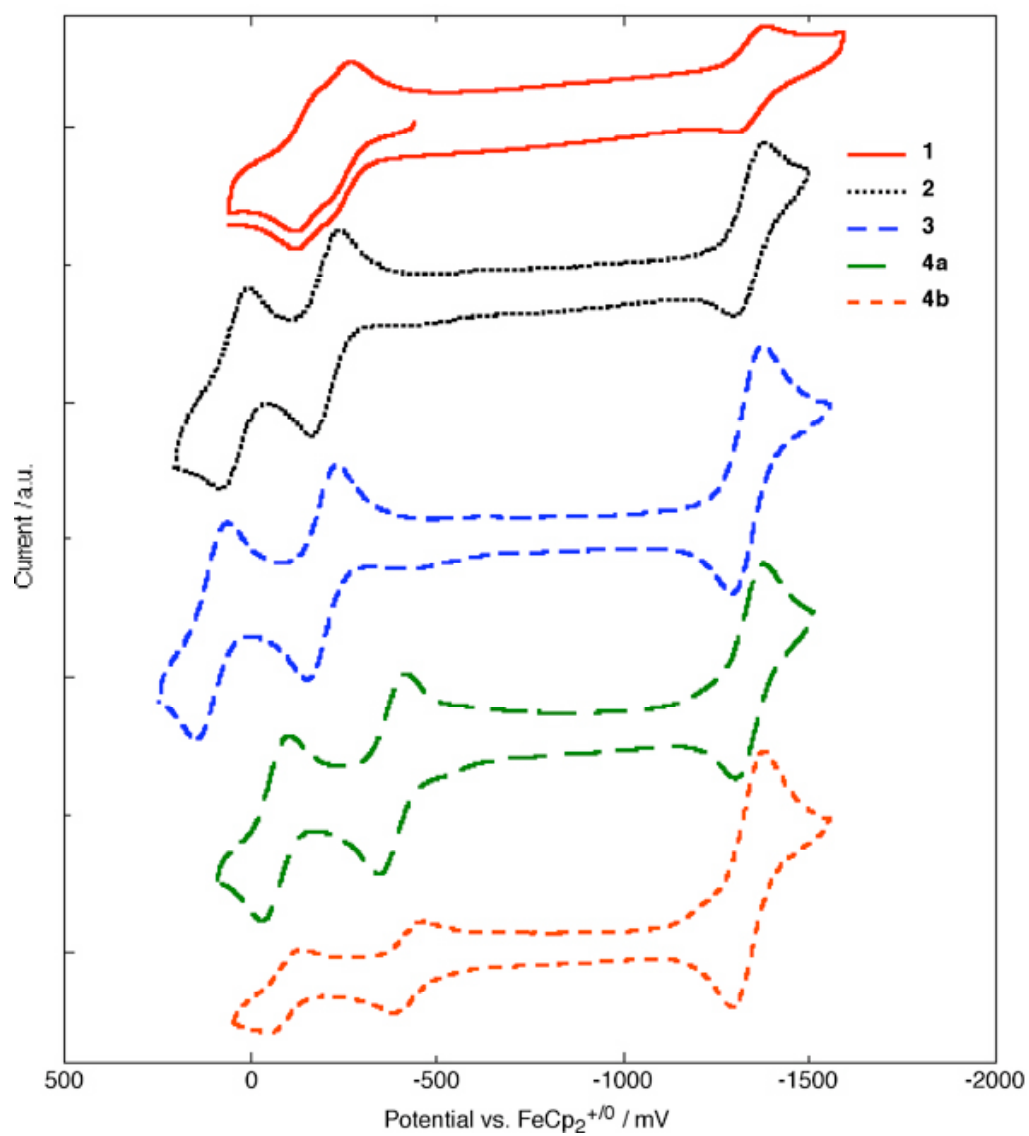
Figure 3.6. Cyclic voltammetry of compounds **1**-**4** in 0.1 M tetra-*n*-butylamino hexafluorophosphate in dichloromethane at 50 mV/s, shown with $Cp_2Co^{+/0}$ as the internal reference.

The oxidation potentials for compounds **1**-**4** are shown in Table 3.2; additionally Table 3.2 includes redox potentials of related bis[di-(4-(methoxy)phenyl]amine analogues,[23,40,45] the structures of which are shown in Figure 3.1. Comparisons with these analogs indicate compounds **1**-**4** are rather more readily oxidized than analogues with 1,4-phenylene, biphenyl-4,4'-diyl, or *E*-stilbene-4,4'-diyl bridges. The dithienopyrrole-based bridges results in the most electron-rich compounds, which are *ca*. 0.2 V more readily oxidized than their dithienothiophene-bridged analogues, consistent with the ionization potential of the simple pyrrole (8.2 eV) and thiophene (8.9 eV) heterocycles,[46] with the *N*-alkyl derivative (**4b**) being slightly more electron-rich than its *N*-aryl analogue (**4a**).

Table 3.2. Redox potentials for bis[di(4-alkoxyphenyl)amino] compounds determined by CV in 0.1 M tetra-*n*-butylammonium hexafluorophosphate in dichloromethane (CH$_2$Cl$_2$) or acetonitrile (CH$_3$CN).

	CH$_2$Cl$_2$			CH$_3$CN		
Compound	$E_{1/2}^{+/0}$	$E_{1/2}^{2+/+}$	$\Delta E_{1/2}$	$E_{1/2}^{+/0}$	$E_{1/2}^{2+/+}$	$\Delta E_{1/2}$
1	−0.23	−0.14	0.09	−0.22[a]		a
2[b]	−0.20	−0.04	0.16	−0.14	-0.02	0.12
3	−0.19	+0.13	0.32	−0.19	+0.03	0.22
4a	−0.40	−0.08	0.32	−0.31	−0.07	0.24
4b	−0.43	−0.10	0.33	−0.37	−0.15	0.22
I[c]	+0.08	+0.22	0.14	–	–	–
IIa[d,14]	+0.09	+0.31	0.22	–	–	–
IIIa[d]	−0.15	+0.34	0.49	–	–	–

[a] Separation not resolvable. [b] Values for **2** in acetonitrile / 0.1 M [^{n}Bu$_4$N]$^+$[PF$_6$]$^-$ reported in reference[40] are similar. Potentials for **IVa**, **IVb**, and longer Ph-terminated species in benzonitrile / 0.1 M [^{n}Bu$_4$N]$^+$[PF$_6$]$^-$ are reported in reference.[28] [c] Data for reference.[23] [d] Data from reference. [14]

The difference between the first and second redox potentials, $\Delta E_{1/2}$, for all four compounds is greater in the less polar solvents, consistent with the predictions of the dielectric continuum model for the electrostatic contribution to $\Delta E_{1/2}$.[47] This model assumes that the more polar solvents stabilize the positive and negative charges, therefore resulting in the second oxidation occurring at lower potentials due to the stabilization of the first positive charge. Although $\Delta E_{1/2}$ values have often been used as measures of electronic coupling in MV species, it has been shown that they provide a very poor guide and must be used with extreme caution.[48] The values of $\Delta E_{1/2}$ in Table 3.2 show no clear relation with the couplings, V, in Table 3.3 (see later discussion of this table). However, it is worth noting that the $\Delta E_{1/2}$ values for compounds **3**, **4a**, and **4b** are rather large compared to many of the other species included in the table, indicating that the corresponding radical cations are relatively stable to disproportionation.

3.1.4. Electronic Spectra of the Radical Monocations of Bis(diarylamine) Derivatives

As in previously reported studies, the radical cations of compounds **1**-**4** were generated in dichloromethane solution by addition of the excess diamine to a solution of tris(4-bromophenyl)aminium hexachloroantimonate.[22,23,25,49] The visible-NIR absorption spectra of the resulting solutions are shown in Figure 3.7.
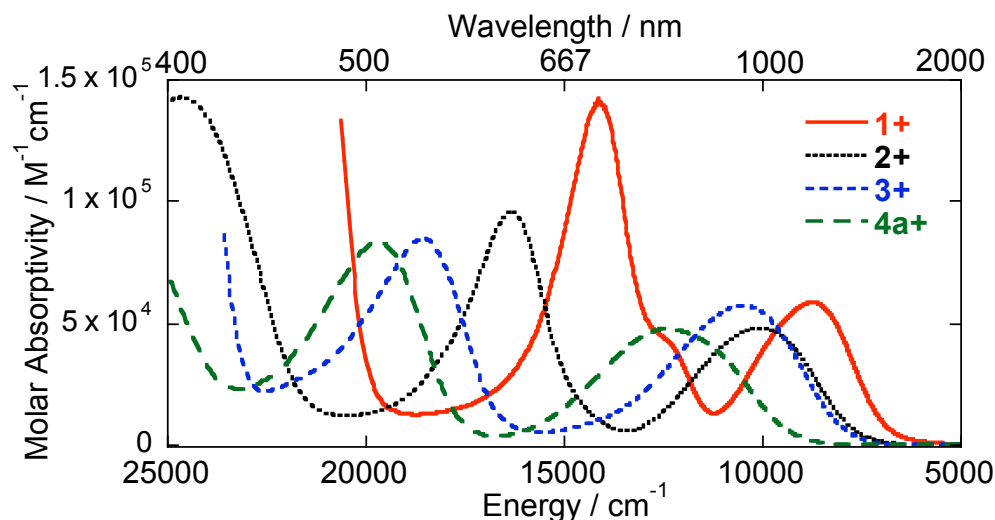
Figure 3.7. Visible-near-IR absorption spectra of monocations **1-4a$^+$** in dichloromethane. The onsets of strong absorption at high energy (at *ca.* 20000 for **1$^+$** and *ca.* 23000 cm^{-1} for **2$^+$**, **3$^+$** and **4a$^+$**) correspond to absorption by the excess neutral diamines present; the absorptivity scale applies only to the lower energy absorptions attributable to the radical cations.

Radical cations **4a$^+$** and **4b$^+$** show very similar spectra, the similarity reflecting the lack of pyrrole nitrogen contributions to the relevant orbitals (Figure 3.8). For clarity the spectrum for **4b$^+$** was not shown in Figure 3.7.
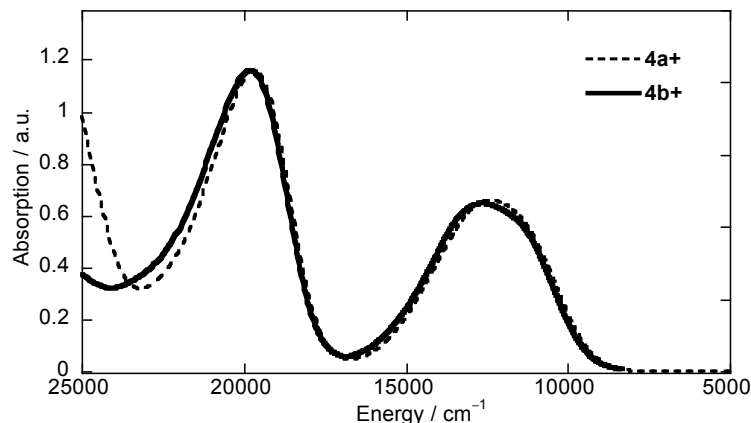
Figure 3.8. Normalized visible-near-IR absorption spectra of monocations **4a$^+$** and **4b$^+$** in dichloromethane. The onsets of strong absorption at high energy (at ca. 23000 cm^{-1}) correspond to absorption by the excess neutral diamines present.

Monocations **1⁺-4⁺** show intense absorption bands in the NIR region that are similar in terms of energy and, absorptivity and lineshape to the IVCT absorptions previously observed for other strongly coupled bis(diarylamine) monocations, data for some examples of which are also included in Table 3.3. Specifically, the bandwidths at half height, $\bar{\nu}_{1/2[obs]}$, are narrower than the width predicted by Hush theory for a class-II MV species according to:

$$\bar{\nu}_{1/2[Hush]} = \sqrt{2310 \times \bar{\nu}_{max}} \qquad (3.1)$$

where both $\bar{\nu}_{1/2[Hush]}$ and $\bar{\nu}_{max}$ are in cm⁻¹. In the case of radical cations **1⁺**, **3⁺**, and **4⁺**, the bands are strongly asymmetric (as gauged by $\bar{\nu}_{1/2[high]}/\bar{\nu}_{1/2[low]}$), with twice the bandwidth on the high-energy side being in the vicinity of the Hush limit, $\bar{\nu}_{1/2[Hush]}$. These asymmetric lineshapes were originally interpreted in terms of a cut-off on the low-energy side of the band due to the thermal population of the electron-transfer barrier top.[14][50] Definitively localized class II bis(diarylamino) MV systems show more-or-less symmetrical Gaussian IVCT bands that have widths in excess of that predicted by equation 3.2.[14,22,23,26,51,52] According to this model, this situation is predicted for any system belonging to Robin and Day's class II[53] (valence-localized) but lying very close to the borderline with class III (delocalized), i.e. with a low barrier to intramolecular electron transfer. Subsequent work suggested that these lineshapes could also arise from coupling of the electron transfer in class-III and class-II/class-III borderline systems to symmetric vibrations.[54] A number of other bis(diarylamine) MV cations have been found to exhibit similar lineshapes. Crystallographic and vibrational studies[15,23,55] and variable-temperature measurements of the IVCT band shape[56] support the latter of the two

interpretations. Although the near-IR absorptions of radical cations **4a⁺** and **4b⁺** are also consistent with delocalized structures in that both $\bar{v}_{1/2[obs]}$ and $\bar{v}_{1/2[high]}$ are well below $\bar{v}_{1/2[Hush]}$, the bands are the broadest of the species under consideration ($\bar{v}_{1/2[obs]}$ over 600 cm^{-1} greater than for the next broadest, that of radical cation **3⁺**) and are considerably less asymmetric as gauged by $\bar{v}_{1/2[high]}/\bar{v}_{1/2[low]}$ (compare the values of 1.34 and 0.95 for radical cations **3⁺** and **4⁺**, respectively). Thus, the characteristics of the low-energy near-IR absorptions strongly support the assignment of radical cations **1⁺**-**4⁺** to Class III, along with the previously studied radical cation **I⁺**.

The DFT geometry optimization results (see supporting information for details) of the radical cations **1⁺**, **2⁺**, **3⁺**, **4a⁺** and **I⁺** also suggest all these systems should be assigned to class III. While use of DFT often leads to overdelocalization and, therefore, may suggest a symmetric class-III structure for a class-II species, it has previously been found to give good agreement with structural and spectroscopic features when applied to species shown experimentally to belong to class III.[15,18,23] The TD-DFT transition energies and transition dipole moments are included in Table 3.3. The calculated energies are slightly overestimated for the ethylene-bridged species **1⁺** and **I⁺** and slightly underestimated for **2⁺** and for the fused-ring species **3⁺** and **4a⁺**, with the variation in $\bar{v}_{max}$ between compounds being well-reproduced. This further supports the assignment of the cations to class III. The transition dipole moments are generally less well-reproduced by TD-DFT calculations than in the case of the corresponding neutral species.

In all cases, the TD-DFT results indicate that the lowest energy transition is dominated by a SOMO–1 to SOMO transition, with other configurations playing a slightly more important role in the more extended species. The SOMO and SOMO–1 of

the radical cations very closely resemble the HOMO and HOMO–1, respectively, of the neutral species (see Figure 3.4). Thus, the transition is between combinations of diarylamino-based orbitals (dominated by amine nitrogen p-orbitals) with opposite parity, this orbital picture closely resembling that previously reported for other delocalized bis(diarylamino) radical cations,[15,18,29,30,57,58] and thus supporting the identification of the lowest energy band in $\mathbf{1^+}$-$\mathbf{4^+}$ as IVCT transitions.

The electronic structure calculations also provide some insight into the differences in experimental band shapes. The relaxation energy associated with the lowest excited state of the radical cations was estimated using DFT to be 2873 cm^{-1}, 3480 cm^{-1}, 3331 cm^{-1}, and 3943 cm^{-1} for radical cations $\mathbf{1^+}$, $\mathbf{2^+}$, $\mathbf{3^+}$, and $\mathbf{4a^+}$, respectively, and, thus, follow a similar trend as seen in experimental values of $\bar{v}_{1/2[\text{obs}]}$ (2720 cm^{-1}, 3338 cm^{-1}, 3640 cm^{-1}, and 4260 cm^{-1}, respectively). Thus the increase in the bandwidth when going from radical cations $\mathbf{3^+}$ to $\mathbf{4a^+}$ could be related to a significant (about 600 cm^{-1}) increase in the corresponding relaxation energy. Usually larger relaxation energies result in a more symmetric (Gaussian-like) band shape, which is consistent with the broader, more symmetric, lineshape of the IVCT of radical cation $\mathbf{4a^+}$ relative to that of $\mathbf{3^+}$.

3.1.5. Calculation of the Electronic Coupling of the Radical Cations of the Bis(diarylamine) Derivatives

According to Hush theory the electronic coupling, V, between two redox centers can be obtained from the transition dipole moment, μ_{ge}, and the absorption maximum, $\bar{v}_{\text{max}}$, of the IVCT band of the MV species according to

$$V = \frac{\mu_{ge}\bar{\nu}_{max}}{eR} \tag{3.2}$$

where e is the electronic charge and R is the diabatic electron-transfer distance, i.e. the distance between donor and acceptor in the absence of any electronic coupling.[59][60] In the case of Class-III MV systems, the coupling can also be obtained directly from the IVCT maximum:

$$V = \bar{\nu}_{max}/2 \tag{3.3}$$

Estimates of V from eq 3.2, obtained by assuming R to be the geometric N—N separation, are given in Table 3.3, along with values from eq 3.3. According to either estimate, radical cations $\mathbf{1^+}$, $\mathbf{2^+}$, $\mathbf{3^+}$, and $\mathbf{4a^+}$ all show rather large couplings, as one would anticipate from the electron-rich character of the thiophene-containing bridges. Comparison of the dithienylethylene derivative with the stilbene species ($\mathbf{1^+}$ and $\mathbf{I^+}$), respectively, or of the bithophene and biphenyl species ($\mathbf{2^+}$ and $\mathbf{IIa^+}$), respectively, shows that replacement of phenylene with thienylene groups leads to increased coupling. The coupling suggested by equation 3.3 in the dithienopyrrole-bridged species ($\mathbf{4a^+}$), is the strongest yet reported for a bis[di(4-alkoxyphenyl)amino] MV species inlcuding $\mathbf{IIIa^+}$ (a stronger coupling of $V_{[eq3]} = 5790$ cm^{-1} is obtained for the 1,4-bis(diphenylamino)benzene radical cation ($\mathbf{IIIb^+}$)[15] emphasizing that the relative electron-richness of the bridge and end groups is important, while a value of $V_{[eq3]} = $ ca. 5550 cm^{-1} for $\mathbf{IVb^+}$ can be deduced from the published spectrum[28]). For all the compounds in Table 3.3, the couplings estimated according to equation 3.2 are signficantly smaller than those obtained from equation 3.3. This discrepancy is at least partly attributable to the nitrogen—nitrogen separation being greater than the true diabatic electron-transfer distance; i.e. the redox centers cannot be regarded as centered on the nitrogen atoms, but are displaced somewhat

into the bridge. Assuming the validity of equations 3.2 and 3.3, the appropriate values of R would have to be approximately half to two-thirds of the geometric nitrogen—nitrogen separation. In view of the reduced adiabatic electron-transfer distances in all these species, it is interesting to ask to what extent these species can still be regarded as diamino MV species, rather than being "bridge-oxidized" species. To obtain information pertinant to this question, the monocations were next examined by ESR.

Table 3.3. Parameters from the low-energy near-IR absorptions of radical cations **1⁺**, **2⁺**, **3⁺**, **4a⁺** and other symmetric bis[di(4-alkoxyphenyl)amino] radical cations in dichloromethane or, for **IIa⁺** and **IIIa⁺**, dichloromethane / 0.1 M [$^nBu_4N$]⁺[PF_6]⁻ with some values from TD-DFT calculations[a] in italics.

	$\bar{v}_{max}$/cm^{-1}		ε_{max}/ M^{-1}cm^{-1}	$\bar{v}_{1/2[obs]}$/ cm^{-1}	$\bar{v}_{1/2[Hush]}^b$/ cm^{-1}	$\bar{v}_{1/2[high]}$/ $\bar{v}_{1/2[low]}^c$	$\bar{v}_{1/2[high]}$/ $\bar{v}_{1/2[Hush]}^d$	μ_{ge} / D		$V_{[eq2]}^e$/ cm^{-1}	$V_{[eq3]}$/ cm^{-1}
1⁺	8750	*9480*	56500	2720	4500	1.37	0.70	13.0	*9.3*	2150	4375
2⁺	10100	*10020*	47900	3338	4830	1.17	0.75	12.3	*9.6*	2820	5050
3⁺	10500	*10300*	57100	3640	4920	1.34	0.85	14.0	*10.4*	3400	5250
4a⁺	12500	*11600*	49000	4260	5380	0.95	0.77	12.3	*9.7*	3480	6270
I⁺	6080[f]	*6980*	39300[f]	2760[f]	3750[f]	1.40[f]	0.86	13.5[f]	*15.5*	1400	3020
IIa⁺	6360[g]	*6920[h]*	28000[g]	3170[g]	3830	1.45[g]	0.98	11.6[g]	*14.5[h]*	1550	3180
IIIa⁺	9350[g]	*9250[h]*	22700[g]	3640[g]	4647	1.76[g]	0.99	9.17[g]	*10.1[h]*	3240	4675

[a] B3LYP/6-31G(d,p) level. [b] Calculated using eq 1. [c] Ratio of bandwidth on high-energy side to that on low-energy side. [d] Ratio of twice the band of the high-energy side to the bandwidth from eq 1. [e] Estimated from eq 2 using the experimental values of $\bar{v}_{max}$ and μ_{ge} and the geometric N—N distance. [f] Data taken from reference [22,23]. [g] Data from reference [14]. [h] TD-DFT values from reference [54].

3.1.6 Electron-Spin Resonance of Radical Cations of the Bis(diarylamine) Derivatives

Room temperature X-band ESR spectra were acquired for the same dichloromethane solutions of radical cations **1⁺-4⁺** used for measurement of the visible-NIR absorption spectra. The ESR spectra show more resolvable coupling than the spectra of bis(diarylamino) MV species that have been previously reported.[22,23,25] The spectra are of monocations **1⁺-4a⁺** are shown in Figure 3.9. The spectra are reminiscent of those of the radical cations of bis(diphenylamino)-terminated oligothiophenes such as the monocations of **IVa⁺** and **IVb⁺** (structures in Figure 3.1), where coupling constants to the $I = 1$ (^{14}N nuclei) and the $I = \frac{1}{2}$ (^{1}H nuclei) of the bridging ligand are of comparable magnitude.[28] Figure 3.9 shows the spectra, along with the previously reported spectrum of monocation **I⁺**,[22] and spectra simulated using WinSim. In all cases, the spectra are centered at $g = 2.004$, a typical value for triarylamine radical cations.[61] In each case the spectra were fitted by assuming coupling to two equivalent ^{14}N nuclei and to varying numbers of pairs of ^{1}H nuclei (i.e., assuming the cations to be symmetrical, at least on a timescale of $>10^{-7}$ s.
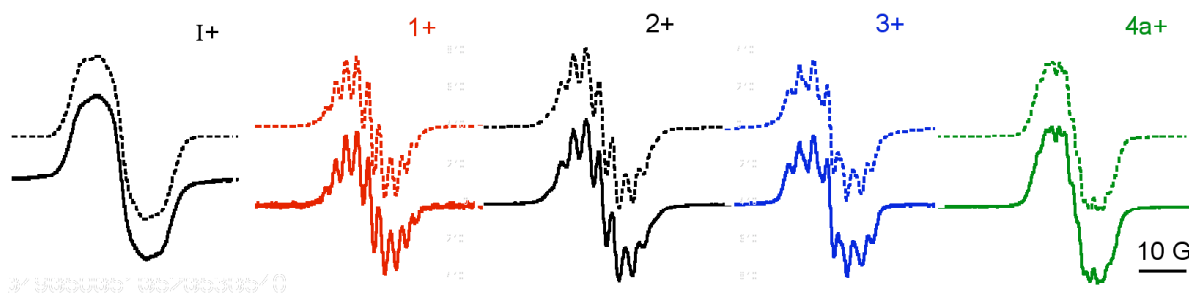
Figure 3.9. Experimental X-band ESR Spectra (lower, red solid line) of monocations **I⁺** and **1⁺**-**4a⁺** in dichloromethane with simulations (upper, blue dotted line) used to obtain coupling constants.

The ESR spectra for the radical cations **4a⁺** and **4b⁺** are essentially identical, indicating that the spin density is relatively small on the nuclei of the *N*-substituent of the dithienopyrrole ring of these radical cations. The ESR spectra of the monocations of **4a⁺** and **4b⁺** are shown in Figure 3.10, on the same scale for x-axis but offset to show each spectral shape clearly.
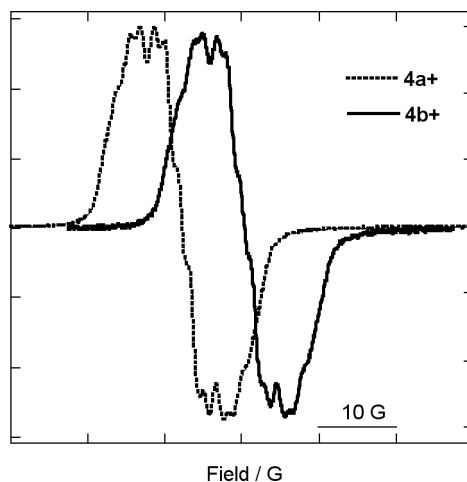
Figure 3.10. Experimental X-band ESR spectra of monocations **4a⁺** (left) and **4b⁺** (right) in dichloromethane offset on the x-axis.

The coupling constants obtained from the simulation are given in Table 3.4. Values obtained from DFT calculations, also given in the table, are in good agreement

with the experimental data, and allow assignment to the resolvable ^{1}H coupling, as indicated in Table 3.4. Moreover, the good agreement between experimental and DFT coupling constants suggests that DFT describes the spin distribution in the radical cations well and justifies using DFT spin densities as a means of assessing the degree to which the oxidation can be regarded as amine-based.

Table 3.4. Experimental and theoretical (italics) ESR hyperfine coupling constants (G) for some bis[di(4-alkoxyphenyl)amino] radical cations.[a]

	1^+		2^+		3^+		$4a^+$		I^+	
$A_{N(a)}$	2.68	*2.91*	3.20	*3.30*	3.44	*3.43*	3.17	*3.15, 3.18*	3.80[c]	*3.65*
$A_{H(a)}{}^b$	2.00	*1.90*	2.70	*2.45*	2.15	*1.85*	1.24	*1.17, 1.20*	d	*0.76, 0.82[e]*
$A_{H(b)}{}^b$	2.28	*2.09*	2.20	*2.13*	–	–	–	–	d	*0.26, 0.30[e]*
$A_{H(c)}{}^b$	1.90	*1.79*	–	–	–	–	–	–	d	*0.82*
$A_{N(b)}{}^f$	–	–	–	–	–	–	1.61	*1.22*	–	–

[a] Calculated values, from open-shell DFT at the B3LYP/6-31G(d,p) level, are absolute values of the isotropic Fermic contact couplings whereas the experimental values are moduli, $|A|$. [b] H(a), H(b), and H(c) are defined in Figure 3.8.[c] Previously a somewhat larger value was reported[22] for this coupling constant by inspection of the experimental spectrum; however, the spectra are better simulated with the present value.[d] Not resolvable in the experimental spectrum.[e] The first and second values are H(a/b) and H(a'/b') respectively.[f] This nitrogen is that in the pyrrole ring of **4a**⁺.

Figure 3.11 shows the labeling scheme for the structures of the monocations for which hyperfine coupling constants are reported in Table 3.4.
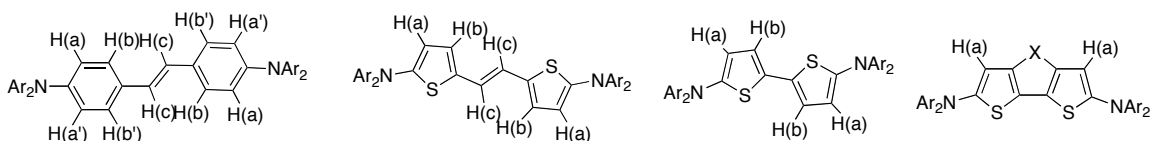
Figure 3.11. Labeling scheme for ^{1}H and ^{14}N nuclei for which coupling constants are given in Table 3.4.

A value of A_N = 8.97 G has been reported for the radical cation of tri(4-methoxyphenyl)amine ($[(p\text{-MeOC}_6\text{H}_4)_3\text{N}]^+$) in acetonitrile.[62] Thus, a notional class-III (or rapidly exchanging) MV system consisting of two such redox centers would be expected to show A_N = ca. 4.5 G. The experimental (and calculated) A_N values are lower, decreasing in the order $\mathbf{I^+} > \mathbf{3^+} > \mathbf{2^+} > \mathbf{4a^+} > \mathbf{1^+}$, suggesting the total spin density for the two ^{14}N atoms is reduced relative to that in $[(4\text{-MeOC}_6\text{H}_4)_3\text{N}]^+$, consistent with the bridge character of the oxidation increasing in the order $\mathbf{I^+} < \mathbf{3^+} < \mathbf{2^+} < \mathbf{4a^+} < \mathbf{1^+}$. DFT-calculated spin densities (see Table 3.5 and Supporting Information) are consistent with this picture. Even in $\mathbf{I^+}$ there is considerably more spin density on the stilbene bridge than on the terminal aryl groups, consistent with the shift of the diabatic states into the bridge suggested by the NIR data and with the appearance of the SOMO (corresponding to the HOMO of the neutral species shown in Figure 3.5). In the thiophene-containing radical cations, the spin density on the bridge is increased at the expense of that on nitrogen and that on the terminal aryl groups with the bridge character increasing in the same order as deduced from the values of A_N. Nevertheless, the calculations indicate the amino nitrogen atoms bear greater spin density than any of the other atoms, suggesting that, although the bridge character of the oxidation is increased in monocations $\mathbf{1^+}$ - $\mathbf{4^+}$ relative

145

to that in analogues such as **I⁺**, the species with thiophene-based bridges can still be regarding as having significant MV diamine character.

Table 3.5. DFT-calculated Spin Densities for Different Portions of the Radical Cations of **1⁺**, **2⁺**, **3⁺**, **4a⁺**, and **I⁺**.

	1⁺	**2⁺**	**3⁺**	**4a⁺**	**I⁺**
Terminal Aryl	0.12	0.15	0.17	0.13	0.27
Amino N atoms	0.25	0.28	0.29	0.27	0.31
Bridging group	0.63	0.57	0.54	0.60	0.42

3.2 Summary of the Analysis of Bis(diarylamine)s and Their Radical Cations

Di(4-alkoxyphenyl)amines can be coupled to bromothiophene and related derivatives in good yield under palladium-catalyzed conditions. At least in some cases, microwave irradiation leads to improved yields and fewer side reactions. Five bis[di(4-alkoxyphenyl)amino] species with thiophene-based bridges have been synthesized. The ease of oxidation of these materials may lead to potential application as hole-injection materials in organic light-emitting diodes, while the 5-[di-(4-*n*-butoxyphenyl)amino]-2-formylthiophene intermediate used in the synthesis of one of these compounds has potential utility as a stable and potent π-donor for incorporation into electrooptic chromophores. The radical cations of the bis[di(4-alkoxyphenyl)amine] compounds have been generated. Their NIR spectra are indicative of strong coupling between the two redox centers, stronger than that observed in species with phenylene-based bridging groups of comparable length. This can be attributed to high-lying orbitals of the thiophene-based bridging units. ESR spectroscopy and quantum-chemical calculations indicate increased spin density on the bridging groups than in comparable species with

phenylene-based bridges, with a concommitant reduction in spin density on the amino nitrogen centers.

3.3. Experimental Details for Chapter 3

3.3.1 Computational Methods

Note: All DFT and TD-DFT calculations in this chapter were performed by Kelly Lancaster and Vaeceslav Coropceanu in the research group of Prof. Jean-Luc Brédas at Georgia Institute of Technology.

The geometries of the bis(diaryl)amine compounds of the neutral and radical cation ground and first excited states were optimized at the DFT level. The excitation energies and transition dipole moments of the low-lying excited states were calculated at the TD-DFT level. All DFT and TD-DFT calculations are performed using with the 6-31G(d,p) split valence plus double polarization basis set[63-66] and with the B3LYP functional.[67,68] All calculations were carried out using the Gaussian 03 suite of programs.[69]

Simulations of EPR experiments were accomplished using WinSim, a simulation program for Windows, which is currently provided for free download at the National Institutes for Environmental Health Sciences of the National Institutes of Health website at http://www.niehs.nih.gov/research/resources/software/tools/index.cfm.

3.3.2 General Experimental Methods

Starting materials were reagent grade and were used without further purification unless otherwise indicated. Starting materials were purchased from Acros Chemical Co. except for tris(dibenzylideneacetone)dipalladium(0) (Pd$_2$dba$_3$) and tri-*tert*-butylphosphine solution in hexane, both of which were purchased from Strem Chemicals, Inc. Solvents were dried by passing through columns of activated alumina in a manner similar to that described in the literature (tetrahydrofuran, toluene, dichloromethane)[70] or by distillation from calcium hydride (acetonitrile), or were obtained as anhydrous grade from Acros Organics. Chromatographic separations were performed using standard flash column chromatography methods using silica gel purchased from Sorbent Technologies (60 Å, 32-63 μm) or basic alumina purchased from Aldrich Chemical Company. Elemental analyses were performed by Atlantic Microlabs. The microwave used was a CEM Discover Labmate. Mass spec FAB was performed on a VG Instruments 70SE. GCMS data were acquired on an Agilent 5790 GC/ 6850 MS. Electrochemical measurements were carried out under nitrogen in dry deoxygenated dichloromethane or acetonitrile solutions ca. 10^{-4} M in analyte and 0.1 M in tetra-*n*-butylammonium hexafluorophosphate using a BAS 100 W Potentiostat, a glassy carbon working electrode, a platinum auxillary electrode, and, as a pseudo-reference electrode, a silver wire anodized in 1 M aqueous potassium chloride. Potentials were referenced to ferrocenium / ferrocene at 0 V by using cobaltocenium hexafluorophosphate (–1.32 V in dichloromethane) or decamethylferrocene (–0.52 V in acetonitrile) as an internal reference (since many of the redox events of interest were at similar potentials to that of ferrocene). Cyclic voltammograms were recorded at a scan rate of 50 mVs^{-1}. UV-visible-NIR spectra were recorded in 1 cm cells using a Varian Cary 5E spectrometer. Room-temperature ESR

spectra were acquired using a Bruker EMX spectrometer. Monocation solutions (*ca.* 0.00005 M) visible-NIR and ESR spectroscopy were generated by addition of < 0.1 eq. tris(4-bromophenyl)aminium hexachloroantimonate (Aldrich) in dry dichloromethane; absorptivities were calculated assuming all of the oxidizing agent added resulted in formation of monocation and that disproportionation is negligible at these concentration ratios.

3.3.3 Synthesis of Bis(diarylamine) Derivatives and Precursors

*Note: Some of the compounds reported in this section (specifically compounds **1**, **3**, **7a**, **9**, and **10**) were initially synthesized by Luca Beverina with the assistance of Natalie Thompson in the research group of Prof. Seth Marder at Georgia Institute of Technology. Kelly Lefler, also in the same research group, provided assistance with synthesis and characterization (specifically with the resynthesis of compound **4a**).*

Di(4-methoxyphenyl)amine (7b). This compound was synthesized as described in the literature.[34] ^{1}H NMR (300 MHz, C_6D_6) δ 6.81 (d, J = 9.3 Hz, 4H), 6.75 (d, J = 9.0 Hz, 4H), 4.75 (s, 1H), 3.35 (s, 6H). ^{13}C NMR (75 MHz, C_6D_6) δ 154.8, 138.4, 119.8, 115.0, 55.1.

Di(*n*-butoxyphenyl)amine (7a), conventional heating. To a 100 mL round-bottomed flask was added anhydrous deoxygenated toluene (50 mL), 4-*n*-butoxyaniline (**6**, 8.4 g, 51 mmol), and 1-bromo-4-*n*-butoxybenzene (**5**, 11.6 g, 50 mmol) under nitrogen. Then tris(dibenzylideneacetone)dipalladium   (0)   (0.46   g,   0.50   mmol),   1,1'-

bis(diphenylphosphino)ferrocene (0.56 g, 1.0 mmol), and sodium *tert*-butoxide (6.0 g, 62 mmol) were added. A reflux condenser was attached, and the reaction solvent was brought to reflux. After one hour, the reaction appeared complete by TLC. The reaction mixture was cooled, and hexanes (50 mL) was added. The resulting mixture was run through a short pad of silica gel, eluting with hexanes (1 L) to remove any starting bromide, and then with hexanes / ethyl acetate (9:1, 2 L) to give the crude product (15.7 g), which was crystallized from boiling hexanes to give an off-white semicrystalline solid (11.45 g, 73%). ^{1}H NMR (300 MHz, C_6D_6) δ 6.84 (s, 8H), 3.67 (t, *J* = 6 Hz, 4H), 1.60 (quintet, *J* = 8 Hz, 4H), 1.36 (m, 4H), 0.83 (t, *J* = 7 Hz, 6H). ^{13}C{^{1}H} NMR (100 MHz, acetone-d_6) δ 154.1, 139.2, 119.5, 116.0, 68.5, 32.2, 19.9, 14.1. HRMS-EI (*m/z*) [M]$^+$ calcd for $C_{20}H_{27}NO_2$, 313.20418; found, 313.20416. Anal. Calcd for $C_{20}H_{27}NO_2$: C, 76.64; H, 8.68; N, 4.47. Found C, 76.42; H, 8.80; N, 4.40.

Di(*n*-butoxyphenyl)amine (7a), microwave heating. To a 100 mL round-bottomed flask was added anhydrous deoxygenated toluene (50 mL), 4-*n*-butoxyaniline (**6**, 8.4 g, 51 mmol), and 1-bromo-4-*n*-butoxybenzene (**5**, 11.6 g, 50 mmol) under nitrogen. Then tris(dibenzylideneacetone)dipalladium (0) (0.46 g, 0.50 mmol), 1,1'-bis(diphenylphosphino)ferrocene (0.56 g, 1.0 mmol), and sodium *tert*-butoxide (6.0 g, 62 mmol) were added. The reaction flask was assembled in a microwave reactor with a reflux condenser attached, and the reaction mixture was heated at 80 Watts, which reached a maximum temperature of 84 ºC. The reaction was monitored by TLC after every 15 minute heating cycle. After 45 minutes of heating, the starting amine appeared consumed by TLC, and the reaction mixture was cooled. The reaction mixture was

worked up in the same way as the conventional reaction (12.6 g crude material; 9.2 g, 59% after recrystallization). The recrystallized product showed essentially the same ^{1}H NMR spectrum as that observed for the same compound synthesized using conventional heating.

2-[Di(4-*n*-butoxyphenyl)amino]thiophene (9), conventional heating. To a 100 mL round-bottomed flask, anhydrous deoxygenated toluene (20 mL), tris(dibenzylideneacetone)dipalladium (0) (0.091 g, 0.10 mmol), and tri(*tert*-butylphosphine) (0.25 mmol, 10% weight solution in hexanes) were added under nitrogen. The solution was stirred at room temperature under nitrogen for 20 minutes. Di(4-*n*-butoxyphenyl)amine (**7a**, 2.40 g, 7.70 mmol), 2-bromothiophene (**8**, 3.2 g, 20 mmol), and sodium *tert*-butoxide (3.0 g, 31 mmol) were added. A reflux condenser was attached to the flask, and the reaction mixture was heated to reflux under nitrogen. After 5 hours of heating, the reaction appeared complete by TLC (SiO$_2$, 5% ethyl acetate in hexanes), and the reaction flask was removed from the oil bath, and the reaction mixture was concentrated by rotary evaporation. The crude product was redissolved in 5% ethyl acetate in hexanes and was run through a short pad of silica gel, eluting with the same solvent. The crude product was concentrated and then chromatographed on a column of silica gel. ^{1}H NMR spectroscopy showed the title compound with minor impurities (73%). Purification with the same chromatographic system of a small portion of product afforded that which was used for analytical characterization. ^{1}H NMR (300 MHz, [D$_2$]dichloromethane) δ 7.03 (dt, J = 9.0, 2.4 Hz, 4H), 6.52 (dd, J = 1.8 Hz, 1H), 3.93 (t, J = 6.6 Hz, 4H), 1.76 (quintet, J = 8.1 Hz, 4H), 1.50 (sextet, J = 7.2 Hz, 4H), 0.97 (t, J =

7.2 Hz, 6H). ^{13}C {^{1}H} NMR (75 MHz, CD$_2$Cl$_2$) δ 155.4, 153.7, 141.8, 126.0, 124.3, 118.0, 117.5, 115.1, 68.3, 31.7, 19.6, 14.0. HRMS-EI (*m/z*): [M]$^+$ calcd for C$_{24}$H$_{29}$NO$_2$S, 395.1919; found, 395.1924. Anal. Calcd for C$_{24}$H$_{29}$NO$_2$S: C, 72.87; H, 7.39; N, 3.54. Found: C, 72.86; H, 7.48; N, 3.60.

2-[Di(4-*n*-butoxyphenyl)amino]thiophene (9), microwave heating. To a 100 mL round-bottomed flask, anhydrous deoxygenated toluene (20 mL), tris(dibenzylideneacetone)dipalladium (0) (0.091 g, 0.10 mmol), and tri(*tert*-butylphosphine) (0.25 mmol, 10% wt. in hexanes) were added under nitrogen. The catalyst mixture was stirred at room temperature under nitrogen for 20 minutes. Di(4-*n*-butoxyphenyl)amine (**7a**, 2.40 g, 7.70 mmol), 2-bromothiophene (**8**, Acros, 3.2 g, 20 mmol), and sodium *tert*-butoxide (3.0 g, 31 mmol) were added. The reaction flask was assembled in a microwave reactor with a reflux condenser attached to the flask. The reaction mixture was heated to 80 Watts for 15 minutes (reaching a maximum temperature of 85 °C) after which TLC showed the reaction was complete. After concentration by rotary evaporation, the crude product was redissolved in 5% ethyl acetate in hexanes and was run through a short pad of silica gel, eluting with the same solvent. The crude product was concentrated and was then chromatographed on a column of silica gel to give slightly impure material (95%), shown to be principally the title compound by comparison of its ^{1}H NMR spectrum to the same target obtained by conventional heating.

5-[Di-(4-*n*-butoxyphenyl)amino]-2-formylthiophene **(10)**. Phosphorus oxychloride (2.94 g, 19.3 mmol) was added dropwise to a stirred mixture of 2-[di(4-*n*-butoxyphenyl)amino]thiophene, **(9**, 6.9 g, 17.5 mmol) and anhydrous *N,N*-dimethylformamide (50 mL) at 0 °C under nitrogen. The reaction mixture was stirred for 4 hours at 0 °C after which the reaction was brought to room temperature for 1 hour. The reaction mixture was poured into aqueous sodium carbonate, and a yellow-orange precipitate formed. The aqueous layer was extracted with ethyl acetate (2 × 200 mL), and the organic layer was subsequently washed with aqueous sodium carbonate (1 M, 3 × 200 mL) and water (2 × 200 mL). The organic layer was dried with anhydrous magnesium sulfate, was filtered, and was concentrated by rotary evaporation. Chromatography on a column of silica gel, eluting with hexanes / ethyl acetate / triethylamine (100:10:1), gave the title compound as a yellow oil (5.29 g, 71%). ^{1}H NMR (300 MHz, CD_2Cl_2) δ 9.52 (s, 1H), 7.43 (d, J = 4.5 Hz, 1H), 7.23 (dd, J = 4.5, 2.1 Hz, 4H), 6.90 (dd, J = 8.7, 1.5 Hz, 4H), 6.16 (d, J = 4.5 Hz, 1H), 3.97 (t, J = 6.6 Hz, 4H), 1.78 (quintet, J = 7.8 Hz, 4H), 1.50 (sextet, J = 7.8 Hz, 4H), 0.99 (t, J = 7.2 Hz, 6H). ^{13}C{^{1}H} NMR (75 MHz, CD_2Cl_2) δ 180.7, 166.2, 157.8, 139.1, 138.8, 128.6, 127.4, 115.1, 108.9, 68.3, 31.6, 19.6, 14.0. HRMS-EI (*m/z*): [M]$^+$ calcd for $C_{25}H_{29}NO_2S$, 423.1868; found, 423.1845. Anal. Calcd for $C_{25}H_{29}NO_2S$: C, 70.89; H, 6.90; N, 3.31. Found: C, 71.13; H, 7.04; N, 3.34.

E-**1,2-Bis(5-{di[4-(*n*-butoxy)phenyl]amino}-2-thienyl)ethylene** **(1)**. In a flame-dried 100 mL round-bottomed flask, allowed to cool under a flow of nitrogen, zinc (0.26 g, 4.0 mmol) was suspended in anhydrous deoxygenated tetrahydrofuran (10 mL). The

suspension was cooled in a dry ice / acetonitrile bath until the temperature fell below –20

°C. Titanium tetrachloride (0.37 g, 0.070 mmol) was slowly added, and a reflux

condenser was attached, following which the mixture was heated at reflux for 50 minutes

under nitrogen. The reaction was then recooled in the dry ice / acetonitrile bath, and a

solution of anhydrous pyridine (0.23 g, 2.9 mmol) and aldehyde **3** (0.40 g, 1.0 mmol) in

anhydrous deoxygenated tetrahydrofuran (10 mL) was added slowly. The resulting dark

suspension was heated to reflux for 2 hours. The reaction mixture was cooled and was

poured into 100 mL of 3:2 mixture of dichloromethane / water. The resulting dark

suspension was filtered through Celite. The organic phase was separated, was washed

with water (150 mL), was dried over anhydrous magnesium sulfate, and was concentrated

by rotary evaporation to afford a dark oil. Column chromatography on silica gel, eluting

with hexanes / ethyl acetate / triethylamine / dichloromethane (95:3:1:1), gave the title

compound as a bright yellow solid (0.28 g, 68%). ^{1}H NMR (300 MHz, DMSO-d_6) δ 7.03

(d, J = 9.6 Hz, 8H), 6.87 (d, J = 9.3 Hz, 8H), 6.71 (d, J = 3.9 Hz, 2H), 6.59 (s, 2H), 6.16

(d, J = 3.9 Hz, 2H), 3.91 (t, J = 6.6 Hz, 8H), 1.66 (quintet, J = 8.1 Hz, 8H), 1.41 (sextet, J

= 7.8 Hz, 8H), 0.91 (t, J = 7.2 Hz, 12H). ^{13}C{^{1}H} NMR (125 MHz, acetone-d_6) δ 157.1,

153.6, 142.0, 134.4, 126.2, 126.1, 120.3, 116.2, 116.1, 68.7, 32.3, 20.0, 14.1. UV/Vis

(dichloromethane) λ_{max} (ε): 442 (41300), 294 (19800), 247 nm (25700 M^{-1}cm^{-1}). HRMS-

EI (m/z): calcd for $C_{50}H_{58}N_2O_4S_2$, 814.3838; found, 814.3799. Anal. Calcd for

$C_{50}H_{58}N_2O_4S_2$: C, 73.67; H, 7.17; N, 3.44. Found: C, 73.91; H, 7.41; N, 3.36.

5,5'-Bis{di(4-methoxyphenyl)amino}-2,2'-bithiophene (2). To tube-shaped a Schlenk

flask containing anhydrous deoxygenated toluene (15 mL) was added

tris(dibenzylideneacetone)dipalladium (0) (0.036 g, 0.040 mmol) and tri(*tert*-butylphosphine) (10% wt. solution in hexanes, 1.5 mL). After stirring for 25 minutes, 5,5'-dibromo-2,2'-bithiophene (**11**, 0.26 g, 0.79 mmol), di(4-methoxyphenyl)amine (**7b**, 0.40 g, 1.75 mmol), and sodium *tert*-butoxide (1.49 g, 15.5 mmol) were added. The reaction mixture was heated to reflux for 100 minutes, after which the crude product was concentrated and was then run through a short pad of basic alumina, eluting with 10%, 20%, then 33% ethyl acetate in hexanes, collecting the product as a yellow-orange solid. After crystallization from boiling ethyl acetate / methanol, a rusty-orange solid was isolated. Finally, the product was run through a pad of basic alumina, eluting with toluene, then precipitated again from ethyl acetate / methanol to obtain the pure product as a yellow-orange solid (0.37 g, 76%). ^{1}H NMR (300 MHz, C$_6$D$_6$) δ 7.12 (d, *J* = 8.7 Hz, 8H), 6.73 (d, *J* = 3.9 Hz, 2H), 6.68 (d, *J* = 9 Hz, 8H), 6.34 (d, *J* = 3.9 Hz, 2H), 3.24 (s, 12H). UV/Vis (dichloromethane) λ_{max} (*ε*): 406 (25800), 296 nm (17900 M^{-1}cm^{-1}). HRMS-FAB (*m/z*): [M]$^+$ calcd for C$_{36}$H$_{32}$N$_2$O$_4$S$_2$, 620.1804; found, 620.1808. Anal. Calcd for C$_{36}$H$_{32}$N$_2$O$_4$S$_2$: C, 69.65; H, 5.20; N, 4.51. Found: C, 69.28; H, 5.11; N, 4.41.

2,6-Bis{di(4-*n*-butoxyphenyl)amino}dithieno[3,2-*b*;2',3'-*d*]thiophene (3). A mixture of di(4-*n*-butoxyphenyl)amine (**7a**, 0.69 g, 2.2 mmol), 2,6-dibromodithieno[3,2-*b*;2',3'-*d*]thiophene (**12**, 0.36 g, 1.00 mmol), and sodium *tert*-butoxide (0.24 g, 2.5 mmol) were suspended under nitrogen in anhydrous deoxygenated toluene (3 mL). In a separate flask, a suspension of tris(dibenzylideneacetone)dipalladium (0) (0.04 g, 0.04 mmol) and tri(*tert*-butylphosphine) (0.17 mL, 10 % wt. solution in hexane) in anhydrous and deoxygenated toluene (2 mL) was stirred under nitrogen for 10 minutes and was then

added to the reaction mixture. The resulting brown-yellow solution was heated under microwave irradiation at a constant power of 80 Watts for 50 minutes, during which time the reaction temperature reached 110 °C. The solvent was removed, and the residue was dissolved in dichloromethane and was run through a short silica gel column. The solvent was removed by rotary evaporation, affording a viscous yellow oil that was further purified by column chromatography (silica gel, hexane / ethyl acetate (95:5)) to give the product as a light yellow oil (0.60 g, 73%). ^{1}H NMR (500 MHz, C_6D_6) δ 7.10 (d, J = 8.8 Hz, 8H), 6.73 (d, J = 8.9 Hz, 8H), 6.57 (s, 2H), 3.57 (t, J = 6.3 Hz, 8H), 1.52 (quintet, J = 6.4 Hz, 8H), 1.30 (sextet, J = 7.4, 8H), 0.79 (t, J = 7.3 Hz, 12H). ^{13}C{^{1}H} NMR (125 MHz, C_6D_6) δ 155.9, 153.1, 141.6, 137.1, 129.1, 124.6, 115.4, 112.2, 67.8, 31.7, 19.6, 14.0. UV/Vis (dichloromethane) λ_{max} (ε): 387 (32100), 290 nm (27500 $M^{-1}cm^{-1}$). MS-FAB m/z (%): 818 (100) [M^+], 762 (7), 669 (9), 404 (3). Anal. Calcd for $C_{48}H_{54}N_2O_4S_3$: C, 70.38; H, 6.64; N, 3.42. Found: C, 70.45; H, 6.65; N, 3.38.

2,6-Bis{di(methoxyphenyl)amino}dithieno[3,2-*b*;2',3'-*d*]thiophene (3b). To a tube-shaped Schlenk flask were added tris(dibenzylideneacetone)dipalladium (0) (0.022 g, 0.034 mmol), tri(*tert*-butyl)phosphine (1.0 mL, 10% wt. in hexane), and anhydrous deoxygenated toluene (10 mL) under nitrogen atmosphere. 2,6-Dibromodithieno[3,2-*b*;2',3'-*d*]thiophene (**12**, 0.19 g, 0.53 mmol), bis(4-methoxyphenyl)amine (**7b**, 0.31 g, 1.3 mmol), and sodium *tert*-butoxide were added. A reflux condenser was attached, and the reaction mixture was brought to reflux for 30 minutes, after which the reaction flask was removed from the heat, and the crude product was run through a tall pad of basic alumina, eluting with ethyl acetate/toluene (1:9). The crude product was crystallized

from ethyl acetate and methanol, giving an orange-yellow solid (0.17 g, 49%). ^{1}H NMR (300 MHz, C$_6$D$_6$) δ 7.09 (d, J = 8.7 Hz, 8H), 6.69 (d, J = 9.0 Hz, 8H), 6.57 (s, 2H), 3.23 (s, 12H). ^{13}C{1H} NMR (125 MHz, C$_6$D$_6$) δ 156.4, 153.2, 141.8, 137.2, 125.4, 114.2, 114.1, 113.1, 55.1. HRMS-EI (m/z): [M]$^{+}$ calcd. for C$_{36}$H$_{30}$N$_2$O$_4$S$_3$, 650.1369; found, 650.13388. Anal. Calcd for C$_{36}$H$_{30}$N$_2$O$_4$S$_3$: C, 66.44; H, 4.65; N, 4.30. Found: C, 66.09; H, 4.58; H, 4.18.

N-(4-*tert*-Butylphenyl)-2,6-bis{di(4-methoxyphenyl)amino}dithieno[3,2-*b*;2',3'-*d*]pyrrole (4a). To an ampoule was added dry deoxygenated toluene (20 mL), tris(dibenzylideneacetone)dipalladium (0) (0.060 g, 0.065 mmol), and tri(*tert*-butylphosphine) (10% wt. in hexane, 1.5 mL) under nitrogen. After stirring for 10 minutes at room temperature, *N*-(4-*tert*-Butylphenyl)-2,6-dibromodithieno[3,2-*b*;2',3'-*d*]pyrrole (**14a**, 0.15 g, 0.32 mmol), bis(4-methoxyphenyl)amine[34] (**7b**, 0.175 g, 0.76 mmol), and sodium *tert*-butoxide (0.20 g, 2.1 mmol) were added. The reaction was subjected to three freeze/pump/thaw cycles, and the reaction vessel, still under vacuum, was immersed in an oil bath at 110 ˚C. After stirring for 40 minutes, the reaction flask was removed from the heat, and the reaction mixture was run through a column of basic alumina, eluting with toluene, then 2% ethyl acetate in toluene (using deoxygenated solvents and running the column under nitrogen) to give the title product (0.16 g, 67%). ^{1}H NMR (500 MHz, C$_6$D$_6$) δ 7.23 (d, J = 8.5 Hz, 2H), 7.20 (d, J = 8.5 Hz, 8H), 7.00 (d, J = 8.5 Hz, 2H), 6.96 (s, 2H), 6.71 (d, J = 8.5 Hz, 8H), 3.27 (s, 12H), 1.02 (s, 9H). ^{13}C{1H} NMR (125 MHz, C$_6$D$_6$) δ 156.1, 150.9, 148.6, 139.4, 137.6, 126.8, 124.2, 122.3, 114.9, 112.7, 106.9, 55.0, 34.4, 31.3. UV/Vis (dichloromethane) λ_{max} (ε): 382 (34100), 304 nm

157

(32200 $M^{-1}cm^{-1}$). MS-EI (*m/z*): 765 (M^+). Anal. Calcd for $C_{46}H_{43}N_3O_4S_2$: C, 72.13; H, 5.66; N, 5.49. Found: C, 71.78; H, 5.60; N, 5.42.

***N*-(*tert*-Butyl)-2,6-bis{di(4-*n*-methoxyphenyl)amino}dithieno[3,2-*b*;2',3'-*d*]pyrrole (4b)**. To a 100 mL Schlenk ampoule was added dry deoxygenated toluene (15 mL), tris(dibenzylideneacetone)dipalladium (0) (0.060 g, 0.065 mmol), and tri(*tert*-butylphosphine) (1.5 mL, 10% solution by weight in hexanes) under a positive pressure of nitrogen. After stirring for 20 minutes at room temperature, *N*-(*tert*-Butyl)-2,6-dibromo[3,2-*b*;2',3'-*d*]pyrrole (**14b**, 0.12 g, 0.51 mmol), di(4-methoxyphenyl)amine (**7b**, 0.26 g, 1.12 mmol), and sodium *tert*-butoxide (0.22 g, 2.3 mmol) were added. The reaction mixture was subjected to three freeze/pump/thaw cycles, and the reaction vessel, still under vacuum, was immersed in an oil bath at 110 °C for 30 minutes. The reaction flask was removed from the oil bath, and the reaction mixture was through a column of basic alumina under nitrogen, eluting with toluene, then 2% ethyl acetate in toluene (using deoxygenated solvents and running the column under nitrogen). The yellow fractions containing the desired product were concentrated to give a viscous yellow-orange oil, which was precipitated from ethyl acetate / hexanes to give the product as a bright yellow powder (0.13 g, 26%). ^{1}H NMR (300 MHz, C_6D_6) δ 7.25 (d, *J* = 9 Hz, 8H), 7.01 (s, 2H), 6.73 (d, *J* = 9 Hz, 8H), 3.27 (s, 12H), 1.22 (s, 9H). ^{13}C{^{1}H} NMR (75 MHz, C_6D_6) δ 156.0, 149.2, 142.6, 138.5, 124.0, 114.9, 112.4, 110.1, 57.5, 55.0, 30.2. UV/Vis (dichloromethane) λ_{max} (ε): 376 (30600), 299 nm (24700 $M^{-1}cm^{-1}$). HRMS-FAB (*m/z*): calcd for $C_{40}H_{39}N_3O_4S_2$, 689.2317; found, 689.2321. Anal. Calcd for $C_{40}H_{39}N_3O_4S_2$: C, 69.64; H, 5.70; N, 6.09. Found: C, 69.55; H, 6.08; N, 5.87.

3.4 References

(1)   Rumi, M.; Ehrlich, J. E.; Heikal, A. A.; Perry, J. W.; Barlow, S.; Hu, Z.; McCord-Maughon, D.; Parker, T. C.; Röckel, H.; Thayumanavan, S.; Marder, S. R.; Beljonne, D.; Brédas, J.-L. *J. Am. Chem. Soc.* **2000**, *122*, 9500-9510.

(2)   Pond, S. J. K.; Rumi, M.; Levin, M. D.; Parker, T. C.; Beljonne, D.; Day, M. W.; Brédas, J. L.; Marder, S. R.; Perry, J. W. *J. Phys. Chem. A.* **2002**, *106*, 11470-11480.

(3)   Cho, B. R.; Lee, S. H.; Lim, J. C.; Kang, T. I.; Jeon, S.-J. *Mol. Cryst. Liq. Cryst.* **2001**, *370*, 77-82.

(4)   Cho, B. R.; Park, S. B.; Lee, S. J.; Son, K. H.; Lee, S. H.; Lee, M.-J.; Yoo, J.; Lee, Y. K.; Lee, G. J.; Kang, T. I.; Cho, M.; Jeon, S.-J. *J. Am. Chem. Soc.* **2001**, *123*, 6421-6422.

(5)   Moylan, C. R.; Twieg, R. J.; Lee, V. Y.; Swanson, S. A.; Betterton, K. M.; Miller, R. D. *J. Am. Chem. Soc.* **1993**, *115*, 12599-12600.

(6)   Ermer, S.; Lovejoy, S. M.; Leung, D. S.; Warren, H.; Moylan, C. R.; Twieg, R. J. *Chem. Mater.* **1997**, *9*, 1437-1442.

(7)   Bösch, M.; Fisher, C.; Cai, C.; Liakatas, I.; Bosshard, C.; Günter, P. *Synth. Met.* **2001**, *2001*, 241-243.

(8)   Staub, K.; Levina, G. A.; Barlow, S.; Kowalczyk, T. C.; Lackritz, H. S.; Barzoukas, M.; Fort, A.; Marder, S. R. *J. Mater. Chem.* **2003**, *13*, 825-833.

(9)   Ramos-Ortiz, G.; Cha, M.; Thayumanavan, S.; Mendez, J.; Marder, S. R.; Kippelen, B. *Appl. Phys. Lett.* **2004**, *85*, 3348-3350.

(10)   Ramos-Ortiz, G.; Cha, M.; Kippelen, B.; Walker, G. A.; Barlow, S.; Marder, S. R. *Opt. Lett.* **2004**, *29*, 2515-2517.

(11)   Belfield, K. D.; Hagan, D. J.; Van Stryland, E. W.; Schaefer, K. J.; Negres, R. A. *Org. Lett.* **1999**, *1*, 1575-1578.

(12)   Thomas, J.; Fuentes-Hernandez, C.; Yamamoto, M.; Cammack, K.; Matsumoto, K.; Walker, G. A.; Barlow, S.; Kippelen, B.; Meredith, G.; Marder, S. R.; Peyghambarian, N. *Adv. Mater.* **2004**, *16*, 2032-2036.

(13)   Spangler, C. W. *J. Mater. Chem.* **1999**, *9*, 2013-2020.

(14)   Lambert, C.; Nöll, G. *J. Am. Chem. Soc.* **1999**, *121*, 8434-8442.

(15)   Szeghalmi, A. V.; Erdmann, M.; Engel, V.; Schmitt, M.; Amthor, S.; Kriegisch, V.; Nöll, G.; Stahl, R.; Lambert, C.; Leusser, D.; Stalke, D.; Zabel, M.; Popp, J. *J. Am. Chem. Soc.* **2004**, *126*, 7834-7845.

(16)   Lambert, C.; Risko, C.; Coropceanu, V.; Schelter, J.; Amthor, S.; Gruhn, N. E.; Durivage, J. C.; Brédas, J. L. *J. Am. Chem. Soc.* **2005**, *127*, 8508-8516.

(17)   Nöll, G.; Avola, M. *J. Phys. Org. Chem.* **2006**, *19*, 238-241.

(18)   Low, P. J.; Paterson, M. A. J.; Goeta, A. E.; Yufit, D. S.; Howard, J. A. K.; Cherryman, J. C.; Tackley, D. R.; Brown, B. *J. Mater. Chem.* **2004**, *14*, 2516-2523.

(19)   Lambert, C.; Nöll, G. *Chem. Eur. J.* **2002**, *8*, 3467-3477.

(20)   Lambert, C.; Amthor, S.; Schelter, J. *J. Phys. Chem. A* **2004**, *108*, 6474-6486.

(21)   Heckmann, A.; Amthor, S.; Lambert, C. *Chem. Commun.* **2006**, 2959-2961.

(22) Barlow, S.; Risko, C.; Coropceanu, V.; Tucker, N. M.; Jones, S. C.; Levi, Z.; Khrustalev, V. N.; Antipin, M. Y.; Kinnibrugh, T. L.; Timofeeva, T.; Marder, S. R.; Brédas, J. L. *Chem. Commun.* **2005**, 764-766.

(23) Barlow, S.; Risko, C.; Chung, S.-J.; Tucker, N. M.; Coropceanu, V.; Jones, S. C.; Levi, Z.; Brédas, J. L.; Marder, S. R. *J. Am. Chem. Soc.* **2005**, *127*, 16900-16911.

(24) Amthor, S.; Lambert, C. *J. Phys. Chem. A* **2006**, *110*, 1177-1189.

(25) Jones, S. C.; Coropceanu, V.; Barlow, S.; Kinnibrugh, T.; Timofeeva, T.; Brédas, J.-L.; Marder, S. R. *J. Am. Chem. Soc.* **2004**, *126*, 11782-11783.

(26) Lambert, C.; Nöll, G.; Hampel, F. *J. Phys. Chem. A* **2001**, *105*, 7751-7758.

(27) Cheng, L.-T.; Tam, W.; Stevenson, S. H.; Meredith, G. R.; Rikken, G.; Marder, S. R. *J. Phys. Chem.* **1991**, *95*, 10631-10643.

(28) Rohde, D.; Dunsch, L.; Tabet, A.; Hartmann, H.; Fabian, J. *J. Phys. Chem. B* **2006**, *110*, 8223-8231.

(29) Casado, J.; Ruiz Delgado, M. C.; Shirota, Y.; Hernández, V.; LópezNavarrete, J. T. *J. Phys. Chem. B* **2003**, *107*, 2637-2644.

(30) Lacroix, J. C.; Chane-Ching, K. I.; Maquère, F.; Maurel, F. *J. Am. Chem. Soc* **2006**, *128*, 7264.

(31) Hush, N. S. *Prog. Inorg Chem.* **1967**, *8*, 391-444.

(32) Wolfe, J. P.; Wagaw, S.; Buchwald, S. L. *J. Am. Chem. Soc.* **1996**, *118*, 7215.

(33) Driver, M. S.; Hartwig, J. F. *J. Am. Chem. Soc.* **1996**, *118*, 7217.

(34) Pratt, D. A.; Di Labio, F. A.; Valgimigli, L.; Pedulli, G. F.; Ingold, K. U. *J. Am. Chem. Soc* **2002**, *124*, 11085-11092.

(35) Zeika, O.; Hartmann, H. *Synthesis* **2004**, *3*, 377-380.

(36) Hooper, M. W.; Utsunomiya, M.; Hartwig, J. F. *J. Org. Chem.* **2003**, *68*, 2861-2873.

(37) Ogawa, K. R., K. R.; Rothstein, S. D.; Rasmussen, S.C. *J. Org. Chem.* **2001**, *66*, 9067-9070.

(38) Watanabe, M.; Yamamoto, T.; Nishiyama, M. *Chem. Commun.* **2000**, *2*, 133-134.

(39) Bedworth, P. V.; Cai, Y. M.; Jen, A.; Marder, S. R. *J. Org. Chem.* **1996**, *61*, 2242-2246.

(40) Gerstner, P.; Tohde, D.; Hartmann, J. *Synthesis* **2002**, *17*, 2487-2489.

(41) Kisselev, R. T., M. *Chem. Commun.* **2002**, *14*, 1530-1531.

(42) Kwon, O.; Barlow, S.; Odom, S. A.; Beverina, L.; Natalie J. Thompson; Zojer, E.; Brédas, J.-L.; Marder*, S. R. *J. Phys. Chem. A* **2005**, *109*, 9346-9352.

(43) Li, P.; Ahrens, B.; Feeder, N.; Raithby, P. R.; Teat, S. J.; Khan, M. S. *Dalton Trans.* **2005**, *5*, 874-883.

(44) Frey, J.; Bond, A. D.; Holmes, A. B. *Chem. Commun* **2002**, 2424-2425.

(45) Lambert, C.; Nöll, G. *J. Am. Chem. Soc* **1999**, *1999*, 8434-8442.

(46) Sell, J. A.; Kuppermann, A. *Chem. Phys. Lett* **1978**, *61*, 355.

(47) Ferrere, S.; Elliott, C. M. *Inorg. Chem.* **1995**, *34*, 5818-5824.

(48) Barriere, F.; Camire, N.; Geiger, W. E.; Mueller-Westerhoff, U. T.; Sanders, R. *J. Am. Chem. Soc.* **2002**, *124*, 7262 -7263.

(49) Coropceanu, V.; Gruhn, N. E.; Barlow, S.; Lambert, C.; Durivage, J. C.; Bill, T. G.; Nöll, G.; Marder, S. R.; Brédas, J.-L. *J. Am. Chem. Soc.* **2004**, *126*, 2727-2731.

(50) Nelsen, S. F. *Chem. Eur. J.* **2000**, *2000*, 581-588.

(51) Bonvoisin, J.; Launay, J.-P.; Van der Auweraer, M.; De Schryver, F. C. *J. Phys. Chem.* **1994**, *98*, 5052-5057.

(52) Bonvoisin, J.; Launay, J.-P.; Verbouwe, W.; Van der Auweraer, M.; De Schryver, F. C. *J. Phys. Chem.* **1996**, *100*, 17079-17082.

(53) Robin, M. B.; Day, P. *Adv. Inorg. Chem. Radiochem.* **1967**, *10*, 247-422.

(54) Coropceanu, V.; Malagoli, M.; André, J. M.; Brédas, J. L. *J. Am. Chem. Soc.* **2002**, *124*, 10519-10530.

(55) Low, P. J.; Paterson, M. A. J.; Puschmann, H.; Goeta, A. E.; Howard, J. A. K.; Lambert, C.; Cherryman, J. C.; Tackley, D. R.; Leeming, S.; Brown, B. *Chem. Eur. J.* **2004**, *10*, 83-91.

(56) Coropceanu, V.; Lambert, C.; Nöll, G.; Brédas, J. L. *Chem. Phys. Lett.* **2003**, *373*, 153-160.

(57) Coropceanu, V.; Malagoli, M.; Andre, J. M.; Brédas, J. L. *J. Chem. Phys.* **2001**, *115*, 10409.

(58) Rohde, D.; Dunsch, L.; Tabet, A.; Hartmann, H.; Fabian, J. *J. Phys. Chem. B* **2006**, *110*, 8223-8231.

(59) Cave, R. J.; Newton, M. D. *Chem. Phys. Lett.* **1996**, *249*, 15.

(60) Creutz, C.; Newton, M.; Sutin, N. *J. Photochem. Photobiol.* **1994**, *A82*, 47.

(61) Bamberger, S.; Hellwinkel, D.; Neugebauer, F. A. *Chem. Ber.* **1975**, *108*, 2416-2421.

(62) Seo, E. T.; Nelson, R. F.; Fritsch, J. M.; Marcoux, L. S.; Leedy, D. W.; Adams, R. N. *J. Am. Chem. Soc.* **1966**, *88*, 3498-3503.

(63) Ditchfield, R.; Hehre, W. J.; Pople, J. A. *J. Chem. Phys.* **1971**, *54*, 724.

(64) Hehre, W. J.; Ditchfield, R.; Pople, J. A. *J. Chem. Phys.* **1972**, *56*, 2257.

(65) Gordon, M. S. *Chem. Phys. Lett* **1980**, *76*, 163.

(66) Hariharan, P. C.; Pople, J. A. *Theor. Chim. Acta* **1973**, *28*, 213.

(67) Becke, A. D. *Phys. Rev.* **1988**, *A38*, 3098-3100.

(68) Becke, A. D. *J. Chem. Phys.* **1993**, *98*, 5648-5652.

(69) Frisch, M. J.; Trucks, G. W.; Schlegel, H. B.; Scuseria, G. E.; Robb, M. A.; Cheeseman, J. R.; Montgomery, J., J. A.; Vreven, T.; Kudin, K. N.; Burant, J. C.; Millam, J. M.; Iyengar, S. S.; Tomasi, J.; Barone, V.; Mennucci, B.; Cossi, M.; Scalmani, G.; Rega, N.; Petersson, G. A.; Nakatsuji, H.; Hada, M.; Ehara, M.; Toyota, K.; Fukuda, R.; Hasegawa, J.; Ishida, M.; Nakajima, T.; Honda, Y.; Kitao, O.; Nakai, H.; Klene, M.; Li, X.; Knox, J. E.; Hratchian, H. P.; Cross, J. B.; Bakken, V.; Adamo, C.; Jaramillo, J.; Gomperts, R.; Stratmann, R. E.; Yazyev, O.; Austin, A. J.; Cammi, R.; Pomelli, C.; Ochterski, J. W.; Ayala, P. Y.; Morokuma, K.; Voth, G. A.; Salvador, P.; Dannenberg, J. J.; Zakrzewski, V. G.; Dapprich, S.; Daniels, A. D.; Strain, M. C.; Farkas, O.; Malick, D. K.; Rabuck, A. D.; Raghavachari, K.; Foresman, J. B.; Ortiz, J. V.; Cui, Q.; Baboul, A. G.; Clifford, S.; Cioslowski, J.; Stefanov, B. B.; Liu, G.; Liashenko, A.; Piskorz, P.; Komaromi, I.; Martin, R. L.; Fox, D. J.; Keith, T.; Al-Laham, M. A.; Peng, C. Y.; Nanayakkara, A.; Challacombe, M.; Gill, P. M. W.; Johnson, B.; Chen, W.; Wong, M. W.; Gonzalez, C.; Pople, J. A. *Gaussian03, Revision B.05*; Gaussian Inc.: Wallingford, CT, 2004.

(70) Pangborn, A. B.; Giardello, M. A.; Grubbs, R. H.; Rosen, R. K.; Timmers, J. F. *Organometallics* **1996**, *15*, 1518-1520.

CHAPTER 4

ELECTRONIC COUPLING AND INTRAMOLECULAR ELECTRON

TRANSFER RATES IN BIS(TRIARYLAMINE)S

4.1 Introduction

In this chapter, the electronic coupling of triarylamine redox centers in the mixed valence radical cations of 1,4-bis[4-(diarylamino)styryl]benzenes, and related 2,5-bis[4-(diarylamino)styryl]heteroarenes, and later with bis(diarylaminophenylene)-based derivatives with bridges of different conjugation length and degrees of unsaturation (C=C versus C≡C) are compared. The comparison includes derivatives with variation in the electron donor strength of the terminal aryl groups and / or of the phenylene, thienylene, or pyrrolylene bridges, as well as in the degree of unsaturation in the bridges. The bis(diarylamino)-substituted derivatives were investigated by cyclic voltammetry (CV), and their corresponding monocations – generated by chemical oxidation – were studied by visible-near infrared (visible-NIR) absorption and electron paramagnetic resonance (EPR) spectroscopies. For some monocations, variable temperature EPR (VT-EPR) experiments were used to determine rates of electron exchange between the triarylamine redox centers.

4.1.1 Coupling in Organic Mixed-Valence Species

In many organic mixed-valence (MV) systems, the separation between redox centers precludes direct orbital overlap between the orbitals associated with the redox

centers. In such systems, electronic coupling can be considered as arising through interaction of bridge-based orbitals with the "redox group" orbitals.[1] In π-conjugated organic systems, the highest filled bridge orbitals are generally the most relevant to the ground state character of the oxidized species. In Figure 4.1 a rough approximation of the highest occupied molecular orbitals (HOMOs) for a simple diamino derivative with a bithiophene bridge are shown to illustrate the relevance of the interaction of the HOMOs of the building blocks to the electronic coupling in a monocation.

When two nitrogen atoms are used as starting points, there are two possible combinations of HOMOs: in-phase and out-of-phase. Because the nitrogen atoms separated over a relatively large distance, they are considered to be essentially non-interacting, so the energies of both combinations of orbitals are approximately the same. The HOMO of bithiophene has an in-phase and out-of-phase interaction with the nitrogen-nitrogen (N-N) HOMO. The in-phase combination is at lower energy than the bridge HOMO and is more bridge-based than N-N based. The out-of-phase combination is at higher energy and is more N-N based than bridge-based. The HOMO of bithiophene has no net overlap with the in-phase N-N MO set, so the HOMO of the in-phase nitrogen-nitrogen pair remains at approximately the same energy as where it started in this model. Of course, in reality it is possible for in the in-phase N-N HOMO to interact with the LUMO – a destabilizing effect – and the HOMO-1 – a stabilizing effect. For simplicity, the HOMO is shown at the same energy in this simple model because it is now known whether the N-N HOMO will interact more with the LUMO or the HOMO-1, thus being destabilized or stabilized. In total, three orbitals were used as starting points, and, as required when generating MO diagrams, three orbitals were obtained.
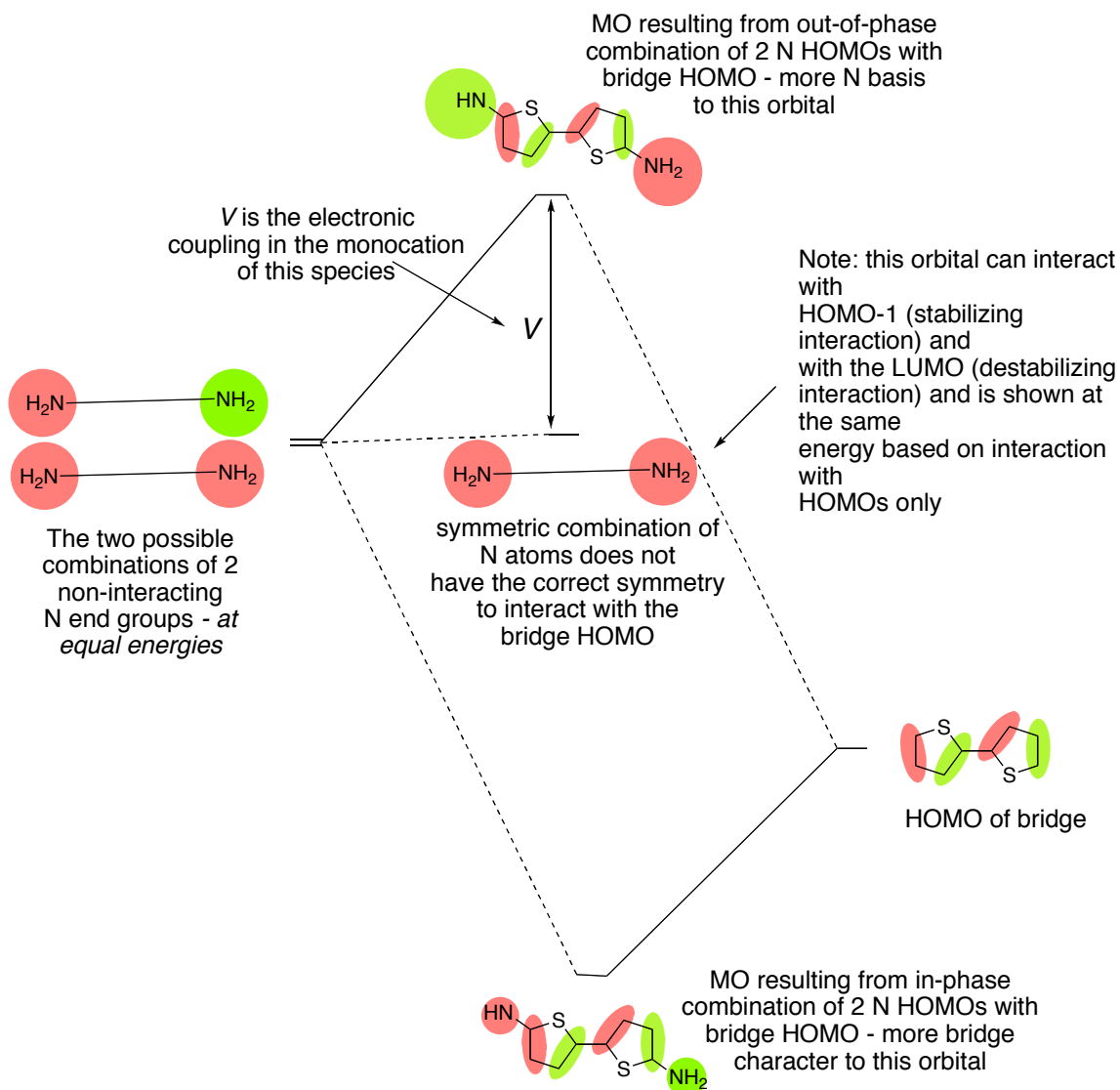
Figure 4.1. Rough approximation for HOMOs of N-N and bridge building blocks.

In the neutral version of this simple model. The MOs are filled with paired electrons. When an electron is removed, generating the monocation, there is a vacancy in the orbital drawn at highest energy. There is now a transition (labeled *V*) that is equivalent to the electronic coupling. The strength of the resultant electronic coupling is expected to increase with increased overlap between local orbitals associated with the redox-active fragment and with the bridge, and this overlap increases as the energy

bridge-based orbitals approaches that of the end-group orbitals. A model for orbital mixing of the bridging and triarylamine frontier molecular orbitals is shown below, showing a case in which the energy of the bridging orbitals approaches the energy of the triarylamine orbitals.
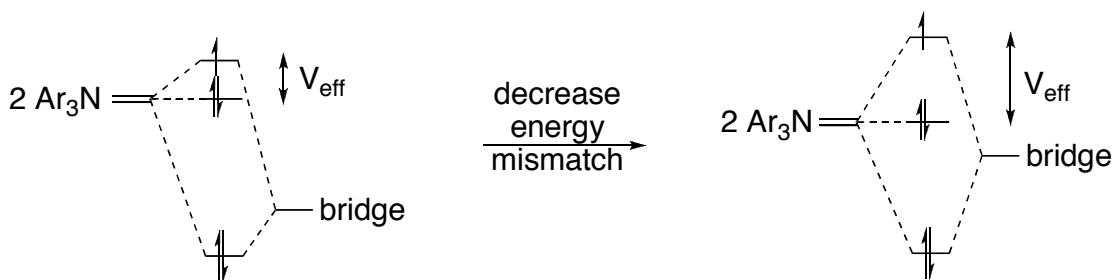
Figure 4.2. Model for orbital mixing in a class III bis(triarylamine) monocation.

The role of the end group can be seen in the couplings found for the radical cations of bis(diphenylamino)-terminated biphenyls or benzenes exceeding those of their analogs with bis(di-p-anisylamino)-terminated end groups.[2-5] The role of the bridge is illustrated by varying the arene cores in the radical cations of bis[4-(di-p-anisylamino)phenylethynyl]arenes [6,7] and by the strong couplings observed in species incorporating thiophene groups in the bridge (see results from Chapter 3). Increasing coupling via bridging orbitals leads to an increased contribution of bridge orbitals to the semi-occupied molecular orbital, resulting in increased bridge character to the radical cation. This displaces the redox center from its formal triarylamine position into the bridge, giving a reduction in the diabatic electron-transfer distance (R_{ab}). This means that the redox centers can no longer be regarded as centered on the triarylamines and that the diabatic transfer distance required for Hush analysis of the IVCT band (equation 4.2, see below) will be reduced relative to the nitrogen-nitrogen distance.

As described in previous chapters, in a class-III system, the electronic coupling is directly proportional to the energy of absorption of the IVCT band

$$\bar{\nu}_{max} = 2V \qquad (4.1)$$

The electronic coupling between two redox centers (V) can also be estimated for both class II and III systems from characteristics of the IVCT band using the Hush expression

$$V = \frac{\mu_{ge}\bar{\nu}_{max}}{eR_{ab}} \qquad (4.2)$$

where e is the electronic charge, R_{ab} is the diabatic electron-transfer distance, and μ_{ge} is the transition dipole moment.

For bis(diarylamino)-substituted species, computational estimates suggest values of R_{ab} are considerably reduced from the nitrogen–nitrogen distance;[8] in the case of class-III (valence-delocalized) systems, reduced R_{ab} values are a requirement for consistency between estimates of the electronic coupling (V) from equations 4.1 and 4.2 (see Chapter 3). Moreover, as shown in Chapter 3, DFT calculations, which are supported by EPR measurements, suggest that replacing the stilbene bridge of a bis(diarylamino)-substituted monocation with a more easily ionized dithienylethene bridge leads to an increase in the spin density on the bridge at the expense of that on the nitrogen atoms and the terminal aryl groups (see Chapter 3).

The first portion of this chapter (4.2) focuses on incorporating electron-rich bridges into bis(diarylaminostyryl)arenes, as well as modifiying the electron-richness of

the bis(diarylamino) end groups. In addition to CV studies of the bis(diarylaminostyryl)arene derivatives, the monocations were analyzed by visible-NIR and EPR spectroscopies in order to examine the change in spectral characteristics upon increasing V and thus decreasing R_{ab}. The second portion of the chapter (4.3) focuses on determining the difference in the rates of electron transfer (ET) from one triarylamine redox center to another, which – in some cases – can be determined by VT-EPR experiments. By comparing VT-EPR spectra of MV monocations with varying degrees of electronic coupling, it could be possible to determine the different rates of ET on the EPR time scale for some of the Class II MV species. From that data, it may be possible to determine barriers to ET and to, therefore, gain experimental insight into the extent of deviation of R_{ab} from the nitrogen-nitrogen distance.

4.2 Previous Analysis of Bis(diarylaminostyryl)arenes and Their Radical Cations

The monocations of several previously synthesized bis(diarylaminostyryl)arenes (**I**-**VII**)[8-10] were studied as MV radical cations. The compounds (Figure 4.2) were chosen for comparison as MV systems with variation in the electron-richness of the end groups (alkyl versus alkoxy versus no substituent) and / or of the bridging aromatic group (phenylene, 2,5-disubstituted *p*-phenylene, 3,4-dialkoxythiophene-2,5-diyl, pyrrole-2,5-diyl, or 3,4-dialkoxypyrrole-2,5-diyl). The derivatives were previously studied by CV experiments, and the visible-NIR absorption spectra were recorded for the monocations in dichloromethane, and were analyzed by Marcus-Hush theory.[11]
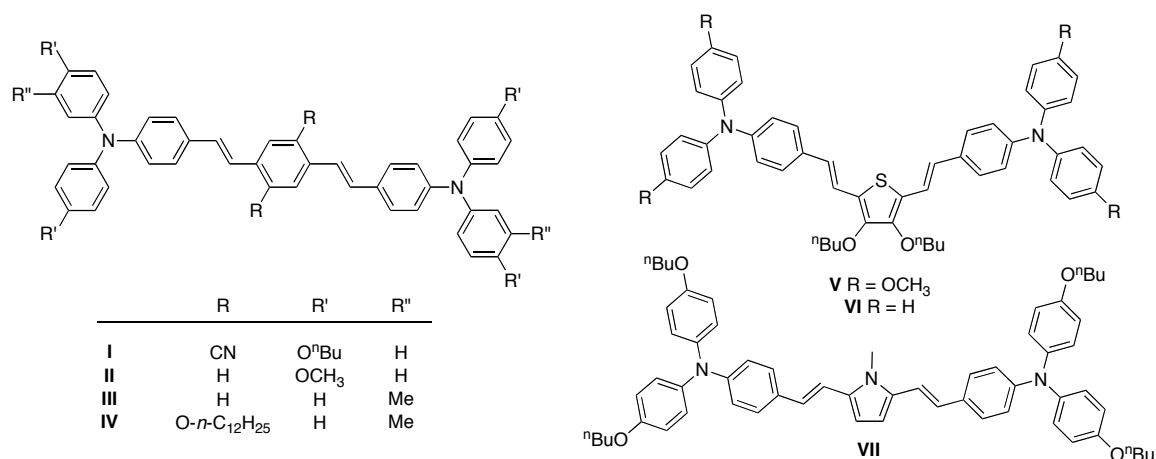
Figure 4.3. 1,4-Bis[4-(diarylamino)styryl]benzenes and related 2,5-bis[4-(diarylamino)styryl]heterocycles.

Electrochemical data for **II** and **V** in dichloromethane have been previously published.[8,10] The redox potentials of the remaining neutral compounds were investigated using CV in 0.1 M tetra-*n*-butylammonium hexafluoroantimonate (^{n}Bu$_4$NPF$_6$) in dichloromethane. For compounds **I**-**VI**, the first and second electrons are removed at similar potentials, and the separation between first and second oxidation potentials was not resolvable using CV. Compounds **I**-**VI** also exhibited a third one-electron oxidation at higher potential. Additionally, for compound **V**, a fourth oxidation is evident within the solvent window. For compound **VII**, three separate one-electron oxidations are observed in the CV experiment. The $E_{1/2}^{+/0}$ values reflect the overall electron-richness of the molecules and are consistent with expectations based on the electron-withdrawing or electron-donating character of the bridging and terminal substitutents, and on the relative ionization potentials of benzene (9.2 eV),[12] thiophene (8.9 eV),[13] and pyrrole (8.2 eV).[14]

Spectroscopic data for **II⁺** has been previously published.[8] The visible-NIR absorption spectra for monocations **I⁺** and **III⁺**-**VI⁺** were also previously recorded.[11] In the spectra of **I⁺** and **II⁺**, the lowest energy features are approximately symmetric Gaussians, which are broader than the Hush prediction for class-II compounds ($\overline{v}_{1/2}$[Hush], equation 4.3) and were therefore assigned to the intervalence charge transfer (IVCT) transitions of class-II MV compounds.

$$\overline{v}_{1/2[Hush]} = \sqrt{2310 \times \overline{v}_{max}} \qquad (4.3)$$

Compound **III** has less electron-rich end groups than **II** and a more electron-rich bridge compared to **I**. The IVCT band of **III⁺** is qualitatively different to that seen for those cations **I⁺** and **II⁺**; the band has neither the symmetric Gaussian lineshape typical of class-II systems nor the characteristic shape of class-III bis(triarylamine) MV IVCT bands, leading to its tentative assignment as a class-II / class-III borderline species. Compound **IV** has a more electron-rich bis(alkoxy)-substituted bridge than **III**; the IVCT band of its monocation is higher in energy than that seen for **III⁺**, and it has a lineshape typical for class-III bis(triarylamine)s.[3,4,8]. Further increasing the electron-richness of the bridge in 3,4-dialkoxythiophene-bridged compounds **V⁺** and **VI⁺** gives similar IVCT lineshapes as at increased energies relative to **IV⁺**, consistent with class III species having increased electronic coupling as a result of raising the bridge energy.

Lastly, the maximum of the IVCT of the pyrrole-bridged cation **VII⁺** occurs at higher energy than even those of **IV⁺**-**VI⁺**; the band shape is rather different: broader and less strongly asymmetric. However, because the absorption spectrum was recorded at unknown concentration of monocation, some of the terms relevant to Marcus-Hush

analysis of the IVCT band could not be calculated. In addition to obtaining a quantitative spectrum of the radical cation of **VII⁺**, because the character of the IVCT band changed throughout the series of monocations **I⁺-VI⁺**, it would be interesting to raise the orbital energy of the bridge relative to the end groups even further to see the effect on the IVCT band in the absorption spectra of the monocations, and also to evaluate whether the species can still be considered MV systems or are better described as bridge-based monocations.

4.2.1 Bis(diarylaminostyryl)pyrrole Derivatives and Bridge-Based Model Compounds

As a first comparison to bis(diarylaminostyryl)pyrrole derivative **VII**, compound **1** (Figure 4.3) was designed as an analog with less electron-rich end groups; the *n*-butoxyphenyl groups were replaced with *tert*-butylphenyl groups. Compound **2** (Figure 4.3) was designed as a derivative that also incorporated the less electron-rich end groups and additionally incorporated a more electron-rich 3,4-propylenedioxy-substituted pyrrole bridge. It has been previously reported that 3,4-propylenedioxy-*N*-alkylpyrroles are approximately 0.1 V easier to oxidize than *N*-alkylpyrroles,[15] so it was expected that compound **2** would be easier to oxidize than compound **1**.
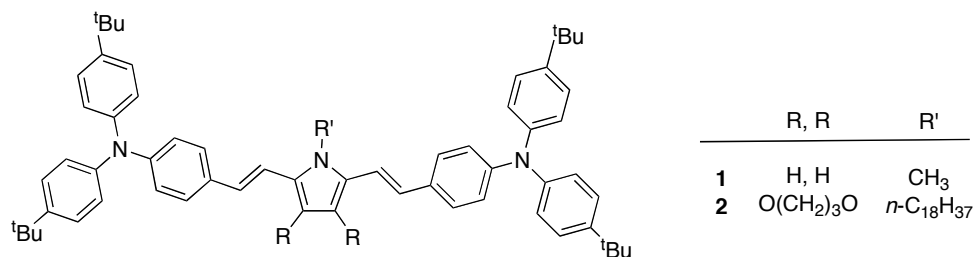
Figure 4.4. Bis(diarylaminostyryl)pyrrole derivatives.

Figure 4.4 shows the extent to which the electron-richness of end and bridging groups is varied among compounds **I**-**VII** and **1**-**2**, as measured by the HOMO energies, calculated at the AM1 level, for the triarylamine (**E1-4**) and divinylbenzene or divinylheterocycle (**B1-6**) fragments. From this data, it is reasonable to expect that monocations of compounds **VII**, **1**, and **2** will have greater bridge character.
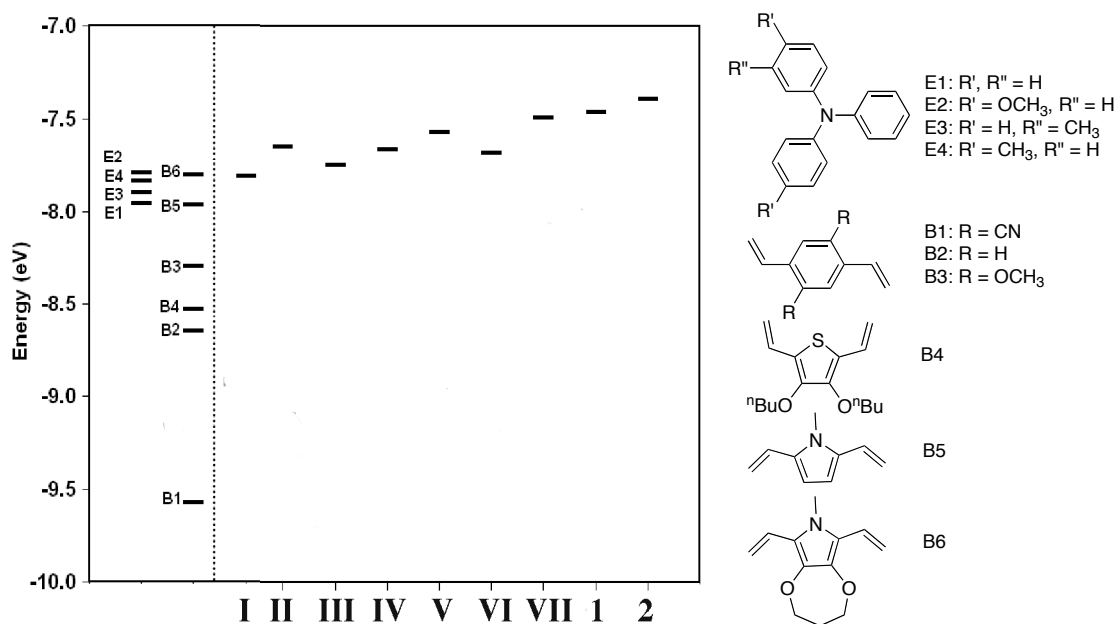
Figure 4.5. HOMO energies calculated at the AM1 level of theory for compounds **I**-**VII** and **1**-**2** and for the constituent end group (**E1-E4**) and bridging group (**B1-B6**) fragments (some alkyl groups were replaced by methyl groups in the calculations).

Additionally, in order to compare the properties of the new and previously analyzed bis(diarylaminostyryl)arene derivatives with their corresponding bridges – in part to help determine if any of the monocations are bridge-based and exhibit the same properties independently of the diarylamino substitution – model compounds **3**-**7** (Figure 4.5) were synthesized. The model compounds are bis(styryl)arenes that are

functionalized at the 4-positions of the outer phenyl ring with *tert*-butyl or methoxy groups in attempt to block the presumably most reactive positions in the isolated bridges. The methoxy group was used in the case of compound **7** in order to obtain a more electron-rich bridge model compound compared to **6**.
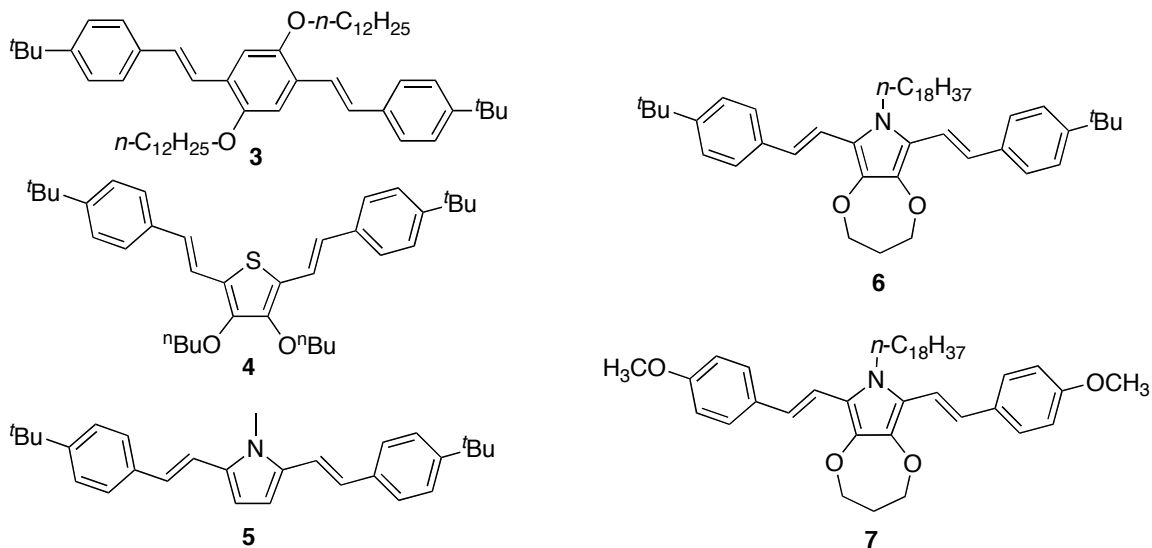
Figure 4.6. Bis(4-*tert*-butylstyryl)arenes and a bis(4-methoxystyryl)pyrrole as model compounds for the bis(diarylaminostyryl)arene derivatives.

4.2.2 Syntheses of Bis(diarylaminostyryl)arene Derivatives and Model Compounds

The syntheses of compounds **II**-**VII** have been previously described in the literature.[8-10,16] Compound **I** was previously synthesized[17] under typical Horner-Emmons conditions[18,19] from 4-[bis(4-*n*-butoxyphenyl)amino]benzaldehyde and tetraethyl 2,5-dicyano-1,4-xylene-α,α'-diyldiphosphonate.[20] 4-[Bis(4-*n*-butoxyphenyl)amino]-benzaldehyde was synthesized via a Buchwald-Hartwig[21,22] coupling of 4-bromobenzaldehyde and bis(di-4-*n*-butoxyphenyl)amine (Chapter 3).

Diethyl bis(4-*tert*-butylphenyl)aminobenzylphosphonate (**11**, Scheme 4.1) was common to the syntheses of compounds **1** and **2**. The phosphonate was synthesized by the formylation of bis(4-*tert*-butylphenyl)aniline (**8**)[23] to obtain 4-bis(4-*tert*-butylphenyl)aminobenzaldehyde (**9**),[23] which was followed by reduction with sodium borohydride in ethanol to obtain 4-bis(4-*tert*-butylphenyl)aminobenzyl alcohol (**10**), which was ultimately reacted with triethylphosphite / iodine to obtain phosphonate **11** under previously published conditions.[24]
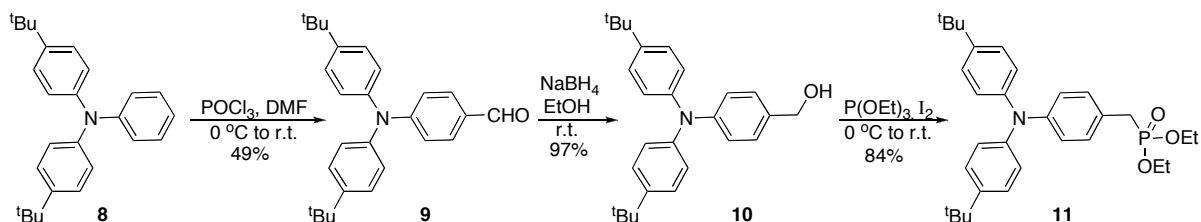
Scheme 4.1. Synthesis of diethyl bis(4-*tert*-butylphenyl)aminobenzylphosphonate.

2,5-Bis(di(4-*tert*-butylphenyl)aminostyryl-*N*-methylpyrrole (Scheme 4.2) was synthesized in a Horner-Emmons reaction of diethyl bis(4-*tert*-butylphenyl)aminobenzylphosphonate (**11**) with *N*-methylpyrrole-2,5-dicarboxaldehyde (**12**)[25] in reasonable yield.
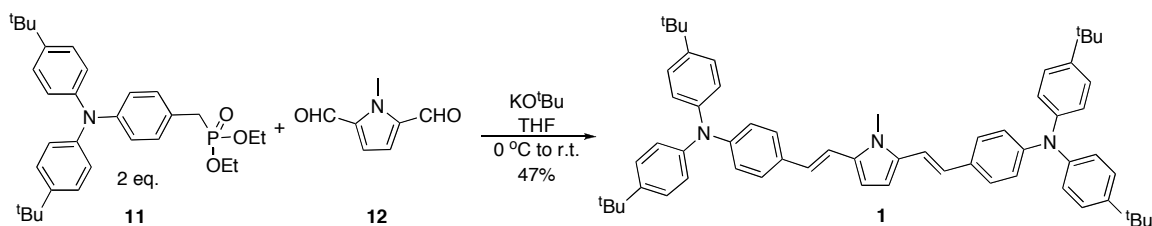
Scheme 4.2. Synthesis of 2,5-bis(di(4-*tert*-butylphenyl)aminostyryl-*N*-methylpyrrole.

Similarly, to obtain 2,5-bis(di(4-*tert*-butylphenyl)aminostyryl-3,4-[2,3,4,7-tetrahydro-[1,4]dioxepino]-*N*-methylpyrrole (**2**, Scheme 4.3), the same reaction conditions were used to react diethyl bis(4-*tert*-butylphenyl)aminobenzylphosphonate (**11**) with 3,4-[2,3,4,7-tetrahydro-[1,4]dioxepino]-*N*-methylpyrrole-2,5-dicarboxaldehyde (**13**).
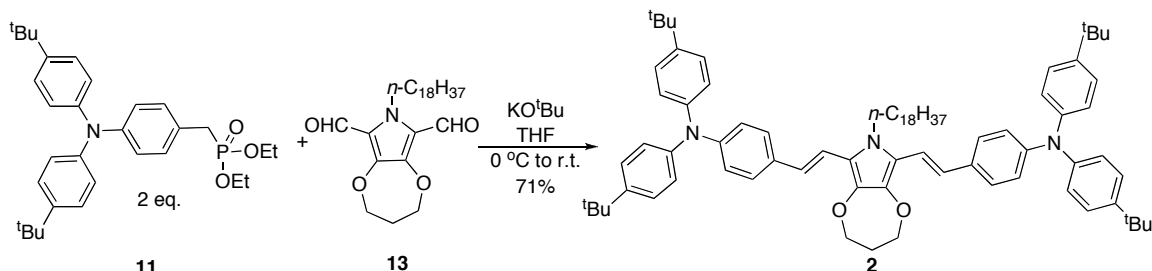
Scheme 4.3. Synthesis of 2,5-Bis(di(4-*tert*-butylphenyl)aminostyryl-3,4-[2,3,4,7-tetrahydro-[1,4]dioxepino]-*N*-methylpyrrole.

Bis(4-*tert*-butylstyryl)-2,5-di(*n*-dodecyloxy)benzene (**3**, Scheme 4.4) was synthesized as a model compound for compound **IV**. A Horner-Emmons reaction was used to react diethyl 4-*tert*-butylbenzylphosphonate[26] (**14**) with 1,4-di(*n*-dodecyloxy)benzene-2,5-dicarboxaldehyde[27] (**15**).
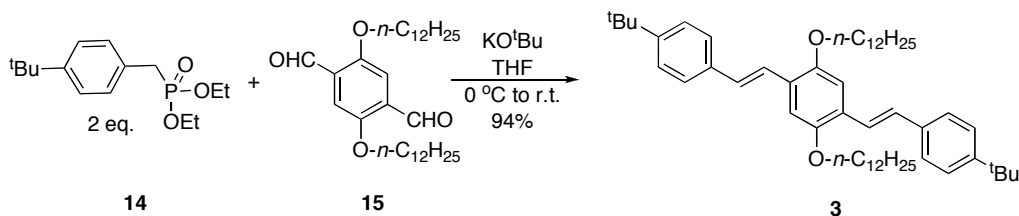
Scheme 4.4. Synthesis of 1,4-bis(4-*tert*-butylstyryl)-2,5-di(*n*-dodecyloxy)benzene.

2,5-bis(4-*tert*-butylstyryl)-3,4-di(*n*-butoxy)thiophene   (**4**,   Scheme   4.5)   was synthesized by a Horner-Emmons reaction of diethyl 4-*tert*-butylbenzylphosphonate[26] (**14**) with 3,4-di(*n*-butoxy)thiophene-2,5-dicarboxaldehyde[28] (**16**).   Compound **4** was synthesized as a model compound for compounds **IV** and **V**.
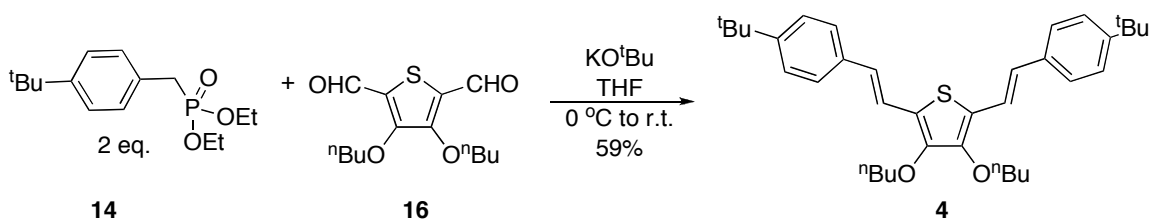
Scheme 4.5. Synthesis of 2,5-bis(4-*tert*-butylstyryl)-3,4-di(*n*-butoxy)thiophene.

Similarly,   2,5-bis(4-*tert*-butylstyryl)-*N*-methylpyrrole   (**5**,   Scheme   4.6)   was synthesized by a Horner-Emmons reaction of diethyl 4-*tert*-butylbenzylphosphonate[26] (**14**) with *N*-methylpyrrole-2,5-dicarboxaldehyde (**12**).[25]
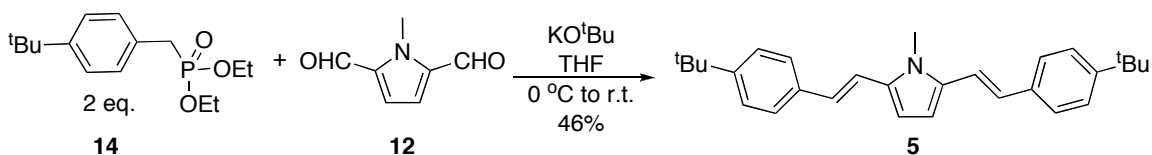
Scheme 4.6. Synthesis of 2,5-bis(4-*tert*-butylstyryl)-*N*-methylpyrrole.

Lastly,   bis(2,5-bis(4-*tert*-butylstyryl)-3,4-propylenedioxy-*N*-methylpyrrole   (**6**, Scheme 4.7) and 2,5-bis(4-methoxystyryl)- 3,4-propylenedioxy-*N*-methylpyrrole (**7**) were synthesized from diethyl 4-*tert*-butylbenzylphosphonate[26] (**14**) or commercially

available diethyl 4-methoxybenzylphosphonate (**15**) with 3,4-propylenedioxy-*N*-methylpyrrole-2,5-dicarboxaldehyde (**13**) as model compounds for compound **2**.
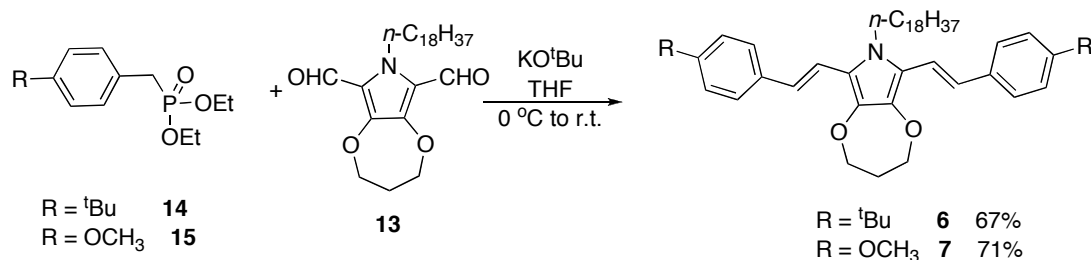
Scheme 4.7. Synthesis of 2,5-bis(4-*tert*-butylstyryl)-3,4-propylenedioxy-*N*-methylpyrrole.

4.2.3 Electrochemical Characterization of Bis(diarylaminostyryl)pyrrole Derivatives and Model Compounds

CV experiments were performed on bis(diarylaminostyryl)pyrroles **1** and **2**. As was the case for the previous bis(diarylaminostyryl)pyrrole derivative (**VII**), compounds **1** and **2** showed three separate one-electron oxidations (Figure 4.6). The cyclic voltammogram of compound **1** is shown with $Cp^*_2Fe^{+/0}$ as the internal reference at -0.55 V, and that of compound **2** is shown with $Cp_2Co^{+/0}$ as the internal reference at -1.32 V.
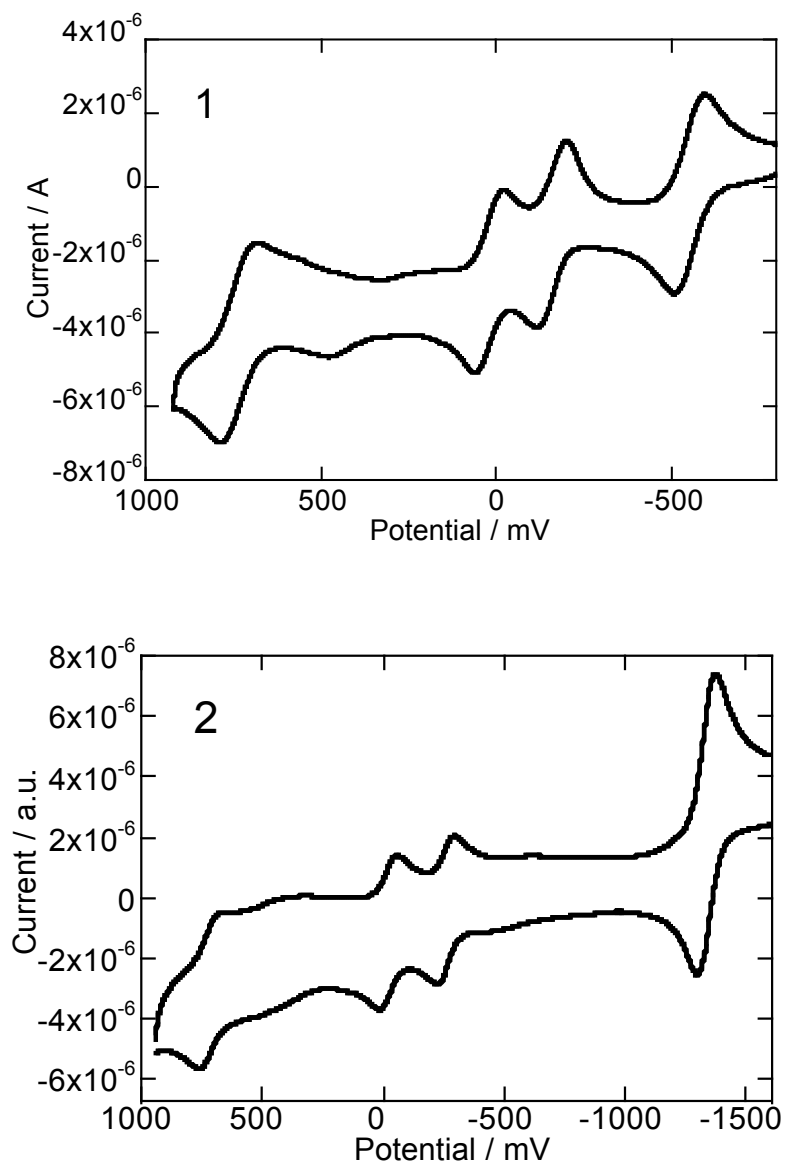
Figure 4.7. Cyclic voltammogram of compound **1** in 0.1 M nBu$_4$NPF$_6$, shown with Cp*$_2$Fe$^{+/0}$ as the internal reference at -0.55 V (top); cyclic voltammogram of compound **2** in 0.1 M ^{n}Bu$_4$NPF$_6$, shown with Cp$_2$Co$^{+/0}$ at -1.32 V as the internal reference (bottom), potentials referenced to Cp$_2$Fe$^{+/0-}$ at 0 V.

The half-wave oxidation potentials of compounds **I**-**VII** and **1**-**2** are shown below in Table 4.1. The first and second oxidations of **VII** and **1** occur at relatively similar potentials, while the third oxidation of **1** is 0.15 V more difficult than of $\mathbf{VII^{+/0}}$; the more difficult third oxidation potential in **1** is consistent with the less electron-rich end group compared to compound **VII**. This difference also suggests that the first and second oxidations depend more on the character of the bridge than on the end groups in the cases of **VII** and **1**. Upon introduction of the 3,4-propylenedioxy-pyrrole bridge in compound **2** while also retaining the less electron-rich end groups, the first oxidation of **2** becomes easier than that of **1** by ca. 0.1 V; this difference is also consistent with the first oxidation being strongly bridge-based and also correlates with the difference between the oxidation potentials of 3,4-propylenedioxy-*N*-alkylpyrroles and *N*-alkylpyrroles.[15] The second oxidation is slightly easier in compound **2** than in **1**, which may also be a contribution from the alkoxy groups on the pyrrole in **2**. The third oxidation occurs at the same potential for **1** and **2**, which have the same end groups, and is again consistent with the third oxidation depending more on the end groups than on the bridge.

Table 4.1. Half-wave oxidation potentials (V) versus $Cp_2Fe^{+/0}$ at 0 V, in 0.1 M nBu_4NPF_6 in dichloromethane) for 1,4-bis[4-(diarylamino)styryl]benzenes and 2,5-bis[4-(diarylamino)styryl]heteroarenes.[a]

compound	+/0	2+/+	3+/2+
I	+0.26[b]		+0.94
II	+0.20[b]		+0.81
III	+0.31[b]		+0.97
IV	+0.24[b]		+0.91
V	+0.05[b]		+0.70[c]
VI	+0.15[b]		+0.97
VII	–0.18	+0.01	+0.58
1	-0.16	+0.02	+0.73
2	–0.26	–0.02	+0.73

[a] All processes were reversible. [b] The separation between first and second oxidation were not resolvable.

CV experiments (Figure 4.7) were also performed on the bridge-based model compounds (**3**-**7**). Of the derivatives with *tert*-butyl functionalization, compounds **3** and **4** showed reasonably reversible oxidations, while pyrrole-based compounds **5** and **6** displayed partially reversible oxidations, suggesting that the radical cations of compounds **5** and **6** are not stable. Generally, the more electron-rich the bridge is, the smaller difference there is between the first oxidation potentials of the model compounds and their corresponding bis(diarylaminostyryl)arene derivatives, which suggests that the oxidation of the bis(diarylaminostyryl)arene derivative becomes more bridge-based when the frontier molecular orbital energy of the bridge is raised.

In the case of the bridge-based pyrrole model compound with methoxy end groups (**7**), the difference in oxidation potential between the model compounds and its bis(diarylaminostyryl)pyrrole derivative (**2**) is 0.04 V. Although the model compound is oxidized at a similar potential to its bis(diarylaminostyryl)arene counterpart, the oxidation of the model compound is not reversible, suggesting that **7**$^+$ is unstable.

Because the lack of diarylamino-donor substitution leads to irreversible oxidations of the pyrrole-based model compounds in CV experiments, this suggests that di(styryl)pyrrole monocations requires the donor substitution for stability, and, thus, the monocation of compounds **IV**, **1**, and **2** cannot be entirely bridge-based.
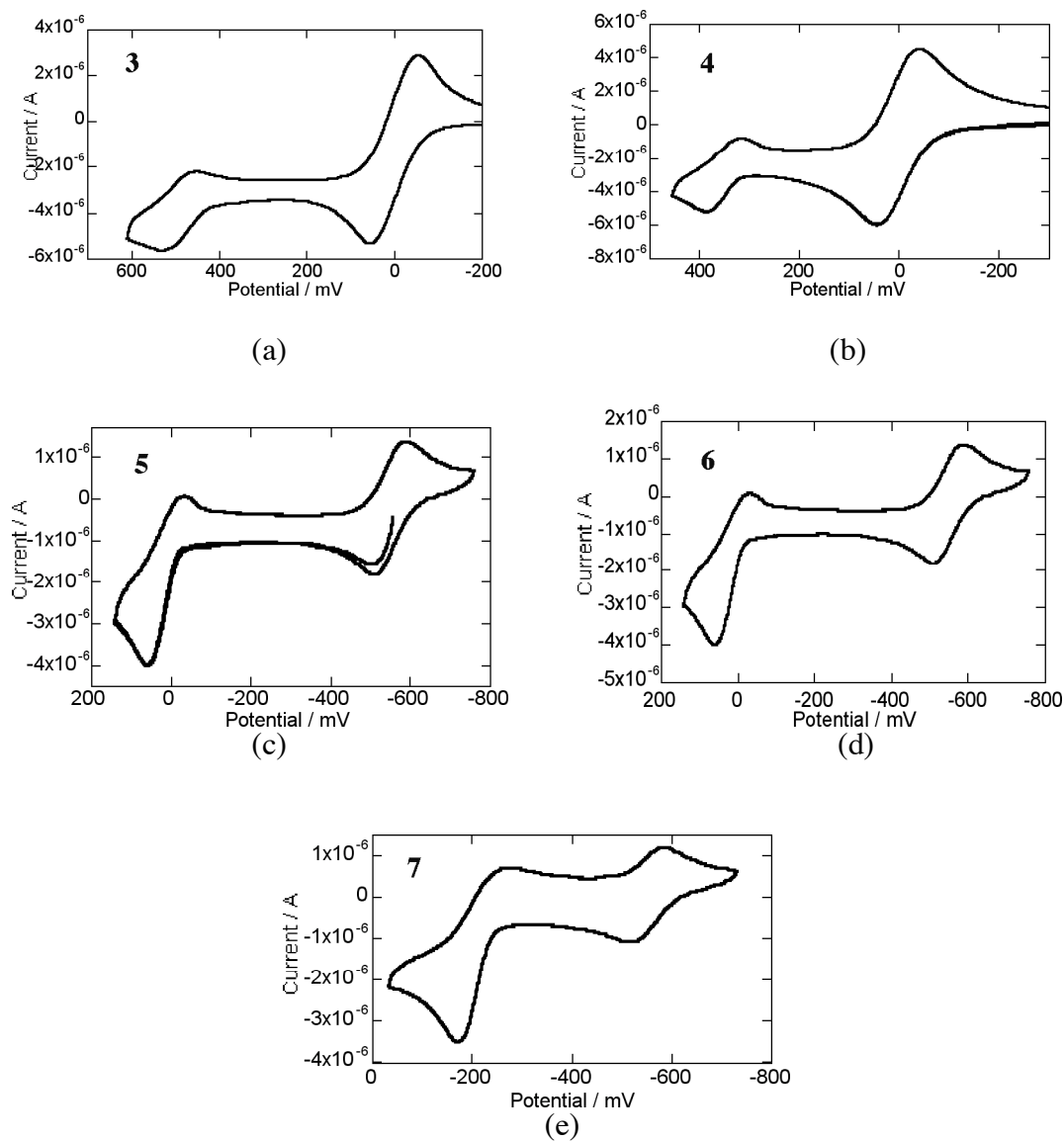
Figure 4.8. Cyclic voltammograms of (a) **3** with $Cp_2Fe^{+/0}$; (b) **4** with $Cp_2Fe^{+/0}$; (c) **5** with $Cp*_2Fe^{+/0}$; (d) **6** with $Cp*_2Fe^{+/0}$; and (e) **7** with $Cp*_2Fe^{+/0}$ as the internal reference. All CV experiments were recorded in 0.1 M nBu_4NPF_6 in dichloromethane at 50 mV/s.

Table 4.2 shows the oxidation potentials for the bridge-based model compounds as well as the first oxidation potentials for the corresponding bis(diarylaminostyryl)arene derivatives. One can see that as the $E_{1/2}^{+/0}$ for the model compound decreases, there is also a decrease in the $E_{1/2}^{+/0}$ for the bis(diarylaminostyryl)arene derivatives. Furthermore, the difference in the oxidation potentials decreases as the bridge becomes easier to oxidize, which is consistent with the oxidation becoming more bridge-based when the bridge is more electron-rich.

Table 4.2. Oxidation potentials for bridge-based model compounds **3**-**7** with the first oxidation potentials of relevant reference compounds; difference in oxidation potentials between model and reference compounds.

Compound	$E_{1/2}^{+/0}$ (V)	Relevant Bis(diarylamino) Derivative	$E_{1/2}^{+/0}$ (V)	$\Delta E_{1/2}^{+/0}$ (V)
3	+0.49	**I**	+0.26	0.23
4	+0.35	**V**	+0.05	0.30
		VI	+0.15	0.20
5	+0.01	**VII**	-0.18	0.19
		1	-0.16	0.17
6	-0.14	**2**	-0.26	0.12
7	-0.22	**2**	-0.26	0.04

4.2.4 Visible-NIR Absorption Spectra of the Monocations of the Bis(diarylaminostyryl)pyrrole Derivatives

As in Chapters 2 and 3, solutions containing the MV radical cations were obtained in dichloromethane using tris(4-bromophenyl)aminium hexachloroantimonate ($E_{1/2}^{+/0}$ = 0.70 V versus $Cp_2Fe^{+/0}$ at 0 V in dichloromethane[29]) as the oxidant. Spectroscopic data for **II⁺** has been previously reported,[8,10] and the absorption spectra of the remaining monocations of **I** and **III–VII** were previously recorded. The absorption spectra of monocations **VII⁺** and **2⁺** were recorded at known concentration, and are plotted below

with the IVCT bands of the monocations previously assigned as class III MV species (**V⁺** and **VI⁺**) in Figure 4.8. The monocation of **1⁺** appears to be very unstable in comparison to the other monocations of the bis(diarylamino) derivatives. It is not obvious why this monocation was unstable when **VII⁺** and **2⁺** were relatively stable, but because of the instability, it is difficult to know the real molar absorptivity of the IVCT band as well as the properly analyze the shape of the band because of the presence of decomposition products in the spectrum.
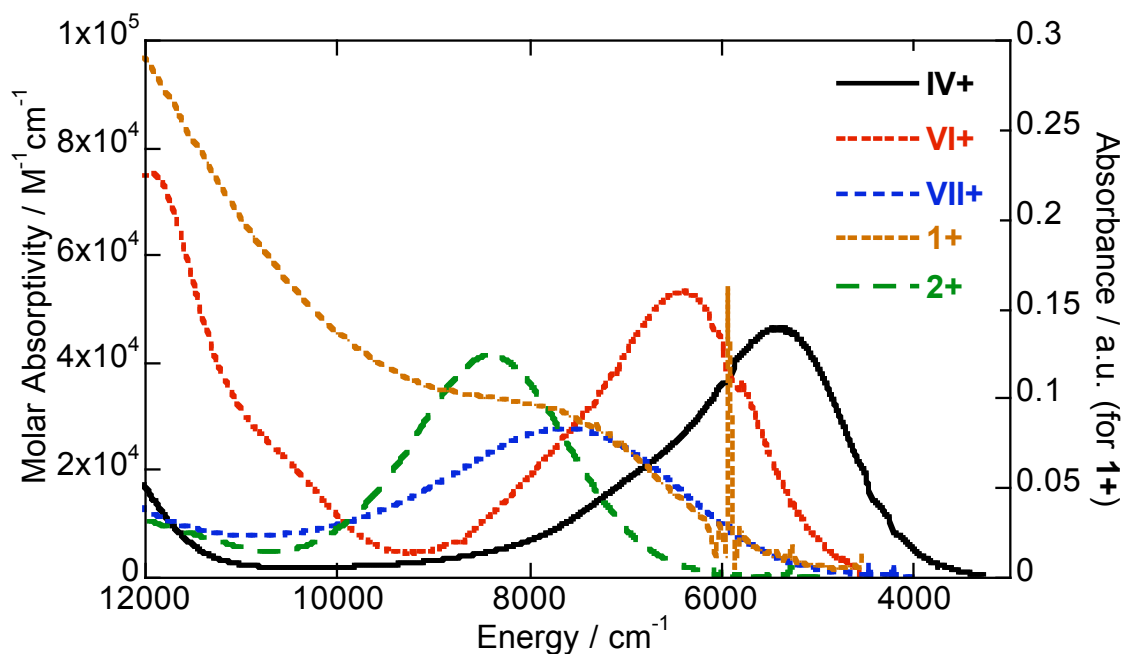
Figure 4.9. Molar absorptivities of the IVCT bands of monocations **IV⁺**, **VI⁺**, **VII⁺**, **1⁺**, and **2⁺** in dichloromethane.

Parameters obtained from the IVCT absorptions of the monocations are summarized in Table 4.3. $\bar{v}_{max}$ is the energy of absorption of the IVCT band, and ε_{max} is the molar absorptivity at the absorption maximum of the IVCT band. The half height

($\bar{\nu}_{1/2}$[obs]) is defined as the width of the IVCT absorption at half-height. The width predicted for class II compounds by Hush theory ($\bar{\nu}_{1/2}$[Hush]) is shown for comparison (Equation 4.1). $\bar{\nu}_{1/2}$[high] and $\bar{\nu}_{1/2}$[low] are compared to evaluate the symmetry of the band. The transition dipole moment (μ_{ge}) is also included. For **1$^+$**, fewer parameters are included because of the inability to properly analyze the IVCT band; it should also be noted that the parameters that are shown have larger error than the other monocations, due to the greater error in the energy of maximum absorption of the IVCT band.

Table 4.3. Experimental parameters characterizing the intervalence absorptions of the radical cations of bis(diarylamino)styrylbenzenes and bis(diarylamino)styrylheteroarenes in dichloromethane.

	$\bar{\nu}_{max}$ / cm^{-1}	ε_{max} / M^{-1}cm^{-1}	$\bar{\nu}_{1/2}$[obs] / cm^{-1}	$\bar{\nu}_{1/2}$[Hush] / cm^{-1}	$\bar{\nu}_{1/2}$[high] / $\bar{\nu}_{1/2}$[low]	$\bar{\nu}_{1/2}$[high] / $\bar{\nu}_{1/2}$[Hush]	μ_{ge} / D
I$^+$	7450	6100	4490[a]	4150	1[a]	1.08[a]	5.78[a]
II$^+$	6130	15500	4310[a]	3760	1[a]	1.15[a]	10.3[a]
III$^+$	4860	21300	3380	3350	2.15	1.38	11.8
IV$^+$	5400	46300	1980	3530	1.50	0.67	13.6
V$^+$	5660	45800	2450	3620	1.81	0.97	13.9
VI$^+$	6390	53000	1980	3840	1.41	0.60	12.9
VII$^+$	7630	27600	3090	4200	1.25	0.82	10.4
1$^+$	7810	–	–	4247	–	–	–
2$^+$	8420	41100	1920	4410	1.01	0.44	9.65

[a]Appear to be approximately symmetrical and assumed to be so due to overlap with other bands on high-energy side

The absorption maximum of the IVCT band of the pyrrole-bridged cation **VII$^+$** is at yet higher energy than **IV$^+$–VI$^+$**, and the band shape is rather different, being broader and less strongly asymmetric (Figure 4.7). However, the band is still narrower than the Hush limit (Equation 4.1), suggesting a symmetric cation (i.e. bridge-based on a class III MV species). Interestingly, the IVCT of a bis(diarylamino)dithienopyrrole radical cation shows a rather different band shape to analogues with bithiophene or dithienothiophene

bridges (Chapter 3). The IVCT band of 1^+ appears to be more blue-shifted than that of

VII^+, although it is difficult to determine with certainty due to the rapid decomposition of

1^+; if the absorption of 1^+ is indeed blue-shifted with respect to VII^+, the coupling in 1^+

would be stronger than in VII^+, which is what was predicted. The IVCT of the

dialkoxypyrrole-bridged monocation 2^+ is strongly symmetric and is much narrower than

the IVCT band of VII^+, the width being less than half of the Hush limit, suggesting that it

is a symmetric class III mixed valent monocation. Also, because CV experiments

suggested that the monocation of the bridge model compounds (**6** and **7**) for **2** were not

stable, this provides support that the monocation of **2** can still be considered as having

some MV diamine character rather than being a completely bridge-localized species.

4.2.5 Evaluation of the Coupling in Bis(diarylaminostyryl)pyrrole Derivatives from IVCT Absorptions

Equations 4.2 and 4.3 can be used to calculate the electronic coupling in class III

MV species. While the transition dipole moment (μ_{ge}) can be readily evaluated from the

experimental spectra, identifying the appropriate value of diabatic ET distance (R_{ab}) is

often problematic, since the diabatic states are often displaced into the bridge. Theoretical

estimates of R_{ab} can be obtained from

$$R_{ab} = \frac{2|\mu_\pm|}{e} \tag{4.4}$$

where $\mu_\pm$ is the transition dipole moment between the adiabatic surfaces at the symmetric

geometry corresponding to the crossing point of the diabatic surfaces,[30] or from

$$R_{ab} = \frac{\sqrt{\Delta\mu_{12}^2 + 4\mu_{ge}^2}}{e} \qquad (4.5)$$

where μ_{ge} and $\Delta\mu_{12}$ are the transition dipole moment and static dipole moment change associated with the IVCT transition.[31,32] In the case of equation 4.4, TD-DFT values are used to calculated $\mu_\pm$, and for equation 4.5, experimental values are used for μ_{ge}, and AM1/CI values are used to calculate $\Delta\mu_{12}$.

Table 4.4 compares estimates of V from equations 4.2 (for class III systems only) and 4.3; for equation 4.3, three sets of values for V were calculated: 1) using the nitrogen-nitrogen distance (R_{NN}) and the alternative estimates of R, 2) using R_{ab} calculated from equation 4.4, and 3) using R_{ab} calculated from equation 4.5. Note that for **1⁺**, only the value of V from equation 4.2 was used because the molar absorptivity for this monocation is not known. The values for V when using alternate estimates for R with equation 4.3 are larger by a factor of ca. 3 (**IV⁺-VI⁺**) or 4 (**VII⁺** and **2⁺**) than the values obtained from equation 4.3 using R_{NN}. Additionally, for the class III systems, the value for V using equation 4.2 give similar values to those used with equation 4.3 when the alternate estimates for R are employed. These discrepancies at least partially reflect the fact that the diabatic electron-transfer distance, R_{ab}, is shorter than the geometric nitrogen-nitrogen separation, meaning that the centers of the two redox sites are considerably displaced into the bridge, rather than centered on the amine nitrogen atoms.

Table 4.4. Electronic coupling (cm^{-1}) calculated by various estimates of R with equation 4.3, and from equation 4.2 for class III species.

	$V_{[eq\ 4.3]}$ with R_{NN}	$V_{[eq\ 4.3]}$ with $R_{[eq\ 4.4]}$	$V_{[eq\ 4.3]}$ with $R_{[eq\ 4.5]}$	$V_{[eq\ 4.2]}$
I$^+$	480	1020	530	–
II$^+$	700	1500	1460	–
III$^+$	640	1500	1400	–
IV$^+$	810	2130	2010	2700
V$^+$	960	2370	2080	2830
VI$^+$	1000	2970	2260	3200
VII$^+$	920	2350	3720	3820
1$^+$	–	–	–	3905
2$^+$	940	2840	4080	4210

The values of V calculated using R_{NN} vary by a factor of two depending on the redox properties of the terminal and bridging groups. However, R_{ab} is likely to decrease as the electron-richness of the bridge is raised or that of the end group is lowered; accordingly the true variation in V between the most weakly and most strongly coupled systems is likely to be even greater than the variation in V based on R_{NN} suggested by Table 4.4.

4.2.6 EPR Spectra of the Monocations of the Bis(diarylaminostyryl)arene Derivatives

Because the diabatic electron-transfer distance (R_{ab}) appears to decrease upon increasing the frontier molecular orbital energies of the bridges, in principle this change should be observable as the coupling to the nitrogen nuclei decreases and coupling to the bridging hydrogen nuclei increases. If the cation becomes more bridge-based, then,

instead of showing coupling to two nitrogen nuclei at room temperature, it is possible that the unpaired electron would be more coupled to the hydrogen nuclei of the bridge and therefore have smaller coupling to the nitrogen nuclei. Therefore the EPR spectra of several bis(diarylaminostyryl)arene monocations were recorded to compare spectral features in the different species.

The same solutions of monocations generated for visible-NIR absorption spectra were used for measurement with an X-band EPR spectrometer. The spectra (Figure 4.9) were all centered at $g = 2.004$ and, in many cases, no coupling was resolvable in the EPR spectra; the poor resolution could be caused by coupling to large numbers of inequivalent protons, which could blur any pattern in the EPR signal. For example, the poor resolution of the tri(biphenyl-4-yl)aminium monocation, the poor resolution in the EPR spectrum is attributed to the large number of unique hydrogen nuclei.[33] In the cases of $\mathbf{I^+}$ and $\mathbf{II^+}$, however, five-line spectra were observed in dichloromethane, consistent with coupling to two equivalent nitrogen centers ($I = 1$ ^{14}N) with hyperfine coupling constant (A_N) of 4.3 G and 3.6 G, respectively, noting though that the simulation to $\mathbf{I^+}$ was not a perfect fit (this will be further addressed in section 4.3). These values are similar to half of the magnitude of the coupling constant reported for the mononuclear triarylamine radical cation $[(4\text{-}MeOC_6H_4)_3N]^+$ in acetonitrile,[34] which is reasonable since the amount of charge localized on each nitrogen nucleus in an apparently delocalized system should be approximately half that reported for one triarylamine, assuming minimal contributions from coupling to hydrogen nuclei. It is not surprising that the coupling to nitrogen is larger for $\mathbf{I^+}$ than for $\mathbf{II^+}$ because the bridge energy is higher in $\mathbf{II^+}$ than in $\mathbf{I^+}$, and therefore, it is expected that there would be slightly more charge on the bridge than the

triarylamine in $\mathbf{II^+}$ than in the case of $\mathbf{I^+}$. The observation of coupling to both nitrogen

centers is consistent either with a delocalization of the unpaired electron (class III MV

species) or with an intramolecular electron exchange rate in excess of ca. 1.7×10^7 s^{-1}, the

approximate magnitude for a coupling constant to nitrogen of ca. 5.8 G.
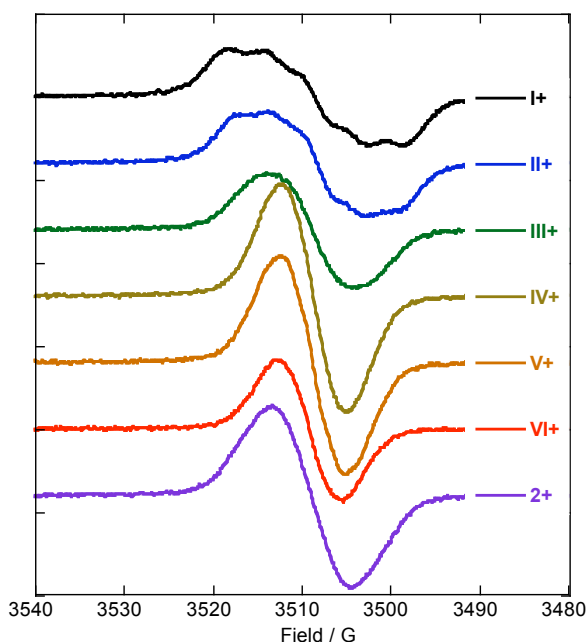
Figure 4.10. EPR spectra of the monocations of some bis(diarylaminostyryl)arene derivatives in dichloromethane.

Although the EPR spectrum of $\mathbf{III^+}$ does not show a fine pattern, the overall shape

of the spectrum is narrower than the spectra for $\mathbf{I^+}$ and $\mathbf{II^+}$. The spectra of $\mathbf{IV^+}$ and $\mathbf{V^+}$ are

narrower than that of $\mathbf{III^+}$. The spectra for these three monocations support the idea that

the charge has more bridge character and that the coupling to the nitrogen nuclei

continues to decrease as the bridge energy is increased. Interestingly, the EPR spectrum

of $\mathbf{VI^+}$, with higher bridge energy than $\mathbf{V^+}$, is broader than that of $\mathbf{V^+}$; the broadening

189

could be due to coupling to the nitrogen nucleus in the pyrrole ring. While intermolecular ET has been shown to cause line narrowing in EPR spectra when the concentration of monocation of a bis(triarylamine) derivative was increased,[35] the concentrations of the monocations is sufficiently dilute that intermolecular exchange was not expected to be a factor in the line shape, and the concentrations were similar to those reported in the literature for which line narrowing was not observed.[35] Additionally, the line shapes (when integrated) are not Lorentzian in shape, which also supports the notion that the spectra are free from intermolecular exchange.

Finally, in the case of **2⁺**, with a more electron-rich pyrrole-based bridge than **VI⁺**, the EPR spectrum is broader than that of **VI⁺**, which could result from even more bridge basis in **2⁺**, which could give an even larger coupling to the central nitrogen nucleus, again broadening the spectrum. Unfortunately, since there is no splitting pattern in the EPR spectra of the class III monocations, the spectra cannot be simulated with WinSim to analyze this proposed explanation for the spectral narrowing and eventual broadening upon increasing the energies of the bridges. Additionally, because the bridge-based model compounds are not stable as monocations, it is not possible to examine their EPR spectra for comparison. Hopefully future DFT calculations will lead to predictions of hyperfine coupling constants that could be used to simulate the EPR spectra to determine if the prediction of the trend in line shape is replicated.

4.3 Determination of the Barrier to Electron Exchange in the Monocations of Bis(diarylamino) Derivatives

In MV compounds the inherent ET properties and patterns of charge

(de)localization strongly depend on the interplay between the electronic coupling (V) and reorganization energy (λ). While analysis of IVCT bands in the framework of Hush semi-classical[36] or vibronic coupling models [30,37] have been used to extract information quantifying both microscopic parameters in MV bis(triarylamine)s, this approach suffers from the ambiguity in deriving the ET distance between redox centers, as was discussed previously section 4.1. [2,30]

In the conventional semi-classical model,[36]1 the barrier to thermal intramolecular ET ($\Delta G^{\ddagger}$) is also related to electronic coupling and reorganization energy through

$$\Delta G^{\ddagger} = \frac{\left(\lambda - 2V\right)^2}{4\lambda} \tag{4.6}$$

and, thus, the determination of the ET barrier can also be used to gain insight into the microscopic parameters.

A widely applied experimental method to probe the ET barrier is based on the measurements of the ET rates by means of EPR spectroscopy. [38,39] However, most of the previously investigated MV triarylamines have been strongly electronically coupled and are either completely delocalized (class III) or are likely to exhibit ET rates much faster than the typical EPR timescale. While VT-EPR has been used to determine the rates of intermolecular ET in the monocation of spiro-fused bis(triarylamine) derivative, in this study, the spectra at all temperatures were 5-line in nature, and no optical data was provided for comparison.[40] The goal of this study was to observe a transition from approximately 5-line to 3-line from high to low temperatures and to try to gain insight about the ET rates in the bis(diarylamino) monocations.

191

Because the radical cations of some of the bis(triarylamine)s in the first portion of this chapter appeared to be class II MV species, the possibility was reasonable for observation of a difference in the rate of electron exchange in the monocation in a VT-EPR experiment. If spectral changes occurred in VT-EPR, it should allow for rates of electron exchange to be extracted (from simulations of the EPR spectra), ultimately using an Arrhenius plot to determine the barrier to electron exchange.

4.3.1 Bis(triarylamine)s for Variable Temperature EPR Studies

This portion of the chapter focuses on the analysis and interpretation of VT-EPR experiments of radical cations $\mathbf{I^+}$, $\mathbf{II^+}$, and $\mathbf{VIII^+}$-$\mathbf{XI^+}$ (Figure 4.10). Some of the monocations ($\mathbf{I^+}$, $\mathbf{II^+}$, and $\mathbf{IX^+}$-$\mathbf{X^+}$) were chosen because of their weak electronic coupling (*V*), as calculated based on Hush analysis of their IVCT absorptions, while $\mathbf{VIII^+}$ has been assigned as a strongly coupled MV species on the basis of visible-NIR absorption, vibrational spectroscopy,[8,41] and X-ray diffraction analysis of a crystal of the monocation salt. In alkene-based derivatives ($\mathbf{I^+}$, $\mathbf{II^+}$, and $\mathbf{VIII^+}$), the frontier molecular orbital energy and length of the bridge were chosen for comparison of bis(triarylamine)s with similar structure with slight variations that affect the electronic coupling between the two redox centers. In another family of bis(triarylamine)s with alkyne-based bridges ($\mathbf{IX^+}$-$\mathbf{X^+}$), the bridge length is varied. In one additional example, a diarylaminophenylacetylene ($\mathbf{XI^+}$) was studied as a non-MV control species. In particular, the magnitudes of the electronic coupling and the hyperfine interactions in MV cations $\mathbf{I^+}$ and $\mathbf{IX^+}$ lead to the observation of a transition from delocalized (room temperature) to localized (low temperature) behavior on the EPR timescale. Rates extracted from simulations of the VT-EPR spectra

were used to obtain the thermal barrier to ET and to show that the ET falls in the adiabatic regime.
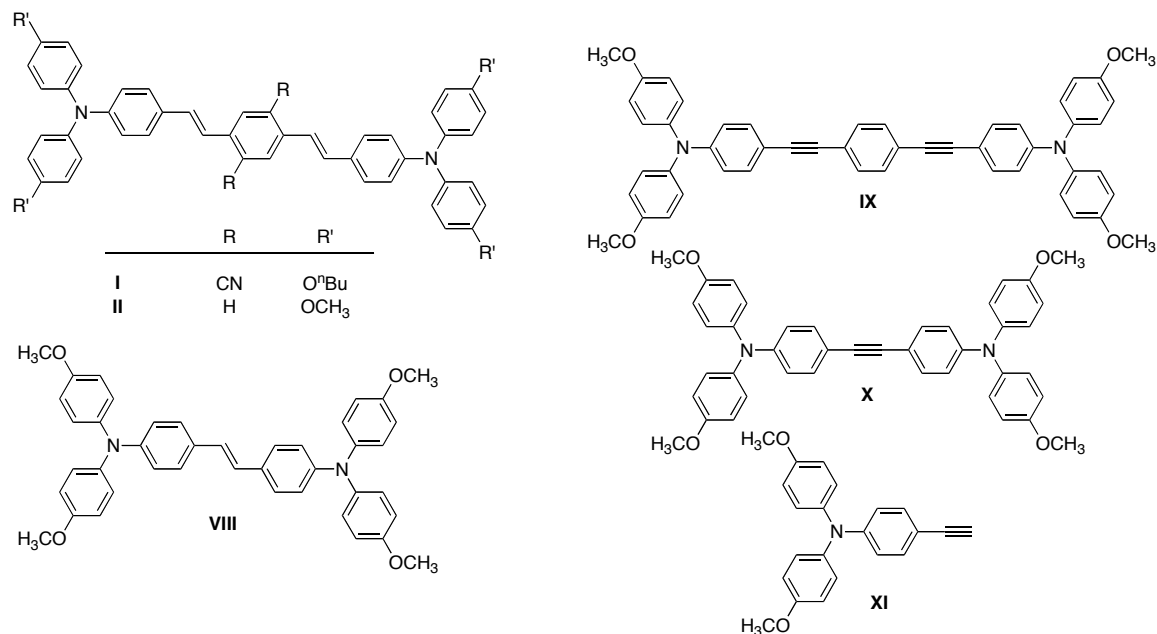
Figure 4.11. Bis(triarylamine)s and a control compound studied for which the radical cations were studied by VT-EPR experiments.

4.3.2 Room temperature EPR Spectra of the Monocations of the Bis(triarylamine)s and the Control Compound

For room temperature EPR spectra, the monocations of compounds $\mathbf{I^+}$, $\mathbf{II^+}$, and $\mathbf{VIII^+}$-$\mathbf{XI^+}$ were generated by addition of a 10-fold excess of neutral compound to one equivalent of tris(4-bromophenyl)aminium hexachloroantimonate in dichloromethane with concentrations of ca. 3×10^{-4} M in oxidizing agent. The EPR spectra for the radical cations are shown in Figure 4.11. The EPR spectra for the radical cations of the bis(triarylamino) derivatives all show approximately 5-line spectra, consistent with coupling to two nitrogen nuclei ($I = 1$, ^{14}N). In the cases of monocations $\mathbf{I^+}$ and $\mathbf{IX^+}$, the shape of the spectrum is difficult to model with WinSim, given that the height of the first

line is taller than the height of the second line, which is not typical for coupling to two nitrogen nuclei in a fast-exchange or delocalized regime. The nature of these line shapes will be explored further in the next sections. The EPR spectrum of the radical cation of the control triarylamine (**XI**$^+$) has a 3-line spectrum, consistent with coupling to one nitrogen nucleus, as was expected for this monocation.
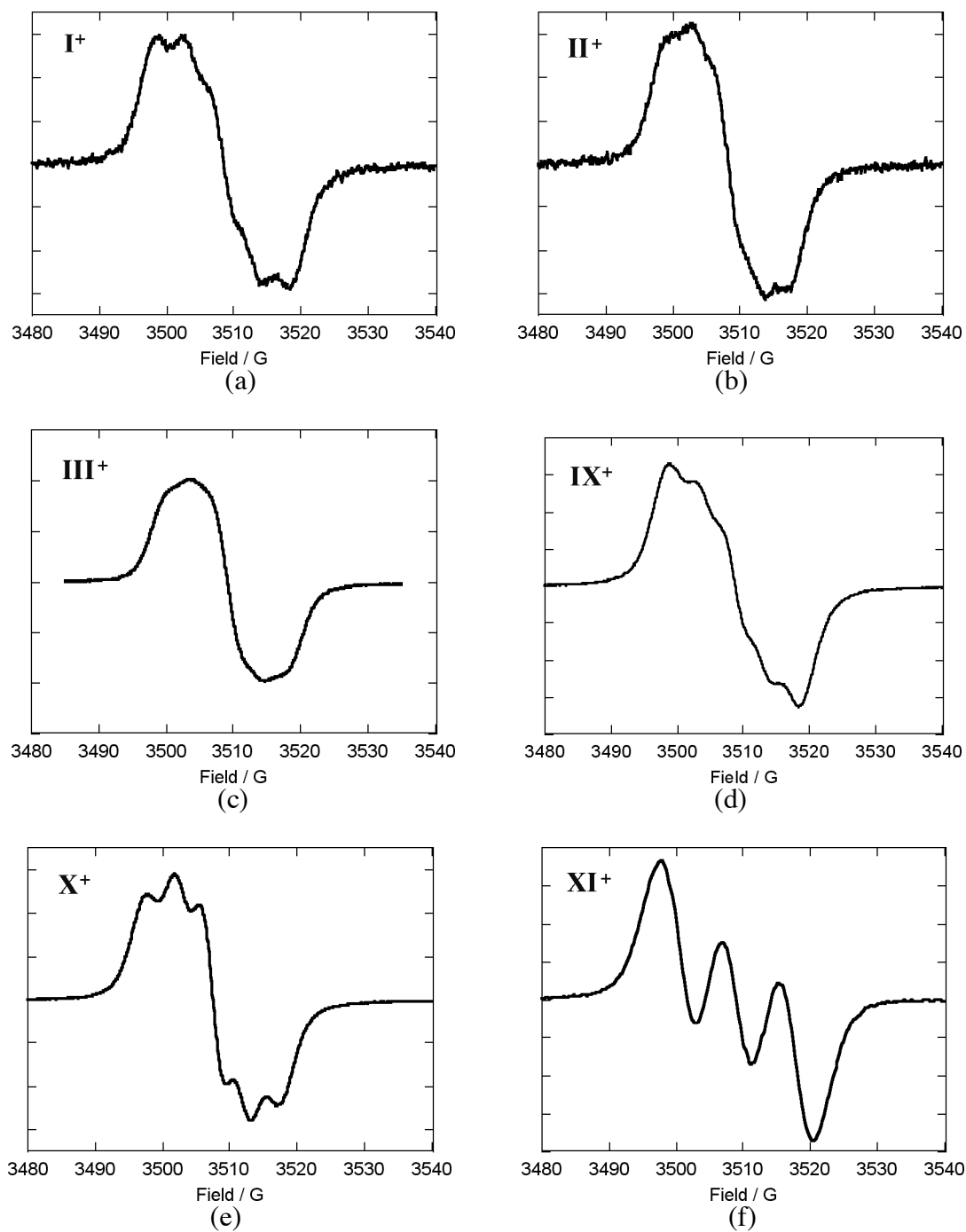
Figure 4.12. Room temperature EPR spectra for monocations $\mathbf{I}^+$ (a), $\mathbf{II}^+$ (b), and $\mathbf{VIII}^+$ (c), $\mathbf{IX}^+$ (d), $\mathbf{X}^+$ (e), and $\mathbf{XI}^+$ (f).

4.3.3 VT-EPR Spectra of the Monocations of the Bis(triarylamine)s

This section describes the experimental and simulated VT-EPR spectra of the monocations of the bis(triarylamine)s (**I⁺**, **II⁺**, and **VIII⁺-X⁺**) and of the model triarylamine (**XI⁺**). For the VT-EPR experiments, monocations **I⁺**, **II⁺**, and **VIII⁺-XI⁺** were also generated by adding a 10-fold excess of neutral compound to one equivalent of tris(4-bromophenyl)aminium hexachloroantimonate in dichloromethane, with concentrations ranging from ca. 3×10^{-4} M to 3×10^{-3} M in oxidizing agent.

4.3.4.1 Experimental and Simulated EPR Spectra of I⁺

VT-EPR spectra were recorded of monocation **I⁺** at ca. 10 K intervals from 298 to 191 K in dichloromethane. The spectra change shape from approximately a 5-line spectrum at room temperature to approximately 3-line spectrum at low temperature, suggesting a dynamic delocalization at room temperature and localization onto one triarylamine at low temperatures on the EPR time scale. The room temperature EPR spectrum could not be simulated with a good fit in WinSim, which assumes a static delocalization of the lone electron. Instead, the room temperature spectrum was simulated with an EPR-EXN program, which allows for the possibility of ET between multiple redox centers, giving a rate of $k_{ET} = 6.7 \times 10^8$ s⁻¹. The VT-EPR spectra were simulated at all temperatures using the EPR-EXN program and are shown in Figure 4.12. As expected, the rate of ET decreases upon cooling, reaching a minimum of 8.4×10^7 s⁻¹ at 191 K.

EXPERIMENTAL   SIMULATED

T = 298 K   6.7 x 10^8 s^{-1} = k$_{ET}$
288 K   6.5 x 10^8 s^{-1}
278 K   5.7 x 10^8 s^{-1}
268 K   4.9 x 10^8 s^{-1}
258 K   4.2 x 10^8 s^{-1}
248 K   3.6 x 10^8 s^{-1}
238 K   3.0 x 10^8 s^{-1}
228 K   2.4 x 10^8 s^{-1}
218 K   1.9 x 10^8 s^{-1}
208 K   1.3 x 10^8 s^{-1}
198 K   9.4 x 10^7 s^{-1}
191 K   8.4 x 10^7 s^{-1}

10 G
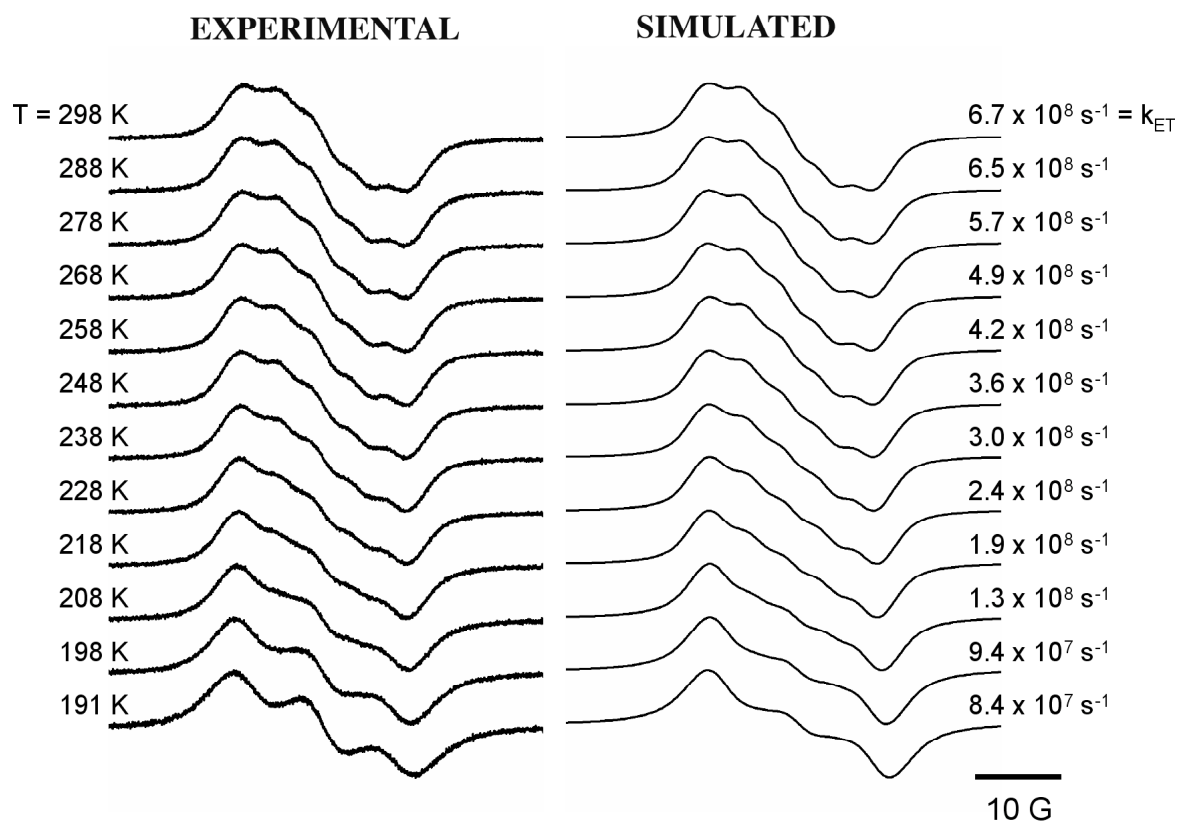
Figure 4.13.   Experimental (left) and simulated (right) VT-EPR spectra of **I**⁺ in dichloromethane.

At high temperatures, the simulations give reasonable fits to the experimental data, but at colder temperatures – where the spectra appear to be in an intermediate regime between the 5- and 3-line limits – the fits of the simulations do not match the experiments well. This may be because the model for fitting the electron exchange is purely classical and does not take into account nuclear tunneling effects. The rate data from the simulations will be further evaluated in Section 4.3.5.

4.3.4.2 Experimental and Simulated EPR Spectra of II⁺

EPR spectra of monocation $\mathbf{II^+}$ were also recorded in dichloromethane at variable temperatures. As is shown in Figure 4.13, the overall shape of the EPR spectra does not change much upon cooling from 300 to 195 K, suggesting that this approximately 5-line spectrum represents either a statically delocalized (class III) or rapidly dynamic delocalization of electron exchange between the two triarylamine redox centers on the EPR time scale. This is not surprising because, based on the optical data for the radical cations, monocation $\mathbf{II^+}$ is more strongly coupled ($V = 700$ cm^{-1}) than monocation $\mathbf{I^+}$ ($V = 480$ cm^{-1}) - based on equating R_{NN} to the diabatic ET distance - and should, therefore, have a lower barrier to electron exchange than does $\mathbf{I^+}$.
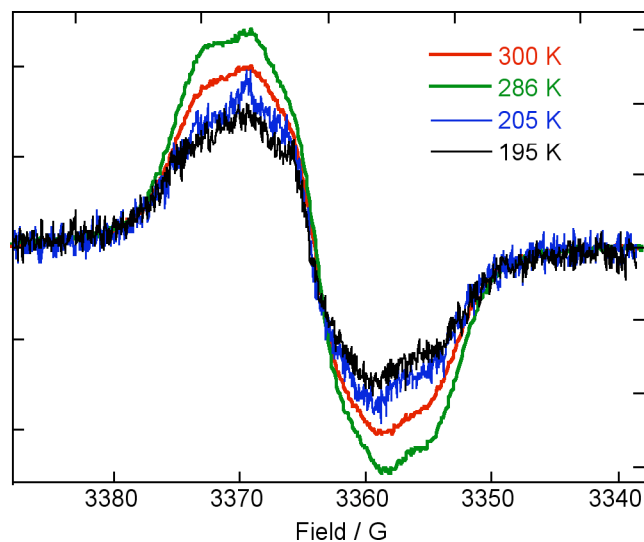
Figure 4.14. EPR spectra of monocation **II**⁺ in dichloromethane at multiple temperatures.

The room temperature spectrum was simulated with WinSim (Figure 4.14) to fit coupling to two nitrogen nuclei, giving a coupling constant $A_N = 3.9$ G, consistent with a monocation that is delocalized or in a fast exchange regime on the EPR time scale.
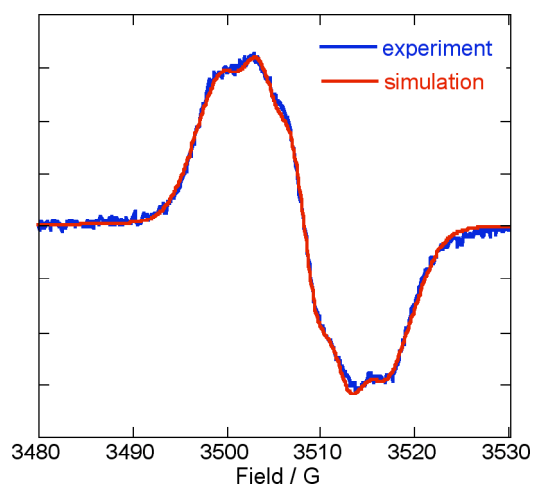
Figure 4.15. Experimental (blue) and simulated (red) EPR spectra for **II**⁺ at room temperature in dichloromethane.

4.3.4.3 Experimental and Simulated EPR Spectra of VIII⁺

VT-EPR spectra were also acquired for monocation **VIII⁺** in dichloromethane. The room temperature and low temperature spectra are nearly identical (Figure 4.15). Overall it appears that the spectrum is approximately a broadened 5-line spectrum at 205 K, which suggests that this monocation is in the fast regime of electron exchange on the EPR time scale. For the monocation to be in the fast regime at cold temperatures is not surprising because the optical data for **VIII⁺** suggest that it a strongly coupled (V = 1400 cm^{-1}) class III MV species. The observation of a 5-line spectrum at all temperatures is consistent with the previous assignment of **VIII⁺** as a class III MV species.
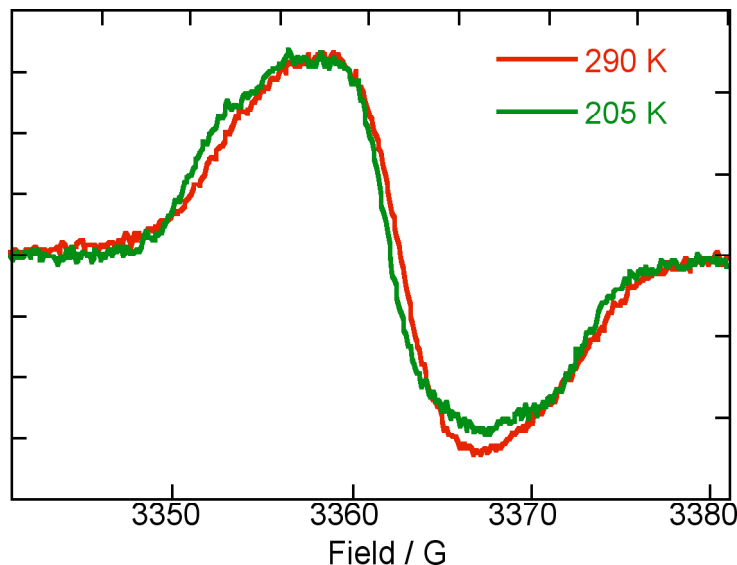
Figure 4.16. EPR spectra of monocation **VIII⁺** at 290 (red) and 205 (blue) K in dichloromethane.

Simulations of the room temperature EPR spectra of **VIII⁺** with WinSim gave a good fit to the experimental spectrion, showing coupling to two nitrogen nuclei with

coupling constant $A_N = 3.8$ G. The experimental and simulated spectra are shown in Figure 4.16.
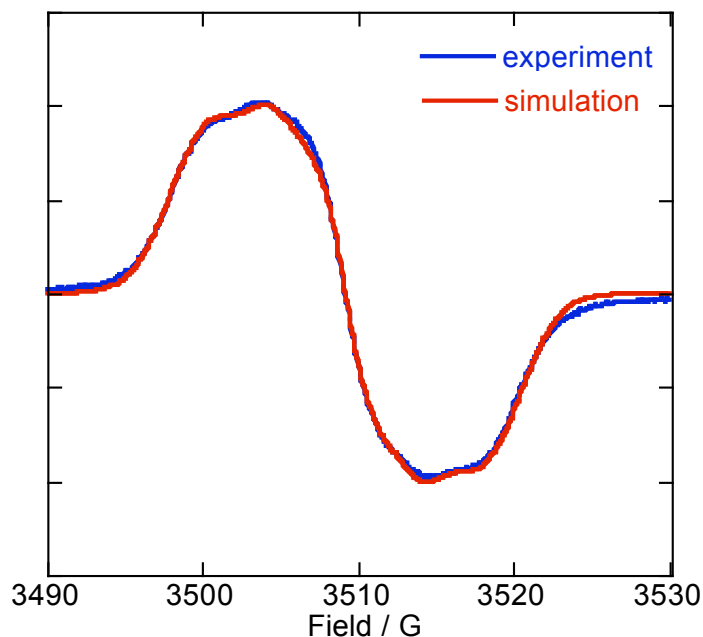
Figure 4.17. Experimental (blue) and simulated (red) EPR spectra of **VIII⁺** at room temperature in dichloromethane.

4.3.4.4 Experimental and Simulated EPR Spectra of IX⁺

VT-EPR spectra recorded for monocation **IX⁺** in dichloromethane show that the monocation appears to be in an intermediate regime of electron exchange at room temperature and reaches an approximately 3-line spectrum at lower temperatures. Again it is not surprising that the VT-EPR spectrum of **IX⁺** showed spectral changes upon cooling; in comparison to monocation **II⁺**, which has a similar bridge length to that of **IX⁺**, the electronic coupling in **IX⁺** (V = 490 cm⁻¹) is smaller than in **II⁺** (V = 700 cm⁻¹),

The room temperature EPR spectrum of **IX⁺** can only be simulated as a localized charge with hyperfine coupling to one triarylamine (A_N = 8.4 G) and thermal exchange rate on the order of ca. 3.5×10^8 s^{-1}. The shape of the spectrum cannot be reproduced (with WinSim) under the assumption of a delocalized charge. The VT-EPR spectra of **IX⁺** were simulated with the EPR-EXN program at each temperature, and a rate of electron exchange was extracted from each simulation (Figure 4.17). As expected, the rate of ET decreases with decreasing temperature, reaching a minimum of 3.5×10^7 s^{-1} at 185 K.
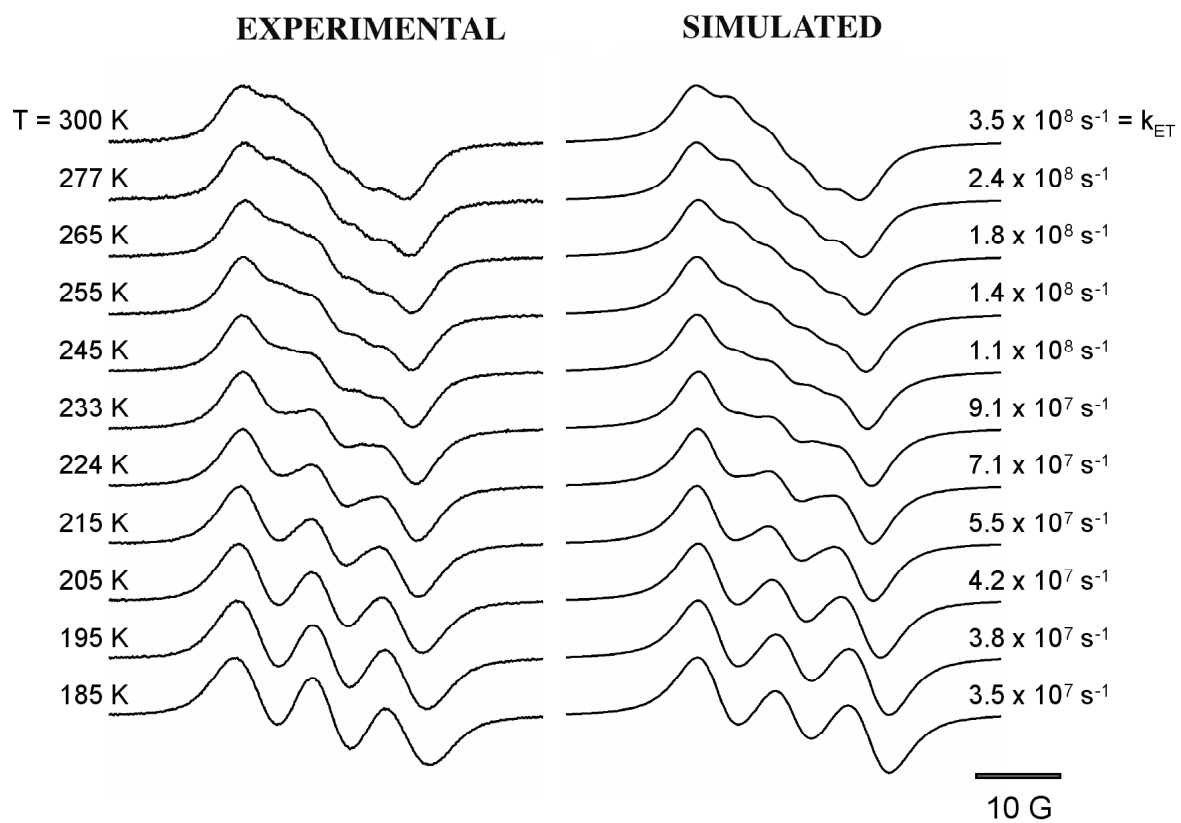
Figure 4.18. Experimental (left) and simulated (right) VT-EPR spectra of $\mathbf{IX^+}$ in dichloromethane.

In general, the simulations are in good agreement with the experimental spectra, although in some cases (particularly 255, 265, and 277 K), the center of the spectra do not match well. This is again presumably due to the treatment of this system as a classical model of electron exchange, as was described in the discussion of the fits for the VT-EPR spectra of $\mathbf{I^+}$, neglecting electron tunneling effects.

4.3.4.5 Experimental and Simulated EPR Spectra of X⁺

VT-EPR spectra were recorded for $\mathbf{X^+}$ in dichloromethane. Both the low temperature and room temperature spectra show a 5-line pattern, consistent with coupling to two nitrogen nuclei (Figure 4.18). This result suggests that the rate of intermolecular electron exchange is in the fast regime on the EPR time scale at both temperatures. This is consistent with stronger coupling in $\mathbf{X^+}$ (as determined from the analysis of the IVCT absorption band, assuming $R_{ab} = R_{NN}$) is ca. 1080 cm^{-1}, compared to that for $\mathbf{IX^+}$ ($V = 490$ cm^{-1}).
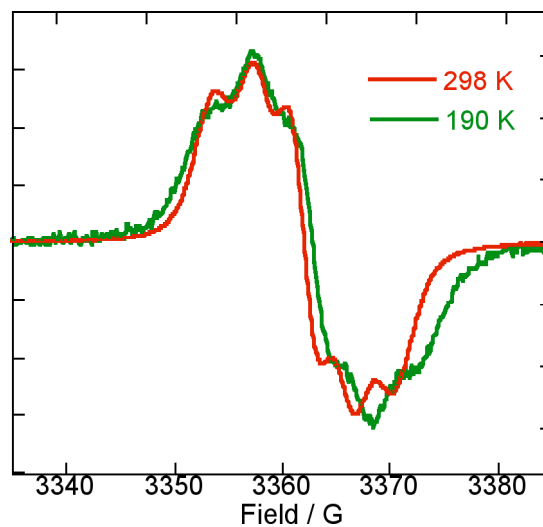
Figure 4.19. EPR spectra of $\mathbf{X^+}$ at 180 (green) and 295 (red) K in dichloromethane, slightly offset on the x-axis.

The room temperature EPR spectrum of $\mathbf{X^+}$ can be simulated as a delocalized charge with hyperfine coupling to two equivalent triarylamine moieties (A_N = 4.2 G, Figure 4.19). The line shape is consistent with either a static delocalization class III) or rapid dynamic delocalization; however IR and visible-NIR analysis of this monocation suggest that it is a class II species.
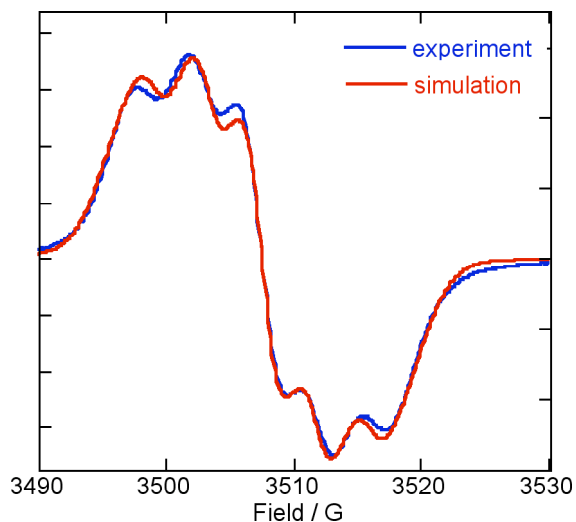
Figure 4.20. Room-temperature experimental (blue) and simulated (red) EPR spectra for **X⁺** in dichloromethane.

4.3.4.6 Experimental and Simulated EPR Spectra of XI⁺

For comparison of the hyperfine coupling constant to nitrogen in the EPR spectra of a one-site monocation, VT-EPR spectra were recorded for monocation **XI⁺** in dichloromethane (Figure 4.20). At the two temperature extremes (298 and 198 K), the spectra are 3-line in nature, although there are slight changes in the height of the ratio of the inner to outer peaks upon cooling. This may be due to a change in coupling to hydrogen nuclei at different temperature due changes in conformational populations.
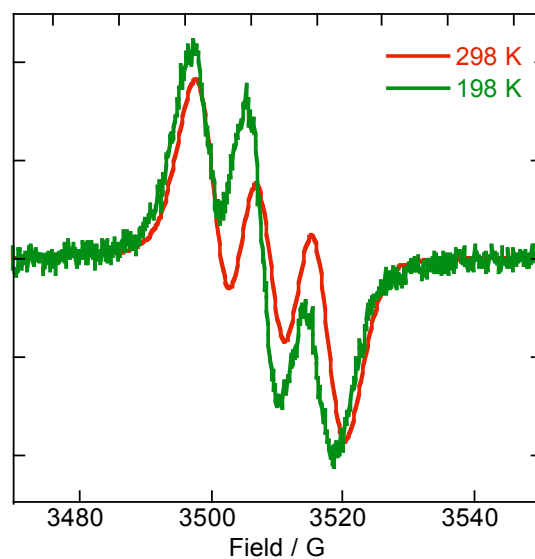
Figure 4.21. EPR spectra of **XI⁺** at 298 (red) and 198 (green) K in dichloromethane.

Since there is only one triarylamine, the simulation for monocation **XI⁺** (Figure 4.21) was expected to fit one nitrogen nucleus, possibly with additional coupling to hydrogen nuclei. In this case simulation with WinSim to one nitrogen nucleus ($I = 1$, 8.3 G) is adequate indeed to describe the EPR spectrum at room temperature.
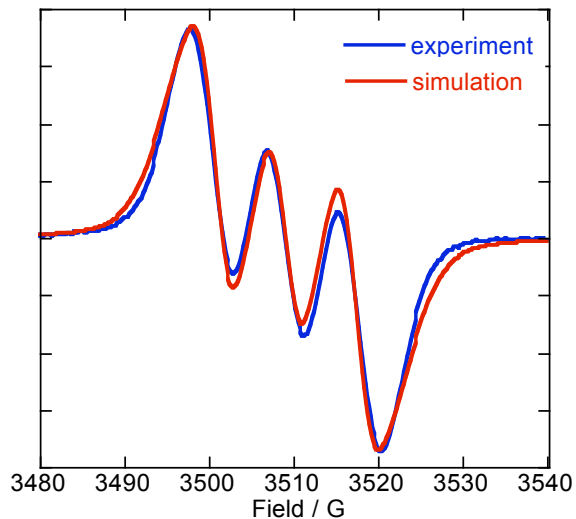
Figure 4.22. Experimental (blue) and simulated (red) room-temperature EPR spectra for **XI⁺** in dichloromethane.

4.3.4.7 Summary of Simulated EPR Spectra

The hyperfine coupling constants to nitrogen for monocations **I⁺**, **II⁺**, **VIII⁺**, **IX⁺**, **X⁺**, and **XI⁺** are shown below in Table 4.5, including whether the simulation used was from a static delocalization (WinSim) or using a thermal exchange rate over two nitrogen nuclei (EPR-EXN).

Table 4.5. Hyperfine coupling constants (G) fitted from WinSim or EPR-EXN for **I⁺**, **II⁺**, **VIII⁺**, **IX⁺**, **X⁺**, and **XI⁺** from the room temperature EPR spectra.

Compound	A_N from WinSim	Number of nuclei	A_N from EPR-EXN	Thermal exchange rate (s⁻¹)
I	-	-	8.4	6.7×10^8
II	3.9	2	-	-
VIII	3.8	2	-	-
IX	-	-	8.4	3.5×10^8
X	4.2	2	-	-
XI	8.3	1	-	-

4.3.5 Arrhenius Plots of the Kinetic Data Obtained from EPR Simulations

From the simulated data in Figures 4.12 and 4.16, the plot of $\ln(k_{ET})$ versus the inverse of the temperature (1/T) for **I⁺** and **IX⁺** (Figure 4.22) both yield a linear relationship between these quantities, suggesting that ET rate obeys an Arrhenius-type equation

$$k_{ET} = A\exp\left(-\frac{\Delta G^*}{k_B T}\right) \tag{4.7}$$

where k_B denotes the Boltzmann constant and T is the temperature. From this equation the prefactor (A) and the free activation energy for electron exchange ($\Delta G^{\ddagger}$) were estimated as $A \approx 3 \times 10^{10}$ and 4×10^{10} s⁻¹ and $\Delta G^{\ddagger} \approx 760$ and 970 cm⁻¹ for **I⁺** and **IX⁺**, respectively. Note that some of the temperatures (hollow triangles and hollow squares) were left out of the fit because the experimental spectra could not be well-simulated at these temperatures, and therefore, the obtained rates should be regarded as less reliable.
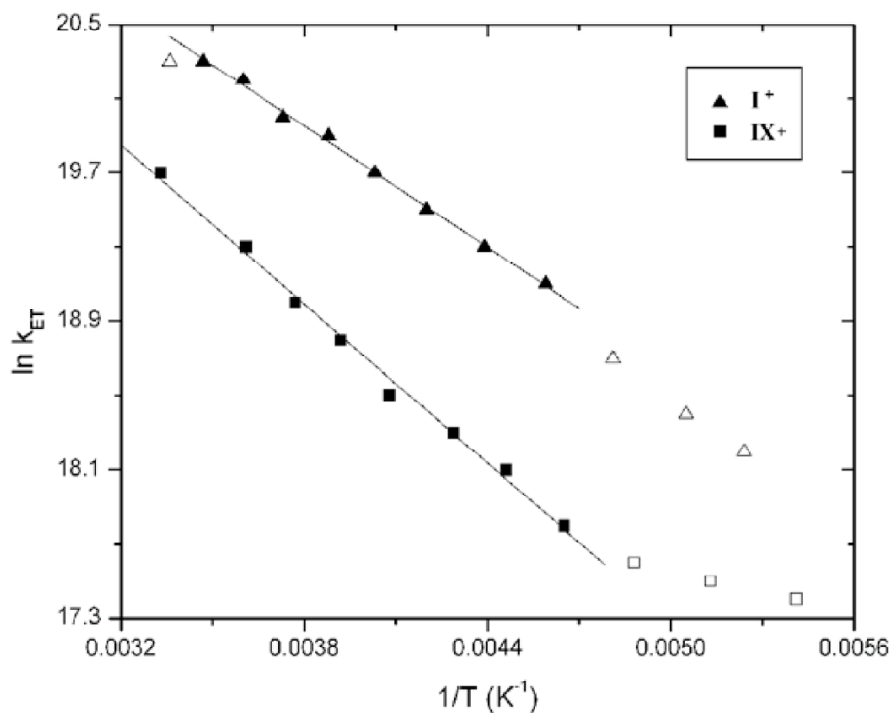
Figure 4.23. Arrhenius plots for $\mathbf{I^+}$ ($\blacktriangle$ and $\triangle$) and $\mathbf{IX^+}$ ($\blacksquare$ and $\square$), shown with linear fits.

It is interesting to compare the EPR estimate of the barrier ($\Delta G^{\ddagger}$) with that derived from optical data shown earlier in this chapter. The Hush analysis of IVCT band of $\mathbf{I^+}$ measured in dichloromethane gives $\lambda = 7450$ cm^{-1} and $V = 480$ cm^{-1} (Section 4.2), assuming that R is equal to the nitrogen-nitrogen distance. From equation 4.1, these values result in an activation barrier of $\Delta G^{\ddagger} = 1410$ cm^{-1}, which is much higher than that derived from the VT-EPR data ($\Delta G^{\ddagger} = 760$ cm^{-1}). Similarly, the Hush analysis of IVCT band of $\mathbf{IX^+}$ measured in dichloromethane gives $\lambda = 7780$ cm^{-1} and $V = 490$ cm^{-1},[8] resulting in an activation barrier of $\Delta G^{\ddagger} = 1520$ cm^{-1}, which is also much higher than that derived from the VT-EPR data ($\Delta G^{\ddagger} = 970$ cm^{-1}). As stated before, both sets of results suggest that the distance for ET (or R) was overestimated in the calculations based on the optical data, and really the diabatic ET distance is shorter than the nitrogen-nitrogen

distance. Note that this is *not* to be confused with the adiabatic ET distance, i.e. the actual distance moved by the electron.

Table 4.6. Parameters for electron exchange calculated from Hush analysis of IVCT bands and simulations of the VT EPR spectra for compounds I^+ and IX^+.

	I^+		IX^+	
	Optical data	VT EPR data	Optical data	VT EPR data
ΔG^* (cm^{-1})	1410	760	1520	970

4.3.6 Conclusions from VT-EPR Experiments

In earlier work[8,41] on the basis of the analysis of the IVCT bands, it was concluded that X^+ displays a weaker electronic coupling than its vinylene analogue $VIII^+$. Although the VT-EPR did not demonstrate variable rates in these monocations, both MV compounds appear delocalized on the EPR timescale. However, now it can be demonstrated that the longer bridge in IX^+ reduces the electronic coupling to such an extent that the rate of ET is not in the fast limit at room temperature. In contrast, its vinylene analogue II^+ exhibits the five-line signature of a bis(triarylamine) MV monocation with an ET rate faster than the EPR timescale. This shape persists even at temperatures as low as 195 K. Thus it can be concluded that the electronic coupling through CH=CH is stronger than through C≡C, consistent with previous work.[8] Additionally, it has been demonstrated that modification of the energy of the frontier molecular orbitals of a conjugated bridge while keeping the energies of the end groups and remaining conjugated structures constant, can modify the rates of intermolecular ET, as was the case in the comparison of monocations I^+

and $\mathbf{II}^+$.

4.4 Overall Conclusions from Chapter 4

It has been shown that bis(diarylaminostyryl)arene derivatives can be systematically modified by altering the orbital energies of the bridge and end groups to alter the MV character of the monocations gradually, making the transition from class II to class III, as demonstated by visible-NIR absorption and EPR spectroscopies. Ultimately, a completely bridge-localized monocation was not obtained, as demonstrated by the instability of the monocations of relevant bridge model compounds (specifically **6** and **7**). Additionally, for the first time, triarylamine-based MV systems ($\mathbf{I}^+$ and $\mathbf{IX}^+$) have been shown to exhibit a delocalized-to-localized transition on the EPR timescale as a function of temperature. The analysis of EPR spectra in these monocations and other related systems allowed for a deeper insight into the nature of ET processes in organic MV systems. Importantly, for the class III pyrrole compounds in section 4.2 (**VII** and **2**) and for the class II systems of section 4.3 (**I** and **IX**), the R_{ab} has been shown to be shorter than R_{NN} for the monocations.

4.5 Experimental Section for Chapter 4

4.5.1 EPR Computational Details

Note: All EPR simulations using the EPR-EXN program and rate calculations were done by Kelly Lancaster and Vaeceslav Coropceanu of the research group of Prof. Jean-Luc Brédas at Georgia Institute of Technology.

Room-temperature EPR spectra for the MV compounds were simulated in one of two ways. The first corresponds to the static case, where it was assumed that the charge is completely delocalized over both triarylamine moieties; for this method, the WinSim program was used. The second corresponds to the dynamic case, where it was assumed that a charge localized on one triarylamine can transfer to the other triarylamine upon thermal activation; for this case, the EPR-EXN program was employed.

4.5.2 Computational Details

Note: All AM1 and DFT calculations were done by Dr. Chad Risko of the research group of Prof. Jean-Luc Brédas at Georgia Institute of Technology.

Geometry optimizations and energies of the HOMOs for the fragments for the neutral molecules were performed using both the semiempirical Hartree-Fock Austim Model 1 (AM1). A correlated semiempirical AM1/CI method was utilized for the investigations of the radical cations, including the determination of R_{12}. Density Functional Theory (DFT) methods were also used in calculations of $\mu_{\pm}$ and μ_{12}, which were used to calculate R_{ab} in equations 4.4 and 4.5. The DFT calculations were carried out using the B3LYP functional, in which Becke's three-parameter hybrid exchange

functional is combined with the Lee-Yang-Parr correlation functional, with a 6-31G* split valence plus polarization basis set.

4.5.3 Electrochemical Methods

*Note: CV data for new compounds **I**-**VII** were obtained by Dr. Stephen Barlow in the research group of Prof. Seth R. Marder at Georgia Institute of Technology.*

Electrochemical measurements were carried out under nitrogen on dry deoxygenated dichloromethane solutions ca. 10^{-4} M in analyte and 0.1 M in tetra-*n*-butylammonium hexafluorophosphate ($^nBu_4NPF_6$) using a BAS 100W Potentiostat, a glassy carbon working electrode, a platinum auxillary electrode, and, as a pseudo-reference electrode, a silver wire anodized in 1 M aqueous potassium chloride. Potentials were referenced to ferrocenium / ferrocene by using cobaltocenium hexafluorophosphate (–1.32 V versus ferrocenium / ferrocene) or decamethylferrocenium / decamethylferrocene (-0.55 B versus ferrocenium / ferrocene). Cyclic voltammograms were recorded at a scan rate of 50 mVs^{-1}.

4.5.4 Visible-NIR Absorption Spectra of the Radical Cations

*The visible-NIR absorption spectra for the monocations of compounds **I**-**IV** were obtained by Dr. Stephen Barlow; for compounds **V**-**VI**, the same spectra were recorded by Dr. Shijun Zheng, also of the same research group. The initial visible-NIR absorption spectra for the monocation of **VII** was obtained by Dr. Luca Beverina, also a member of the research group of Prof. Seth R. Marder at Georgia Institute of Technology.*

Monocations and dications were generated in solution by addition of appropriate amounts of tris(4-bromophenyl)aminium hexachloroantimonate (Aldrich) in dry solvents (< 0.1 eq. for monocations). Absorptivities were calculated assuming complete ET and, in the case of monocations, negligible disproportionation. Visible-NIR spectra were recorded in 1 cm cells using a Varian Cary 5E spectrometer.

4.5.5 EPR Experimental Details.

EPR spectra were acquired on a X-band Bruker EMX spectrometer in dichloromethane solutions. Dichloromethane was dried by passing through columns of activated alumina in a manner similar to that described in the literature.[42] Tris(4-bromophenyl)aminium hexachloroantimonate was purchased from Aldrich Chemical Company. In all cases a ca. 10-fold excess of either diarylamine or bis(diarylamine) derivative was added to a solution of tris(4-bromophenyl)aminium hexachloroantimonate in dichloromethane, thus generating a solution with molarity of radical cation that was approximately the same as the molarity of the original oxidant in solution. For EPR spectra recorded at room temperature, the solutions were ca. 3×10^{-4} M in tris(4-bromophenyl)aminium hexachloroantimonate and were recorded from samples in 4 mm EPR tubes. For EPR spectra recorded at variable temperatures, the solutions were ca. 3×10^{-3} to 3×10^{-4} M in tris(4-bromophenyl)aminium hexachloroantimonate and were obtained from samples in 2 mm EPR tubes supported inside 4 mm EPR tubes or in 3 mm tubes independently supported.

215

4.5.6 Synthetic Details

*Note: Compound **I** and 4-bis(4-n-butoxyphenyl)aminobenzaldehyde were synthesized and characterized by Dr. S. Thayumanavan of the research group of Prof. Seth R. Marder at the University of Arizona. The experimental data are included here for completeness. Compound **II**[8] was synthesized by Neil Tucker; **III**[9] and **IV**[9] by Dr. Stephen Barlow; **V**,[10] **VI**,[16] and **VIII**[41] by Shijun Zheng; **VII**[16] by Dr. Luca Beverina; and **IX**,[2] **X**,[43] and **XI**[44] by Dr. Simon Jones and Zerubba Levi, all as described in the literature. Compound **13** was synthesized by members of the research group of Prof. John Reynolds at the University of Florida.*

Compounds **8**,[23] **9**,[23] and **12**[25] were synthesized as described in the literature.

Starting materials were reagent grade and were used without further purification unless otherwise indicated. Starting materials were purchased from Acros Chemical Co. except for tris(dibenzylideneacetone)dipalladium(0) and tri-*tert*-butylphosphine solution in hexane, both of which were purchased from Strem Chemicals, Inc. Solvents were dried by passing through columns of activated alumina in a manner similar to that described in the literature (tetrahydrofuran, toluene, dichloromethane)[42] or were obtained as anhydrous grade from Acros Organics. Chromatographic separations were performed using standard flash column chromatography methods using silica gel purchased from Sorbent Technologies (60 Å, 32-63 μm) or basic alumina purchased from Aldrich Chemical Company. Elemental analyses were performed by Atlantic Microlabs. FAB and EI mass spectra were obtained from a VG Instruments 70SE. GCMS data were acquired on an Agilent 5790 GC/ 6850 MS.

4-Bis(4-*n*-butoxyphenyl)aminobenzaldehyde.   4-Bromobenzaldehyde (17.7 g, 95.7 mmol) was added to a solution of tris(dibenzylideneacetone) palladium(0) (0.44 g, 0.48 mmol) and 1,1'-bis(diphenylphosphino)ferrocene (0.40 g, 0.72 mmol) in dry toluene (150 mL) under nitrogen. After 15 minutes of stirring, sodium *tert*-butoxide (8.59 g, 89.3 mmol) and bis(di-4-*n*-butoxyphenyl)amine (20.0 g, 63.8 mmol, prepared as previously described (Chapter 3)) were added. The reaction mixture was heated to 90 °C for 24 hours. After allowing the reaction mixture to cool to room temperature, water was added, and the reaction mixture extracted with diethyl ether. The product was purified by column chromatography on silica gel, eluting with ethyl acetate / hexane (1:9) to give the product as a yellow oil (22.2 g, 83%). ^{1}H NMR (300 MHz, CD$_2$Cl$_2$) δ 9.76 (s, 1H), 7.63 (d, *J* = 8.8 Hz, 2H), 7.15 (d, *J* = 8.8 Hz, 4H), 6.92 (d, *J* = 8.8 Hz, 4H), 6.84 (d, *J* = 8.8 Hz, 2H), 3.97 (t, *J* = 6.4 Hz, 4H), 1.77 (m, 4H), 1.01 (t, *J* = 7.4 Hz, 6H). ^{13}C{^{1}H} NMR (75 MHz, CD$_2$Cl$_2$) δ 190.2, 157.5, 154.5, 139.0, 131.5, 128.6, 128.2, 116.8, 116.0, 68.5, 31.8, 19.7, 14.0. HRMS-FAB (*m/z*): [M$^+$] calcd. for C$_{27}$H$_{31}$NO$_3$, 417.2304; found, 417.2307.

***E,E*-1,4-Bis{4-[di(4-*n*-butoxyphenyl)amino]styryl}-2,5-dicyanobenzene   (I).** To a mixture of tetraethyl 2,5-dicyano-1,4-xylene-α,α'-diyl diphosphonate[20] (0.83 g, 1.9 mmol) and 4-bis(4-*n*-butoxyphenyl)aminobenzaldehyde (1.62 g, 3.88 mmol) in tetrahydrofuran (15 mL) at 0 °C was added potassium *tert*-butoxide (0.87 g, 7.8 mmol) in tetrahydrofuran (10 mL) dropwise. The resultant solution was stirred at 0 °C for 30 minutes, then at room temperature for 4 hours. The reaction mixture was then poured into water and was extracted with ether, then concentrated by rotary evaporation, and the residue was purified using flash column chromatography on silica, eluting with hexane /

dichloromethane (2:1) to give the product as a red solid (1.24 g, 67%). ^{1}H NMR (300 MHz, CD$_2$Cl$_2$) δ 7.99 (s, 2H), 7.38 (d, J = 8.5 Hz, 4H), 7.23 (d, J = 16.1 Hz, 2H), 7.14 (d, J = 16.1 Hz, 2H), 7.06 (d, J = 8.7 Hz, 8H), 6.85 (d, J = 8.6 Hz, 12H), 3.94 (t, J = 6.5 Hz, 8H), 1.74 (m, 8H), 1.48 (m, 8H), 0.97 (t, J = 7.4 Hz, 12H). ^{13}C{^{1}H} NMR (CD$_2$Cl$_2$, 75 MHz) δ 156.6, 150.4, 140.2, 138.9, 134.5, 129.6, 128.6, 127.7, 127.4, 119.3, 118.8, 117.3, 115.8, 114.7, 68.4, 31.8, 19.7, 14.1. HRMS-FAB (m/z): [M$^+$] calcd. for C$_{64}$H$_{66}$N$_4$O$_4$, 954.50841; found, 954.50717. Anal. Calcd. for C$_{64}$H$_{66}$N$_4$O$_4$: C, 80.47; H, 6.96; N, 5.87; found: C, 80.42; H, 6.98; N, 5.94. Cyclic voltammetry in 0.1 M ^{n}Bu$_4$NPF$_6$ in dichloromethane: E$_{1/2}$$^{+/0, 2+/+}$: +0.26; E$_{1/2}$$^{3+/2+}$: +0.94 V versus Cp$_2Fe^{+/0}$ at 0 V.

4-[Bis(4-*tert*-butylphenyl)amino]benzylalcohol (10). 4-[Bis(4-*tert*-butylphenyl)amino]benzaldehyde (1.0 g, 2.6 mmol) was dissolved in ethanol (80 mL) using heat and sonication, and the solution was sparged with nitrogen gas; sodium borohydride (0.13 g, 3.5 mmol) was added under nitrogen atmosphere, and the reaction mixture was stirred for 1 hour. Water (50 mL) and diethyl ether (100 mL) were added, and the layers were separated; the organic layer was washed with water (1 × 100 mL) and was dried over anhydrous magnesium sulfate. Concentration by rotary evaporation gave the title compound as an off-white solid (0.84 g, 97%). ^{1}H NMR (300 MHz, CDCl$_3$) δ 7.31 (2 overlapping d, J = 9 Hz, 6H), 7.11 (d, J = 8 Hz, 2H), 7.06 (d, J = 9 Hz, 4H), 4.67 (s, 2H), 1.34 (s, 18H). ^{13}C{^{1}H} NMR (75 MHz, CDCl$_3$) δ 147.8, 145.6, 145.0, 134.1, 128.2, 126.0, 123.8, 123.2, 65.2, 34.2, 31.4. EI-MS (m/z): 388.3 (MH$^+$). Anal. calcd. for C$_{27}$H$_{33}$NO: C, 83.66; H, 8.58; N, 3.61; found: C, 83.40; H, 8.69; N, 3.57.

Diethyl 4-[bis(4-*tert*-butylphenyl)amino]benzylphosphonate (11). 4-[Bis(4-*tert*-butylphenyl)amino]benzylalcohol (1.0 g, 2.6 mmol) was dissolved in triethylphosphite (10 mL); the mixture was deoxygenated and cooled in ice-water under nitrogen. Iodine (0.68 g, 2.7 mmol) was added, and the reaction was allowed to warm to room temperature and was stirred for 3 hours under nitrogen. Residual triethylphosphite was removed by distillation under vacuum, and the remaining product was purified by passing through a pad of silica gel, eluting with hexanes / ethyl acetate (4:1) to give an off-white solid (0.58 g, 84%). ^{1}H NMR (300 MHz, CDCl$_3$) δ 7.25 (d, J = 8.7 Hz, 4H), 7.15 (dd, J = 2.1, 8.4 Hz, 2H), 7.04 – 6.98 (m, 6H), 4.04 (q, J = 7.2 Hz, 4H), 3.11 (d, J = 21 Hz, 2H), 1.33 (s, 18 H), 1.23 (t, J = 7.2 Hz, 2H). ^{13}C{^{1}H} NMR (75 MHz, CDCl$_3$) δ 146.8 (d, J_{CP} = 4.0 Hz), 145.2, 144.8, 130.2 (d, J_{CP} = 9.6 Hz), 123.5, 123.1 (d, J_{CP} = 2.9 Hz), 61.8 (d, J_{CP} = 6.8 Hz), 34.0, 32.8 (d, J_{CP} = 137.3 Hz) 31.3, 16.2 (d, J_{CP} = 5.7 Hz). EI-MS (*m/z*): 508.3 (MH$^+$). Anal. calcd. for C$_{31}$H$_{42}$NO$_3$P: C, 73.35; H, 8.34; N, 2.76; found: C, 73.43; H, 8.46; N, 2.71.

2,5-bis(4-bis(4-*tert*-butylphenyl)aminostyryl)-*N*-methylpyrrole (1). To a 100 mL round-bottomed flask was added diethyl bis(4-*tert*-butylphenyl)aminobenzyl phosphonates (0.20 g, 0.40 mmol), *N*-methylpyrrole-2,5-dicarboxaldehyde (0.025 g, 0.18 mmol), and dry tetrahydrofuran (10 mL) under nitrogen. Potassium *tert*-butoxide (0.12 g, 1.1 mmol) was added, and the reaction immediately turned from tan to bright yellow. The reaction mixture was stirred for 30 minutes at room temperature after which the solvent was removed by rotary evaporation. The crude product was run through a tall pad of silica gel, eluting with hexanes / ethyl acetate (20:1), collecting the product as an

orange-yellow solid.   After Recrystallization from ethyl acetate / methanol, the title

compound was isolated as a yellow solid (0.070 g, 47%). ^{1}H NMR (400 MHz, acetone-

d_6) δ 7.43 (d, J = 8.2 Hz, 4H), 7.34 (d, J = 8.2 Hz, 8H), 7.10 (d, J = 16 Hz, 2H), 6.98 (d, J

= 8.2 Hz, 8H), 6.93 (d, J = 8.2 Hz, 4H), 6.90 Id, J = 16 Hz, 2 H), 3.75 (s, 3H), 1.29 (s, 36

H).   A ^{13}C NMR spectrum was not obtained for this compound due to low solubility.

HRMS-EI (*m/z*): [M$^+$] calcd. for $C_{61}H_{69}N_3$, 843.54915; found, 843.55666.   Cyclic

voltammetry in 0.1 M $^nBu_4NPF_6$ in dichloromethane: $E_{1/2}{}^{+/0}$: –0.16; $E_{1/2}{}^{2+/+}$: +0.02; $E_{1/2}{}^{3+/2+}$:

+0.94 V versus $Cp_2Fe^{+/0}$ at 0 V.

***N-n*-Octadecyl-3,4-propyenedioxy-pyrrole-2,5-dicarbaldehyde (13).**   This compound

was provided as a gift from the research group of Prof. John Reynolds at the University

of Florida.   A procedure for this compound has not been published and has not been

provided.

**2,5-Bis(4-(bis(4-*tert*-butylphenyl)amino)styryl)-*N-n*-octadecyl-3,4-propylenedioxy-

pyrrole (2)**.   Dry   deoxygenated   tetrahydrofuran   (2   mL),   *N-n*-octadecyl-3,4-

propylenedioxypyrrole-2,5-dicarbaldehyde (0.076 g, 0.17 mmol), diethyl bis(4-*tert*-

butylphenyl)aminobenzylphosphonate (0.20 g, 0.39 mmol), and potassium *tert*-butoxide

(0.11 g, 1.0 mmol) were stirred under nitrogen for 10 minutes. The solvent was then

removed under reduced pressure, and the residue was passed through a column of basic

alumina, eluting with hexanes / ethyl acetate (10:1). The product was recrystallized from

ethyl acetate and methanol to give a yellow solid (0.15 g, 76%). ^{1}H NMR (500 MHz,

C_6D_6) δ 7.68 (d, J = 16 Hz, 2H), 7.39 (d, J = 8.5 Hz, 4H), 7.17 (s, 8H), 7.01 (d, J = 16 Hz,

2H), 3.79 (t, J = 5 Hz, 4H), 3.65 (t, J = 7 Hz, 2H), 1.78 (m, 2H), 1.58 (quintet, J = 7.5 Hz, 2H), 1.05–1.35 (m, 30H), 1.23 (s, 36H), 0.91 (t, J = 6.5 Hz, 3H). $^{13}C\{^1H\}$ NMR (125 MHz, C_6D_6) δ 147.5, 146.1, 145.9, 139.0, 133.9, 127.2, 126.7, 126.4, 124.7, 124.2, 118.1, 115.0, 43.2, 24.8, 23.3, 32.5, 31.7, 30.4, 30.34, 30.32, 30.27, 30.2, 30.1, 30.01, 29.79, 27.2, 23.3, 14.6 (4 alkyl peaks missing, presumably due to overlap). FAB-MS (m/z): 1154 (M$^+$). Anal. calcd. for $C_{81}H_{107}N_3O_2$: C, 84.25; H, 9.34; N, 3.64; found: C, 83.18; H, 9.45; N 3.59. Cyclic voltammetry in 0.1 M $^nBu_4NPF_6$ in dichloromethane: $E_{1/2}^{+/0}$: –0.26; $E_{1/2}^{2+/+}$: –0.02; $E_{1/2}^{3+/2+}$: +0.73 V versus $Cp_2Fe^{+/0}$ at 0 V.

1,4-Bis(4-*tert*-butylphenylvinyl)-2,5-di(*n*-dodecyloxy)benzene (3). To an oven-dried 50 mL round-bottomed flask cooled under nitrogen was added diethyl 4-*tert*-butylbenzyl phosphonate (0.22 g, 0.75 mmol), 1,4-di(*n*-dodecyloxy)benzene-2,5-dicarboxaldehyde (0.11 g, 0.22 mmol), and dry tetrahydrofuran (5 mL). Potassium *tert*-butoxide (0.22 g, 2.0 mmol) was added under nitrogen atmosphere. After stirring the reaction mixture for 60 minutes at room temperature, the solvent was removed by rotary evaporation, and the crude product was run through a tall pad of silica gel, eluting with hexanes/ethyl acetate (20:1), yielding 0.16 g (94%) of the title compound as a bright yellow solid. ^1H NMR (300 MHz, C_6D_6) δ 8.00 (d, J = 16 Hz, 2H), 7.61 (d, J = 8.1 Hz, 4H), 7.44 (d, J = 16 Hz, 2H), 7.33-7.32 (m, 6H), 3.83 (t, J = 6.3 Hz, 4H), 1.76 (quintet, J = 6.6 Hz, 4H), 1.49 (m, 4H), 1.30 – 1.40 (m, 32H), 0.91 (t, J = 6.9 Hz, 6H). $^{13}C\{^1H\}$ NMR (75 MHz, C_6D_6) δ 151.8, 150.6, 135.9, 129.1, 127.6, 126.8, 126.0, 123.5, 111.0, 69.4, 34.6, 32.3, 31.4, 30.2, 30.1 (2 peaks separated by 0.04 ppm), 29.9 (2 peaks separated by 0.04 ppm), 29.8, 26.7, 23.1, 14.4. HRMS-EI (m/z): [M$^+$] calcdd for $C_{54}H_{82}O_2$, 762.63148; found, 762.63201.

Anal. calcd. for $C_{54}H_{82}O_2$: C, 84.98; H, 10.83; found: C, 84.41; H, 10.90. Cyclic voltammetry in 0.1 M $^nBu_4NPF_6$ in dichloromethane: $E_{1/2}^{+/0}$: +0.49 V versus $Cp_2Fe^{+/0}$ at 0 V.

2,5-Bis(4-*tert*-butylphenylvinyl)-3,4-di-*n*-butoxy-thiophene (4). In an oven-dried 50 mL round-bottomed flask, diethyl 4-*tert*-butylbenzyl phosphonate (0.22 g, 0.77 mmol), 3,4-di-*n*-butoxythiophene-2,5-dicarboxaldehyde (0.22 g, 0.34 mmol), and dry tetrahydrofuran (10 mL) were combined under nitrogen. Potassium *tert*-butoxide (0.22 g, 2.0 mmol) was added, and the reaction mixture was stirred for 50 minutes at room temperature after which the solvent was removed by rotary evaporation. The crude product was passed through a tall pad of silica gel, eluting with hexanes / ethyl acetate (20:1), and was concentrated by rotary evaporation to obtain the title compound as a yellow-orange oil (0.11 g, 59%). ^{1}H NMR (300 MHz, C_6D_6) δ 7.63 (d, J = 16 Hz, 2H), 7.40 (d, J = 8.4 Hz, 4H), 7.23 (d, J = 8.4 Hz, 4H), 7.18 (d, J = 16 Hz, 2H), 4.04 (t, J = 6.3 Hz, 4H), 1.65 (quintet, J = 6.6 Hz, 4H), 1.42 (sextet, J = 6.6 Hz, 4H), 1.21 (s, 18H), 0.86 (t, J = 7.5 Hz, 6H). ^{13}C{^{1}H} NMR (75 MHz, C_6D_6) δ 150.6, 148.3, 135.1, 127.1, 126.5, 126.0, 124.4, 118.3, 73.8, 34.6, 32.4, 31.3, 19.5, 14.0. EI-MS (*m/z*): 544.2 [M$^+$]. Cyclic voltammetry in 0.1 M $^nBu_4NPF_6$ in dichloromethane: $E_{1/2}^{+/0}$: +0.35 V versus $Cp_2Fe^{+/0}$ at 0 V.

2,5-Bis(4-*tert*-butylphenylvinyl)-*N*-methylpyrrole (5). To an oven-dried 50 mL round-bottomed flask cooled under nitrogen was added diethyl 4-*tert*-butylbenzyl phosphonate (0.22 g, 0.75 mmol), *N*-methylpyrrole-2,5-dicarboxaldehyde (0.047 g, 0.34 mmol), and

dry tetrahydrofuran (5 mL). Potassium *tert*-butoxide (0.22 g, 2.0 mmol) was added upon which the reaction immediately turned yellow. After 30 minutes of stirring at room temperature, the reaction mixture was extracted with ethyl acetate (2 × 50 mL), and the organic layer was washed with water (1 × 50 mL). After drying the organic layer with anhydrous magnesium sulfate, the organic layer was concentrated by rotary evaporation. The crude product was run through a tall pad of basic alumina, eluting with hexanes/ethyl acetate (20:1). The product was recrystallized from ethyl acetate/methanol, yielding 0.062 g (46%) of the title compound as a bright yellow solid. ^{1}H NMR (500 MHz, C_6D_6) δ 7.40 (d, J = 8.5 Hz, 4H), 7.33 (d, J = 8.5 Hz, 4H), 7.03 (d, J = 16 Hz, 2H), 6.90 (d, J = 16 Hz, 2H), 6.69 (s, 2H), 2.93 (s, 3H), 1.25 (s, 18H). ^{13}C{^{1}H} NMR (125 MHz, C_6D_6) δ 150.0, 135.9, 134.0, 126.3, 126.2, 125.9, 117.0, 108.3, 34.6, 31.4, 29.9. Anal. calcd. for $C_{29}H_{35}N$: C, 87.60; H, 8.87; N, 3.52; found: C, 87.55; H, 8.94; N, 3.62. HRMS-EI (*m/z*): [M$^+$] calcd. for $C_{29}H_{35}N$, 397.27695; found, 397.27804. Cyclic voltammetry in 0.1 M $^nBu_4NPF_6$ in dichloromethane: $E_{1/2}^{+/0}$: +0.01 V versus $Cp_2Fe^{+/0}$ at 0 V.

2,5-Bis(4-*tert*-butylphenylvinyl)-7-*n*-octadecyl-3,5-propylenedioxy-pyrrole **(6)**.
Diethyl 4-*tert*-butylbenzylphosphonate[26,45] (0.11 g, 0.37 mmol), *N-n*-octadecyl-3,4-propylenedioxypyrrole-2,5-dicarbaldehyde (0.076 g, 0.17 mmol), anhydrous deoxygenated tetrahydrofuran (10 mL) were combined in a 50 mL oven-dried round-bottomed flask. Potassium *tert*-butoxide (0.11 g, 1.0 mmol) was added, and the reaction mixture was stirred under nitrogen atmosphere at room temperature for 30 minutes. The solvent was removed by rotary evaporation, and the crude product was passed through a pad of silica gel, eluting with hexanes / ethyl acetate (9:1). Recrystallization from ethyl

acetate and methanol gave the title compound as a bright yellow powder (0.080 g, 67%).

^{1}H NMR (500 MHz, C$_6$D$_6$) δ 7.76 (d, J = 16 Hz, 2H), 7.54 (d, J = 8 Hz, 4 H), 7.31 (d, J = 8 Hz, 4H), 7.16 (d, J = 16 Hz, 2H), 3.84 (t, J = 5.0 Hz, 4H), 3.74 (t, J = 7.5 Hz, 2H), 1.66 (quintet, J = 5.0 Hz, 2H), 1.62 (quintet, J = 7.0 Hz, 2H), 1.10–1.35 (m, 30H), 1.25 (s, 18H), 0.91 (t, J = 6.5 Hz, 3H). ^{13}C\{^{1}H\} NMR δ (125 MHz, C$_6$D$_6$) δ 149.6, 138.8, 136.8, 126.5, 125.9 (2 peaks, 0.01 ppm apart), 117.8, 115.8, 105.1, 71.7, 71.1, 43.0, 34.6, 32.3, 31.5, 30.21, 20.19, 30.17, 30.11, 30.07, 29.88, 29.80, 29.57, 27.0, 23.1, 14.4 (4 alkyl peaks missing, presumably due to overlap). MS-FAB (m/z): [M$^+$] calcd. for C$_{49}$H$_{73}$NO$_2$, 707.56; found, 707.5. Anal. calcd. for C$_{49}$H$_{73}$NO$_2$: C, 83.11; H, 10.39; N, 1.98; found: C, 82.60; H, 10.45; N, 1.99. Cyclic voltammetry in 0.1 M ^{n}Bu$_4$NPF$_6$ in dichloromethane: E$_{1/2}$$^{+/0}$: –0.14 V versus Cp$_2Fe^{+/0}$ at 0 V.

2,5-Bis(4-methoxyphenylvinyl)-*N*-octadecyl-3,4-propylenedioxy-pyrrole (7). In a 25 mL oven-dried round-bottomed flask were combined diethyl 4-methoxy lbenzylphosphonate (0.096 g, 0.37 mmol), 7-*n*-octadecyl-2,3,4,7-tetrahydro-[1,4]dioxepino[2,3-*c*]pyrrole-2,5-dicarbaldehyde (0.076 g, 0.17 mmol), anhydrous deoxygenated tetrahydrofuran (5 mL), and potassium *tert*-butoxide (0.11 g, 1.0 mmol). After 30 minutes, the reaction mixture was concentrated by rotary evaporation, and the crude product was run through a tall pad of basic alumina, eluting with hexanes/ethyl acetate (1:1), then with ethyl acetate, yielding a bright yellow. Recrystallization from ethyl acetate / methanol afforded the product as a yellow solid (0.078 g, 71%). ^{1}H NMR (300 MHz, C$_6$D$_6$) δ 7.71 (d, J = 16 H, 2H), 7.47 (d, J = 8.7 Hz, 2H), 7.04 (d, J = 16 Hz, 2H), 6.82 (d, J = 8.7 Hz, 4H), 3.86 (t, J = 5.4 Hz, 4H), 3.74 (t, J = 7.2 Hz, 2H), 3.30 (s,

6H), 1.69 (quintet, $J = 5.1$ Hz, 2H), 1.63 (m, 2H), 1.10-1.35 (m, 30H), 0.91 (t, $J = 6.6$ Hz, 3H). Cyclic voltammetry in 0.1 M nBu$_4$NPF$_6$ in dichloromethane: $E_{1/2}^{+/0}$: –0.22 V versus Cp$_2$Fe$^{+/0}$ at 0 V.

4.6 References

(1)   Brunschwig, B. S.; Creutz, C.; Sutin, N. *Chem. Soc. Rev*. **2002**, *31*, 168–184.

(2)   Lambert, C.; Nöll, G. *J. Am. Chem. Soc* **1999**, *1999*, 8434-8442.

(3)   Low, P. J.; Paterson, M. A. J.; Puschmann, H.; Goeta, A. E.; Howard, J. A. K.; Lambert, C.; Cherryman, J. C.; Tackley, D. R.; Leeming, S.; Brown, B. *Chem. Eur. J*. **2004**, *10*, 83-91.

(4)   Szeghalmi, A. V.; Erdmann, M.; Engel, V.; Schmitt, M.; Amthor, S.; Kriegisch, V.; Nöll, G.; Stahl, R.; Lambert, C.; Leusser, D.; Stalke, D.; Zabel, M.; Popp, J. *J. Am. Chem. Soc*. **2004**, *126*, 7834-7845.

(5)   Coropceanu, V.; Gruhn, N. E.; Barlow, S.; Lambert, C.; Durivage, J. C.; Bill, T. G.; Nöll, G.; Marder, S. R.; Brédas, J.-L. *J. Am. Chem. Soc*. **2004**, *126*, 2727-2731.

(6)   Lambert, C.; Nöll, G.; Schelter, J. *Nature Mater*. **2002**, *1*, 69-73.

(7)   Lambert, C.; Amthor, S.; Schelter, J. *J. Phys. Chem. A* **2004**, *108*, 6474-6486.

(8)   Barlow, S.; Risko, C.; Chung, S.-J.; Tucker, N. M.; Coropceanu, V.; Jones, S. C.; Levi, Z.; Brédas, J. L.; Marder, S. R. *J. Am. Chem. Soc*. **2005**, *127*, 16900-16911.

(9)   Rumi, M.; Ehrlich, J. E.; Heikal, A. A.; Perry, J. W.; Barlow, S.; Hu, Z.; McCord-Maughon, D.; Parker, T. C.; Röckel, H.; Thayumanavan, S.; Marder, S. R.; Beljonne, D.; Brédas, J.-L. *J. Am. Chem. Soc*. **2000**, *122*, 9500-9510.

(10)   Zheng, S.; Barlow, S.; Risko, C.; Kinnibrugh, T. L.; Khrustalev, V. N.; Antipin, M. Y.; Tucker, N. M.; Timofeeva, T.; Coropceanu, V.; Jones, S. C.; Jean-Luc Brédas; Marder, S. R. *J. Am. Chem. Soc*. **2006**, *128*, 1812-1817.

(11)   Barlow, S.; Zheng, S.; Beverina, L.; Marder, S. R. *Unpublished Work*.

(12)   Lindholm, E.; Asbrink, L. *Chem. Phys. Lett*. **1970**, *5*, 192.

(13)   Sell, J. A.; Kuppermann, A. *Chem. Phys. Lett*. **1979**, *61*, 355-362.

(14)   Kupperman, A. *Chem. Phys. Lett*. **1978**, *61*.

(15)   Schottland, P.; Zong, K.; Gaupp, C. L.; Thompson, B. C.; Thomas, C. A.; Giurgiu, I.; Hickman, R.; Abboud, K. A.; Reynolds, J. R. *Macromolecules* **2000**, *33*, 7051-7061.

(16)   Zheng, S.; Beverina, L.; Barlow, S.; Zojer, E.; Fu, J.; Padilha, L. A.; Fink, C.; Kwon, O.; Yi, Y.; Shuai, Z.; Stryland, E. W. V.; Hagan, D. J.; Brédas, J.-L.; Marder, S. R. *Chem. Commun*. **2007**, *published on the web*.

(17)   Thayumanavan, S.; Marder, S. *Unpublished Work*.

(18)   Horner, L. *Chem. Ber*. **1958**, *83*, 733.

(19)   Wadsworth, W. S.; Emmons, W. D. *J. Am. Chem. Soc*. **1961**, *83*, 1733.

(20)   Wenseleers, W.; Stellacci, F.; Meyer-Friedrichsen, T.; Mangel, T.; Bauer, C. A.; Pond, S. J. K.; Marder, S. R.; Perry, J. W. *J. Phys. Chem. B*. **2002**, *106*, 6853-6863.

(21)   Driver, M. S.; Hartwig, J. F. *J. Am. Chem. Soc*. **1996**, *118*, 7217.

(22)   Wolfe, J. P.; Wagaw, S.; Buchwald, S. L. *J. Am. Chem. Soc*. **1996**, *118*, 7215.

(23)   Jeong, H. C.; Piao, M. J.; Lee, S. H.; Jeong, M.-Y.; Kang, K. M.; Park, G.; Jeon, S.-J.; Cho, B. R. *Adv. Funct. Mater*. **2004**, *14*, 64.

(24)   Zheng, S.; Barlow, S.; Parker, T. C.; Marder, S. R. *Tet. Lett*. **2003**, *44*, 7989-7992.

(25) Van Der Looy, J. F. A.; Thys, G. J. H.; Dieltiens, P. E. M.; SDe Schrijver, D. D.; Van Alsenoy, C.; Geise, H. J. *Tetrahedron* **1997**, *53*, 15069-15084.

(26) Lock, J. S.; May, B. L.; Clements, P.; Lincoln, S. F.; Easton, C. J. *Org. Biomol. Chem.* **2004**, *2*, 337-344.

(27) Shao, P.; Li, Z.; Luo, J.; Wang, H.; Qin, J. *Syn. Commun.* **2005**, *35*, 49-53.

(28) Ono, N.; Okumura, H.; Murashima, T. *Heteroatom Chemistry* **2001**, *12*, 414-417.

(29) Connelly, N. G.; Geiger, W. E. *Chem. Rev.* **1996**, *96*, 877-910.

(30) Coropceanu, V.; Malagoli, M.; André, J. M.; Brédas, J. L. *J. Am. Chem. Soc.* **2002**, *124*, 10519-10530.

(31) Nelsen, S. F.; Newton, M. D. *J. Phys. Chem. A* **2000**, *104*, 10023.

(32) Johnson, R. C.; Hupp, J. T. *J. Am. Chem. Soc.* **2001**, *123*, 2053.

(33) Pearson, G. A.; Rocek, M.; Walter, R. I. *J. Phys. Chem.* **1978**, *82*, 1185-1192.

(34) Seo, E. T.; Nelson, R. F.; Fritsch, J. M.; Marcoux, L. S.; Leedy, D. W.; Adams, R. N. *J. Am. Chem. Soc.* **1966**, *88*, 3498-3503.

(35) Veregin, R. P.; Harbour, J. R. *J. Phys. Chem.* **1990**, *94*, 6231-6237.

(36) Hush, N. S. *Prog. Inorg Chem.* **1967**, *8*, 391-444.

(37) Tang, S. W.; VanSlyke, S. A. *Appl. Phys. Lett.* **1987**, *51*, 913.

(38) Nelsen, S. F.; Ismagilov, R. F.; II, D. A. T. *Science* **1997**, *289*, 846.

(39) Lindeman, S. B.; Rosokha, S. B.; Sun, D.; Kochi, J. K. *J. Am. Chem. Soc* **2002**, *124*, 843.

(40) Hirao, Y.; Urabe, M.; Ito, A.; Tanaka, K. *Angew. Chem. Int. Ed.* **2007**, *36*, 3300-3303.

(41) Barlow, S.; Risko, C.; Coropceanu, V.; Tucker, N. M.; Jones, S. C.; Levi, Z.; Khrustalev, V. N.; Antipin, M. Y.; Kinnibrugh, T. L.; Timofeeva, T.; Marder, S. R.; Brédas, J. L. *Chem. Commun.* **2005**, 764-766.

(42) Pangborn, A. B.; Giardello, M. A.; Grubbs, R. H.; Rosen, R. K.; Timmers, J. F. *Organometallics* **1996**, *15*, 1518-1520.

(43) Lambert, C.; Noll, G. *Angew. Chem. Int. Ed.* **1998**, *37*, 2107-2110.

(44) Lambert, C.; Noll, G.; Schmalzlin, E.; Meerholz, K.; Brauchle, C. *Chem. Eur. J.* **1998**, *4*, 2129-2135.

(45) Bellucci, C.; Gualtieri, F.; Chiarini, A. *Eur. J. Med. Chem* **1987**, *22*, 473-477.

CHAPTER 5

MIXED-VALENCE MONOCATIONS OF 1,3,5-TRIS(DIARYLAMINO) DERIVATIVES AROUND A CENTRAL BENZENE CORE

5.1. Introduction

In comparison to two-site mixed-valence (MV) systems, three-site MV systems have had a rather limited investigation in the literature. In many three-site MV systems, either the intervalence charge-transfer (IVCT) band is too weak to study, or the IVCT band overlaps in energy with other strong transitions in the radical species such that it cannot be readily studied. This is often the case in 1,3,5-trisubstituted benzene derivatives in which the redox sites are often poorly coupled due to poor conjugation through the *meta*-positions of the benzene ring. In attempt to learn more about the nature of three-site MV species, the synthesis and characterization of new three-site MV species in an attempt obtain more strongly coupled MV species with IVCT bands that are well-separated from other absorption bands are described in this chapter.

5.1.1 Coupling in Three-Site MV Monocations

MV species are useful systems to study as simple models for electron transfer processes. Understanding fundamental electron transfer processes has relevance in complicated biological systems as well as in charge transport materials in organic electronic devices. While two-site MV species provide the simplest systems for investigation and have been studied in numerous publications, [1-4] investigations of three-site MV species have been rather more limited. [5-16] However, when considering a

situation in which multiple positions are available to accept an electron – such as in the case of an oxidized or reduced conjugated oligomeric or polymeric system in which there are more than two redox sites available for electron transfer – then a three-site model system may be more helpful in understanding the nature of electron transfer. Yet another example of intermolecular electron transfer in a molecular solid, where multiple redox sites could be more readily available than in solution measurements. Rather than having one redox center with which electronic coupling can occur, a three-site MV species has more options for electron transfer because there are two potential redox sites available (Figure 5.1).
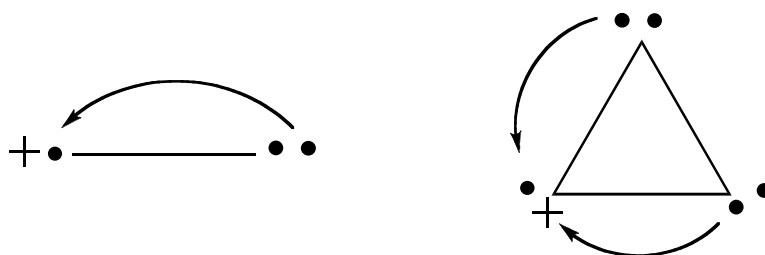
Figure 5.1. Potential for electron transfer reactions in a two-site (left) and three-site (right) MV species, examples shown for cationic MV species.

While some publications have addressed the theory concerning electron transfer in centrosymmetric three-site MV species,[5,6,8,17] these species are often more difficult to study because of the smaller electronic coupling in systems that are convenient to synthesize. For example, when considering three-site MV systems in which the three redox centers are strictly equivalent (in the neutral version of the MV system), a fairly simple system to synthesize and study is a 1,3,5-trisubstituted benzene ring with three redox centers attached to the benzene core. However, the *meta*-substitution in such systems prevents effective conjugation between the substitutents in comparison to the

para-substition in similar two-center MV species, the result of which is weaker electronic coupling, and, therefore, less intense IVCT bands compared to similar two-site species with *para*-substition around a phenylene bridge. This chapter focuses on the synthesis and characterization of potentially more strongly coupled three-site MV species with 1,3,5-substitution around a central benzene ring than those reported in the literature, thus potentially retaining the synthetic ease in a trisubstituted benzene derivative with the advantage of stronger coupling and therefore greater ease in studying the characteristics of the IVCT bands.

5.1.2 *Previous Studies of the Monocations of Tris(diarylamine)s*

A few examples of symmetric three-site MV species have been reported in the literature, i.e. three-site species with strict three-fold symmetry in the neutral species.[8,17,18] Concerning symmetrically substituted organic MV species, Launay's reports on the mono-, di-, and tri-cations of tris(diarylamine)s[5,6] have been among the few. In Launay's reports,[5,6] the monocation of 1,3,5-tris(di(4-ethylphenyl)aminophenyl)benzene (**I**) and a related two-site system – the monocation of a 1,3-bis(di(4-alkylphenyl)aminophenyl)benzene derivative (**II**)[6] – have been studied as MV species. These compounds are shown in Figure 5.2.
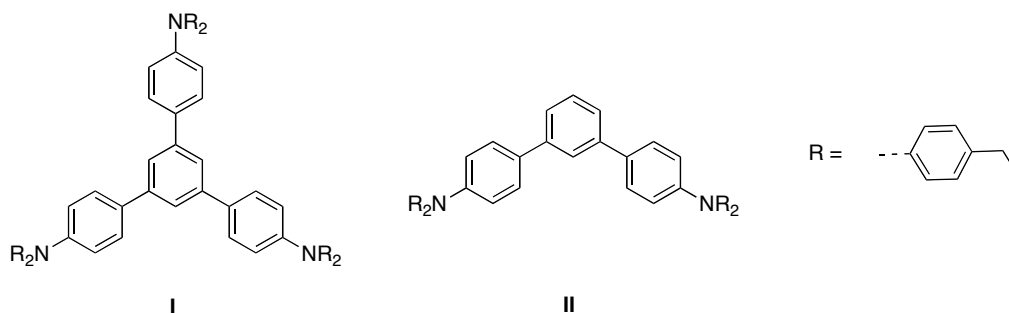
Figure 5.2. A tris(triarylamine) and related two-site derivative for which the monocations were studied as MV species.[5,6]

Cyclic voltammetry (CV) experiments of compound **I** have been reported in dichloromethane.[5] For this derivative, one reversible oxidation wave was observed, which presumably corresponds to three one-electron oxidations of each triarylamine moiety, occurring at experimentally indistinguishable potentials. This result suggests that the oxidation of one triarylamine does not effect the other triarylamine enough to cause the second and third oxidations to occur at higher potentials, as far as could be detected by the CV experiment.

The visible-NIR absorption spectra of the mono-, di-, and tri-cation of compound **I** were reported in tetra-n-butylammonium hexafluorophosphoate ($^nBu_4NPF_6$) in dichloromethane.[5] The bands associated with the triarylamine monocation absorption (from 500 to 900 nm) are similar in the mono-, di-, and tri-cation, and increase in intensity from mono- to tri-cation, as was expected for the transitions associated with the individual redox centers. The IVCT band of the monocation was measured, having an absorption maximum at ca. 1400 nm. The dication of **I** is also a MV species in which there are two redox centers with electronic vacancies and one neutral center. In comparison to the IVCT band of monocation $\mathbf{I^+}$, the absorption of the IVCT band of the two-site monocation $\mathbf{II^+}$ is slightly red-shifted and is less intensely absorbing. The signal-

to-noise ratio was small for the IVCT bands, and although Launay and coworkers analyzed the band using Hush theory[19] – obtaining electronic couplings (V) of 205 and 181 cm^{-1} for $\mathbf{I^+}$ and $\mathbf{II^+}$, respectively – more confidence could be ascribed to the shape and analysis of the IVCT absorption if a spectrum with higher signal-to-noise ratio had been obtained and if the IVCT bands were more separated from the triarylaminium absorption features.

The main goal of this chapter was – in comparison to an analog of $\mathbf{I}$ for comparison – to study a more strongly coupled monocation of a tris(diarylamino) derivative in order to obtain a more strongly absorbing IVCT band, and in which the IVCT band did not have an absorption energy coincident with the other triarylaminium transitions. In addition to Hush analysis[19] of the IVCT band of the monocation, electron paramagnetic resonance (EPR) studies could possibly shed light as to the nature of the delocalization of the monocations on the EPR time scale, potentially similar to the studies in section 4.3 of this thesis.

5.1.3   Tris(diarylamino) Derivatives and Model Compounds

In order to determine if the measurements obtained for compound $\mathbf{I}$ could be replicated in a derivative with a similar structure and to investigate a 1,3,5-tris(di(4-alkylphenyl)aminophenyl)benzene derivative using DPV, initially compound $\mathbf{1}$ was synthesized, replacing ethyl groups with *tert*-butyl groups (Figure 5.3). Because many bis(diarylamino) derivatives that have been studied in the literature incorporate 4-alkoxyphenyl rather than 4-alkylphenyl end groups, a derivative with di(4-methoxyphenyl)amino end groups ($\mathbf{2}$, Figure 5.3) was designed as a more electron-rich

π-system. To obtain potentially more strongly coupled three-site MV systems, two derivatives were synthesized in which phenylene bridges were replaced with thienylene bridges (**3** and **4**, Figure 5.3). The difference in ionization potentials of benzene (9.2 eV)[20] and thiophene (8.9 eV)[21] could lead to stronger coupling through the less aromatic and more easily oxidized thiophene rings. In Chapter 3, for example, it was shown that the monocations of bis(diarylamino) derivatives with thiophene-based bridges have stronger electronic coupling than the equivalent derivatives with phenylene-based bridges.
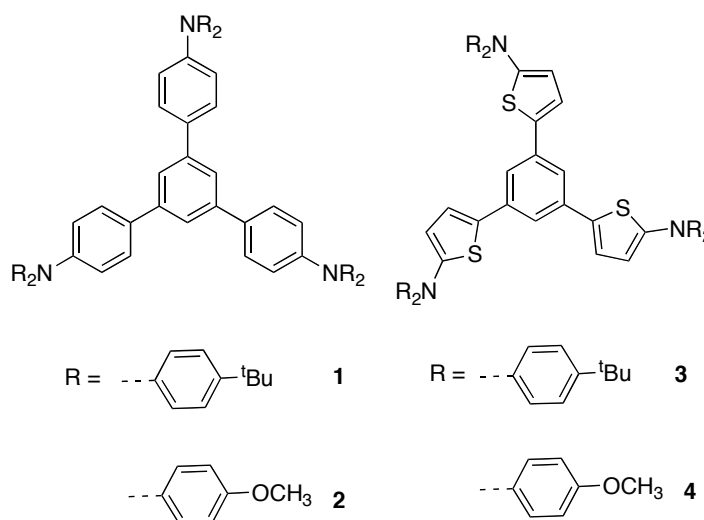
Figure 5.3. Tris(diarylamino) derivatives to be discussed in this chapter.

Additionally, for comparison to one of the thiophene-based three-site systems (**3**), a two-site version (**5**) was designed as a two-site MV monocation that should have an IVCT band, and a one-site version (**6**) was designed as a triarylamine monocation that should not have an IVCT transition (Figure 5.4). It would be interesting to see, in a set of

233

similar two- and three-site MV species, if the trends in energies of absorption maxima and electronic coupling were consistent with the trends observed in the case of $\mathbf{I^+}$ and $\mathbf{II^+}$. In this way, a comparison of the IVCT bands of $\mathbf{3^+}$ and $\mathbf{5^+}$ could lead to more information about the difference in electron transfer between similar two- and three-site MV species.
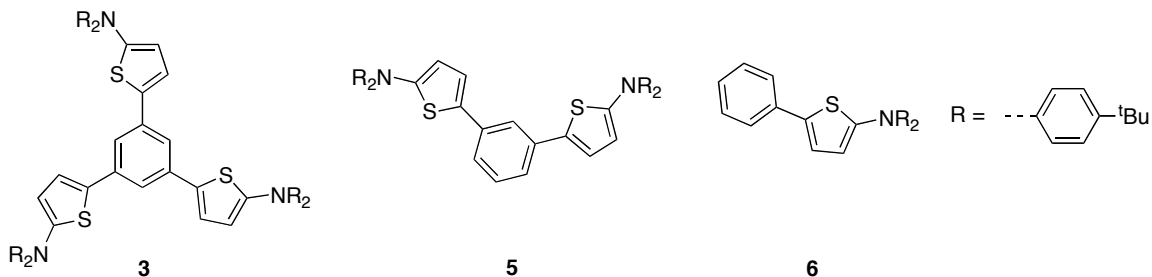
Figure 5.4. A three-site compound for study as a MV monocation, and corresponding two- and one-site control compounds.

5.2 Results and Discussion

5.2.1 Synthesis of Tris(diarylamino) Derivatives and Model Compounds

The synthesis of the tris(diarylamino) derivatives and model compounds employed extensive use of palladium-catalyzed amination reactions and condensation reactions. The 1,3,5-tris(diarylaminophenyl)benzene derivatives (**1** and **2**) were synthesized in two steps (Scheme 5.1). First, commercially available 1-acetyl-4-iodobenzene (**7**) was cyclized in a condensation reaction with silicon tetrachloride to form known compound 1,3,5-tris(4-iodophenyl)benzene (**8**).[22,23] Next the triiodide was coupled with a di(4-*tert*-butylphenyl)amine (**9**) or di(4-methoxyphenyl)amine (**10**) in a palladium-catalyzed amination reaction, yielding the desired triply aminated products (**1** or **2**, Scheme 5.1).
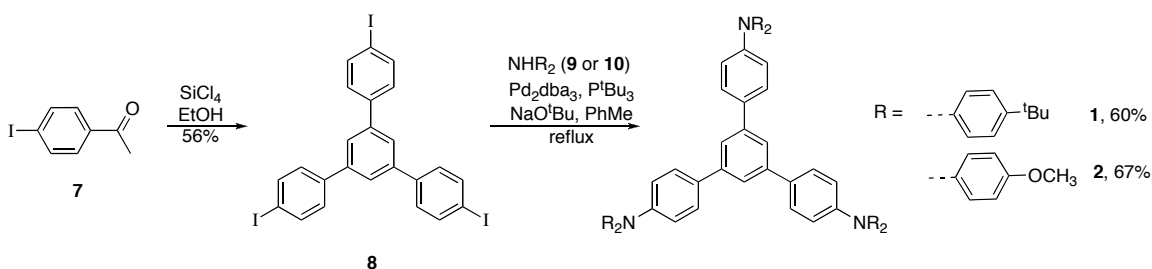
Scheme 5.1. Synthesis of 1,3,5-tris(di(aryl)aminophenyl)benzene derivatives.

Similarly the 1,3,5-tris(5-di(aryl)aminothien-2-yl)benzene derivatives (**3** and **4**) were synthesized in a palladium-catalyzed amination of 1,3,5-tris(5-bromothien-2-yl)benzene (**13**) with diarylamine (**9** or **10**). To obtain the triply brominated core, originally 2-acetyl-5-bromothiophene was reacted with silicon tetrachloride, following a published procedure to obtain compound **13**,[24] but the product isolated from the reaction was a mixture of tribromo-, dibromo-monochloro-, monobromo-dichloro-, and trichloro-products, as was determined by mass spectrometry and ^{1}H NMR spectroscopy. Instead, 2-acetylthiophene (**11**) was cyclized to form 1,3,5-tris(thien-2-yl)benzene (**12**),[23] which was triply brominated with *N*-bromosuccinimide to form 1,3,5-tris(5-bromothien-2-yl)benzene (**13**, Scheme 5.2).
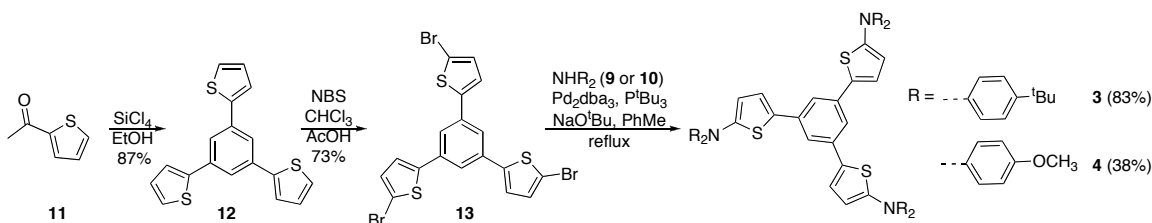
Scheme 5.2. Synthesis of 1,3,5-tris(diarylamino-5-thien-2-yl)benzene derivatives.

A palladium-catalyzed Stille coupling of 1,3-dibromobenzene and 2-tri(*n*-butyl)stannylthiophene was used to synthesize commercially available 1,3-bis(thien-2-yl)benzene (**14**), which was brominated to obtain 1,3-bis(5-bromothien-2-yl)benzene (**15**). Reaction of **15** with bis(4-*tert*-butylphenyl)amine (**9**) in a palladium-catalyzed amination reaction yielded 1,3-bis(di(4-*tert*-butylphenyl)amino-5-thien-2-yl)benzene (**5**, Scheme 5.3).
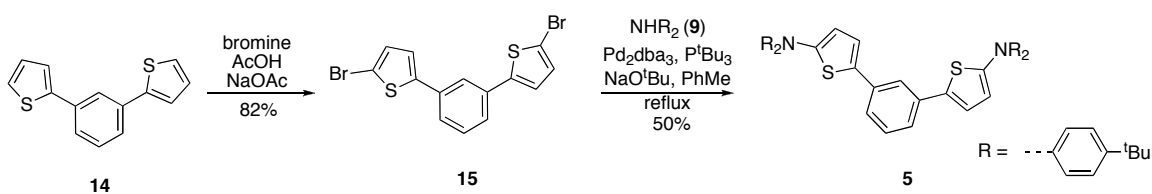
Scheme 5.3. Synthesis of 1,3-bis(di(4-*tert*-butylphenyl)amino-5-thien-2-yl)benzene.

The one-site version of the above product was also synthesized in a similar fashion to the original synthesis of the two- and three-site species. First 2-phenylthiophene (**16**) was brominated[25] (Scheme 5.4). Then palladium-catalyzed amination of 2-bromo-5-phenylthiophene (**17**) with bis(4-*tert*-butylphenyl)amine (**9**) yielded 2-bis(4-*tert*-butylphenyl)amino-5-phenyl-thiophene (**6**) as an off-white solid.
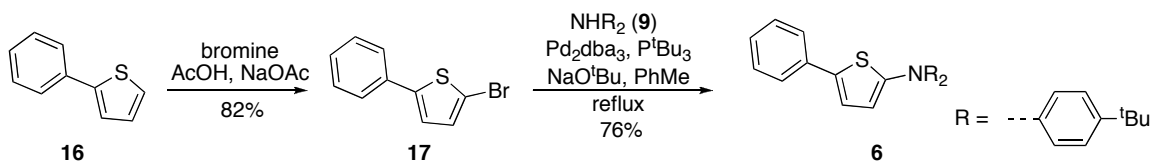
Scheme 5.4. Synthesis of 2-bis(4-*tert*-butylphenyl)amino-5-phenyl-thiophene.

5.2.2 Electrochemical Characterization

Compounds **1**–**6** were analyzed by CV to determine oxidation potentials; for the two- and three-site derivatives, DPV was used in attempt to determine any differences in potential between successive oxidations. When multiple oxidations in the same molecule occur at the same potential, the oxidation of one redox center does not affect the potentials of the other redox centers to a sufficient extent that a difference in the multiple processes can be observed. However, if the two redox centers are sufficiently close in space, electrostatic interactions can cause the presence of one positive charge to make the second and further oxidations more difficult. Also, if the conjugation between the redox centers is sufficiently large, and thus the monocation is delocalized to some extent over both redox centers, then the second and further oxidations will also occur at higher potentials.

In all cases, CV and DPV experiments were run in 0.1 M $^nBu_4NPF_6$ in dichloromethane, and decamethylferrocenium / decamethylferrocene ($Cp*_2Fe^{+/0}$) was used as the internal reference at –0.55 V versus ferrocenium / ferrocene ($Cp_2Fe^{+/0}$) at 0 V. As was the case with the published characterization of compound **I**,[5] the cyclic voltammogram of compound **1** (Figure 5.5, left) is consistent with three overlapping, unresolved one-electron oxidations at +0.42 V, referenced to $Cp_2Fe^{+/0}$ at 0 V. DPV experiments showed no separation in the multiple oxidations (Figure 5.5, right).

Figure 5.5. Cyclic voltammogram (left) and differential pulse votammogram (right) of compound **1** in 0.1 M ^{n}Bu$_4$NPF$_6$ in dichloromethane, both shown with Cp*$_2$Fe$^{+/0}$ as the internal reference and referenced to Cp$_2$Fe$^{+/0}$ at 0 V.

The cyclic voltammogram of compound **2** (Figure 5.6, left) is also consistent with three overlapping, unresolved reversible one-electron oxidations. DPV experiments (Figure 5.6, right) did not show any separation of the multiple oxidations. The oxidation of **2** (E$_{1/2}$$^{+/0}$ = +0.27 V) occurs at lower potential than that of compound **1** (E$_{1/2}$$^{+/0}$ = +0.42 V), which is consistent with the more electron-rich alkoxy end groups in compound **2**.
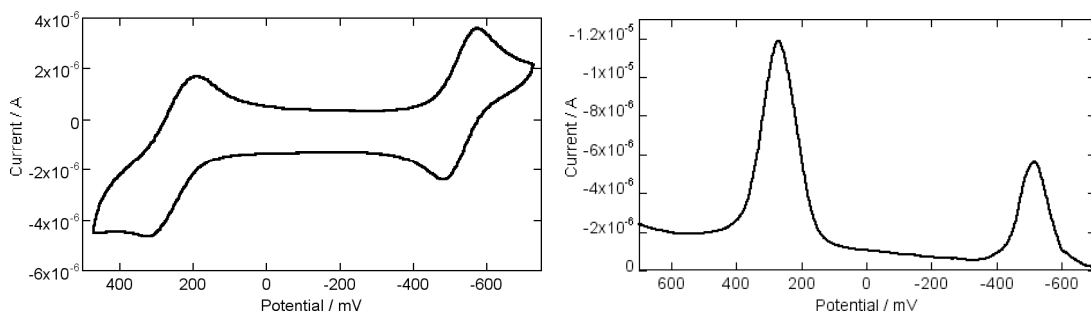
Figure 5.6. Cyclic voltammogram (left) and differential pulse voltammogram (right) of compound **2** in 0.1 M ^{n}Bu$_4$NPF$_6$ in dichloromethane, both shown with Cp*$_2$Fe$^{+/0}$ as the internal reference and referenced to Cp$_2$Fe$^{+/0}$ at 0 V.

The cyclic voltammogram of compound **3** is consistent with multiple oxidations at different potentials (Figure 5.7, left), although it is not possible to determine the positions of each oxidation from the cyclic voltammogram without simulation. The three

238

oxidations are separated in the DPV experiments (Figure 5.7, right). Compound **3** is considerably easier to oxidize ($E_{1/2}^{+/0}$ = +0.22 V) than its phenylene-based analog **1** ($E_{1/2}^{+/0}$ = +0.42 V), which was expected because of the lower ionization potential of thiophene relative to benzene. Also, because the oxidations are separable in compound **3**, this result implies that the oxidation of each triarylamine moiety affects the potentials of the others, which could be due to greater electronic coupling of the redox centers in compound **3** than in compound **1**. Because the nitrogen-nitrogen distance in **3** is shorter than that in **1**, the lower distance between nitrogen nuclei might lead to greater electrostatic contributions to the difference in oxidation potentials. Regardless of the cause of the increase in $\Delta E_{1/2}$, the result of the increase is that monocation **3$^+$** is more stable with respect to disproportionation and makes acquisition of the monocation [only] spectra easier.
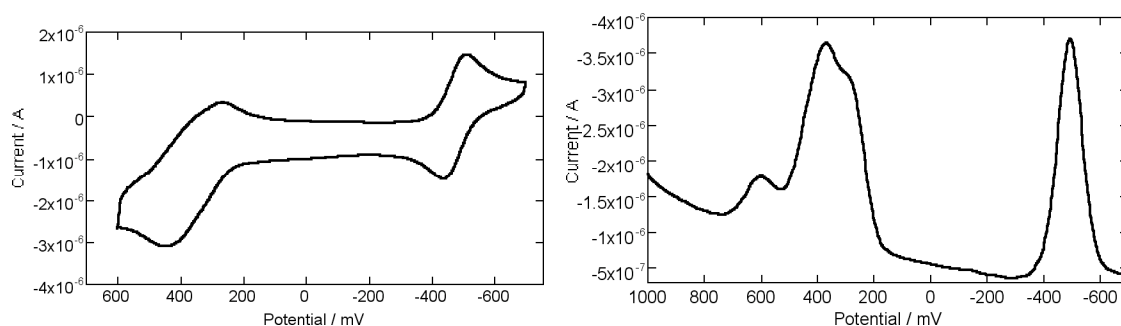
Figure 5.7. Cyclic voltammogram (left) and differential pulse voltammogram (right) of compound **3** in 0.1 M $^nBu_4NPF_6$ in dichloromethane, both shown with $Cp^*_2Fe^{+/0}$ as the internal reference and referenced to $Cp_2Fe^{+/0}$ at 0 V.

The oxidations in compound **4** are also somewhat separated in CV experiments (Figure 5.8, left) and are better resolved in the DPV experiments (Figure 5.8, right). The first

oxidation of compound **4** occurs at lower potential ($E_{1/2}^{+/0}$ = +0.20 V) than compound **3** ($E_{1/2}^{+/0}$ = +0.22 V), consistent with the more electron-rich end groups in compound **4**.
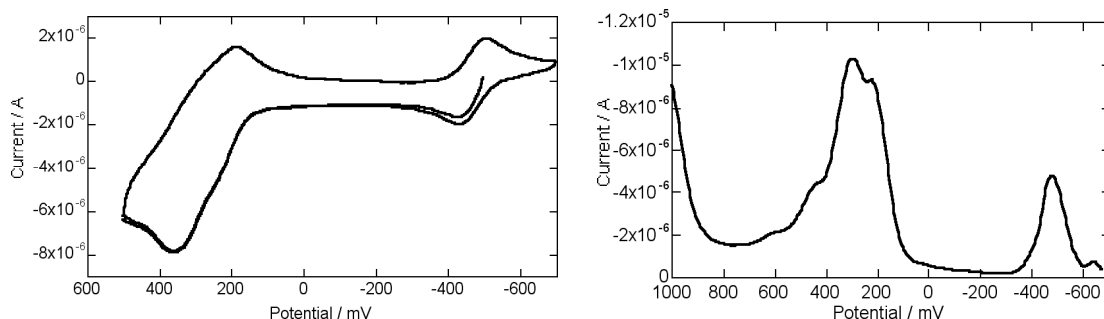
Figure 5.8.   Cyclic voltammogram (left) and differential pulse voltammogram (right) of compound **4** in 0.1 M ^{n}Bu$_4$NPF$_6$ in dichloromethane, both shown with Cp*$_2$Fe$^{+/0}$ as the internal reference and referenced to Cp$_2$Fe$^{+/0}$ at 0 V.

The cyclic voltammogram and differential pulse voltammogram of the two-site compound (**5**) are shown in Figure 5.9, displaying two reversible oxidations with separation of ca. 0.09 V.   The separation in oxidation potentials suggests that – as was the case for the equivalent three-site compound (**3**) – the oxidation of one triarylamine affects the oxidation of the second triarylamine.   The first oxidation potential of **5** is similar to that of **3**, consistent with the relatively weak coupling expected from *meta*-substitution around the central benzene ring, which implies that the monocation of **3** is not more stabilized than **5**, despite it having additional redox sites.
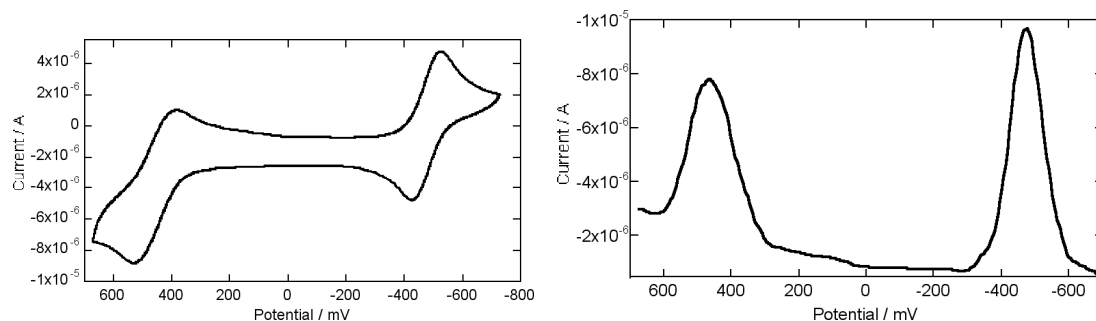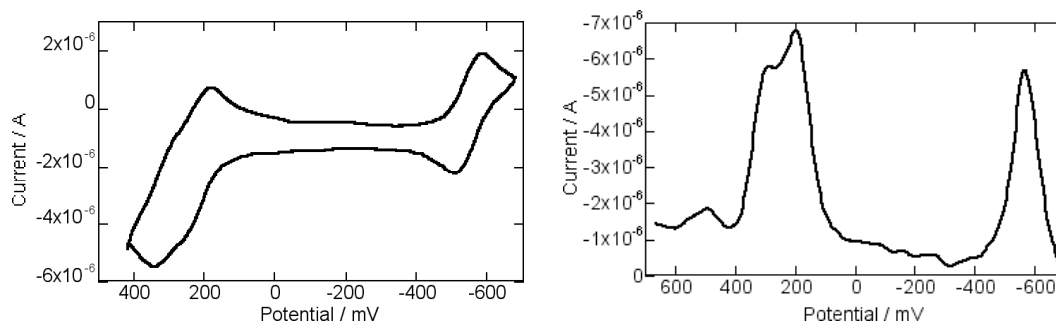
Figure 5.9. Cyclic voltammogram (left) and differential pulse voltammogram (right) of two-site compound **5** in 0.1 M $^nBu_4NPF_6$ in dichloromethane, both shown with $Cp*_2Fe^{+/0}$ as the internal reference and referenced to $Cp_2Fe^{+/0}$ at 0 V.

The cyclic voltammogram of the one-site compound (**6**) is shown below in Figure 5.10. In this case, one oxidation is observed at a similar oxidation potential ($E_{1/2}^{+/0} = +0.22$ V) to the two- (**5**) and three-site (**3**) analogs. Because there is only one triarylamine moiety in compound **6**, it is reasonable that only one oxidation was observed.
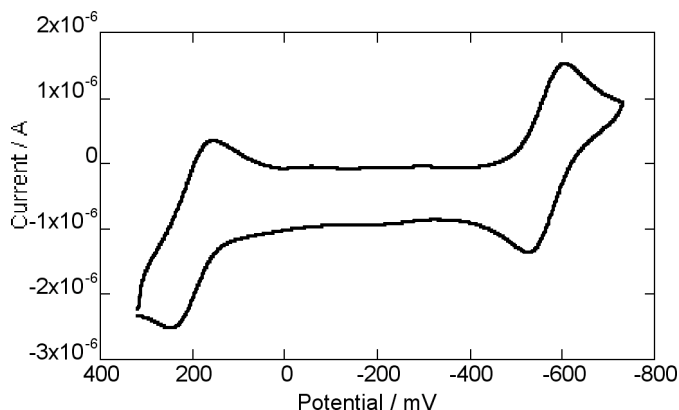
Figure 5.10. Cyclic voltammogram of compound **6** in 0.1 M nBu_4NPF_6 in dichloromethane at 50 mV/s, shown with $Cp*_2Fe^{+/0}$ as the internal reference and referenced to $Cp_2Fe^{+/0}$ at 0 V.

The oxidation potentials of compounds **1–6** are summarized in Table 5.1. The oxidation potential reported for **I** (which was initially reported as $E_{1/2} = +0.822$ V versus a standard calomel electrode (SCE) and converted assuming a value of referencing $Cp_2Fe^{+/0}$ to

241

SCE from Connelly and Geiger[26]) is slightly lower than that obtained for **1**. Here potentials are referenced to $Cp_2Fe^{+/0}$ because this is the standard reference recommended by the International Union for Pure and Applied Chemistry.[26]

Table 5.1.   Half-wave oxidation potentials (V) of **I**[5] and **1–6** in 0.1 M $^nBu_4NPF_6$ in dichloromethane, referenced to $Cp_2Fe^{+/0}$ at 0 V.

Compound	+/0	2+/+	3+/2+
I		+0.36[a,b,c]	
1		+0.42[c]	
2		+0.27[c]	
3	+0.22[d]	+0.30[d]	+0.52[d]
4	+0.20[d]	+0.28[d]	+0.40[d]
5	+0.22[d]	+0.31[d]	–
6	+0.22	–	–

[a] value reported from a literature reference.[5] [b] value corrected from its initial report of an oxidation potential versus a standard calomel electrode. [c] separation between first, second, and third oxidations were not resolvable. [d] values determined using a combination of CV and DPV experiments

5.2.3 Visible-NIR Absorption Spectra of the Monocations

Monocations **1⁺–4⁺** were generated by adding a 10-fold excess of the neutral compound to a solution of tris(4-bromophenyl)aminium hexachloroantimonate in dichloromethane or d_2-dichloromethane. Visible-NIR absorption spectra of monocations **1⁺**, **3⁺**, and **4⁺** are shown in Figure 5.11. Knowing the initial concentration of oxidizing agent in solution allowed for the determination of the molar absorptivities of the resultant monocations, assuming complete electron transfer and no disproportionation. The visible-NIR absorption spectrum of **1⁺** shows similar features to the published spectrum of **I⁺**. In addition to the triarylamine monocation transitions (at ca. 10500 cm^{-1} and higher), there is a weak IVCT band at ca. 7000 cm^{-1}. In the case of the thiophene-based monocations **3⁺** and **4⁺**,

both species showed similar triarylamine absorptions and IVCT bands to those observed for **1⁺**, although the line shapes are narrower and molar extinction coefficients for the triarylaminium absorption bands are lower for both **3⁺** and **4⁺** than for **1⁺**. The extinction coefficients of the IVCT bands are similar for all three monocations.
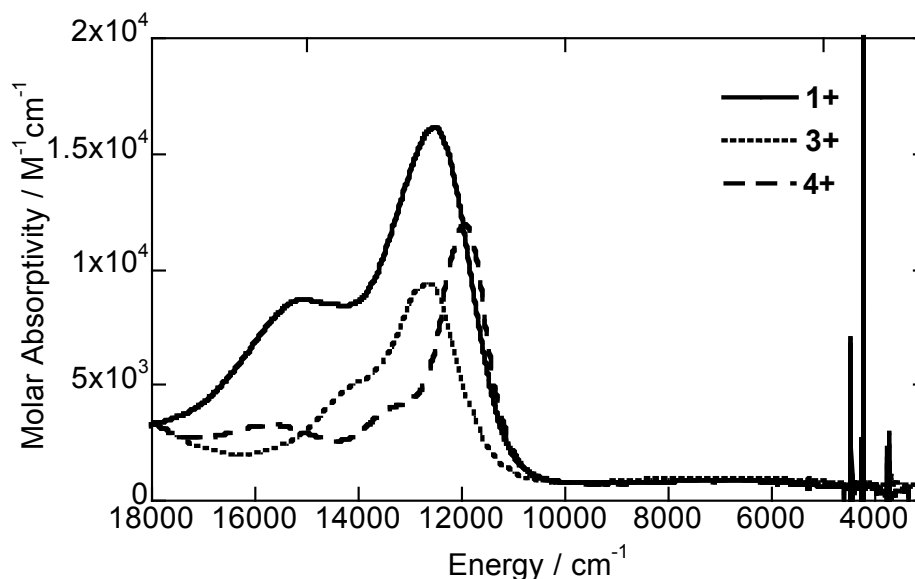
Figure 5.11. Visible-NIR absorption spectra of monocation **1⁺** in dichloromethane, and monocations **3⁺** and **4⁺** in d_2-dichloromethane.

Unexpectedly, visible-NIR absorption spectrum resulting from the oxidation of compound **2** (Figure 5.12) does not show a distinct IVCT band and shows a long tail that overlaps with the triarylamine monocation transition. It is possible that the energy of the IVCT band is higher in **2⁺** than that of **1⁺**, resulting in the appearance of the tail and lack of a distinct IVCT band. The energy of the IVCT band depends on the reorganization energy – not the electronic coupling – in a class II MV system, so this could mean that the reorganization energy is larger for **2⁺** than for **1⁺**. The visible-NIR absorption spectrum for the oxidation of

compound **2** is shown in Figure 5.12. In this case, the spectrum is shown from a solution with higher concentration of monocation than the solutions for which spectra were recorded in Figure 5.11. However, even at high concentrations, the IVCT band cannot be clearly observed; a shoulder from ca. 9000 – 12000 cm^{-1} precluded analysis of what might be the tail of an IVCT band apparent from 5000 – 9000 cm^{-1}. Another possibility is that the spectrum observed is not of **2$^+$** at all. For this reason, no Hush analysis[19] was done for the visible-NIR absorption spectrum recorded upon oxidation of compound **2**.
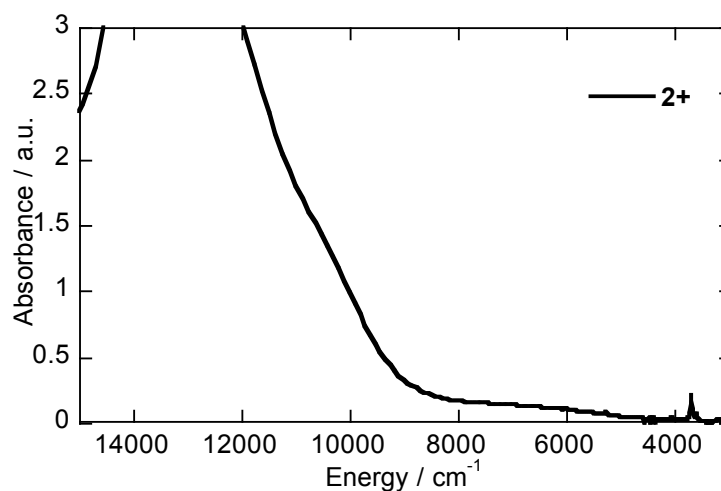
Figure 5.12. Visible-NIR absorption resulting from the oxidation of **2** in dichloromethane.

An expansion of the IVCT bands of **1$^+$**, **3$^+$**, and **4$^+$** is shown in Figure 5.13. In this expansion, one can see that the separation of the IVCT bands from the triarylaminium absorption is more distinct for **3$^+$** and **4$^+$** than for **1$^+$**.
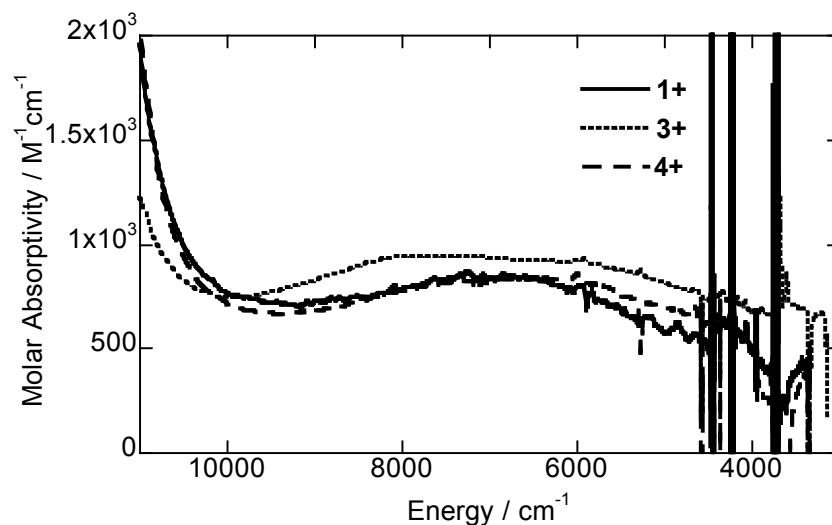
Figure 5.13. IVCT bands of **1⁺**, **3⁺**, and **4⁺** in dichloromethane.

The visible-NIR absorption spectra of three-site monocation **3⁺** and its relevant two-site (**5⁺**) and one-site (**6⁺**) model compounds are shown in dichloromethane (Figure 5.14). Unfortunately the shape of the IVCT band of **5⁺** is not reliable because there is an impurity peak that varies in intensity with the concentration of the monocation in solution (Figure 5.15). Since the extent of the absorption spectrum of the impurity is unknown, the IVCT band could not be confidently analyzed because its apparent line shape and absorption maximum could be affected by the absorption of the impurity. However, it is at least evident that there is an IVCT band for **5⁺** that occurs at similar energy and similar intensity as that for **3⁺**, so the spectrum is shown for comparison. As expected, **6⁺** does not show an IVCT band and does show a triarylaminium absorption similar to those observed in **3⁺** and in **5⁺**.
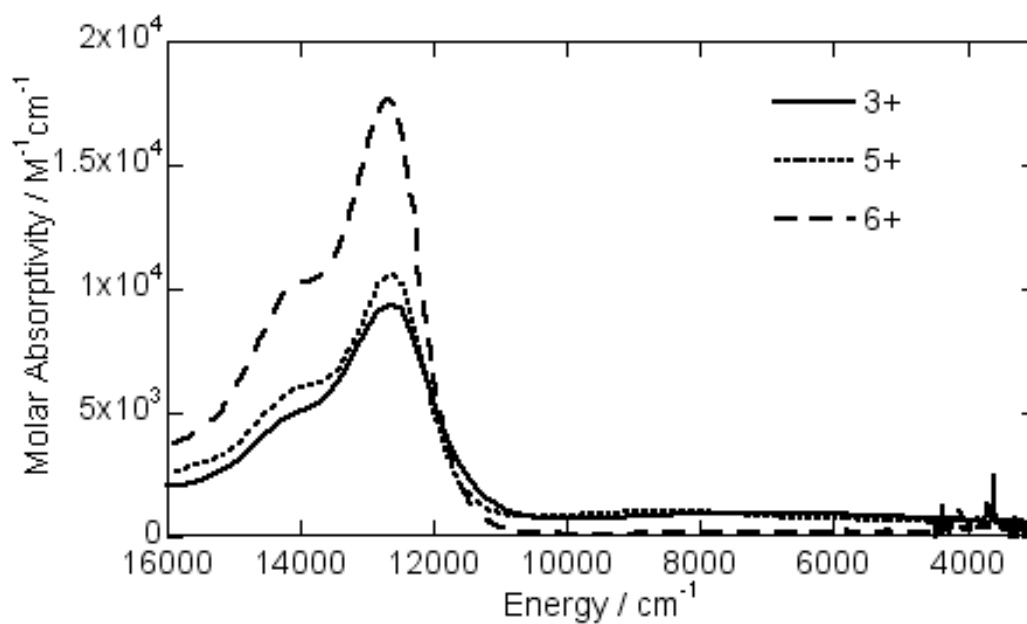
Figure 5.14. Visible-NIR absorption spectra of monocations **3⁺**, **5⁺**, and **6⁺** in dichloromethane.

The visible-NIR absorption spectrum of **5⁺** is shown in Figure 5.15 when recorded at different concentrations. In this figure, one can see the change in relative amounts of the impurity peak with absorption maximum at ca. 8500 cm⁻¹.
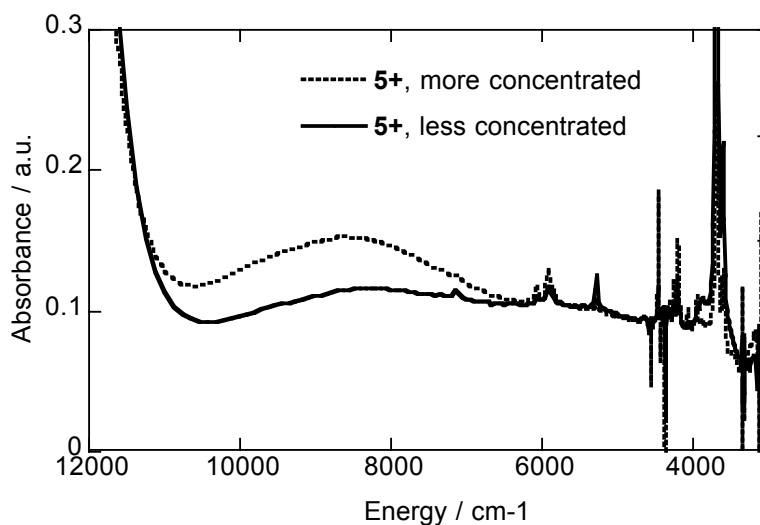
Figure 5.15. Visible-NIR absorption spectra recorded for 5^+ at two concentrations in dichloromethane.

As a consequence of overlap between the IVCT absorption and the triarylaminium absorption, the tail of the triarylaminium absorption and the IVCT for 1^+, 3^+, and 4^+ were fitted as two symmetric Gaussians, the sum of which is are shown in Figure 5.16. The Gaussian used to fit the IVCT band were used for the Hush analysis of the monocations.
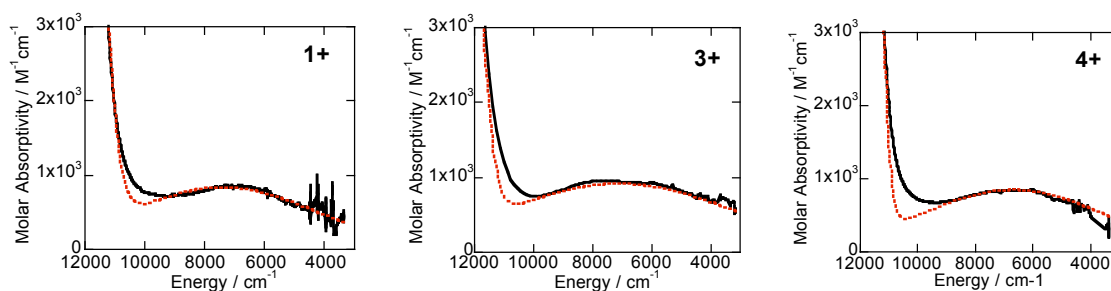
Figure 5.16. Sum of two Gaussian fits to the NIR absorption bands of 1^+, 3^+, and 4^+ from spectra recorded in dichloromethane.

The Gaussian fits of the IVCT bands of $\mathbf{1^+}$, $\mathbf{3^+}$, and $\mathbf{4^+}$ were analyzed by Hush theory and are compared with the data provided in the literature for $\mathbf{I^+}$, although the absorption spectrum for $\mathbf{I^+}$ was recorded in $^nBu_4NPF_6$ in dichloromethane (the monocation was generated electrochemically, thus requiring the presence of an electrolyte). The full width at half maximum predicted by Hush theory[19] ($\nu_{1/2[Hush]}$) was calculated using

$$\overline{\nu}_{1/2[Hush]} = \sqrt{2310 \times \overline{\nu}_{max}} \tag{5.1}$$

In the spectra of $\mathbf{1^+}$, $\mathbf{3^+}$, and $\mathbf{4^+}$, the lowest energy features are approximately symmetric Gaussians, which are broader than the Hush prediction for class-II compounds and were therefore assigned to the IVCT transitions of class II MV compounds.

The transition dipole moment (μ_{ge}) was calculated using the integration of the Gaussian fits of the IVCT bands rather than the raw experimental absorption spectra, since the original spectra would have overlap of the IVCT and triarylaminium absorption bands with each other. In addition to calculating μ_{ge} using the area under the Gaussian curve, for comparison with $\mathbf{I^+}$ and $\mathbf{II^+}$ for which μ_{ge} was not provided, μ_{ge} was also calculated using the molar absorptivity multiplied by $\nu_{1/2}$ because, even though this method is less accurate, both the molar absorptivity and $\nu_{1/2}$ were provided for $\mathbf{I^+}$ and $\mathbf{II^+}$, so this method for calculating μ_{ge} allows for comparison with published data. Using μ_{ge} calculated from the Gaussian fits, the electronic coupling (V) can be estimated for both class II and III systems from characteristics of the IVCT band using the Hush expression, modified for a three-site MV species[7]

$$V_{Hush} = \frac{\mu_{ge}\overline{\nu}_{max}}{\sqrt{2}eR_{ab}} \tag{5.2}$$

where e is the electronic charge, and R_{ab} is the diabatic electron-transfer distance. R_{ab} was assumed to be the nitrogen-nitrogen distance (R_{NN}), the value for which was calculated using an MM2 geometry minimization of the neutral species, though this value may not be the real R_{ab}; the more strongly coupled the MV species is, the more likely R_{ab} is likely to be smaller than R_{NN}. Because the ionization potentials of the thiophene bridges are lower than the phenylene bridges, it was expected that the coupling in the thiophene-based monocations should be stronger than their equivalent phenylene-based systems, because the monocation could have more bridge character in the thiophene-based species, moving the redox centers closer. Spectral characteristics and calculations for transition dipole moment and electronic coupling based on the experimental data for the IVCT absorptions for 1^+, 3^+, and 4^+ are shown in Table 5.2.

Table 5.2. Experimental parameters characterizing the intervalence absorptions of the monocations of tris(diarylamino) derivatives in dichloromethane.

compound	ν_{max} / cm^{-1}	ε / M^{-1}cm^{-1}	$\nu_{1/2}$ / cm^{-1}	$\nu_{1/2[Hush]}$ / cm^{-1}	μ_{ge}[b] / D	μ_{ge}[c] / D	V_{Hush} / cm^{-1}
I[a]	6935	797	5650	4002	–[d]	2.4	205
II[a]	5981	258	7898	4271	–[d]	1.8	181
1	7400	830	10300	4130	2.8	3.2	244
3	7100	910	13000	4050	3.3	3.9	296
4	6700	840	10600	3930	3.0	3.5	254

[a] values from published data,[6,7] [b] calculated using the area under the Gaussian, [c] calculated using the molar absorptivity multiplied by $\nu_{1/2}$ instead of the area, [d] value not provided

From this data, the electronic coupling obtained for 1^+ is slightly larger than that obtained for I^+ in the literature, which – since the molar absorptivities for the two monocations are similar – is presumably due to the larger $\nu_{1/2}$ obtained from the Gaussian fit for 1^+. The electronic coupling found for thiophene-based monocation 3^+ is also slightly

larger than those found for phenylene-based monocations $\mathbf{I^+}$ and $\mathbf{1^+}$, which was expected based on the predicted increase in electronic coupling due to the lower ionization potentials of thiophene compared to benzene. It is more difficult to know what trend in electronic coupling to expect for $\mathbf{1^+}$ versus $\mathbf{4^+}$ because both the end groups and the bridging groups are changed. It is unfortunate that the IVCT band of the two-site monocation $\mathbf{5^+}$ could not be reliably evaluated in this series to see how the electronic coupling compares to that of $\mathbf{3^+}$.   In conclusion, as was expected based on the relative ionization potentials of thiophene and benzene, the electronic coupling in the thiophene-based MV monocations is slightly stronger than in the phenylene-based MV monocations.

5.2.4   EPR Spectra of the Monocations

EPR spectra were recorded of monocations $\mathbf{1^+}$–$\mathbf{6^+}$. One reason to obtain this data was to correlate any hyperfine coupling in the EPR spectra with the (de)localization of the monocation both throughout each arm of the tris(diarylamine) derivative and whether the monocation was coupled to multiple triarylamine moieties on the EPR time scale. If the monocation showed a spectrum that indicated hyperfine coupling to all three nitrogen nuclei, then it would be considered in the fast limit of intramolecular exchange; if coupling to one nitrogen nucleus is observed in the EPR spectrum, then the monocation is considered in the slow limit of intramolecular exchange. It should be noted that coupling to three nitrogen nuclei does not necessarily imply that the monocation is delocalized over all three triarylamine moieties; this result implies either delocalization of the monocation or that the rate of intramolecular exchange is greater than the coupling constant to nitrogen. Recording the EPR spectra at variable temperatures could allow – if the spectrum changes with

temperature – for the determination of rates of intramolecular exchange, which could give a barrier to intramolecular electron transfer, as was shown for two monocations in Chapter 4. The second reason to record EPR spectra was to determine – if hyperfine coupling was observed – the extent to which the monocation is delocalized within the triarylamine moiety itself; for example, if the hyperfine coupling constant (HFCC) to nitrogen varies in magnitude from one monocation to another, this difference suggests that the monocation with the smaller HFCC to nitrogen (assuming coupling to the same number of nitrogen nuclei) is more delocalized throughout the aryl group(s).

EPR spectra of monocations $\mathbf{1}^+$–$\mathbf{6}^+$ were recorded in dichloromethane. In the same way as was reported in section 5.2.2, the monocations were generated by addition of a 10-fold excess of neutral compound to tris(4-bromophenyl)aminium hexachloroantimonate in dichloromethane. EPR spectra were initially recorded at room temperature on a Bruker X-band EPR spectrometer at concentrations of ca. 5×10^{-4} M. Additionally, DFT calculations were used to predict HFCCs based on predictions for spin densities in the monocations.

Figure 5.l7 shows the EPR spectra of $\mathbf{1}^+$ and $\mathbf{2}^+$, which are nearly identical in shape. Neither EPR spectrum shows any resolvable hyperfine coupling, so modeling the spectra (as was done for the EPR spectra of some of the monocations in Chapters 2, 3, and 4) would serve little purpose here. The EPR spectra of $\mathbf{1}^+$ and $\mathbf{2}^+$ demonstrate the presence of a radical but do not allow for the determination of whether the monocation is in a fast or slow limit of electron exchange on the EPR time scale. However, because the integrated peaks of the EPR spectra of $\mathbf{1}^+$ and $\mathbf{2}^+$ are essentially Gaussian in shape (not shown), this rules out intermolecular electron exchange as the reason for the lack of hyperfine coupling. It is

possible that no hyperfine coupling is observed because of coupling to a large number of inequivalent hydrogen nuclei.
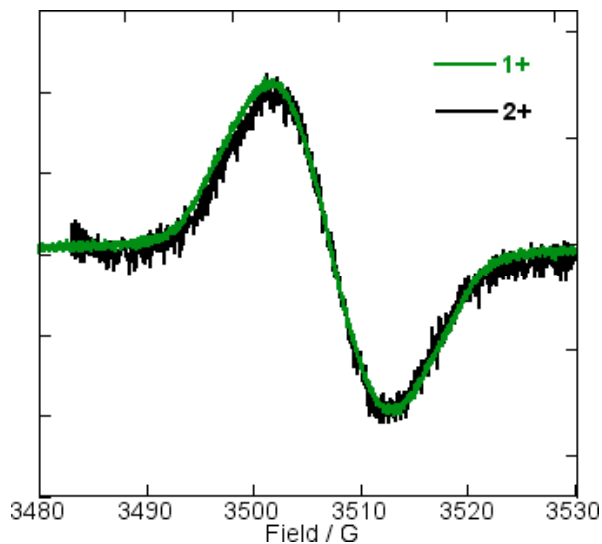
Figure 5.17. EPR spectra of 1^+ and 2^+ in dichloromethane at room temperature.

When cooled to 200 K, the EPR spectrum of 1^+ (Figure 5.18) shows a three-line spectrum (A_N = 7.7 G), consistent with coupling to one nitrogen nucleus; therefore, at low temperature the rate of intramolecular electron transfer between the multiple redox centers is in the slow regime on the EPR time scale.
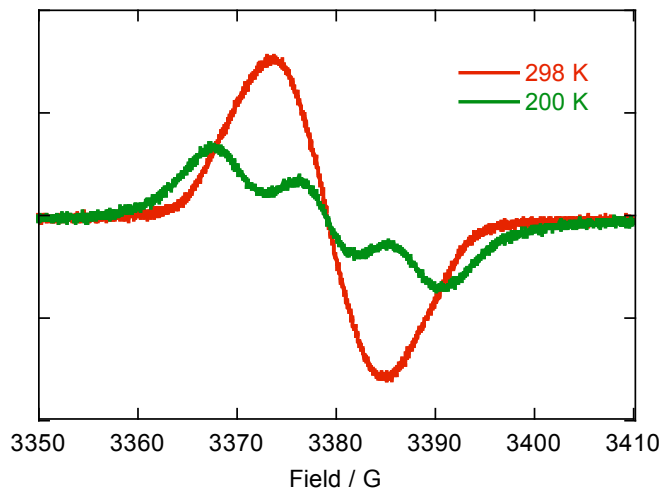
Figure 5.18. EPR spectra of **1⁺** in dichloromethane at 298 and 200 K.

The EPR spectra of **3⁺** and **4⁺** are shown in Figure 5.19. While the spectrum of **4⁺** shows no hyperfine coupling – as was the case for both phenylene-based monocations **1⁺** and **2⁺** – the spectrum of **3⁺** does show hyperfine coupling, the simulation of which will be discussed shortly. The integrated peaks in the EPR spectrum of **4⁺** is Gaussian in shape, which rules out the possibility for intermolecular exchange being the cause of the lack of hyperfine coupling.
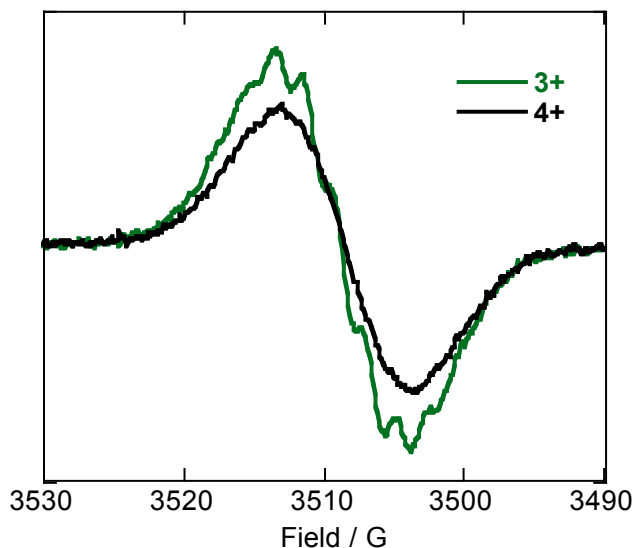
Figure 5.19. EPR of monocations **3⁺** and **4⁺** in dichloromethane at room temperature.

Variable temperature EPR (VT-EPR) spectra of monocation **3⁺** were obtained (Figure 5.20) in order to determine if the spectrum changed upon cooling. When cooled, the intensity of the signal observed by EPR initially diminished slightly – presumably due to decomposition of the monocation over the time required to record the spectra at multiple temperatures or because of precipitation of the monocation at the bottom of the EPR tube –

but retained the same shape until below 240 K, where the splitting pattern was lost. Retention of the same splitting pattern suggests that the spectrum observed at room temperature is in either a fast or slow limit of intramolecular exchange on the time scale of the EPR experiment.
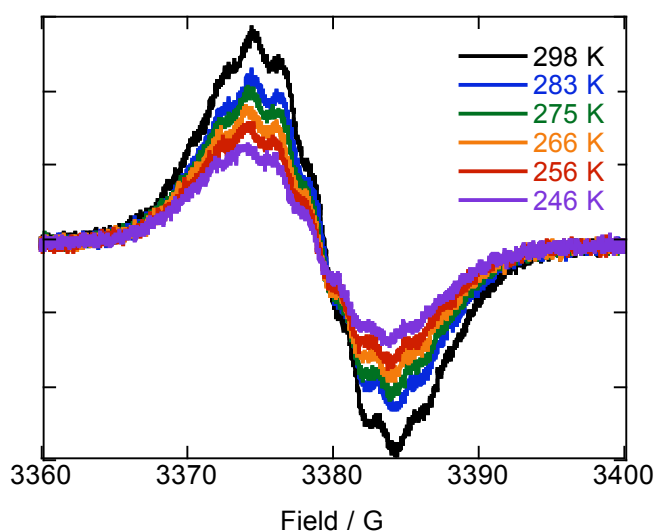
Figure 5.20. VT-EPR of **3⁺** in dichloromethane, from 298 to 246 K.

In Figure 5.21, the normalized EPR spectra of **3⁺** at 298 and 206 K are shown. While the fine structure of the EPR spectrum is lost at low temperatures, the overall line shape is similar.
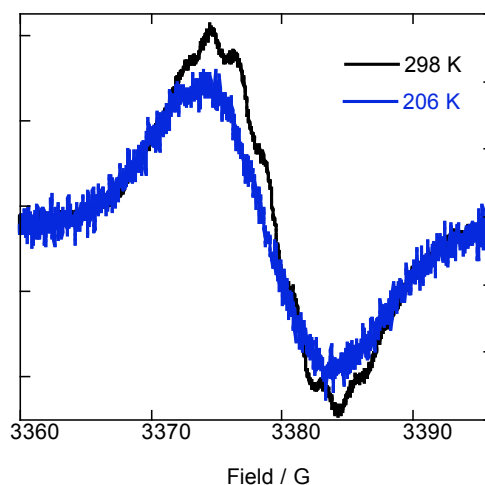
Figure 5.21. Normalized EPR spectra of **3⁺** at 298 and 206 K in dichloromethane.

EPR spectra of monocations **3⁺**, **5⁺**, and **6⁺** are shown in Figure 5.22. The monocations have different splitting patterns; while the spectra of the monocations of the two- (**5⁺**) and three-site (**3⁺**) compounds have similar line widths, the spectrum of the monocation of the one-site species (**6⁺**) is much broader. While the broadness of the EPR spectrum of **6⁺** was not expected, simulations of the spectrum give reasonable fits. The shapes and splitting patterns will be discussed further when the EPR simulations are presented.
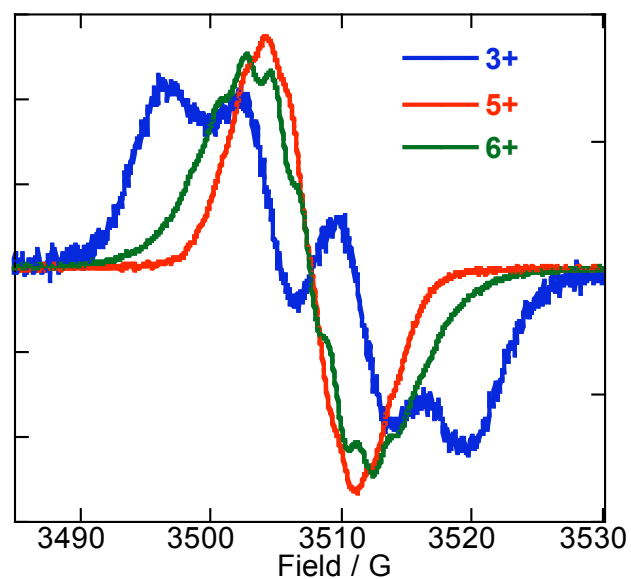
Figure 5.22. EPR spectra of monocations $\mathbf{3^+}$, $\mathbf{5^+}$, and $\mathbf{6^+}$ in dichloromethane at room temperature.

VT-EPR spectra of $\mathbf{5^+}$ in dichloromethane (Figure 5.23) show little change in the shape of the spectrum upon cooling, suggesting that the intramolecular electron transfer is either in a fast or slow limit on the time scale of the EPR experiment.
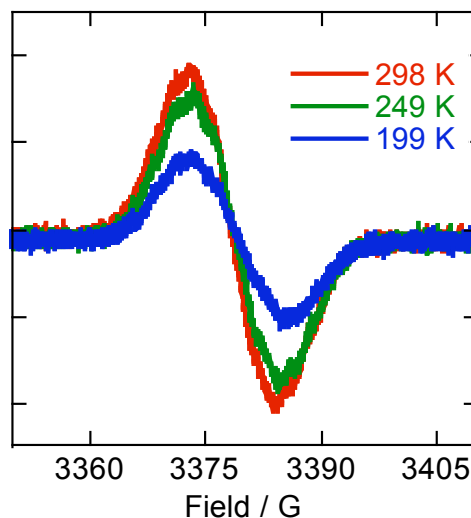
Figure 5.23. VT-EPR of **5⁺** in dichloromethane at 298, 248, and 199 K.

VT-EPR spectra of **6⁺** in dichloromethane (Figure 5.24) were recorded for comparison with the two- and three-site species, even though intramolecular electron exchange was not expected. The EPR spectra show some change upon cooling, but overall the spectrum is still four-line in nature. The changes in spectral shape may be due to a difference coupling to hydrogen nuclei at different temperature because of changes in conformational populations.
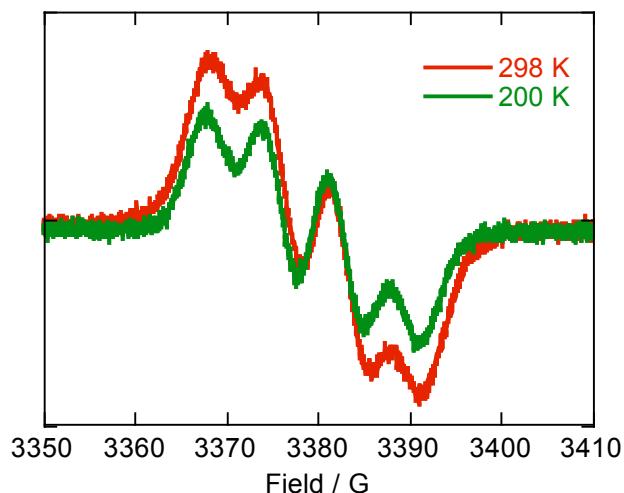
Figure 5.24. VT-EPR of **6⁺** in dichloromethane at 298 and 200 K.

The EPR spectra of **1⁺**, **3⁺**, **5⁺**, and **6⁺** were analyzed using WinSim to obtain simulations (Figure 5.25) and hyperfine coupling constants (HFCCs, A_N, Table 5.3) to specific types of nuclei. The EPR spectrum of **1⁺** at low temperature gives a fairly good fit to coupling to one nitrogen nucleus (A_N = 7.7 G); coupling to additional hydrogen nuclei did not improve the fit. This value is lower than that of the magnitude of the HFCC reported for the mononuclear triarylamine monocation $[(4\text{-}CH_3C_6H_4)_3N]^+$ in acetonitrile (A_N = 9.45 G),[27] and is presumably lowered by some delocalization onto the central benzene ring. The EPR spectrum of **3⁺** can be simulated with a good fit to one set of three equivalent nitrogen nuclei (A_N = 1.8 G) and two sets of three equivalent hydrogen nuclei (A_H = 2.7, 2.3 G). Considering that the unpaired electron is coupled to three nitrogen nuclei, the magnitude of the HFCC seems reasonable; the HFCC to nitrogen is slightly smaller than one third of the HFCC to the nitrogen nucleus in a triarylamine monocation.[27] Comparison to DFT calculations for HFCCs for **3⁺** was not possible in this case because the calculation for **3⁺** did not converge, possibly

due to complications from the degeneracy of the highest occupied molecular orbital in the neutral compound. The fits from the simulation suggest that there is electron delocalization or fast exchange on the time scale of the EPR experiment, meaning that the intramolecular electron exchange rate is much greater than ca. 10^7 s^{-1}. A good fit could not be obtained when coupling to one or two nitrogen nuclei were used, regardless of how many hydrogen nuclei were used, further supporting the fit to three nitrogen nuclei.

For the two-site monocation (**5$^+$**), the simulation shows a good fit to two nitrogen nuclei ($A_N = 3.1$ G), one set of two hydrogen nuclei ($A_H = 2.5$), and one additional hydrogen nucleus ($A_H = 1.8$ G), consistent with a monocation that is delocalized or in a fast exchange regime on the time scale of the EPR experiment. The HFCC to nitrogen is reasonable because it is approximately 3/2 that of the A_N obtained from the simulation of **3$^+$**; the value for A_N is also consistent with that predicted by DFT calculations ($A_N = 3.05$ G), assuming a delocalized monocation for the calculation of spin density. A good simulation to this EPR spectrum could not be obtained using only one nitrogen nucleus, even when given the possibility for coupling to multiple hydrogen nuclei, again supporting that this monocation is not in the slow limit of intramolecular electron exchange on the EPR time scale.

Lastly, the EPR spectrum of the one-site monocation (**6$^+$**) was simulated, giving a reasonable fit to one nitrogen nucleus ($A_N = 6.5$ G), three hydrogen nuclei ($A_H = 5.2$, 2.6, and 1.6 G), as well as a few more hydrogen nuclei with HFCCs of 1 G or less. Unsurprisingly, the HFCC to nitrogen is larger than in the cases of **3$^+$** and **5$^+$**; the value for A_N is similar to that predicted by DFT calculations ($A_N = 5.83$ G). The unusually large HFCC to a hydrogen nucleus was also similarly predicted by DFT calculations ($A_H = 4.72$ G), which was calculated to be the hydrogen atom at the 3-position of the thiophene ring.
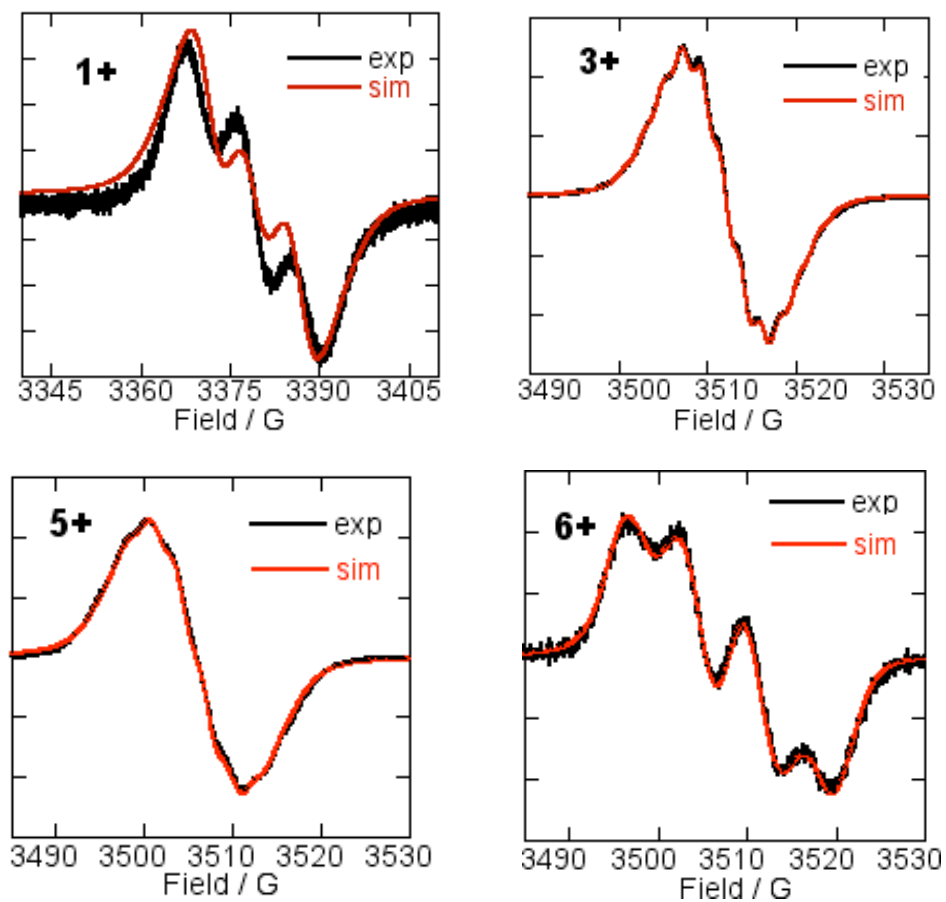
Figure 5.25. Experimental and simulated EPR spectra of **1⁺** (top left), **3⁺** (top right), **5⁺** (bottom left), and **6⁺** (bottom right) in dichloromethane.

The HFCCs obtained from simulated EPR spectra of 3^+, 5^+, and 6^+, with the number of nuclei for which the HFCC applies, are shown in Table 5.3. A summary of the HFCCs predicted from DFT calculations is given in the experimental section.

Table 5.3. HFCCs for the EPR spectra of 3^+, 5^+, and 6^+ from WinSim, with the number of nuclei corresponding to each coupling constant shown in parentheses. Values of HFCCs of 1 G or less were not included in the table.

Compound	A_N / G	A_H / G	A_H / G	A_H / G
1*	7.7 (1)	–	–	–
3	1.8 (3)	2.7 (3)	2.3 (3)	_
5	3.1 (2)	2.5 (2)	1.8 (1)	–
6	6.5 (1)	5.2 (1)	2.6 (1)	1.6 (1)

*from spectra recorded at 200 K in dichloromethane

In summary, from the simulations of the EPR experiments, the thiophene-based MV species (3^+ and 5^+) are in a fast limit of intramolecular exchange or are statically delocalized species at both room temperature and low temperature (where the spectra have similar shapes), compared with the phenylene-based MV species (1^+), which is in the slow limit of intramolecular electron exchange, at least at low temperature.   This observation is consistent with the assignment of monocations 1^+ and 3^+ as class II MV species that have different rates of intramolecular electron exchange (3^+ having a faster rate than 1^+). In this context, it would also be reasonable to assume that 5^+ could be assigned as a class II MV species with a rate of intramolecular exchange that is much greater than ca. 10^7 s^{-1}.   Additionally, the EPR data for the thiophene-based compounds suggests more shifting of the redox site into the thiophene bridge, so R_{ab} should be decreased versus R_{NN}, and, therefore, V should be even larger for the thiophene-based monocations than the phenylene-based monocations than is suggested by simply using R_{NN}.

5.3 Conclusions on Three-site MV Systems

In conclusion, the three-site monocations studied in this chapter can be confidently described as class II MV species. From the CV and DPV data, the more easily oxidized thiophene-based derivatives show separable oxidations whereas the phenylene derivatives do not. From the visible-NIR absorption spectra of the monocations, the thiophene-based derivatives show IVCT bands of similar intensity, and the IVCT bands are more separated from the triarylaminium absorption bands than is the case for the phenylene-based monocation; the IVCT bands of the thiophene-based monocations can, therefore, be more confidently analyzed by Hush theory than the phenylene-based monocations. EPR spectra shed light into the minimum rates of intramolecular electron exchange for some of the thiophene-based derivatives, showing that the electron exchange is in the fast limit, whereas – at least at cold temperatures – the equivalent phenylene-based derivative is in the slow limit. While all of the monocations are class II species, the monocations of the thiophene-based derivatives show evidence of stronger electronic coupling.

5.4 Experimental Section for Chapter 5

5.4.1 Electrochemical Methods

Electrochemical measurements were carried out under nitrogen on dry deoxygenated dichloromethane solutions ca. 10^{-4} M in analyte and 0.1 M in tetra-*n*-butylammonium hexafluorophosphate ($^nBu_4NPF_6$) using a BAS 100W Potentiostat, a glassy carbon working electrode, a platinum auxiliary electrode, and, as a pseudo-reference electrode, a silver wire anodized in 1 M aqueous potassium chloride. Potentials were referenced to ferrocenium / ferrocene using decamethylferrocenium / decamethylferrocene (-0.55 V versus ferrocenium / ferrocene) as an internal reference. Cyclic voltammograms were recorded at a scan rate of 50 mVs^{-1}. Differential pulse voltammetry experiments were run in the same solutions used for cyclic voltammetry experiments, and were run at a scan rate of 20 mVs^{-1}.

5.4.2 Visible-NIR Absorption Spectra of the Monocations

Dr. Stephen Barlow, of the research group of Prof. Seth R. Marder at Georgia Institute of Technology, gave significant input as to the experimental design for collection of the visible-NIR absorption spectra. The visible-NIR absorption spectrum of 1$^+$ was recorded by Dr. Simon Jones, of the same research group.

Monocations were generated in solution by addition of appropriate amounts of tris(4-bromophenyl)aminium hexachloroantimonate (Aldrich) in dry deuterated dichloromethane (< 0.1 equivalents for monocations). Absorptivities were calculated assuming complete electron transfer and negligible disproportionation. Visible-NIR spectra were recorded in 1 cm cells using a Varian Cary 5E spectrometer.

5.4.3 EPR Experimental Details

David Jensen, of the research group of Prof. Bridgette Barry at Georgia Institute of Technology, assisted with the set-up and collection of the VT-EPR data.

EPR spectra were acquired on an X-band Bruker EMX spectrometer in dichloromethane solutions. Dichloromethane was dried by passing through columns of activated alumina in a manner similar to that described in the literature.[28] Tris(4-bromophenyl)aminium hexachloroantimonate was purchased from Aldrich. In all cases a ca. 10-fold excess of tris(diarylamino), bis(diarylamino), or diarylamino derivative was added to a solution of tris(4-bromophenyl)aminium hexachloroantimonate in dichloromethane, thus generating a solution with molarity of monocation that was approximately the same as the molarity of the original oxidant in solution. For EPR spectra recorded at room temperature, the solutions were ca. 3×10^{-4} M in tris(4-bromophenyl)aminium hexachloroantimonate and were recorded from samples in 4 mm EPR tubes. For EPR spectra recorded at variable temperatures, the solutions were ca. 3×10^{-3} to 3×10^{-4} M in tris(4-bromophenyl)aminium hexachloroantimonate and were obtained in 3 mm EPR tubes.

5.4.4 Computational Details

Kelly Lancaster and Dr. Veaceslav Coropceanu, of the research group of Prof. Jean-Luc Brédas at Georgia Institute of Technology, carried out the DFT calculations to obtain theoretical HFCCs.

For obtaining the nitrogen-nitrogen distance in the neutral molecules, geometries were minimized using MM2 calculations in Chem 3-D.   Separately, the ground-state geometries of the neutral and monocation of the tris(diaryl)amino derivatives were optimized at the DFT level.   All DFT calculations were performed using the 6-31G(d,p) split valence plus double polarization basis set[29-32] and with the B3LYP functional.[33,34] All calculations were carried out using the Gaussian 03 suite of programs.[35]

Simulations of EPR experiments were accomplished using WinSim, a simulation program for Windows, which is currently provided for free download at the National Institutes for Environmental Health Sciences of the National Institutes of Health website at http://www.niehs.nih.gov/research/resources/software/tools/index.cfm.

The labeling scheme for **5⁺** and **6⁺** for the HFCCs obtained from DFT calculations are shown below (Figure 5.26).
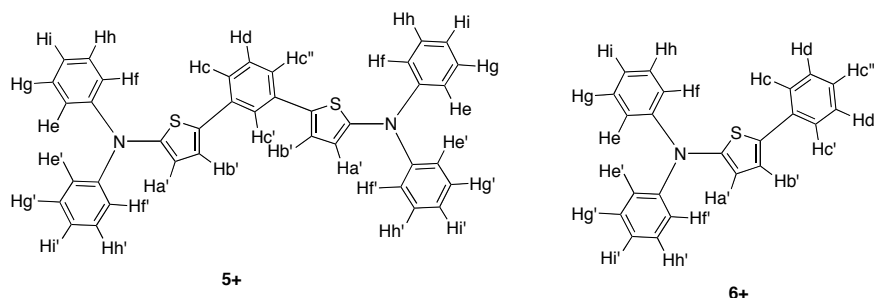
Figure 5.26. Labeling scheme for HFCCs from DFT calculations.

Table 5.4 shows the HFCCs for **5⁺**, and **6⁺** obtained from DFT calculations of the spin densities of the monocations.   These values could not be obtained for **1⁺** and **3⁺** because the calculation did not converge.

Table 5.4. Absolute values of the HFCCs (A_x) for **5$^+$** and **6$^+$** obtained from DFT calculations of spin densities of the monocations.

A_X (G)	5$^+$	6$^+$
A_N	3.05	5.83
A_{Ha}	–*	–*
$A_{Ha'}$	2.31	4.72
A_{Hb}	–*	–*
$A_{Hb'}$	0.06	0.39
A_{Hc}	4.19	2.46
$A_{Hc'}$	0.06	2.54
$A_{Hc''}$	4.19	3.32
A_{Hd}	1.47	0.99
$A_{Hd'}$	–*	1.08
A_{He}	0.57	1.00
$A_{He'}$	0.61	1.05
A_{Hf}	0.57	1.01
$A_{Hf'}$	0.49	0.82
A_{Hg}	0.36	0.64
$A_{Hg'}$	0.34	0.60
A_{Hh}	0.44	0.81
$A_{Hh'}$	0.49	0.92
A_{Hi}	0.68	1.15
$A_{Hi'}$	0.80	1.32

*atom does not exist for this structure

5.4.5 Synthetic Details

Compounds 1 and 2 were initially synthesized and studied by Dr. Simon Jones of the research group of Prof. Seth R. Marder at Georgia Institute of Technology. Dr. Jones also completed the initial characterization of compound 1 and 2. Kelly Lefler, also of the same research group, originally synthesized compound 4 and its precursors.

Starting materials were reagent grade and were used without further purification unless otherwise indicated. Starting materials were purchased from Acros Chemical Co. except for tris(dibenzylideneacetone)dipalladium(0) and tri-*tert*-butylphosphine solution in hexane, both of which were purchased from Strem Chemicals, Inc. Solvents were dried by passing through columns of activated alumina in a manner similar to that described in the literature (tetrahydrofuran, toluene, dichloromethane)[28] or were obtained as anhydrous grade from Acros Organics. Chromatographic separations were performed using standard flash column chromatography methods using silica gel purchased from Sorbent Technologies (60 Å, 32-63 μm) or basic alumina purchased from Aldrich Chemical Company. Elemental analyses were performed by Atlantic Microlabs. Mass spec (FAB and EI) was performed on a VG Instruments 70SE. GCMS data were acquired on an Agilent 5790 GC/ 6850 MS.

1,3,5-Tris(4-iodophenyl)benzene (8). This compound was previously synthesized as previously described in two references.[22,23] ^{1}H NMR (300 MHz, CD_2Cl_2) δ 7.83 (d, J = 8.4 Hz, 6H), 7.34 (s, 3H), 7.45 (d, J = 8.7 Hz, 6H). MS-EI (m/z): 683.6.

1,3,5-Tris(4-(bis(4-*tert*-butylphenyl)amino)phenyl)benzene (1). To an oven-dried tube-shaped Schlenk flask cooled under nitrogen was added anhydrous deoxygenated toluene (10 mL), tris(dibenzylideneacetone)dipalladium(0) (0.050 g, 0.046 mmol), 1,1'-bis(diphenylphosphino)ferrocene (0.019 g, 0.035 mmol), bis(4-*tert*-butylphenyl)amine (0.16 g, 0.58 mmol), and 1,3,5-tris(4-iodophenyl)benzene (0.10 g, 0.15 mmol). A reflux condenser was attached, and the reaction flask was immersed in an oil bath, heating the reaction mixture to reflux. After one hour of heating, the reaction flask was removed from the oil bath. The reaction mixture was diluted by 50% with hexanes and was run through a pad of silica gel, eluting with hexanes/toluene (1:1). After recrystallization from dichloromethane, the product was isolated as an off-white solid (0.10 g, 60%). ^{1}H NMR (300 MHz, CD$_2$Cl$_2$) δ 7.69 (s, 3H), 7.56 (d, J = 8 Hz, 6H), 7.30 (d, J = 8 Hz, 12H), 7.09 (d, J = 8 Hz, 6H), 7.05 (d, J = 8 Hz, 12H), 1.76 (s, 36H). ^{13}C{^{1}H} NMR (100 MHz, CD$_2$Cl$_2$) δ 147.1, 146.5, 145.3, 142.1, 134.5, 128.0, 126.5, 124.5, 123.6, 123.0, 34.6, 31.5. MS (EI, pos.) 1143.5. Anal. calcd for C$_{84}$H$_{93}$N$_3$: C, 88.14; H, 8.19; N, 3.67. Found: C, 87.66; H, 8.62; N, 3.81. Cyclic voltammetry in 0.1 M ^{n}Bu$_4$NPF$_6$ in dichloromethane: $E_{1/2}^{3+/2+, 2+/+, +/0}$: +0.42 V versus Cp$_2Fe^{+/0}$ at 0 V.

1,3,5-Tris(4-(bis(4-methoxyphenyl)amino)phenyl)benzene (2). To an oven-dried tube-shaped Schlenk flask cooled under nitrogen was added anhydrous deoxygenated toluene (10 mL), tris(dibenzylideneacetone)dipalladium(0) (0.050 g, 0.046 mmol), tri(*tert*-butyl)phosphine (1.0 mL, 10% wt. in hexane), bis(4-methoxyphenyl)amine (0.13 g, 0.58 mmol), and 1,3,5-tris(4-iodophenyl)benzene (0.10 g, 0.15 mmol). A reflux condenser was attached, and the reaction flask was immersed in an oil bath, heating the reaction

mixture to reflux. After one hour of heating, the reaction flask was removed from the oil bath, and the reaction mixture was run through a tall pad of silica gel, eluting with hexanes/ethyl acetate (4:1, then 1:1). After recrystallization from ethyl acetate and methanol, 0.086 g (67%) of the desired product was isolated as an off-white solid. ^{1}H NMR (400 MHz, C_6D_6) δ 7.86 (s, 3H), 7.54 (d, J = 8.8 Hz, 6H), 7.21 (d, J = 8.8 Hz, 6H), 7.13 (d, overlapping with benzene signal, so cannot determine J, assumed 12H), 6.74 (d, J = 9.2 Hz, 12H), 3.29 (s, 18H). ^{13}C{^{1}H} NMR (100 MHz, CD_2Cl_2) δ 156.5, 148.8, 142.1, 141.1, 133.2, 127.9, 127.1, 123.2, 120.7, 115.0, 55.8. MS(FAB+) 987.2 (HRMS error: 3.17 ppm). Anal. calcd. for $C_{66}H_{57}N_3O_6$: C, 80.22; H, 5.81; N, 4.25. Found: C, 79.53; H, 5.92; N, 4.02. Cyclic Voltammetry in 0.1 M $^nBu_4NPF_6$ in dichloromethane: $E_{1/2}^{3+/2+, 2+/+, +/0}$: +0.27 V versus $Cp_2Fe^{+/0}$ at 0 V.

1,3,5-Tri(thien-2-yl)benzene (12). This compound was prepared as previously described.[23] ^{1}H NMR (C_6D_6, 500 MHz) δ 7.75 (s, 3H), 7.41 (d, J = 4.0 Hz, 3H), 7.34 (d, J = 5.0 Hz, 3H), 7.13 (dd, J = 4.0, 5.0 Hz, 4H).

1,3,5-Tris(5-bromothien-2-yl)benzene (13). *Note:* In contrast to what is described in the literature, from the cyclization/dehydration reaction of 2-acetyl-5-bromothiophene with $SiCl_4$ in ethanol, a mixture of tri-halogenated (mixture of brominated and chlorinated) derivatives was obtained as an inseparable mixture.[24] Instead, the title compound was obtained using the bromination 1,3,5-tris(thien-2-yl)benzene, as described below:

To a 300 mL round-bottomed flask wrapped in aluminum foil, acetic acid (50 mL) and chloroform (50 mL) were added. The reaction flask was immersed in an ice-water bath, and 1,3,5-tris(thien-2-yl)benzene (0.20 g, 0.62 mmol) was added, followed by *N*-bromosuccinimide (0.37 g, 2.1 mmol, freshly recrystallized from water). After three hours, the reaction flask was removed from the cold bath and was allowed to warm to room temperature, and 0.055 g (0.31 mmol) additional *N*-bromosuccinimide was added to drive the reaction mixture (incomplete by TLC analysis in hexanes/dichloromethane (4:1)) to completion. Dichloromethane (200 mL) was added, and the reaction mixture was washed with water (2 × 200 mL) and sodium bicarbonate (aqueous, saturated solution, 1 × 200 mL), after which it was dried over anhydrous magnesium sulfate. The dichloromethane solution was diluted with hexanes to obtain an approximately 1:1 ratio of hexanes:dichloromethane, and the solution was run through a short pad of silica gel, eluting with hexanes/dichloromethane (1:1). After concentration by rotary evaporation, 0.25 g (73%) of off-white solid was isolated. ^{1}H NMR (CDCl$_3$, 500 MHz) δ 7.31 (s, 1H), 6.67 (d, $J = 4$ Hz, 1H), 6.51 (d, $J = 4$ Hz, 1H). ^{13}C{^{1}H} NMR (125 MHz, CDCl$_3$) δ 144.4, 135.2, 131.0, 124.7, 122.1, 112.4. MS (EI) calcd for C$_{18}$H$_{19}$Br$_3$S$_3$: 561.74; found: 561.7. Anal. calcd. for C$_{18}$H$_{19}$Br$_3$S$_3$: C, 38.53; H, 1.62. Found: C, 38.60; H, 1.60.

1,3,5-Tris(2-bis(4-*tert*-butylphenyl)aminothien-2-yl)benzene (3). To a an oven-dried tube-shaped Schlenk flask cooled under nitrogen was added anhydrous deoxygenated toluene (20 mL), followed by bis(4-*tert*-butylphenyl)amine (0.50 g, 1.8 mmol), 1,3,5-tris(5-bromothien-2-yl)benzene (0.25 g, 0.45 mmol), tris(dibenzylideneacetone)-dipalladium(0) (0.50 g, 0.46 mmol), tri(*tert*-butyl)phosphine (3.0 mL, 10% wt. solution in

hexane), and sodium *tert*-butoxide (0.90 g, 9.4 mmol). A reflux condenser was attached, and the reaction flask was immersed in an oil bath and was heated to reflux. After one hour, the reaction flask was removed from the oil bath, and the reaction mixture was run through a column of silica gel, eluting with toluene. The product was recrystallized from ethyl acetate and methanol, yielding a bright yellow powder (0.44 g, 83%). ^{1}H NMR (500 MHz, C_6D_6) δ 7.64 (s, 3H), 7.27 (d, J = 8 Hz, 12H), 7.20 (d, J = 8 Hz, 12H), 6.80 (d, J = 4.0 Hz, 3H), 6.58 (d, J = 4.0 Hz, 3H), 1.19 (s, 18H). ^{13}C{^{1}H} (500 MHz, C_6D_6) δ 152.6, 146.09, 146.05, 136.8, 136.5, 126.5, 124.2, 123.0, 121.0, 120.9, 34.3, 31.5. MS (EI, pos.) 1161.5. Anal. calcd. for $C_{79}H_{97}N_3S_3$: C, 80.57; H, 7.54; N, 3.61. Found: C, 80.32; H, 7.53; N, 3.60. Cyclic voltammetry in 0.1 M ^{n}Bu$_4$NPF$_6$ in dichloromethane: $E_{1/2}^{+/0}$: +0.22; $E_{1/2}^{2+/+}$ +0.30; $E_{1/2}^{3+/+}$: +0.52 V versus $Cp_2Fe^{+/0}$ at 0 V.

1,3,5-Tris(2-bis(4-methoxyphenyl)aminothien-2-yl)benzene (4). To a an oven-dried tube-shaped Schlenk flask cooled under nitrogen was added anhydrous deoxygenated toluene (20 mL), followed by bis(4-methoxyphenyl)amine (0.41 g, 1.8 mmol), 1,3,5-tris(5-bromothien-2-yl)benzene (0.25 g, 0.45 mmol), tris(dibenzylideneacetone)-dipalladium(0) (0.50 g, 0.46 mmol), tri(*tert*-butyl)phosphine (1.0 mL, 10% wt. solution in hexane), and sodium *tert*-butoxide (0.90 g, 9.4 mmol). A reflux condenser was attached, and the reaction flask was immersed in an oil bath and was heated to reflux. After one hour, the reaction flask was removed from the oil bath, and the reaction mixture was run through a tall pad of silica gel, eluting with hexanes/ethyl acetate (4:1, then 1:1). The product was recrystallized from ethyl acetate and methanol, yielding a bright yellow powder (0.17 g, 38%). ^{1}H NMR (500 MHz, C_6D_c) δ 7.73 (s, 3H), 7.18 (d, J = 9.0 Hz,

12H), 6.89 (d, J = 4.0 Hz, 3H), 6.71 (d, J = 9.0 Hz, 12H), 6.48 (J = 4.0 Hz, 3H), 3.30 (s, 18H). $^{13}C\{^1H\}$ NMR (125 MHz, C_6D_6) δ 156.6, 154.1, 142.0, 136.7, 134.7, 125.2, 123.1, 120.3, 117.7, 115.0, 55.0. MS (FAB+) calcd. for $C_{60}H_{51}O_6N_3S_3$: 1005.29; found: 1005.9. Anal. calcd. for $C_{60}H_{51}O_6N_3S_3$: C, 71.62; H, 5.11; N, 4.18. Found: C, 71.47; H, 5.23; N, 3.78. Cyclic voltammetry in 0.1 M $^nBu_4NPF_6$ in dichloromethane: $E_{1/2}^{+/0}$: +0.20; $E_{1/2}^{2+/+}$: 0.28; $E_{1/2}^{3+/2+}$: 0.40 V versus $Cp_2Fe^{+/0}$ at 0 V.

2-Bromo-5-phenylthiophene (17).   This compound was prepared as previously described for the identical compound.[25] ^1H NMR (500 MHz, CD_2Cl_2) δ 7.54 (d, J = 4.5 Hz, 2H), 7.39 (t, J = 4.5 Hz, 2H), 7.31 (t, J = 4.5 Hz, 1H), 7.09 (d, J = 4.0 Hz, 1H), 7.06 (d, J = 4.0 Hz, 1H). $^{13}C\{^1H\}$ NMR (125 MHz, CD_2Cl_2) δ 146.3, 133.9, 131.4, 129.4, 128.3, 125.9, 123.8, 111.6. GC-MS m/z (% relative intensity): 240 (100), 238 (100), 158 (30), 115 (99).

2-Bis(4-*tert*-butylphenyl)amino-5-phenylthiophene (6). To an oven-dried tube-shaped Schlenk flask cooled under nitrogen atmosphere was added anhydrous deoxygenated toluene (10 mL), tris(dibenzylideneacetone)dipalladium(0) (0.050 g, 0.046 mmol), and tri(*tert*-butyl)phosphine (1.0 mL, 10% wt. in hexane). After 15 minutes, 2-bromo-5-phenylthiophene (0.20 g, 0.84 mmol), bis(4-*tert*-butylphenyl)amine (0.28 g, 1.0 mmol), and sodium *tert*-butoxide (0.40 g, 4.2 mmol) were added. A reflux condenser was attached, and the reaction flask was immersed in an oil bath, bringing the reaction mixture to reflux. After 45 minutes, the reaction flask was removed from the oil bath,

and the reaction mixture was run through a tall pad of silica gel, eluting with hexanes/ethyl acetate (9:1). The product was recrystallized from ethyl acetate and methanol, yielding a pale yellow solid. After a column of silica gel, eluting with hexanes/toluene (10:1), 0.28 g (76%) of the desired product was isolated as a pale yellow solid. ^{1}H NMR (300 MHz, CD$_2$Cl$_2$) δ 7.50 (d, J = 8.1 Hz, 2H), 7.28 – 7.38 (m, 6H), 7.21 (t, J = 6.0 Hz, 1H), 7.13 (d, J = 3.6 Hz, 1H), 7.08 (d, J = 8.0 Hz, 4H), 6.60 (d, J = 3.6 Hz, 1H), 1.31 (s, 18H). ^{13}C{^{1}H} NMR (75 MHz, CD$_2$Cl$_2$) δ 151.9, 146.4, 137.5, 135.0, 129.2, 127.3, 126.4, 125.3, 122.5, 122.1, 121.2, 34.5, 31.5. GC-MS m/z (% relative intensity): 439 (100), 424 (100), 394 (30), 250 (10), 204 (35), 176 (40), 147 (20). Anal. Calcd. for C$_{30}$H$_{33}$NS: C, 81.96; H, 7.57; N, 3.19. Found: C, 81.70; H, 7.56; N, 3.23. Cyclic voltammetry in 0.1 M ^{n}Bu$_4$NPF$_6$ in dichloromethane: E$_{1/2}$$^{+/0}$: +0.22 V versus Cp$_2Fe^{+/0}$ at 0 V.

1,3-Bis(thien-2-yl)benzene (14). In a 100 mL round-bottomed flask were combined 1,3-dibromobenzene (5.0 g, 21 mmol), 2-(tri-n-butylstannyl)thiophene (17 g, 47 mmol), and anhydrous toluene (20 mL). After sparging with nitrogen for 20 minutes, tetrakis(triphenylphosphino)palladium(0) (0.050 g, 0.46 mmol), was added; a reflux condenser was attached, and the reaction flask was immersed in an oil bath and heated to reflux for 15 hours. After removing the reaction flask from the heat, methanol, water, and potassium fluoride were added. The reaction mixture was filtered, giving a white solid (although a large portion of the reaction mixture was discarded because of difficulty in the filtration), which was purified by column chromatography with hexanes/dichloromethane (9:1). After recrystallization from dichloromethane and

273

methanol, a white solid (1.15 g, 22%) was isolated. ^{1}H NMR (300 MHz, C$_6$D$_6$) δ 7.93 (s, 1H), 7.37 (dd, J = 1.8, 7.8 Hz, 2H), 7.00 – 7.08 (m, 3H), 6.83 (dd, J = 1.2, 5.1 Hz, 2H), 6.75 (dd, J = 3.6, 2.1 Hz, 2H). ^{13}C{^{1}H} NMR (75 MHz, C$_6$D$_6$) δ 144.7, 135.5, 129.7, 128.2, 125.4, 125.2, 123.9, 123.8. ^{13}C{^{1}H} NMR (75 MHz, CD$_2$Cl$_2$) δ 144.1, 135.4, 129.8, 128.5, 125.5, 125.3, 123.9, 123.6. GCMS: m/z (% relative intensity): 242 (100), 197 (65), 152 (45), 121 (50). Anal. calcd. for C$_{14}$H$_{10}$S$_2$: C, 69.38; H, 4.16. Found: C, 69.28; H, 4.16.

1,3-Bis(5-bromothien-2-yl)benzene (15). In a 100 mL round-bottomed flask, acetic acid (12 mL), bis(thien-2-yl)benzene (0.61 g, 2.5 mmol), and sodium acetate (0.82 g, 10 mmol) were combined. The reaction flask was immersed in an ice water bath, and bromine (0.80 g, 5.0 mmol) was added dropwise. After one hour, water was added, and the product was extracted with ethyl acetate. The organic layer was washed with aqueous sodium thiosulfate and was dried over anhydrous magnesium sulfate. After concentration by rotary evaporation, the product was recrystallized from dichloromethane and methanol and was filtered to give 0.85 g (85%) of the desired product as a gray semicrystalline solid. ^{1}H NMR (500 MHz, C$_6$D$_6$) δ 7.45 (t, J = 1.5 Hz, 1H), 7.09 (dd, J = 1.5, 8 Hz, 2H), 6.89)t, J = 8 Hz, 1H), 6.65 (d, J = 4 Hz, 2H), 6.54 (d, J = 4 Hz, 2H). ^{13}C{^{1}H} NMR (75 MHz, C$_6$D$_6$) δ 145.3, 134.6, 131.2, 129.8, 125.2, 124.1, 122.8, 112.2. ^{13}C{1H} NMR (CD$_2$Cl$_2$, 75 MHz) δ 145.4, 134.7, 131.4, 130.1, 125.4, 124.3, 122.9, 112.1. GCMS: m/z (% relative intensity): 402 (55), 400 (100), 398 (45), 277 (15), 240 (10), 207 (30), 139 (15). Anal. calcd. for C$_{14}$H$_8$S$_2$Br$_2$: C, 42.02; H, 2.02. Found: C, 41.27; H, 1.83.

1,3-Bis(5-bis(4-*tert*-butylphenyl)aminothien-2-yl)benzene (5). In an oven-dried tube-shaped Schlenk flask cooled under nitrogen atmosphere, anhydrous deoxygenated toluene (15 mL), tris(dibenzylideneacetone)-dipalladium(0) (0.050, 0.046 mmol), and tri(*tert*-butyl)phosphine (1.0 mL, 10% wt. in hexane) were combined. After 15 minutes, 1,3-bis(5-bromothien-2-yl)benzene (0.40 g, 1.0 mmol), bis(4-*tert*-butylphenyl)amine (0.62 g, 2.2 mmol), and sodium *tert*-butoxide (0.58 g, 6.0 mmol) were added; a reflux condenser was attached, and the reaction flask was immersed in an oil bath, bringing the reaction mixture to reflux. After 100 minutes, the reaction flask was removed from the oil bath, and ethyl acetate was added after the reaction mixture reached room temperature. The organic layer was washed with water after which it was concentrated by rotary evaporation. Recrystallization from ethyl acetate and methanol gave 0.40 g (50%) of the desired product as a yellow powder. ^{1}H NMR (500 MHz, C_6D_6) δ 8.13 (t, J = 1.2 Hz, 1H), 7.50 (d, J = 8.5 Hz, 8H), 7.57 (dd, J = 1.5, 6.0 Hz, 2H), 7.54 (d, J = 8.5 Hz, 8H), 7.31 (t, J = 8.0 Hz, 1H), 7.20 (d, J = 3.5 Hz, 2H), 6.91 (d, J = 3.5 Hz, 2H), 1.52 (s, 36H). ^{13}C{1H} NMR (125 MHz, C_6D_6) δ 152.5, 146.1 (2 peaks, 0.04 ppm apart), 137.1, 135.8, 129.6, 126.5, 124.0, 123.0, 122.5, 122.0, 120.9, 34.3, 31.5. HRMS (FAB+), calcd for $C_{54}H_{60}N_2S_2$: 800.41979; found: 800.42197. Anal. calcd. for $C_{54}H_{60}N_2S_2$: C, 80.95; H, 7.55, N, 3.50. Found: C, 80.12; H, 7.42; N, 3.43. Cyclic voltammetry in 0.1 M $^nBu_4NPF_6$ in dichloromethane: $E_{1/2}^{+/0}$: +0.22; $E_{1/2}^{2+/+}$: +0.31 V versus $Cp_2Fe^{+/0}$ at 0 V.

5.5 References

(1)   *Mixed-Valence Compounds: Theory and Applications in Chemistry, Physics and Biology*, Boston, 1980, ed. D. B. Brown, K.

(2)   *Mixed-Valency Systems: Applications in Chemistry, Physics, and Biology*, Boston, 1991, ed. K. Prassides, K.

(3)   Nelsen, S. F.; Tran, H. Q.; Nagy, M. A. *J. Am. Chem. Soc* 1998, *120*, 298-304.

(4)   Demadis, K. D.; Hartshorn, C. M.; Meyer, T. *J. Chem. Rev.* 2001, *101*, 2655-2685.

(5)   Bonvoisin, J.; Launay, J.-P.; Auweraer, M. V.; Schryver, F. C. D. *J. Phys. Chem.* 1994, *98*, 5052.

(6)   Bonvoisin, J.; Launay, J.-P.; Verbouwe, W.; Auweraer, M. V.; Schryver, F. C. D. *J. Phys. Chem.* 1996, *100*, 17097.

(7)   Bonvoisin, J.; Launay, J.-P.; Auweraer, M. V.; Schryver, F. C. D. *J. Phys. Chem.* 1994, *98*, 5052-5057.

(8)   Weyland, T.; Costuas, K.; Toupet, L.; Halet, J.-F.; Lapinte, C. *Organometallics* 2000, *19*, 4228-4239.

(9)   Lambert, C.; Noll, G. *Angew. Chem. Int. Ed.* 1998, *37*, 2107-2110.

(10)   Lambert, C.; Haschler, W.; Schmalzlin, E.; Meerholz, K.; Brauchle, C. *J. Chem. Soc., Perkin Trans. II* 1999, 577-587.

(11)   Haga, M.; Ali, M. M.; Sato, H.; Monjushiro, H.; Nozako, K.; Kano, K. *Inorg. Chem.* 1998, *37*, 2320-2324.

(12)   Sedo, J.; Vidal-Gancedo, J.; Rovira, C.; Bonvoisin, J.; Launay, J.-P.; Veciana, J. *Synth. Met.* 1997, *85*, 1651-1654.

(13)   Mandal, D.; Mikuriya, M.; Fun, H.-K.; Ray, D. *Inorg. Chem. Commun.* 2007, *10*, 657-660.

(14)   Stadler, C.; Daub, J.; Kohler, J.; Saalfrank, R. W.; Coropceanu, V.; Schunemann, V.; Ober, C.; Trautwein, A. X.; Parker, S. F.; Poyraz, M.; Inomata, R.; Cannon, R. D. *J. Chem. Soc. Dalton Trans.* 2001, 3373-3383.

(15)   Pfennig, B. W.; Fritchman, V. A.; Hayman, K. A. *Inorg. Chem.* 2001, *40*, 255-263.

(16)   Lambert, C.; Nöll, G.; Hampel, F. *J. Phys. Chem. A* 2001, *105*, 7751-7758.

(17)   Sedo, J.; Ruiz, D.; Vidal-Gancedo, J.; Rovira, C.; Boncoisin, J.; Launay, J.-P.; Veciana, J. *Adv. Mater.* 1996, *8*, 748.

(18)   Overgaard, J.; Larsen, F. K.; Schiott, B.; Iversen, B. B. *J. Am. Chem. Soc* 2004, *125*, 11088-11099.

(19)   Hush, N. S. *Prog. Inorg Chem.* 1967, *8*, 391-444.

(20)   Lindholm, E.; Asbrink, L. *Chem. Phys. Lett.* 1970, *5*, 192.

(21)   Sell, J. A.; Kuppermann, A. *Chem. Phys. Lett.* 1979, *61*, 355-362.

(22)   Plater, M. J.; McKay, M.; Jackson, T. *Perkin 1* 2000, *16*, 2695-2701.

(23)   Kotha, S.; Dhurke, K.; Kakali, L.; Sunoj, R. B. *Euro. J. Org. Chem.* 2004, *19*, 4003-13.

(24)   Cherioux, F.; Guyard, L. *Adv. Funct. Mater* 2001, *11*, 305-9.

(25)   Vachal, P.; Toth, L. M. *Tet. Lett.* 2004, *45*, 7157-61.

(26)   Connelly, N. G.; Geiger, W. E. *Chem. Rev.* 1996, *96*, 877-910.

(27)   Seo, E. T.; Nelson, R. F.; Fritsch, J. M.; Marcoux, L. S.; Leedy, D. W.; Adams, R. N. *J. Am. Chem. Soc.* 1966, *88*, 3498-3503.

(28)   Pangborn, A. B.; Giardello, M. A.; Grubbs, R. H.; Rosen, R. K.; Timmers, J. F. *Organometallics* 1996, *15*, 1518-1520.

(29)   Ditchfield, R.; Hehre, W. J.; Pople, J. A. *J. Chem. Phys.* 1971, *54*, 724.

(30)   Hehre, W. J.; Ditchfield, R.; Pople, J. A. *J. Chem. Phys.* 1972, *56*, 2257.

(31)   Gordon, M. S. *Chem. Phys. Lett* 1980, *76*, 163.

(32)   Hariharan, P. C.; Pople, J. A. *Theor. Chim. Acta* 1973, *28*, 213.

(33)   Becke, A. D. *Phys. Rev. A* 1988, *38*, 3098.

(34)   Becke, A. D. *J. Chem. Phys.* 1993, *98*, 5648.

(35)   Frisch, M. J.; Trucks, G. W.; Schlegel, H. B.; Scuseria, G. E.; Robb, M. A.; Cheeseman, J. R.; J. A. Montgomery, J.; Vreven, T.; Kudin, K. N.; Burant, J. C.; Millam, J. M.; Iyengar, S. S.; Tomasi, J.; Barone, V.; Mennucci, B.; Cossi, M.; Scalmani, G.; Rega, N.; Petersson, G. A.; Nakatsuji, H.; Hada, M.; Ehara, M.; Toyota, K.; Fukuda, R.; Hasegawa, J.; Ishida, M.; Nakajima, T.; Honda, Y.; Kitao, O.; Nakai, H.; Klene, M.; Li, X.; Knox, J. E.; Hratchian, H. P.; Cross, J. B.; Adamo, C.; Jaramillo, J.; Gomperts, R.; Stratmann, R. E.; Yazyev, O.; Austin, A. J.; Cammi, R.; Pomelli, C.; Ochterski, J. W.; Ayala, P. Y.; Morokuma, K.; Voth, G. A.; Salvador, P.; Dannenberg, J. J.; Zakrzewski, V. G.; Dapprich, S.; Daniels, A. D.; Strain, M. C.; Farkas, O.; Malick, D. K.; Rabuck, A. D.; Raghavachari, K.; Foresman, J. B.; Ortiz, J. V.; Cui, Q.; Baboul, A. G.; Clifford, S.; Cioslowski, J.; Stefanov, B. B.; Liu, G.; Liashenko, A.; Piskorz, P.; Komaromi, I.; Martin, R. L.; Fox, D. J.; Keith, T.; Al-Laham, M. A.; Peng, C. Y.; Nanayakkara, A.; Challacombe, M.; Gill, P. M. W.; Johnson, B.; Chen, W.; Wong, M. W.; Gonzalez, C.; Pople, J. A. *Gaussian 03, Revision B.02* 2004, Gaussian, Inc., Pittsburgh PA, 2003.

CHAPTER 6

CONCLUSIONS

The research in this thesis focused on understanding different aspects of ET and delocalization. In Chapter 2, the main goal was to understand the basic properties of some thiophene-based cores that were incorporated into bis(diarylamino) derivatives in Chapter 3. The study in Chapter 3 focused on determining the electronic coupling in strongly coupled monocations of bis(diarylamino) derivatives and on determining the extent to which the oxidation was amine-based – therefore mixed-valent (MV) – rather than bridge-based. The research in Chapter 4 focused on understanding how electronic coupling changes in MV species when the ioniation potentials of the bridges are changed relative to that of the end groups. The second study in Chapter 4 compared the barrier to ET in some MV species that was obtained from optical data and thermal ET data. Finally, Chapter 5 focused on the properties of a three-site triarylamine and its monocation to determine the properties of a more strongly coupled three-site MV species.

From Chapter 2, some of the properties dithieno[3,2-*b*;2,3-*d*]thiophene (DTT) and dithieno[3,2-*b*;2,3-*d*]pyrrole (DTP) were analyzed. Previously these fused thiophene-based moieties had been synthesized and incorporated into various derivatives for potential use in various optoelectronic applications. Although some data for these cores had been published, some basic characerizations were lacking. One of the most important properties that had not been properly characterized – for lack of the synthesis of suitable derivatives that would lead to the ability to complete this characterization – was the determination of the oxidation potentials of DTT and DTP (with *N*-alkyl or *N*-aryl substitutents) with reasonably reversible

cyclic voltammograms. For incorporation into derivatives for optoelectronic applications, it is important to know the oxidation potentials of the constituent parts of a larger chromophore to know if the energies of the frontier molecular orbitals complement the design of the material. For example, in hole-transporting materials used in organic light-emitting diodes, it is important to have ionization potentials and electron affinities that match the other hole- and electron-transporting materials in the device in order to prevent the charges from being trapped at the interfaces of the different semiconductor layers. In the case of DTT and *N*-substituted-DTP, cyclic voltammetry (CV) gave irreversible oxidations. This is presumably due to oxidative polymerization, which has been shown to occur in thiophene and in DTP derivatives. From irreversible oxidations such as those observed for these derivatives, it is not possible to obtain a reliable half-wave oxidation potential, yet the oxidation potentials of these derivatives were being compared without having a reversible oxidation by CV.

In order to determine the oxidation potentials of DTT and *N*-substituted DTP derivatives, 2,6-dialkyl-substituted derivatives were synthesized, the alkyl groups blocking the positions at which oxidative polymerization has been shown to occur. Additionally, a more commonly used non-fused analog, 2,2'-bithiophene (BIT) was used for comparison, such that the oxidation potentials, when measured, would be relevant to a more standard material. In this case, 5,5'-di(*n*-hexyl)-2,2'-bithiophene was used for comparison. The oxidation potentials of the dialkylated BIT, DTT, *N*-alkyl-DTP, and *N*-aryl-DTP derivatives were measured by CV experiments. The cyclic voltammograms showed reasonably reversible oxidations in the case of the dialkylated derivatives. From this data, it was found that the BIT and DTT derivatives had similar oxidation potentials ($E_{1/2}^{+/0} = 0.69$ and 0.66 V, respectively, versus ferrocenium / ferrocene at 0 V), and both DTP derivatives were significantly easier to

oxidize. Also determined from these experiments was that the *N*-alkyl-DTP derivative was easier to oxidize ($E_{1/2}^{+/0}$ = 0.23 V) than the *N*-aryl-DTP derivative ($E_{1/2}^{+/0}$ = 0.38 V). This data is also relevant in the design of DTP-based materials. Often the substituent on DTP is varied based on solubility, but now it is known that the substitutent on DTP affects more than the solubility; the oxidation potentials of the aromatic cores are also affected.

In the process of synthesizing various derivatives of DTP, the synthesis of DTP was also improved. Previously there had been a few published routes to the synthesis of *N*-substituted DTP derivatives, but each route had a significant draw back, either in number of synthetic steps required to reach unique *N*-substituted derivatives or in the reaction yields. Based on the optimization of a previously published reaction scheme, it is now possible to obtain unique *N*-substituted DTP derivatives in one step (from 3,3'-dibromo-2,2'-bithiophene) in high yields. This makes DTP more appealing as a building block for future materials because a variety of derivatives can be easily synthesized (as was shown in Chapter 2) from a simple intermediate.

The research in Chapter 3 focused on analyzing the electron delocalization in strongly coupled MV monocations of bis(diarylamino) derivatives with thiophene-based cores. Similar derivatives with phenylene-based cores had previously been synthesized, some of the monocations of which had been characterized as strongly coupled Class III MV species. In this chapter, the phenylene-based bridges (stilbene and biphenyl) were replaced with more easily ionizable thiophene-based bridges (di(thien-2-yl)ethene and BIT). Additionally, a fused-ring equivalent to BIT was used (DTT), and a more easily oxidizable DTP bridge was also used. The result of replacing phenylene with thienylene was that the bis(diarylamino) derivatives were more easily oxidized than the phenylene-based derivatives, the most easily

oxidized derivative having an oxidation potential of -0.43 V versus ferrocenium / ferrocene, which compares to an oxidation potential of +0.09 V for bis(dianisylamino)biphenyl. If a hole-transporting material were needed that was very easily oxidized, for example, as a hole-injection layer or where p-doping was desirable, these derivatives would be good candidates because of their low oxidation potentials.

In the monocations, the electronic coupling was increased compared to the equivalent phenylene-based monocations. For example, when comparing the electronic coupling for the bis(dialkoxyphenylamino)BIT derivative (V = 5050 cm^{-1}), the coupling is much larger than the equivalent phenylene-based derivative (V = 3180 cm^{-1}) and is larger than the previously largest value for electronic coupling in a bis(dialkoxyphenylamino) derivative, the 1,4-bis[di(alkoxyphenyl)amino]benzene monocation (V = 4675 cm^{-1}). For the DTP-based derivative, which had the most electron-rich bridge, the electronic coupling is the largest of these series (V = 6270 cm^{-1}). Although the diabatic ET distance in these species is considerably smaller than the nitrogen-nitrogen distance, suggesting redox centers that are bridge-based, electron paramagnetic resonance (EPR) experiments suggest that the monocations are best described as be MV species, not as bridge-based monocations. By simulating the experimental EPR spectra, it was possible to determine the nuclei to which the lone electron was coupled, and because that data agreed well with computational predictions for the degrees of coupling constants to those nuclei, the calculations were used to determine the spin density of the monocations, which has significant character on the nitrogen nuclei.

The first part of Chapter 4 was a continuation of the study started by Barlow and Risko on a series of bis(diarylaminostyryl)arene derivatives. Barlow and coworkers previously showed that the electronic coupling varied in bis(diarylaminostyryl)arene derivatives from

$480 - 3200$ cm^{-1} by changing the ionization potentials of the bridges and cores with respect to each other yet keeping the overall aromatic framework and redox centers the same. At one extreme (where $V = 480$ cm^{-1}), the end groups were di(alkoxyphenyl)amino, and the core was a 1,4-bis(styryl)-2,5-dicyano bridge. At the other extreme ($V = 3200$ cm^{-1}), the end groups were diphenylamino groups, and the core was a 2,5-bis(styryl)-3,4-di(n-butoxy)thiophene. The contribution to this study that is described in Chapter 4 are derivatives with even more easily ionizable pyrrole-based bridges. These derivatives were more easily oxidizable than the most electron-rich derivative of the previous series: -0.26 V for one of the pyrrole derivatives compared to +0.05 V for the most easily oxidized thiophene-based derivative. The electronic coupling values in the pyrrole derivatives were all larger than the previous derivatives, with electronic coupling values as large as 4210 cm^{-1}.

In the second part of Chapter 4, monocations of some Class II bis(diarylamino) derivatives were studied by variable temperature EPR. One set of MV systems studied included the monocations of bis[di(alkoxyphenyl)aminophenyl]ethene, 1,4-bis[di(alkoxyphenyl)amino]benzene, and 1,4-bis[di(alkoxyphenyl)aminostyryl]-2,5-dicyanobenzene derivatives. The second set included the monocations of bis[di(alkoxyphenyl)aminophenyl]acetylene and 1,4-bis[di(alkoxyphenyl)aminophenyl-ethynyl]benzene. All monocations showed approximately 5-line spectra at room temperature, which indicated that there was coupling of the lone electron to both nitrogen nuclei on the EPR time scale. Some of the derivatives showed changes in their EPR spectra upon cooling while others remained the same; the spectra of the monocations that changed moved toward a 3-line spectrum at lower temperatures, which indicates coupling to one nitrogen atom. The derivatives that remained the same had a smaller barrier to ET than the ones for which

changes were observed, as determined by calculating the electronic coupling of the monocations from the Hush analysis of the IVCT bands. By comparing which derivatives underwent changes upon cooling with those that did not, it was possible to compare the different structural aspects of the bis(diarylamino) monocations that lead to differences in barriers for ET. For example, comparison of some of the derivatives indicated that – consistent with conclusions drawn from analysis of the IVCT bands of these monocations – the barrier to intramolecular ET increases when the redox centers are farther apart, i.e. when the bridge length is increased. Additionally, the barrier to intramolecular ET increases when alkene-based bridges are replaced with alkyne-based briges. Finally, this barrier decreases when the energy of the conjugated bridge approaches that of the end groups; specifically in the case of the bis(diarylamino) monocations, the barrier decreases as the energy of the frontier molecular orbitals of the bridge increases. None of the conclusions from the VT-EPR experiments is surprising because we the same conclusions were drawn from Hush analysis of the IVCT bands of the same monocations.

For the EPR spectra that changed with temperature, by simulating the EPR spectra, the rates of intramolecular ET were extracted. An Arrhenius plot gave the barrier to ET and indicated that the ET is in the adiabatic regime. The barrier to ET calculated from the Arrhenius plot was used, in combination with the reorganization energy obtained from the energy of maximum absorbance from the IVCT band, to determine a value for electronic coupling. This value was compared to the electronic coupling found from analysis of the IVCT band using Hush theory using the nitrogen-nitrogen distance as the diabatic ET distance. By comparing these values for electronic coupling, it was found that the diabatic ET transfer distance found from the variable temperature EPR data was 35 – 43% of the nitrogen-

nitrogen distance. This result is significant in that it is the first time for triarylamines (to the best of our knowledge) that two experimental methods (optical and thermal) have been used to compare values for diabatic ET, and it was found to be significantly different for each method. This result suggests, as is consistent with previous suggestions based on IVCT band analysis, that the electronic coupling determined from the Hush equation is underestimated in strongly coupled MV species in which there is a conjugated bridge linking two redox centers when the nitrogen-nitrogen distance is used as the diabatic ET distance. Based on the studies in this chapter, it is underestimated by two to three times the actual value.

The last study is presented in Chapter 5. In this project, three-site compounds which are related to previously studied 1,3,5-tris[di(4-ethylphenyl)aminophenyl]benzene were synthesized in which phenylene bridges were replaced with thienylene bridges. From comparison of the thiophene-based derivatives to the original phenylene-based derivative, it was found that the thiophene-based derivatives were easier to oxidize than the phenylene-based derivatives, which was expected based on the results from Chapter 3 in which a similar bridge replacement was made. Additionally, cyclic voltammetry and differential pulse voltammetry experiments showed different oxidation potentials for the three diarylamino moieties in the thiophene-based derivatives, whereas in the phenylene-based derivatives, the three oxidations occurred at indistinguishable potentials. This means that the oxidation of one diarylamino moiety affects the oxidations of the remaining diarylamino moieties more in the thiophene-based derivative than in the phenylene-based derivative. The electrochemical data is insufficient to determine whether the increase in separation of the redox potentials is due to increase in electronic coupling or if the change might result from contributions from electrostatic effects, ion-pairing, antiferromagnetic exchange, and inductive effects.

Analysis of the IVCT bands of the monocations of the thiophene-based derivatives showed well-resolved bands that were modeled as Gaussians. The Hush analysis using the nitrogen-nitrogen distance as the diabatic ET distance indicated that, as predicted, the electronic coupling in the thiophene-based monocations (V = ca. 300 cm^{-1}) was slightly larger than that of the phenylene-based monocation (V = ca. 200 cm^{-1}).

In the case of one of the thiophene-based monocations, the EPR spectrum at room temperature showed hyperfine coupling, which gave a reasonable fit to a simulation that indicated that the unpaired electron was coupled to all three nitrogen nuclei and, therefore, all three redox centers at room temperature. Again, as has been previously stated, this does not imply that the electron is delocalized over all three redox centers; in fact, the analysis of the IVCT band implies that the electron is *not* delocalized. However, given a Class II cation, these data indicate that the rate of intramolecular ET is in the fast regime at room temperature. Cooling of the solution by 50 K did not change the shape of the spectrum significantly, which implies that the barrier to intramolecular ET is larger than for the examples studied in Chapter 4 for which changes in the EPR spectrum were observed upon cooling by as little as 10 K. Although the results from Chapter 5 are not particularly surprising, they will provide valuable experimental validation for theoretical work for these monocations that is currently underway.

In conclusion, this thesis research has provided insight in ET and delocalization in a variety of MV monocations of bis- and tris-(diarylamino) derivatives. From varying the electronic coupling to examining the barrier to ET, the studies in this thesis have investigated a variety of aspects of ET. From what has been observed, several monocations that exhibit strong electronic coupling have been shown to have MV character. It has been shown that the electronic coupling can be changed significantly in derivatives of the same overall structure

by simple modifications of the ionization potentials of the bridges relative to the redox centers. Lastly, it was possible to compare the diabatic ET distance from data that calculated the thermal barrier to ET from variable-temperature rate-dependent techniques with that calculated from Hush analysis of the IVCT band, which indicated that the diabatic ET distance was overestimated when nitrogen-nitrogen distances were used.

Thanks for reading!